METAGENOMIC AND GENOMIC ANALYSES OF MODERN FRESHWATER MICROBIALITES: UNMASKING A COMMUNITY OF COMPLEX METABOLIC POTENTIAL

by

RICHARD ALLEN WHITE III

Bachelors of Science, California State University East Bay, Hayward, California USA, 2007
Masters of Science, California State University East Bay, Hayward, California USA, 2009

A THESIS SUBMITTED IN PARTIAL FULFILLMENT OF

THE REQUIREMENTS FOR THE DEGREE OF

DOCTOR OF PHILOSOPHY

in

THE FACULTY OF GRADUATE AND POSTDOCTORAL STUDIES

(Microbiology and Immunology)

THE UNIVERSITY OF BRITISH COLUMBIA

(Vancouver)

September 2014

© Richard Allen White III, 2014

Abstract

Microbialites represent the oldest known persistent ecosystems and potentially the earliest evidence of life on the planet, having existed for ~85% of the geologic history of Earth (Dupraz *et al.*, 2009). Despite over one hundred years of active research, little is known about modern freshwater microbialite ecosystems with regards to metabolic potential and microbialite-specific community structure. We performed metagenomic analysis of freshwater thrombolithic clotted microbialites from Pavilion Lake (British Columbia, Canada) and Clinton Creek (Yukon, Canada). In addition, metagenomes were obtained from the surrounding water and sediments to sort out which members of the microbial community were microbialite-specific. Pavilion Lake microbialites are distinct from the surrounding environments in microbial community structure and metabolic potential. The microbialites are dominated by heterotrophic processes with high abundances of heavy metal, antibiotic resistance, and alcohol fermentation pathways from the numerically dominant *Proteobacteria*. Clinton Creek houses the northern-most and fastest growing microbialites, which have a high proportion of photosynthetic genes, supporting isotopic data that photosynthesis drives microbialite formation. Clinton Creek has distinct communities, with microbialites dominated by *Alphaproteobacteria* (photoheterotrophs) and sediments dominated by *Gammaproteobacteria* (mainly heterotrophic nitrogen-fixers). To complement the metagenomic study of Pavilion Lake, a culturing based study was performed that yielded over one hundred new bacterial isolates. The new bacterial isolates were further screened for pigment containing strains that were non-photosynthetic. Amongst these pigment containing bacteria two new isolates were found and designated as an *Exiguobacterium* and an *Agrococcus.* Polyphasic analysis revealed that both are new species, which were named *Agrococcus pavilionensis* strain RW1 and *Exiguobacterium pavilionensis* strain RW2. Genome sequencing of both strain RW1 and

RW2 was completed and a comparative genomic and phylogenetic study was performed to evaluate their evolutionary placement and metabolic potential. Both isolates have low abundance in the Pavilion Lake microbialites, although they contribute heavy metal resistance genes that are found amongst the microbialite metagenomes. Hypothetical carotenoid biosynthesis pathways are also described which may be responsible for the coloration in *Agrococcus* and *Exiguobacterium* and may be related to photo-protection.

Preface

Chapter 2 is based on a manuscript in preparation:

White III RA, Suttle CA. Modern freshwater microbialites reveals distinct microbial community structure and metabolic potential that differs from the surrounding environment.

CAS, RAWIII and AMC designed the project. RAWIII, AMC and CAS conducted field work. RAWIII did the laboratory work and data analysis. RAWIII and CAS wrote the manuscript.

Chapter 3 is based on a manuscript in preparation:

White III RA, Power IM, Hanson NW, Dipple GM, Southam G, Hallam SJ and Suttle CA. Comparative analysis of microbiome of rapidly forming modern microbialites from Canadian Yukon.

CAS, GMD, RAWIII and IMP envisioned the project. RAWIII and IMP designed the experimental approach. IMP did the water chemistry and field sampling. RAWIII processed the genomic samples and did the data analysis with help from NWH and SJH. RAWIII, IMP and CAS wrote the paper.

Chapter 4 is based on a published manuscript and manuscript in preparation:

White III RA, Grassa CJ, Suttle CA. (2013). First draft genome sequence from a member of the genus *Agrococcus*, isolated from modern microbialites. Genome Announc. 1, e00391-13

White III RA, Soles SA, Gavelis G, Gosselin E, Slater GF, and Suttle CA. The genome of *Agrococcus* sp. strain RW1 isolated from modern microbialites reveals genetic promiscuity and elements responsive to environmental stresses. (In preparation).

RAWIII and CAS initiated the project. RAWIII designed and conducted the experiments. EG contributed to experiments on growth and characterization. CJG completed the first draft assembly of the genome (published) and advised on *de novo* assembly and genome finishing. RAWIII revised the assembly, finished the genome and completed annotation. SAS and GFS completed all PLFA experiments and data analysis. GG did the electron microscopy of the isolate. RAWIII, CAS, GS, SAS and GG contributed to writing the manuscript in preparation.

Chapter 5 is based on a published manuscript and manuscript in preparation:

White III RA, Grassa CJ, Suttle CA. (2013). Draft genome sequence of *Exiguobacterium pavilionensis* strain RW-2, with wide thermal, salinity, and pH tolerance, isolated from modern freshwater microbialites. Genome Announc. 1, e00597-13

White III RA, Soles SA, Gavelis G, Gosselin E, Slater GF, and Suttle CA. Illumination of an *Exiguobacterium* through the comparative lenses of classical characterization and comparative genomic analysis. (In preparation).

RAWIII and CAS initiated the project. RAWIII designed and conducted the experiments. EG contributed to experiments on growth and characterization. CJG completed the first draft assembly of the genome (published) and advised on *de novo* assembly and genome finishing. RAWIII revised the assembly, finished the genome and completed annotation. SAS and

GFS completed all PLFA experiments and data analysis. GG did the electron microscopy of the isolate. RAWIII, CAS, GS, SAS and GG contributed to writing the manuscript in preparation.

Table of Contents

Abstract ii

Preface iv

Table of Contents vii

List of Tables xiv

List of Figures xv

List of Abbreviations xix

List of Keywords xxi

Acknowledgments xxiii

Dedication xxiv

Chapter 1: Introduction 1

1.1 What is a microbialite? 1

1.1.1 Physical classification and brief history 1

1.2 Microbialites as the oldest persistent ecosystems 2

1.3 Global distribution of microbialites 2

1.4 Proposed microbialite formation hypotheses 5

1.4.1 Abiotic (spectator hypothesis) 5

1.4.2 Abiotic combined biotic hypothesis 6

1.5 Major microbial taxa and their metabolic pathways that contribute to microbialite formation 8

1.5.1 *Alphaproteobacteria* 8

1.5.2 *Cyanobacteria* 9

1.5.2.1 Planktonic cyanobacteria 9

1.5.2.2 Filamentous cyanobacteria, mat-builders 9

1.5.3 Sulfur-oxidizing bacteria (SOBs) 10

1.5.4 Sulfate-reducing bacteria (SRBs) 11

1.5.5 *Firmicutes* 13

1.5.6 *Actinobacteria* 14

1.5.7 Eukaryotes 15

1.5.8 Viruses 16

1.6 Previously studied microbialite-forming ecosystems 17

1.6.1 Shark Bay microbialites 17

1.6.2 Highbourne Cay microbialites 18

1.6.3 Cuatro Cienegás microbialites: Pozas Azules II and Rios Mesquites 20

1.7 Microbialite-forming ecosystems described in this thesis 21

1.7.1 Pavilion Lake 21

1.7.2 Clinton Creek 23

1.8 Thesis hypotheses 24

1.9 Tables and figures 26

Chapter 2: Modern freshwater microbialite microbial community structure and metabolic potential is distinct from the surrounding environment 32

2.1 Introduction 32

2.2 Materials and methods 33

2.2.1 Sample collection 33

2.2.2 DNA extraction 34

2.2.3 Metagenomic library preparation (454 FLX Titanium and Illumina) 34

2.2.4 Metagenomic data assembly and analysis 35

2.2.5 Recruitment analysis to draft genomes 37

2.2.6 Metagenomic data depositing 37

2.3 Results and discussion 38

2.3.1 Metagenomic assembly statistics 38

2.3.2 Microbialites communities differ from the surrounding environment 38

2.3.3 Pavilion Lake microbialite core microbial community and related pathways 40

2.3.4 Low abundance members of Pavilion Lake microbialite microbial community 45

2.3.5 Metabolic potential relating to photosynthetic or heterotrophic processes 48

2.3.6 Viral community and viral defense 48

2.4 Conclusion 50

2.5 Tables and figures 52

Chapter 3: Comparative analysis of microbiome of rapidly forming modern microbialites from the Canadian Yukon 73

3.1 Introduction 73

3.2 Materials and methods 74

3.2.1 Site description and water chemistry 74

3.2.2 Sampling, DNA extraction, purity and concentration measurements 75

3.2.3 Illumina HiSeq/MiSeq library construction quality control and quantification 75

3.2.4 Analysis of Illumina sequencing data 76

3.2.5 Comparative metagenomics 78

3.2.6 Metagenomic data depositing 79

3.3 Results and discussion 79

3.3.1 Metagenomic assembly and contig properties 79

3.3.2 Community composition 80

3.3.3 Metabolic potential 83

3.3.4 Comparative metagenomic analysis 85

3.4 Conclusion 86

3.5 Tables and figures 88

Chapter 4: The genome of *Agrococcus* sp. strain RW1 isolated from modern microbialites reveals genetic promiscuity and elements responsive to environmental stresses 99

4.1 Introduction 99

4.2 Materials and methods 100

4.2.1 Isolation, growth conditions, phage induction, biochemical and antibiotic susceptibility tests 100

4.2.2 Phospholipid fatty acid analysis 101

4.2.3 Light and scanning electron microscopy (SEM) 102

4.2.4 DNA extraction, PCR and Illumina library construction 103

4.2.5 Phylogenetic analysis 103

4.2.6 Whole genome assembly and genome finishing 104

4.3 Results and discussion 106

4.3.1 Morphology and growth characteristics 106

4.3.2 PLFA characterization and comparative analysis 107

4.3.3 Evolutionary placement of *Agrococcus* sp. RW1 within the genus 108

4.3.4 Biochemical properties and antibiotic susceptibility 110

4.3.5 Mobile DNA and viral elements in *Agrococcus* sp. RW1 111

4.3.6 *Agrococcus* sp. RW1 life in a cold microbialite mat 113

4.3.7 Carotenoid biosynthesis 115

4.4 Conclusions 117

4.5 Tables and figures 119

Chapter 5: Illumination of an *Exiguobacterium* through the comparative lenses of classical characterization and modern genomic analysis 131

5.1 Introduction 131

5.2 Materials and methods 133

5.2.1 Isolation, growth conditions, biochemical and antibiotic susceptibility tests 133

5.2.2 Phospholipid fatty acid analysis (PLFA) 134

5.2.3 Light and scanning electron microscopy (SEM) 135

5.2.4 DNA extraction, PCR and Illumina library construction 135

5.2.5 Whole genome assembly, assembler comparison, genome finishing and annotation 136

5.2.6 Phylogenetic analysis and multiple locus sequence typing (MLST) analysis 137

5.3 Results and discussion 138

5.3.1 Morphology and growth characteristics 138

5.3.2 Biochemical properties and antibiotic susceptibility 140

5.3.3 PLFA characterization and comparative analysis 142

5.3.4 Evolutionary placement of *Exiguobacterium* sp. RW2 within the genus 142

5.3.5 Comparative genome analysis 144

5.3.6 Carbohydrate metabolism 146

5.3.7 Amino acid biosynthesis and catabolism 147

5.3.8 Motility and flagellum biosynthesis 148

5.3.9 Stress response temperature, heavy-metals and salinity 149

5.3.10 Carotenoid biosynthesis 151

5.4 Conclusions 152

5.5 Tables and figures 154

Chapter 6: Conclusion 172

6.1 Summary 172

6.2 Future directions 175

References 177

List of Tables

Table 2.1: Pavilion Lake metagenome assembly statistics 52

Table 2.2: Taxonomic classes (RefSeq) that are overrepresented in microbialites relative to the surrounding environment as determined by ANOVA using STAMP 53

Table 2.3: Functional annotations (SEED subsystem level I) that are overrepresented in microbialites relative to the surrounding environment as determined by ANOVA using STAMP 54

Table 3.1: Assembly statistics for Clinton Creek metagenomes 88

Table 3.2: Domain classification of the microbial community in Clinton Creek (%) 89

Table 4.1: Comparison of physiological properties of *Agrococcus* selected strains 119

Table 4.2: Selected cellular phospholipid fatty acids of *Agrococcus* selected strains (%) 120

Table 4.3: *Agrococcus* spp. final assembly statistics 121

Table 4.4: Biochemical properties of *Agrococcus* spp. selected strains 122

Table 4.5: Antibiotic susceptibility of *Agrococcus* spp. selected strains 123

Table 5.1: Names and isolation location of *Exiguobacterium* species 154

Table 5.2: Properties of *Exiguobacterium* selected strains 156

Table 5.3: Biochemical tests for selected strains of *Exiguobacterium* spp. 157

Table 5.4: Antibiotic susceptibility for selected strains *Exiguobacterium* spp. 158

Table 5.5: Selected phospholipid fatty acids from *Exiguobacterium* spp. strains (%) 159

Table 5.6: *Exiguobacterium* spp. assembly and annotation statistics 160

Table 5.7: *Exiguobacterium* spp. carotenoid biosynthesis genes 161

List of Figures

Figure 1.1: Microbialite morphology and carbonate macrofabric layout 26

Figure 1.2: Microbialite morphology examples..... 27

Figure 1.3: Timeline of microbialite and global atmospheric oxygen concentration over geological time 28

Figure 1.4: Generalized equations for microbialite formation and dissolution 29

Figure 1.5: Pavilion microbialite morphologies 30

Figure 1.6: Pavilion Lake nodular cyanobacterial morphologies 31

Figure 2.1: Pavilion Lake microbialite morphology with GC content and protein isoelectric points (pI)..... 55

Figure 2.2: Pavilion Lake microbial community composition 56

Figure 2.3: PCA and scatter plots using SEED subsystems based on ANOVA in STAMP for Pavilion Lake metagenomes 57

Figure 2.4: MetaCyc pathway annotations for Pavilion Lake metagenomes 58

Figure 2.5: Box and whisker plots for significant taxa represented in water filters and sediments by RefSeq classification using ANOVA in STAMP based on multiple groups..... 59

Figure 2.6: Post-havoc confidence interval plots functional classification for represented metabolic potential in surrounding environment (water filters and sediments) 60

Figure 2.7: Post-havoc confidence interval plots for *Alphaproteobacteria* using RefSeq classification 61

Figure 2.8: Post-havoc confidence interval plots for *Deltaproteobacteria* using RefSeq classification 62

Figure 2.9: Post-havoc confidence interval plots for *Cyanobacteria* using RefSeq classification63

Figure 2.10: Post-havoc confidence interval plots for cyanobacterial based functional genes using SEED subsystem classification and urealytic pathways 64
Figure 2.11: Box and whisker plots for novel functional classifications (SEED subsystem) represented in microbialites based on ANOVA in STAMP using multiple groups 65
Figure 2.12: Box and whisker plots for novel Archael based functional classifications (SEED subsystem) represented in microbialites based ANOVA in STAMP using multiple groups 66
Figure 2.13: *Exiguobacterium* presence in Pavilion Lake microbialite metagenome 67
Figure 2.14: Metagenomic recruitment plot for Pavilion Lake microbialite against *Agrococcus* 68
Figure 2.15: Microbialite metagenome functional annotation ranking using SEED subsystem (Level I) 69
Figure 2.16: Microbialite metagenome carbohydrate related SEED subsystem (Level II) functional annotations 70
Figure 2.17: Box and whisker plots for viruses and CRISPRs in Pavilion Lake..... 71
Figure 2.18: Post-havoc confidence interval plots for viral taxa using RefSeq and viral specific functional genes in SEED 72
Figure 3.1: Clinton Creek sample site and examples of microbialite morphology 90
Figure 3.2: Molecular properties of the Clinton Creek microbialite and sediment contigs..... 91
Figure 3.3: Microbial community structure of Clinton Creek metagenomes 92
Figure 3.4: Extended error plots for functional gene annotations for Clinton Creek metagenomes in STAMP using SEED subsystems 93
Figure 3.5: MetaCyc pathway annotations for Clinton Creek metagenomes 94
Figure 3.6: Functional gene comparative PCA plot for Clinton Creek metagenomes 95
Figure 3.7: Scatter plots of functional gene annotations using SEED subsystem level III 96

Figure 3.8: Comparative functional gene PCA plot for Clinton Creek against whale fall metagenomes..... 97

Figure 3.9: Comparative functional gene PCA plot for Clinton Creek against coral metagenomes 98

Figure 4.1: *Agrococcus* sp. strain RW1 microscopy..... 124

Figure 4.2: Maximum-likelihood tree of 16S rRNA gene sequences for *Agrococcus* spp. and related taxa (~1409 bp) 125

Figure 4.3: MLST (multiple locus sequence typing) maximum-likelihood tree of *Microbacteriaceae* (~2939 amino acids) 126

Figure 4.4: Genome plot (~2.6Mb) of *Agrococcus* sp. strain RW1..... 127

Figure 4.5: Genome synteny and Venn diagrams of *Agrococcus* sp. RW1 vs. *A. lahaulensis* K22-21..... 128

Figure 4.6: *Agrococcus* sp. RW1 LC-RRW783 plasmid genomic plot..... 129

Figure 4.7: Proposed carotenoid biosynthetic pathway for *Agrococcus*..... 130

Figure 5.1: *Exiguobacterium* sp. strain RW2 microscopy..... 162

Figure 5.2: *Exiguobacterium* maximum-likelihood tree based on 16S rRNA gene sequences (~1353 bp)..... 163

Figure 5.3: *Exiguobacterium* combined ribosomal operon maximum-likelihood tree..... 164

Figure 5.4: MLST maximum-likelihood phylogenetic tree..... 165

Figure 5.5: Genome plot (~3 Mb) of *Exiguobacterium* sp. strain RW2..... 166

Figure 5.6: Genome synteny and functional Venn diagrams (SEED) with high amino acid identities (AAIr >80%) to *Exiguobacterium* sp. RW2 167

Figure 5.7: Genome synteny and functional Venn diagrams (SEED) with low amino acid identities (AAIr <65%) to *Exiguobacterium* sp. RW2 168

Figure 5.8: Genome synteny and functional Venn diagrams (SEED) with low amino acid identities (AAIr <65%) to *Exiguobacterium* sp. RW2 169

Figure 5.9: MetaCyc pathway annotations for *Exiguobacterium* genomes 170

Figure 5.10: Proposed carotenoid biosynthesis pathway in the genus *Exiguobacterium* 171

List of Abbreviations

ANOVA: Analysis of variance.
BLAST: Basic local alignment search tool. It finds local similarity between two sequences which can be either protein or nucleotide sequences or a search across these groups.
BLAT: Blast-like alignment tool. Similar to blast but is faster by keeping the entire index of the database. Instead of a set of database sequences it searchs against an index derived from the database in smaller sequences or non-overlapping n-mers.
CRISPR: Clustered regularly interspaced short palindromic repeats. These short repetitions of DNA sequences are imprints of prior viral exposures. CRISPRs are associated with *cas* genes which act combined as a prokaryotic immune system.
CTAB: Cetyl trimethylammonium bromide which is used for nucleic acid extraction for samples with high polysaccharides (e.g. plants and cyanobacteria).
DIC: Dissolved inorganic carbon.
DOC: Dissolved organic carbon.
EPS: Extracellular polymeric substances containing exopolysaccharide formed by filamentous cyanobacteria.
FAMEs: Fatty acid methyl ester analysis.
GC content: Analysis of guanine and cytosine content, often a percentage in a collection of DNA sequences.
Gya: One gigayear ago or 10^9 years ago, which is a billion years ago. See Gyr.
Gyr: One gigayear or 10^9 years, which is a billion years.
LAST: Local alignment search tool. LAST is a blast-like tool that is faster than standard blast; LAST uses adaptive seeds to align and assign similarities between two sequences.
MDS: Multidimensional scaling.
MG-RAST: Metagenomic Rapid Annotations using Subsystems Technology. MG-RAST is an online server for metagenomic annotation and analysis.
MLST: Multiple locus sequence typing commonly used for genotyping clinical bacterial isolates but used here as multiple gene phylogenetic analysis.
Mya: One million ago or 10^6 years ago. See Myr.
Myr: One million years or 10^6 years.
N50: Genomic assembly statistic. Defined as the length for which all contigs of that length or longer contain at least 50% of the total of the lengths of the contigs.
N90: Genomic assembly statistic. Defined as the length for which all contigs of that length or longer contain at least 90% of the total of the lengths of the contigs.
NMDS: Nonmetric multidimensional scaling.
ORFs: Open reading frame related to a protein coding gene.
PCA: Principal component analysis.
pI: Predicted protein isoelectric point.
PAL%: Present atmospheric levels, where 100% PAL equals Earth's atmospheric oxygen at the present day.
PLFAs: Phospholipid fatty acids analysis.
qPCR: quantitative real-time polymerase chain reaction.
R: Statistical programming language.

RAST: Rapid annotations using subsystems technology. It is a web tool that annotates a bacterial, plastid or archaea genome using SEED subsystem classifications.
SEED: A protein sequence database that uses subsystem classifications for metabolic pathways. Each subsystem are functional classifications labeled as levels, with level I the highest followed by functions the lowest level.
SEM: Scanning electron microscopy.
SOB: Sulfur oxidizing bacteria using aerobic sulfur oxidation pathway called *Sox*.
SRB: Sulfate reducing bacteria using anaerobic dissimilatory sulfate reduction via the *dsr* pathway.
STAMP: Statistical Analysis of Metagenomic Profiles. It is a tool used to analyze metagenomic data, in this case from MG-RAST.

List of Keywords

454 FLX Titanium: Roche DNA pyrosequencing technology with read lengths >300bp
Abiotic: A process without biology, meaning geological in this context.
AbySS: A whole genome *de novo* assembler that uses De bruijn graph based method.
Anoxic or Anoxygenic: Not containing or using molecular oxygen. Used to describe photosynthetic processes.
Biotic: A process with biology, in this context biogeochemical.
Celera: A whole genome *de novo* using overlap layout consensus (OLC) following a Hamiltonian path. It attempts to combine overlapping sequences in the nodes into larger contigs.
Clinton Creek: A microbialite containing ecosystem in Yukon, Canada.
Complete genome: A collection of DNA genomic sequence data from a single organism that for bacteria contains one chromosome (usually circular) with possibly many plasmids (usually fewer then five contigs in total).
Contig: A set of overlapping DNA sequence fragments assembled to form a single sequence.
Draft genome: A collection of DNA genomic sequence data from a single organism that is presented as many contigs and scaffolds.
Illumina: DNA sequencing based on reversible chain terminators.
Kelly Lake: A microbialite-forming ecosystem in British Columbia, Canada near Pavilion Lake.
K-mer: A contiguous DNA sequence of *n* length. For example, a K-mer of 39 would contain a unique DNA sequence of 39 base pairs in length.
Leiolites: A type of microbialite that does not fit in any direct classification due to its arranged, not-laminated, and amorphous properties.
Macrofabric: The arrangement of the carbonate in a microbialite.
MetaCyc: A metabolic pathway database.
Metagenomics: Whole community shotgun sequencing as a field or approach.
Metagenome: Whole community shotgun sequencing of a single community.
Metavelvet: A whole genome *de novo* assembler that uses De bruijn graph based method designed specifically for metagenomic data.
Microbialite: Microbially derived organosedimentary carbonate structures.
Oncolite: A type of microbialite that is stromatolithic, meaning it has a laminated internal carbonate layer that is spherical in nature.
Oxic or Oxygenic: Containing or using molecular oxygen. Used to describe photosynthetic processes.
Progressive Mauve: A whole genome alignment program that is useful for genome ordering, editing and detecting rearrangements.
Pavilion Lake: A microbialite-forming ecosystem in British Columbia, Canada.
Ray: A whole genome *de novo* assembler that uses De bruijn graph based method. It has a built-in metagenomic data detector known as Ray Meta but does not require different working commands.
Recruitment analysis: The process of taking metagenomic reads and aligning them to a known genome (commonly a bacterial genome), in order to assess abundances of similar genotype in a community.
RefSeq: A taxonomic protein database.
Scaffold: A collection of non-contiguous contigs with gaps.
SOAP2: A whole genome *de novo* assembler that uses De bruijn graph based method.

Stromatolite: A layered microbially derived organosedimentary carbonate structure.
Thrombolite: A clotted microbially derived organosedimentary carbonate structure.
Velvet: A whole genome *de novo* assembler that uses De bruijn graph based method.
Welch's t-test: An alteration of student's t-test with assumptions that two samples are independent and that both are drawn from a normal population.

Acknowledgments

I thank my supervisor Curtis A Suttle for guidance, help and funding. I particularly appreciate that he let me follow my own ideas and interests and make important decisions on my own. I thank the members of my committee, J. Thomas Beatty, Steven J Hallam, and Sue Baldwin for guidance, advice, and occasional discussions.

I thank all my collaborators, and particularly Christopher J Grassa, Ian M Power, Greg Dipple, Greg Slater, Sarah Soles, Gordon Southam, Jennifer Abel, and Greg Gavelis for their excellent and significant contributions to the publications included in this thesis. Also to thank Allyson Brady, Darlene Lim, Kyung-Mee (Jenny) Moon, and Leonard Foster for significant contributions on my projects not included within the thesis and occasional discussions about the thesis work. I thank all lab mates and friends for helping in sampling and various things needed to survive a PhD.

Dedication

This thesis is dedicated to my loving wife Rachelle Rene' White and our beautiful daughter Elizabeth Baylee White. We did it girls! I couldn't have done it without either of you. I know that the man I am today is because of my love of you girls.

This is also for my Mother, Father, and Uncle Art who are not here to celebrate one of the greatest things a person can ever achieve in their life. This was a promise to my father that I would go "all the way," with my education and obtain a PhD. However, what I didn't expect is that my thirst for knowledge would be greater now, than when I started.

This is only the beginning.

I love you all wherever you are. Always remember that a part of you lives in me and Elizabeth now and forever.

Chapter 1: Introduction

1.1 What is a microbialite?

1.1.1 Physical classification and brief history

The term microbialite refers to a microbially-derived organosedimentary carbonate structure that is our earliest evidence of life (Grotzinger and Knoll, 1999; Schopf 2006; Dupraz *et al.,* 2009). Microbialites are classified into two supergroups according to their macrofabric carbonate layout, as well as gross morphology (Perry *et al.*, 2007; Riding *et al.,* 2011). The first supergroup contains internal laminated carbonate macrofabric stromatolites (thinly layered piles), oncolites (layered, but spherical), and leiolites (amorphous mesofabric) (Perry *et al.*, 2007; Riding *et al.,* 2011; Figure 1.1). The second supergroup contains unlaminated carbonate macrofabric thrombolites (irregular clots), and dendrolites (branched projections that are treelike) (Perry *et al.*, 2007; Riding *et al.,* 2011; Figure 1.1). The classification of microbialites is complicated by their plasticity in nature, with many gradations existing between these basic morphologies. Among living forms, stromatolites and thrombolites are the most common (Dupraz *et al.,* 2009; Figure 1.2).

Microbialites have been intensely studied for over one hundred years (Kalkowsky, 1908). The first mention of the term stromatolite, or "*Stromatolith*," was used to describe early Triassic stromatolites (Kalkowsky, 1908; Riding *et al.,* 2011; Figure 1.1). Pia (1933), was the first to classify oncolites as "unattached, regularly or irregularly spheroidal, concentrically to semiconcentrically laminated bodies" (Figure 1.1). Oncolites were reclassified as "a category of stromatolite structure," thus removing them as a separate category (Pia 1933; Logan *et al.*, 1964). Aitken (1967), was the first to use the term 'thrombolite,' from the Greek meaning "*thrombos* or bloodclot," from their irregular, clot-like arrangement (Figure 1.1). Burne and Moore (1987),

effectively provided the modern definition we use today, as structures "that are accreted as a result of a benthic microbial community trapping and binding detrital sediment and/or forming the locus of mineral precipitation." They broadened the definition from one that included biotic factors to that of a "benthic microbial community", took into account abiotic factors such as "detrital sediment" and added geologic context ("forming the locus of mineral precipitation").

1.2 Microbialites as the oldest persistent ecosystems

Microbialites represent the oldest known persistent ecosystems and potentially the earliest evidence of life (Schopf 2006; Grotzinger and Knoll, 1999). The geologic record indicates that microbialite diversification occurred concurrently with the emergence of life ~3.50 billion years ago (Gya), followed by a period of dominance extending until ~542 million years ago (Mya) following the Cambrian explosion (Allwood *et al.,* 2006; Dupraz and Visscher 2005; Schopf *et al.,* 2007; Rothschild and Mancinelli, 1990; Figure 1.3). With the age of the Earth estimated to be 4.54 billion years (Gyr), the appearance of microbialites in the fossil record at ~3.85 to 3.5 Gyr suggests that microbialites have persisted for ~85% of geological history (Patterson 1956; Dupraz and Visscher 2005; Figure 1.3). Modern microbialites first appear when cyanobacteria emerge (~3.0 Gyr), persisting for roughly 66% of earth's geologic history (Dupraz and Visscher 2005; Figure 1.3). Thus, modern microbialites are the best available representation of Earth's earliest life forms, and their biology may grant insight into the oldest aspects of the biosphere (Grotzinger and Knoll, 1999; Dupraz and Visscher 2005).

1.3 Global distribution of microbialites

Microbialites have adapted to radiate into many environmental conditions, including extremes of temperature, pH and salinity (Dupraz and Visscher 2005). Microbialites are globally distributed, and can be found in oceans (Reid *et al*., 2000; Khodadad and Foster, 2012; Mobberley

et al. 2013), freshwaters (Ferris *et al.,* 1997; Laval *et al*., 2000; Gischler *et al.,* 2008; Breitbart *et al.,* 2009), hypersaline lagoons (Goh *et al.,* 2009; Allen *et al*., 2009), tropical lagoons (Sprachta *et al.,* 2001), hot springs (Bosak *et al.,* 2012), and remnant mining sites (Power *et al.,* 2011a). To a lesser extent, they have also colonized terrestrial environments, such as soils (Maliva *et al.,* 2000) and caves (Lundberg and Mcfarlane, 2011).

Modern microbialite-forming ecosystems have been found globally suggesting that they are not as rare as previously thought. North America and Antarctica harbor many examples of freshwater microbialites, with Cuatro Cienegás and Yellowstone microbialites being the most studied (Breitbart *et al.,* 2009; Bosak *et al.,* 2012). In North America, microbialites are found in the Yukon (Power *et al.,* 2011a), Southwestern British Columbia (Laval *et al.,* 2000; Ferris *et al.,* 1997), Yellowstone National Park in Wyoming (Bosak *et al.,* 2012), Pyramid Lake Nevada (Arp *et al.,* 1999), and in Mexico at Cuatro Cienegás (Breitbart *et al.,* 2009), Lake Pátzcuaro (Bridgwater *et al.,* 1999; Bischoff *et al.,* 2004) and Lake Alchichica (Couradeau *et al.,* 2011). Antarctica is a haven for microbailites, with many found in pristine condition with little human influence. Antarctica has four ecosystems containing conical stromatolites or thrombolites: Lake Untersee (Andersen *et al.,* 2011), Lake Joyce (Hawes *et al.,* 2011), Lake Hoare (Squyres *et al.,* 1991) and Lake Vanda (Andersen *et al.,* 2011).

The microbialites of Central and South America are found in some of the most extreme environments, including lakes containing toxic levels of heavy metals. Microbialites are found in Central and Mesoamerica, including Laguna Bacalar, Mexico, which borders with Belize (Gischler *et al.,* 2008). In South America, microbialites are found in Brazil in the hypersaline lakes of Lagoa Vermelha and Lagoa Salgada (Vasconcelos *et al.,* 2006; Spadafora *et al.,* 2010), in northern Chile in La Brava (Farías *et al.,* 2014) and at the southern tip of Chile (Graham *et al.,* 2014). Laguna

Socompa on the border of Chile and Argentina is an example of an extreme ecosystem that contains microbialites, as it contains high levels of arsenic (18.5 mg L^{-1}) and iron (1 mg L^{-1}) (Farías *et al.,* 2013).

Diverse microbialites, including rare hydromagnesite forms and the largest microbialite ever recorded, are found in Europe. The Ruidera pools in Spain hold a great diversity of freshwater stromatolites (Santos *et al.,* 2010), and Lake Van, Turkey, contains the largest microbialites on record (Kempe *et al.,* 1991; López-García *et al.,* 2005). Salda Gölü Lake, in southern Turkey, also holds the only other example of hydromagnesite microbialites outside of Lake Alchichica, Mexico (Braithwaite and Zedefa, 1994; Couradeau *et al.,* 2011).

Microbialites in Oceania are rare; however, they include modern examples of coral replacement. Hypersaline lakes found in Lake Stonada, Indonesia (Arp *et al.,* 2004), Kiritimati Atoll in the central Pacific (Schneider *et al.,* 2013) and the caldera lakes of Niuafo'ou Island, Tonga (Kazmierczak and Kempe, 2006) contain microbialites. Microbialites in the tropical lagoons of French Polynesia and New Caledonia exist side by side with dead and live corals, illustrating direct competition (Sprachta *et al.,* 2001).

Western Australia has the oldest fossilized examples of microbialites at roughly 3.45 Gyr old (Van Kranendonk *et al.,* 2008), and Shark Bay has one of the few examples of marine stromatolites (Goh *et al.,* 2009; Allen *et al.,* 2009). Two lakes in Australia have documented microbialites, including Lake Thetis (Grey *et al.,* 1990) and Lake Clifton (Konishi *et al.,* 2001). Other lakes in Australia that contain thrombolithic microbialites include Lake Richmond, Lake Walyungup and Lake Coolongup, which are protected and endangered. However, no publications exist describing them.

While China and Russia, the largest combined land mass on the planet, have many examples of microbialite fossils, no studies describe modern versions; or, if studies are available, they have not been translated into English (Wu *et al.,* 2014). In terms of African microbialites, a recent study found some in southern Africa (Smith *et al.,* 2011), and fossils have been found throughout the continent. However, Africa remains largely unstudied when it comes to modern microbialites.

1.4 Proposed microbialite formation hypotheses

There is much debate on whether the formation of ancient microbialites dating back ~3.50 Gya in Western Australia was purely abiotic (Lowe, 1994; Grotzinger and Rothman, 1996) or a combined biotic-abiotic event (Dupraz and Visscher, 2005; Schopf, 2006; Mcloughlin *et al.*, 2008; Dupraz *et al.,* 2009).

1.4.1 Abiotic (spectator hypothesis)

The abiotic model stresses that ancient microbialites and possibly even modern versions are formed completely by abiotic processes (Lowe, 1994; Grotzinger and Rothman, 1996; Mcloughlin *et al.*, 2008). Lowe suggested that the Western Australian stromatolites within the Warrawonna group (3.5 to 3.2 Gyr) lack the structural evidence of biotic processes and therefore are of abiotic origin (1994). Moreover, a laboratory spray deposition experiment showed that stromatolites could be generated abiotically using enamel spray paint with metal-oxide pigment particles (Mcloughlin *et al.,* 2008). A purely abiotic model would suggest that the microbes and/or pathways would be the same between the microbialite and their surrounding environment, as the chemistry alone is driving the formation of the microbialite: microbes would merely be "spectators." Thus, the abiotic model would suggest that microbes have no role in the formation of microbialites.

Abiotic factors are certainly critical to microbialite formation. These include hard water (≥ 121 mg $CaCO_3\,L^{-1}$) with free divalent cations (mainly Ca^{2+} and/or Mg^{2+}), high alkalinity (≥ 121 mg $CaCO_3\,L^{-1}$), stable alkaline pH water (pH ≥ 8), clear water with visible light penetration, and dissolved inorganic carbon (DIC) (Dupraz *et al.*, 2009). No carbonate-derived microbialite-forming ecosystem has been found without at least hard water, high alkalinity and a stable alkaline pH (pH ≥ 8); carbonates cannot form without these factors.

1.4.2 **Abiotic combined biotic hypothesis**

The biotic link to the origin of microbialites has been debated for over one hundred years since it was first suggested by Kalkowsky (1908). Lowe (1995) rejected any biotic role in the formation of the Australian Warrawonna group stromatolites (3.5 to 3.2 Gya). Buick *et al*. (1995), responded that Lowe violated Descartes' fourth rule of science, "omettre rien," directly translating to "omit nothing," suggesting that Lowe (1995) omitted critical examples relating to a combined hypothesis. The examples not included by Lowe (1995) were the post-Isua $\delta^{13}C$ isotopic data, and various microfossil examples illustrating that biotic-abiotic processes are involved in the formation of microbialites (Buick *et al.,* 1995). Since that time, sulfur isotopic measurements in the Australian stromatolites from ~3.45 Gya suggest negative $\delta^{34}S$ isotopic fractionation which can only be explained by biotic processes (Bontognali *et al.*, 2012, Figure 1.3). Ancient microbialites spanning ~3.5 to 3.0 Gya formed under anoxygenic processes, as sufficient oxygen was not present to drive oxygenic photosynthesis, whether cyanobacteria were present or not (Crowe *et al.*, 2013; Planavsky *et al.*, 2014; Figure 1.3).

Biotic metabolism in modern microbialites is an active and highly complex interaction with abiotic factors. Both oxygenic and anoxygenic metabolism within the surface microbial mat on microbialites is highly productive (5000 to 6200 mg biomass $cm^{-2}\,day^{-1}$), and similar to the primary

productivity of tropical forests (6000 mg biomass cm^{-2} day^{-1}) (Stal, 2000; Centreno *et al.*, 2012). Carbonates and free calcium are initially trapped by adhesive biofilms and mats that are often cyanobacterial in origin (Dupraz and Visscher 2005; Dupraz *et al.*, 2009). The cyanobacterial mat is then degraded by heterotrophic bacteria that liberate HCO_3^- and Ca^{2+}, thereby increasing the saturation index and producing nucleation points for carbonate precipitation (Dupraz and Visscher 2005; Dupraz *et al.*, 2009). Cyanobacterial mats contain exopolysaccarides (EPS) that serve as a location of mineral nucleation, while providing a heterotrophic microenvironment favorable for organomineralization via dissimilatory sulfate reduction (Dupraz and Visscher 2005; Dupraz *et al.*, 2009). Light is another critical factor in the biotic-abiotic relationship of microbialite formation. Many microbialite-forming ecosystems are either in shallow locations or have clear light visibility with high light penetration allowing for photoautotrophic microbial mat growth.

The concept that microbes have no role in microbialite formation does not account for evidence that specific mineral precipitation is a function of microbial presence. For the abiotic hypothesis, the question is, why would only certain minerals form, and rates of precipitation differ, with the presence of microbes under similar abiotic conditions? The Atlin wet-land in British Columbia, Canada, contains carbonate precipitating microbial mats. A microcosm experiment showed that abiotic-biotic microcosms promoted carbonate formation at a faster rate and resulted in a completely different mineral (dypingite) than the abiotic microcosm (nesquehonite) (Power *et al.*, 2007). This suggests that both biotic and abiotic forces are required to form particular minerals associated with lithifying microbial mats, including microbialites (Power *et al.*, 2007). Microbialite formation is likely a consequence of complex interactions between both biotic and abiotic factors (Dupraz *et al.*, 2009). However, much is still unknown regarding the effect of microbial community interactions on the formation of microbialites.

1.5 Major microbial taxa and their metabolic pathways that contribute to microbialite formation

Microbialite-forming ecosystems, which include microbial mats, contain highly diverse microbial consortia, including both cellular (bacterial, archaea and eukaryotes) and viral (capsid based) organisms.

1.5.1 *Alphaproteobacteria*

Alphaproteobacteria are abundant in marine, freshwater and artificial marine-derived microbialite-forming systems (Havemann and Foster, 2008; Breitbart *et al.,* 2009; Goh *et al.,* 2009; Khodadad and Foster, 2012) and cyanobacterial non-lithifying mats (Varin *et al.,* 2012). Pozas Azules II within Cuarto Cienegás and the high altitude, hypersaline arsenic-rich stromatolites of Lake Scompa within the Argentinean Andes have a high percentage of *Alphaproteobacteria* sequences (~12-15%), mainly belonging to the *Rhodobacterales* (Breitbart *et al.,* 2009; Farías *et al.,* 2012). The rare hydromagnesite microbialites of Lake Alchichica and the oncolites of Rios Mesquites had cyanobacterial sequences that outnumber the *Alphaproteobacteria* sequences (Breitbart *et al.,* 2009; Couradeau *et al.,* 2011). However, prior amplification of the DNA was used before sequencing in both Lake Alchichica (PCR) and the Rios Mesquites (phi29-MDA), which may have biased the results.

Alphaproteobacteria contain members (e.g. *Rhodobacterales*) that are photoheterotrophic, which could influence the formation of microbialites by anoxygenic photosynthesis and microbialite dissolution through fermentation (Dupraz and Visscher, 2005; Figure 1.4). Anoxygenic photosynthesis would been the only type of photosynthesis within the Precambrian stromatolites prior to the origin of cyanobacteria, and alphaproteobacterial anoxygenic phototrophs could have filled that metabolic niche (Bosak *et al.,* 2007). *Alphaproteobacteria*

appear to be important for microbialite nitrogen fixation, even in the presence of cyanobacterial nitrogen fixation, likely because of diel cycles (Havemann and Foster 2008; Figure 1.4).

1.5.2 *Cyanobacteria*

1.5.2.1 Planktonic cyanobacteria

Cyanobacteria in microbialites exist as planktonic cells and mat builders. The planktonic unicellular cyanobacteria are found in the surrounding water. Cyanobacterial calcification is well documented (Dittricha *et al.,* 2003; Obst *et al.,* 2009). *Synechococcus* sp., a model planktonic cyanobacterium, has been shown in multiple studies to precipitate carbonates using oxygenic photosynthesis (Thompson *et al.,* 1990; Dittricha *et al.,* 2003; Obst *et al.,* 2009; Figure 1.4). *Synechococcus* sp. is known to cause "whiting events," in which calcium carbonate rains down through the water column (Thompson *et al.,* 1997). These "whiting events" are a photosynthetically driven alkalization process that precipitates calcium carbonate principally around the *Synechococcus* cells, which serve as nucleation points of precipitation (Dittricha *et al.,* 2003; Obst *et al.,* 2009). These planktonic cyanobacteria provide the "bricks", in the form of either magnesium or calcium based carbonates, which are the building blocks of microbialites

1.5.2.2 Filamentous cyanobacteria, mat-builders

If the planktonic cyanobacteria provide the "bricks" to make microbialites, then mat-building filamentous cyanobacteria provide the "mortar" that stabilizes the structure. Filamentous cyanobacteria are fundamental in modern microbialites, as they provide nutrients, structure, and directly act in the formation processes. Filamentous cyanobacteria, like their planktonic counterparts, influence carbonate precipitation through photosynthesis-induced alkalinization (Dupraz and Visscher, 2005; Figure 1.4). Mat-building cyanobacteria produce extracellular polymeric substances (EPS) which trap Ca^{2+} ions near dissolved CO_3^{2-}, and provide nucleation

points for precipitation (Dupraz and Visscher, 2005; Dupraz *et al.*, 2009). Commonly found genera of filamentous mat building *Cyanobacteria* in microbialite-forming sites include *Nostoc, Pseudanabaena, Schizothrix, Dichothrix*, and *Lyngbya*, (Laval *et al.*, 2000; Dupraz *et al.*, 2009).

Mat-building filamentous cyanobacteria also provide an essential energy source for heterotrophic bacteria in an oligotrophic water column (Lim *et al.*, 2009). These heterotrophic bacteria in turn mediate further lithification and build-up of the microbialite structure (Omelon *et al.*, 2013). Heterotrophs, release calcium and/or magnesium ions that are bound to cyanobacterial EPS mat by degradation (Dupraz and Visscher, 2005). This allows for more free interaction between cations and CO_3^{2-} anions and leads to carbonate precipitation (Dupraz and Visscher, 2005). Phosphorus, nitrogen and various vitamins and co-factors are critical nutrients required for primary production by filamentous cyanobacteria; these nutrients can be sequestered in the mats and then released by heterotrophic degradation, which feeds further primary production. These cycles of autotrophic and heterotrophic mat breakdown are balanced; otherwise, the structures would likely dissolve and the mats would die. Through primary production, the microbialite cyanobacterial mat is an oasis in a desert-like oligotrophic water column.

1.5.3 Sulfur-oxidizing bacteria (SOBs)

Sulfur-oxidizing bacteria (SOBs) are a double-edged sword for microbialite formation, as they directly cause dissolution of microbialites, but byproducts of this dissolution provide intermediate substrates that allow for colonization by sulfate-reducing bacteria (SRBs; Figure 1.4). Microbialites are often found in highly oxygenic water (Dupraz *et al.*, 2009), and SOBs remove high amounts of oxygen, allowing for further lithification via sulfate reduction by anaerobic sulfate-reducing bacteria (Dupraz and Visscher, 2005). SOBs are chemolithotrophs that promote

dissolution of microbialites through the oxidation of hydrogen sulfide, which in turn releases calcium ions from the microbialite calcium carbonate matrix (Figure 1.4).

The sulfur oxidation pathway encodes the *Sox* gene cluster that is responsible for aerobic sulfur oxidization (Friedrich *et al.,* 2005). *Sox* genes are conserved across *Proteobacteria,* including *Gamma-, Beta-* and *Alpha-proteobacteria* (Friedrich *et al.,* 2005). *Beggiatoa* sp., a ubiquitous filamentous sulfide-oxidizing *Gammaproteobacterium,* would be an excellent candidate for the study of the removal of oxygen from the highly oxygenated surface mat of microbialites (Dupraz and Visscher, 2005). The Sox pathway comprises four protein complexes *SoxYZ, SoxAX, SoxB* and *SoxCD,* which oxidize reduced sulfur species, including sulfide (HS^-), elemental sulfur (S), and sulfite (HSO_3^-) (Friedrich *et al.,* 2005). The diversity and abundance of SOBs, and whether *Sox*-related pathways are found in active microbialite-forming ecosystems, are still unclear. It is also unclear whether sulfur oxidation pathways are a signature of healthy (actively forming) or failing (actively dissolving) microbialites.

1.5.4 **Sulfate-reducing bacteria (SRBs)**

Sulfate-reducing bacteria (SRBs) are a crucial part of the heterotrophic microbial consortia responsible for lithification in microbialites (Visscher *et al.,* 2000; Dupraz and Visscher, 2005; Gallagher *et al.,* 2012; Figure 1.4). Sulfate reduction is an ancient metabolism, predating oxygenic photosynthesis (Canfield *et al.,* 2000). Sulfate reduction was occurring in microbialites prior to the great oxidation event and the appearance of cyanobacterial mats (Canfield *et al.,* 2000; Wacey *et al.,* 2011; Bontognali *et al*., 2012; Figure 1.3).

SRBs reduce sulfate under anaerobic conditions, but also exist in active layers of highly oxygenated mats, which presents a metabolic paradox (Dupraz and Visscher, 2005; Dupraz *et al.,* 2009). SRBs in microbialites must be either oxygen tolerant, find anoxic microenvironments, or

form tight consortia with oxygen-depleting anoxic organisms, such as SOBs (Dupraz and Visscher, 2005). Recent rate measurements suggest that SRBs within microbialites must be oxygen tolerant, as measurable amounts of dissimilatory sulfate reduction occurs in the highly oxygenated surface layers of the cyanobacterial mat (Baumgartner *et al.*, 2006; Gallagher *et al.*, 2012).

SRBs may mediate carbonate precipitation in microbialites by altering the saturation index and increasing alkalinity though dissimilatory sulfate reduction (Baumgartner *et al.*, 2006; Gallagher *et al.*, 2012; Figure 1.4). Active microbialite growth is thus suggested to be related to the heterotrophic breakdown of cyanobacterial-derived mats, which provide a rich and complex carbon source (Dupraz and Visscher, 2005). SRBs need electron donors for functional dissimilatory sulfate reduction: these include organic carbon, as acetate, lactate, ethanol, or formate, or molecular hydrogen (Baumgartner *et al.*, 2006; Gallagher *et al.*, 2012). The concept of lithifying mats and non-lithifying mats could be explained by the rates of dissimilatory sulfate reduction and related to the abundance of metabolically active SRBs (Dupraz and Visscher, 2005; Gallagher *et al.*, 2012). However, this process and the underlaying mechanism are not well understood.

SRBs that use the highly conserved dissimilatory sulfate reduction (or *dsr*) pathway are mainly found among *Proteobacteria*, but are found also in non-proteobacterial lineages. Specifically, the majority of SRB-related taxa are within the class *Deltaproteobacteria*, and fall within the orders *Desulfovibrionales*, *Desulfobacterales*, and *Syntrophobacterales.* Non-proteobacterial lineages that have SRBs include the taxa *Nitrospira, Thermodesulfobacteria, Thermodesulfobiaceae,* and *Firmicutes* (mainly *Clostridia*). The *dsr* pathway consists of sulfate adenyltransferase (*Sat*), adenylylsulfate reductase with the A and B subunit (*apsAB*), and dissimilatory sulfite reductase with alpha and beta subunits (*dsrAB*) (Zhou *et al.*, 2011). The

pathway transports sulfate (reactant) with an electron donor (organic carbon, acetate, lactate, formate, hydrogen and/or ethanol), and through various enzymatic steps yields sulfide (Zhou *et al.,* 2011). The diversity and ocurrence of the *dsr* pathway in microbialites is not known, but it is critical to our understanding of microbialite formation (Baumgartner *et al.,* 2006; Gallagher *et al.,* 2012).

1.5.5 *Firmicutes*

Firmicutes are Gram-positive bacteria that are abundant in a multitude of environments, including microbialites (Breitbart *et al.,* 2009). *Bacillus* spp.were shown over forty years ago to produce carbonates as a "general phenomenon" (Boquet *et al.,* 1973). *Firmicutes* are known to precipitate calcium carbonate with or without the presence of cyanobacteria, with at least one operon (*lcfA*) geared towards carbonate precipitation (Barabesi *et al.,* 2007).

Firmicutes have many mechanisms for facilitating carbonate precipitation. Seven different *Bacillus* species are known to precipitate carbonates, including *B. subtilis* (Barabesi *et al.,* 2007), *B. sphaericus* and *B. lentus* (Dick *et al.,* 2006), *B. megaterium*, *B. cereus*, and *B. thuringiensis* (Dhami *et al.,* 2013), and *B. amyloliquefaciens* (Lee, 2003). *Bacillus* spp., are able to induce carbonate formation through the metabolism of urea (Hammes *et al.,* 2003), heterotrophic ammonification of amino acids (Castanier *et al.,* 1999), carbonic anhydrase (Dhami *et al.,* 2014), EPS formation (Ercole *et al.,* 2007) and the *lcfA* operon (Barabesi *et al.,* 2007). Even at low abundance, members of the *Firmicutes* have metabolic versatility geared towards carbonate precipitation, which may have a role in the formation of microbialites (Paerl *et al.,* 2001; Breitbart *et al.,* 2009; Omelon *et al.,* 2013).

Microbial mats including microbialites have colored pigmented layers (orange to yellow) (Bottos *et al.,* 2008). Little is known about non-photosynthetic pigmented heterotrophic bacteria

in microbialites, although many studies have focused on the oxygenic phototrophs in these layers, and suggested the coloration is related to carotenoid pathways (Nübel *et al.,* 1999; Lionard *et al.,* 2012). Diversity studies (based on 16S rDNA) have found firmicutes in these layers (Bottos *et al.,* 2008; Lionard *et al.,* 2012), and firmicutes synthesize carotenoids that give rise to many different colors of bacteria, including orange (Köcher *et al.,* 2009; Klassen, 2010). To the best of our knowledge, no study has screened for cultivatable isolates of non-photosynthetic, pigmented, heterotrophic members of the *Firmicutes* that could be responsible for the colored layers in microbial mats and microbialites.

1.5.6 *Actinobacteria*

Representatives of the phylum *Actinobacteria* appear to be rare within microbialite-forming ecosystems, and little is known about their abundance, diversity and role. Actinobacteria have been found in smooth and pustular pre-stromatolithic mats in Shark Bay and the dry freshwater stromatolites of Ruidera Pools, Spain (Allen *et al.,* 2009; Santos *et al.,* 2010). Their presence in microbialites does not entail a functional role, but the knowledge gap points to a need for both culture-dependent and independent studies.

Actinobacteria have also been identified in the pigmented layers in microbial mats (Bottos *et al.,* 2008; Lionard *et al.,* 2012), and it has been suggested they may be responsible for the coloration (Klassen, 2010). Although carotenoid biosynthesis also occurs in actinobacteria, to best of our knowledge no study has examined isolates of non-photosynthetic pigmented heterotrophic members of the *Actinobacteria* to determine if they may contribute to the colored layers found in microbial mats and microbialites.

1.5.7 **Eukaryotes**

Eukaryotes in microbialites are present in low abundance (<1%), by physical counts (Power *et al.,* 2011a) and by sequence abundance (Couradeau *et al.,* 2011; Khodadad and Foster, 2012). Even at low abundance, metazoans have been associated with the global decline of microbialites (Awramik, 1971; Garrett 1970, Figure 1.3). Metazoan grazing following the Cambrian explosion has been correlated to a drop in stromatolite diversity about ~500 to 800 Mya (Awramik, 1971; Garrett 1970, Figure 1.3). However, the metazoan grazing hypothesis is hindered by a lack of fossil evidence; as well, protist grazers presumably predated the Cambrian microbialites far earlier (Bernhard *et al.,* 2013). Another major problem is that unicellular or soft body grazers would leave no obvious fossils, possibly contributing to a virtually nonexistent fossil record (Bernhard *et al.,* 2013).

The question remains, why do modern microbialites exist if grazing is the cause of their decline? This is puzzling, as metazoan grazing occurs even under the oligotrophic conditions in which many microbialites are found (Elser *et al.,* 2005). Possibly, metazoan grazing is controlled by abiotic factors such as low nutrients, high temperature, high salinity, and high pH. Cyanobacteria make cytotoxic compounds that can inhibit and kill metazoans, thus cyanobacterial mats in microbialites could also biotically control metazoan grazing (Neilan *et al.,* 2013; Wu *et al.,* 2014). The type of microbial mat that exists on the surface of a marine microbialite is suggested to alter both the microbialite fabric (whether stromatolithic or thrombolithic) and to control the metazoan community structure (Tarhan *et al.,* 2013). Thus the microbial community also likely plays a role in controlling metazoan grazing (Tarhan *et al.,* 2013).

In contrast, photoautotrophic eukaryotes (e.g. algae and other protists) could aid in the organosedimentary formation process via photosynthesis-induced carbonate precipitation (Figure

1.4). Even at low sequence abundances of eukaryotes (<1%) in marine microbialite ecosystems (Highbourne Cay, Bahamas), it is suggested that foraminifera influence the microfabric by stabilizing carbonate grains, and their reticulopods, once encased, act as sheaths that effect the lamination of microbialites (Bernhard *et al.,* 2013; Edgcomb *et al.,* 2013). Thus, foraminifera may help to explain the changes in the microbialite microfabric observed in the late Precambrian (Bernhard *et al.,* 2013). In modern microbialites, foraminifera are suggested to move carbonate grains during diel vertical migration, disrupting lamination critical for stromatolite formation and promote clot formation or thrombolithic structure (Bernhard *et al.,* 2013). Foraminifera were found in microbialites in the Highbourne Cay, Bahamas, including thrombolites and stromatolites; however, the highest diversity was observed in thrombolite mats or mats that were biologically turbated (Bernhard *et al.,* 2013; Edgcomb *et al.,* 2013). Metazoans, *Stramenopiles, Alveolata, Amoeboza* and *Rhizaria* were found to be active metabolically in various microbialites across Highbourne Cay and Shark Bay (Edgcomb *et al.,* 2013).

1.5.8 **Viruses**

The role of viruses in microbialite communities has remained elusive. Viruses are the most prevalent "organisms" on Earth, with an estimated 10^{30} viruses in the ocean, and around 10^{6} - 10^{7} viruses ml^{-1} in most freshwater systems (Suttle, 2005). Viruses are agents of cell lysis and thus play a role in carbon cycling on a global scale (Suttle, 2005). Additionally, new research has found that many viruses harbor auxiliary metabolic genes, including genes that encode the core proteins involved in photosynthesis (*psbA*, *psbD*) and phosphate starvation (*phoH*) (Clokie *et al.,* 2010; Thompson *et al.,* 2011). Viral auxiliary metabolic genes have also been shown to redirect their host's metabolic potential to fuel viral replication (Clokie *et al.,* 2010; Thompson *et al.,* 2011). Some marine cyanophages encode a Calvin cycle inhibitor (*cp12*) that inhibits the carbon-fixation

actions of Rubisco (Ribulose-1,5-bisphosphate carboxylase/oxygenase), and a virally-encoded transaldolase (*talC*) redirects the host metabolism to the pentose phosphate pathway, benefiting viral replication (Clokie *et al.,* 2010; Thompson *et al.,* 2011). This evidence suggests that viruses affect the carbon metabolism of an ecosystem, and may influence the chemistry of microbialite formation or dissolution.

1.6 Previously studied microbialite-forming ecosystems

Shark Bay in Western Australia, Highbourne Cay in Bahamas, and the Cuatro Cienegás basin of Mexico, including Pozas Azules II and Rios Mesquites, are the most studied microbialite-forming assemblages. Metagenomic surveys of the microbial fraction and the viral fraction has been completed for Highbourne Cay, and Cuatro Cienegás microbialites. These sites will provide a valuable reference for comparison with the microbialites from Pavilion Lake and Clinton Creek.

1.6.1 Shark Bay microbialites

The oldest fossil microbialites are found in Western Australia, dating back ~3.5 Gya (Van Kranendonk *et al.,* 2008). Near these fossil microbialites are active, modern versions within Shark Bay at Hamelin Pool in Western Australia. These are the main example of hypersaline marine microbialites (Goh *et al.*, 2009; Allen *et al*., 2009). Shark Bay microbialites range in morphology from columnar, club, spheroidal, domal, nodular, to irregular-shaped morphotypes (Burns *et al.*, 2004).

Shark Bay microbialite diversity has been assessed by three 16S rDNA amplicon studies (Burns *et al.*, 2004; Goh *et al.*, 2009; Allen *et al*., 2009). Currently, only 412 rDNA sequences are available on Genbank from all bacterial surveys of the Shark Bay microbialites. These sequences reveal the distribution of the various bacterial taxa, indicating that *Alphaproteobacteria* (20%), *Actinobacteria* (16%), and *Cyanobacteria* (15%) dominate, with the rest of the sequences

belonging to *Planctomycetes* (11%), *Gammaproteobacteria* (10%), and the *Firmicutes* (9%) (Burns *et al.* 2004; Papineau *et al.*, 2005; Allen *et al.*, 2009; Goh *et al.* 2009). Papineau *et al.* (2005), concluded that Shark Bay microbialites are highly diverse, with 90% of sequences belonging to bacteria and that Shark Bay microbialites have novel *Proteobacteria* representing 28% of the sequences, followed by *Planctomycetes* (17%), and *Actinobacteria* (14%), respectively

Shark Bay is novel compared to other microbialite-forming ecosystems as it has a relatively high abundance of archaea (~10% of 16S rDNA sequence). which are usually <1% of the microbial community in other microbialites (Burns *et al.* 2004; Papineau *et al.*, 2005; Allen et al., 2009; Goh *et al.* 2009). The archaea in Shark Bay microbialites are principally halophiles (Papineau *et al.*, 2005; Allen *et al.*, 2009; Goh *et al.* 2009). Many unclassified haloarchaea have been detected only in Shark Bay microbialites and not in the surrounding seawater, indicating that Shark Bay microbialites are a potential reservoir for these archaea (Papineau *et al.*, 2005; Allen *et al.*, 2009; Goh *et al.* 2009). Currently, no metagenomic data are available for Shark Bay microbialites, and only 16S rDNA based studies on prokaryotic diversity (Burns *et al.* 2004; Papineau *et al.*, 2005; Goh *et al.* 2009), and a RNA-based study on active eukaryotes (Edgcomb *et al.*, 2013), are available for comparison.

1.6.2 **Highbourne Cay microbialites**

Like Shark Bay, Highbourne Cay microbialites are found in shallow depths. They have a high diversity of colored mats covering the microbialites, ranging from pink, green, brown and black (Reid *et al.*, 2000; Myshrall *et al.*, 2010; Mobberley *et al.*, 2012). Highbourne Cay microbialite mats have been classified into three types (I - III) based on morphology (Reid *et al.*, 2000). Type I mats are considered young and are dominated by filamentous cyanobacteria with few heterotrophic bacteria. They have low diversity (~128 OTUs) and low sulfate reduction,

photosynthesis, and aerobic respiration rates, and have been described as non-lithifying mats (Reid e*t al.,* 2000; Myshrall *et al.,* 2010; Khodadad and Foster, 2012; Mobberley *et al.,* 2012). Type II and III mats are considered older lithifying mats with the beginning of carbonate lamination; both have higher rates of sulfate reduction, photosynthesis, aerobic respiration rates than type I mats (Reid *et al.,* 2000; Myshrall *et al.,* 2010; Khodadad and Foster, 2012; Mobberley *et al.,* 2012). Type II and III mats have higher bacterial diversity (~181 OTUs) than type I mats (Reid *et al.,* 2000; Myshrall *et al.,* 2010; Khodadad and Foster, 2012; Mobberley *et al.,* 2012).

Previous bacterial diversity studies based on 16S rDNA amplicons of Highbourne Cay microbialites reveal that bacteria assigned to the *Proteobacteria* dominate all three mat types (52.0%), followed by *Planctomycetes* (12.1%), *Cyanobacteria* (11.6%) and *Bacteroides* (10.4%) (Myshrall *et al.,* 2010; Mobberley *et al.,* 2012). Within the *Proteobacteria*, *Alphaproteobacteria* are dominant, making up 42% of the proteobacterial sequences, followed by 4.9% for both the *Delta-* and *Gamma-proteobacterial* lineages (Myshrall *et al.,* 2010; Mobberley *et al.,* 2012). The surrounding water communities differ from those in the stromatolitic mats I-III, with more taxa assigned to the *Alphaproteobacteria* and *Gammaproteobacteria* in the water, and no *Deltaproteobacteria* detected (Myshrall *et al.,* 2010; Mobberley *et al.,* 2012). Like Shark Bay, *Proteobacteria* are the dominant group in Highbourne Cay, with *Alphaproteobacteria* being the most abundant OTU in the pink thrombolithic mats (Myshrall *et al.,* 2010; Mobberley *et al.,* 2012).

Metagenomes for both the microbial fraction and the viral fraction have been published for Highbourne Cay (Desnues *et al.,* 2008). However, because the surrounding environment was not sampled, including the water, it is hard to know which taxa are specific to the microbialite. Also, multiple displacement amplification (MDA) was used to obtain DNA for sequencing, which is

known to affect quantitative results due to amplification bias (Abulencia *et al.,* 2006; Yilmaz *et al.,* 2010; Abbai *et al.,* 2012).

The Highbourne Cay viral metagenome was dominated by ssDNA microphages, likely due to MDA bias towards circular templates, which enriches for these viral genotypes and skews quantitative results (Kim and Bae, 2011). Moreover, these phage are present in the surrounding seawater (Desnues *et al.,* 2008). Nonetheless, some ssDNA viral genotypes in Highbourne Cay were found to be highly specific, suggesting that microbialites act as islands of viral diversity (Desnues *et al.,* 2008). Highbourne viral metagenomes had contigs that were similar to those in the Sargasso Sea or Cuatro Cienegás. No *Caudovirales* phage sequences were detected, which is unusual, and may be the results of bias from MDA (Desnues *et al.,* 2008).

1.6.3 Cuatro Cienegás microbialites: Pozas Azules II and Rios Mesquites

Cuatro Cienegás, or the "four marshes," is found in the northern Mexican state of Coahuila. Cuatro Cienegás is home to Pozas Azules II or the "blue pools," which have thrombolites, and Rios Mesquites ("mesquite tree rivers"), which have oncolites (Breitbart *et al.,* 2009). Cuatro Cienegás has metagenomic data sets for both the viral and microbial fractions, but not samples from the sediment or water (Desnues *et al.,* 2008; Breitbart *et al.,* 2009).

Comparing the viral metagenomic data in Highbourne Cay and Cuarto Cienegás suggests that microbialites act as islands of novel viral genotypes and reflect an ancient marine origin that has persisted in a freshwater ecosystem (Desnues *et al.,* 2008). However, high abundances of ssDNA viruses within both systems are an artifact of the bias of MDA towards circular templates, which enriches for ssDNA sequences and skews quantitative results (Abulenica *et al.,* 2006; Yilmaz *et al.,* 2010; Kim and Bae, 2011; Abbai *et al.,* 2012). Pozas Azules II is similar to

Highbourne Cay, but has more dsDNA phage sequences, including sequences that are similar to common marine phages, which could be due to cross-contamination from marine samples.

1.7 Microbialite-forming ecosystems described in this thesis

Pavilion Lake and Clinton Creek are freshwater microbialite sites that have not been analyzed for metabolic potential or microbial community structure. Both sites are northern latitude freshwater microbialite-forming ecosystems that are very different from previously studied tropical marine microbialite systems. Described below is what is known about microbialites from these sites, including their morphology, geological classification, abiotic chemistry, and morphologically classified organisms.

1.7.1 Pavilion Lake

Pavilion Lake (50.8 °N, 121.7 °W) lies in Mable Canyon between Squamish and Lillooet, BC, and contains active thrombolithic microbialites (Laval *et al.*, 2000). Pavilion Lake thrombolithic microbialites range from ~2,000 to 12,000 years in age, with the corrected age maximum at ~4,600 years and the uncorrected age maximum at ~12,300, based on Uranium-Thorium dating (Laval *et al.*, 2000). These age estimates put the initial formation of thrombolites in Pavilion Lake after the end of the last ice age (Laval *et al.*, 2000).

Pavilion Lake is a dimictic, alkaline (pH 8.4), oligotrophic (mean total phosphorus - 3.3 µg L^{-1}), freshwater lake with hard water (mean calcium carbonate - 182 mg L^{-1}) (Laval *et al.*, 2000; Lim *et al.*, 2009; Brady *et al.*, 2013; Omelon *et al.*, 2013). Pavilion Lake microbialites consist primarily of calcite thrombolites, which change in morphotype as a function of depth, as follows: shallow domes resembling "open lettuce-beds" at ~10 m, intermediate domes resembling "cabbage heads" at ~20 m, intermediate-deep domes with hollow conical "asparagus-like" outcroppings at

25 m, and deep domes that possess "artichoke leaflets" at ≥25 m (Laval *et al.*, 2000; Brady *et al.*, 2013; Omelon *et al.*, 2013; Figure 1.5).

Morphological characteristics of the cyanobacterial community in Pavilion Lake microbialites have been described (Laval *et al.*, 2000). The microbialites have thin (>5 mm) cyanobacterial-derived mats, comprised of coccoids (*Gloeocapsa* spp.), rods (*Synechococcus* spp.), and filamentous cyanobacteria (*Fischerella* spp. and *Pseudoanabaena* spp.) (Laval *et al.*, 2000). The water column of Pavilion Lake is dominated by *Synechococcus* spp. (8.3×10^4 cells ml^{-1}), the picoplankton known for causing carbonate precipitation "whiting events," (Thompson *et al.*, 1997).

Pavilion Lake microbialites have round filamentous balls of cyanobacteria that are >2 mm at 15 to 20 m, which decrease in size with depth (Figure 1.6, Brady *et al.*, 2010). These filamentous balls of cyanobacteria are called "nodules," which range in pigmentation from purple to green to black. The purple cyanobacterial nodules were morphologically classified as either *Oscillatoria* sp. or *Calothrix* sp. (Laval *et al.*, 2000). Recent clone library analysis suggests that the green nodules are *Leptolyngbya* sp. and the purple nodules are *Tolypothrix* sp. (Russell *et al.*, 2014). *Tolypothrix* spp. and *Calothrix* spp. are morphologically similar and their phylogenetic relationships are not well understood (Berrendero *et al.*, 2011). Green and purple nodules create a microenvironment that has a higher pH and higher dissolved oxygen, and has active lithification of calcite within the filaments (Brady *et al.*, 2010). The nodules are only found at 15 to 25 m depths, which makes it unlikely that they are major players in the formation of the overall microbialite structure, otherwise they would be found at all depths.

The diversity and abundance of microbial taxa and the metabolic potential of Pavilion Lake microbial communities are unknown. Only a single metagenomic study is available for freshwater

microbialites, which did not account for the surrounding environment (e.g. sediments and water column) (Breitbart *et al.,* 2009). Is the microbialite microbial community and metabolic potential the same or different from that in the surrounding environment? This knowledge will either support previous studies that microbial community and metabolic potential are microbialite-specific or will provide evidence of microbes from the surrounding environment (Breitbart *et al.,* 2009; Khodadad and Foster, 2012; Mobberley *et al.* 2013).

1.7.2 **Clinton Creek**

Clinton Creek has a subarctic climate and is located near the Arctic Circle, ~77 km northwest of Dawson City, Yukon, Canada (64°26'42"N and 140°43'25"W). It is a flooded open pit from an abandoned asbestos mine, which was active from 1969 to 1978 (Power *et al.*, 2011a). Clinton Creek has served as a model research site for carbon sequestration studies within industrial mining sites (Power *et al.*, 2011a). Sediment mineralogy is highly variable, containing quartz, muscovite, kaolinite, and chrysotile, as well as minor aragonite and trace calcite (Power *et al.*, 2011a). Aragonite will preferentially lithify abiotically over calcite due the inhibiting effect of the high magnesium to calcium ratio (Power *et al.*, 2011a). Clinton Creek microbialites have a columnar thombolithic morphology that is primarily composed of aragonite with spherulitic texture (Power *et al.*, 2011a). The water in the open pit is subsaline (>3.0 g L^{-1}), alkaline (average pH 8.4), and supersaturated with aragonite (Power *et al.*, 2011a). It is oligotrophic (undetectable phosphorus), has low-iron (~0.04 mg L^{-1}) and light penetrates to the bottom (Power *et al.*, 2011a). The water is very hard (>200 mg L^{-1} and >75 mg Ca L^{-1}) and has high alkalinity (>190 mg HCO_3^- L^{-1}) (Power *et al.*, 2011a). There is minimal nutrient input into the open pit due to the lack of surrounding soil and human activity over the last 35 years (Power *et al.*, 2011a).

Power *et al*. (2011a) were the first to microscopically and isotopically characterize the microbial community of the Clinton Creek microbialite: it was morphologically described to have benthic diatoms (e.g *Brachysira* spp.), filamentous algae (e.g *Oedogonium* spp.), dinoflagellates and cyanobacteria. Power *et al*. (2011a) noted the low microbial growth rates and suggested that the low sediment input had little influence geologically, but did not examine microbe-sediment interactions.

The microbial community structure and metabolic potential of the Clinton Creek microbialites and their surrounding environment are uncharacterized, as are microbialite systems from cold regions in general. As well, the metabolic potential of freshwater microbialites, especially from cold environments, is mostly uncharacterized; only one freshwater microbialite metagenomic dataset exists, which is from a tropical environment and which was biased by using MDA for DNA amplification (Breitbart *et al.,* 2009). Prior metagenomic studies, whether marine or freshwater, did not examine the composition or metabolic potential of the adjacent sediments or surrounding waters; such sampling would provide a context for identifying the microbes and processes that are confined to the microbialites. In Clinton Creek, the microbialite and sediment communities were compared to determine their similarities and differences and which biotic carbonate precipitating pathways, whether photosynthetic or heterotrophic, are enriched in the microbialites over the sediments.

1.8 Thesis hypotheses

Outlined below are the hypotheses considered in this thesis and the chapters where they are addressed.

Hypothesis [1] The microbial community and metabolic potential of modern freshwater microbialites in Pavilion Lake differs from that in the nearby sediments and water.
Presented in Chapter 2.

Hypothesis [2] Modern freshwater microbialites in Clinton Creek have a core functional potential and different pathways relating to carbonate precipitation than in the nearby sediments.
Presented in Chapter 3.

Hypothesis [3] *Agrococcus* sp. strain RW1 represents a new species of *Actinobacteria* that has genomic features associated with carotenoid biosynthesis leading to potential for yellow colony pigmentation.
Presented in Chapter 4.

Objective [4] *Exiguobacterium* sp. strain RW2 represents a new species of *Firmicutes* that has genomic features features associated with carotenoid biosynthesis to potential for orange colony pigmentation.
Presented in Chapter 5.

1.9 Tables and figures

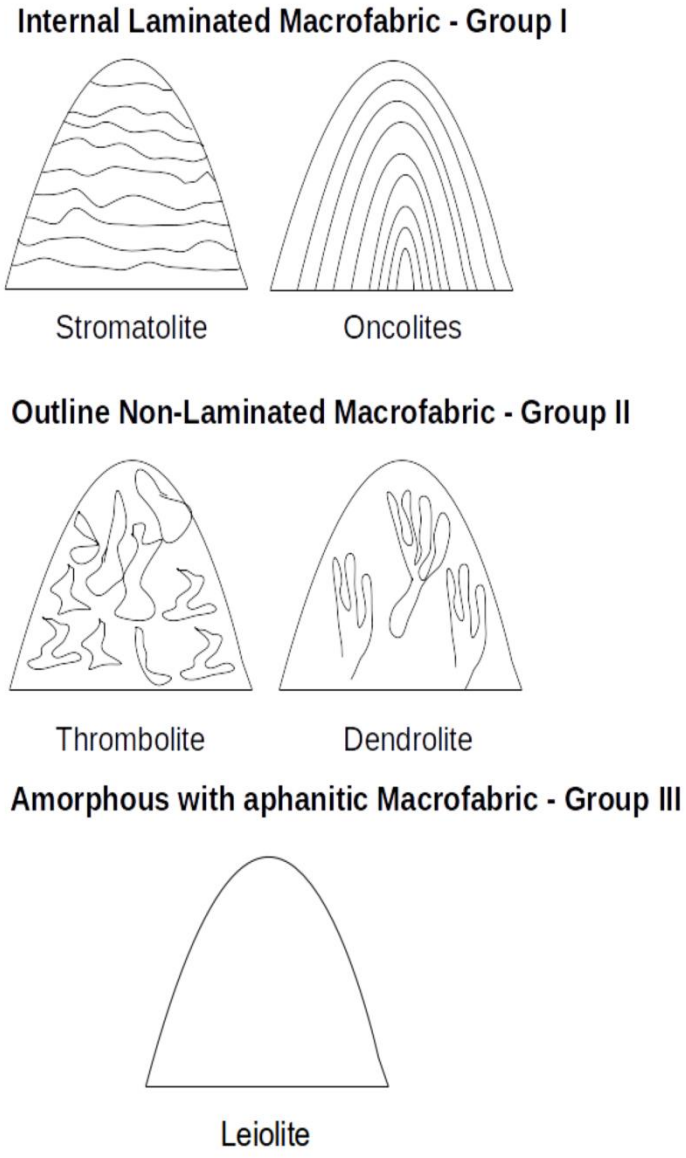

Figure 1.1: Microbialite morphology and carbonate macrofabric layout
Adapted from Riding *et al.*, 2011.

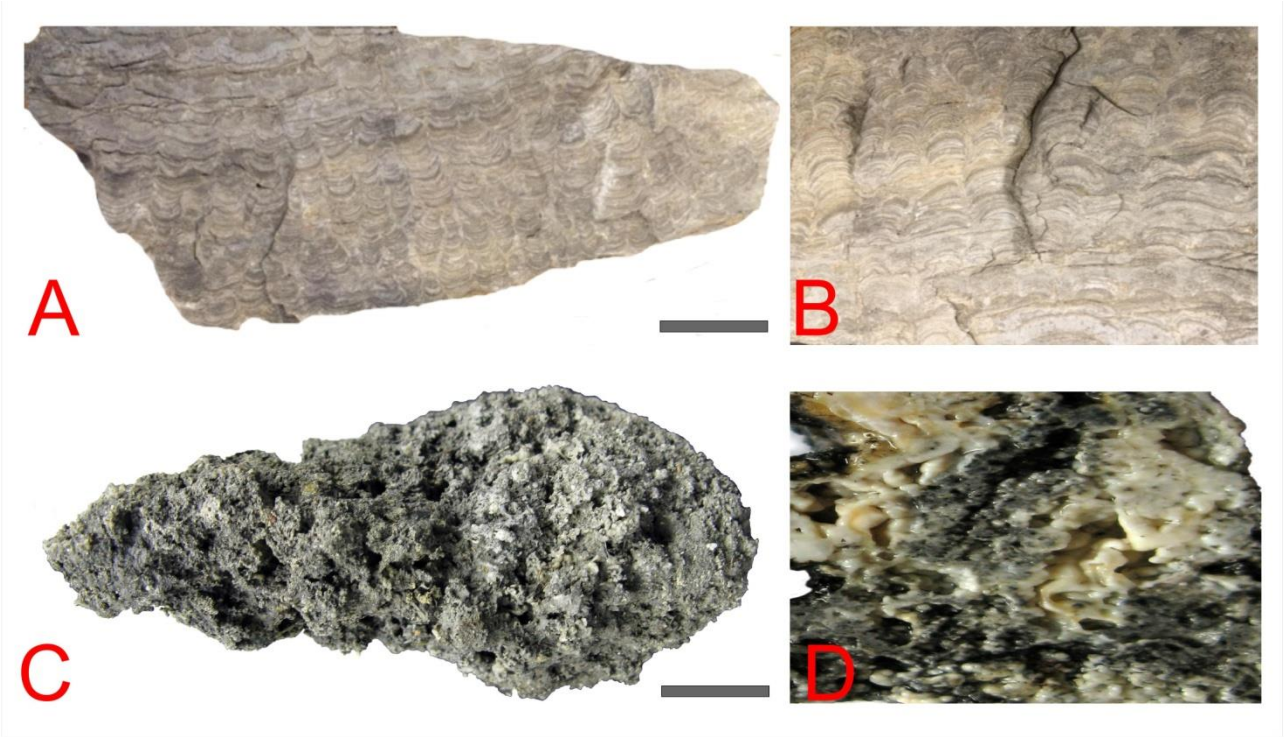

Figure 1.2: Microbialite morphology examples
A) A fossilized stromatolite (~505 Mya). Burgess shale in British Columbia.
Photo courtesy of Dr. David Turner, Beaty Biodiversity with permission. Gray scale bar 7 cm.
B) A close up of the fossilized stromatolite (10x from scale bar).
C) Clinton Creek thrombolite from Clinton Creek, Yukon Canada.
Photo courtesy of Dr. Ian Malcolm Power (University of British Columbia) with permission.
Gray scale bar 3 cms.
D) A close up of the Clinton Creek thrombolite (10x from scale bar).

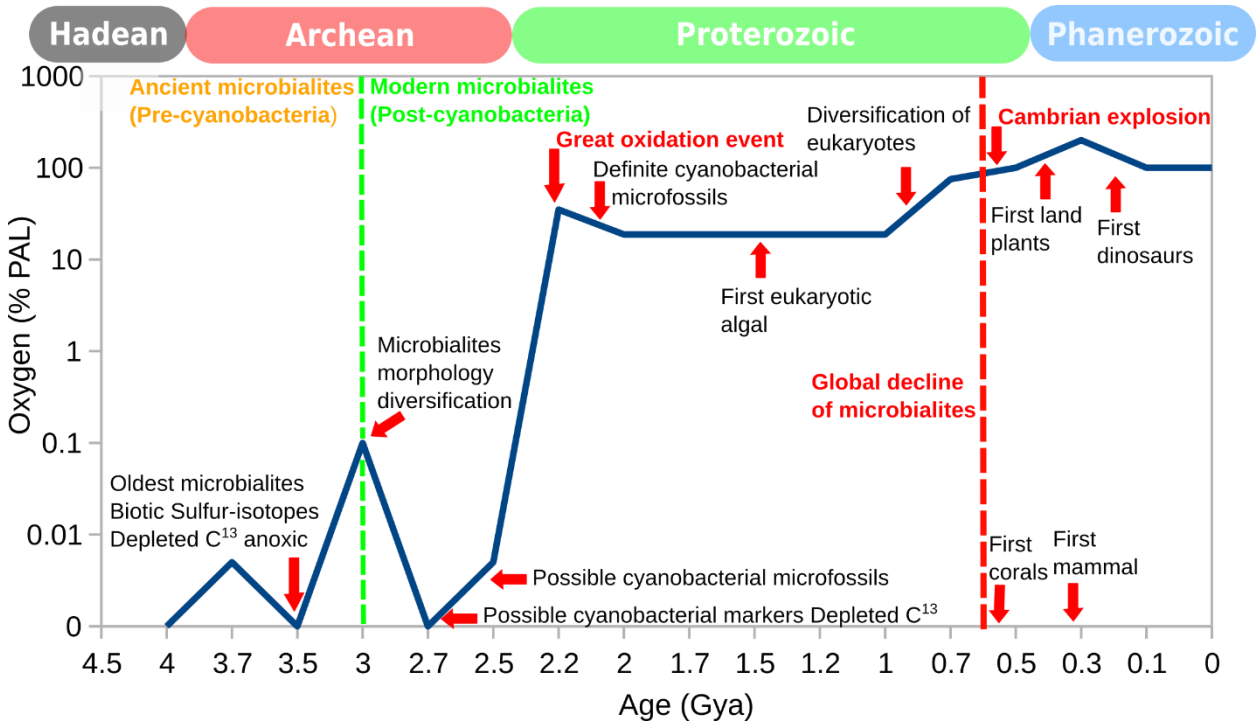

Figure 1.3: Timeline of microbialite and global atmospheric oxygen concentration over geological time

The figure was adapted from Canfield *et al.*, 2005 and Dupraz and Visscher, 2005. The oxygen data was provided by Dr. Sean Crowe (University of British Columbia) with permission, including data from Lyons *et al.*, 2014 and Crowe *et al.*, 2013. Oxygen data is expressed as %PAL or present atmospheric levels.

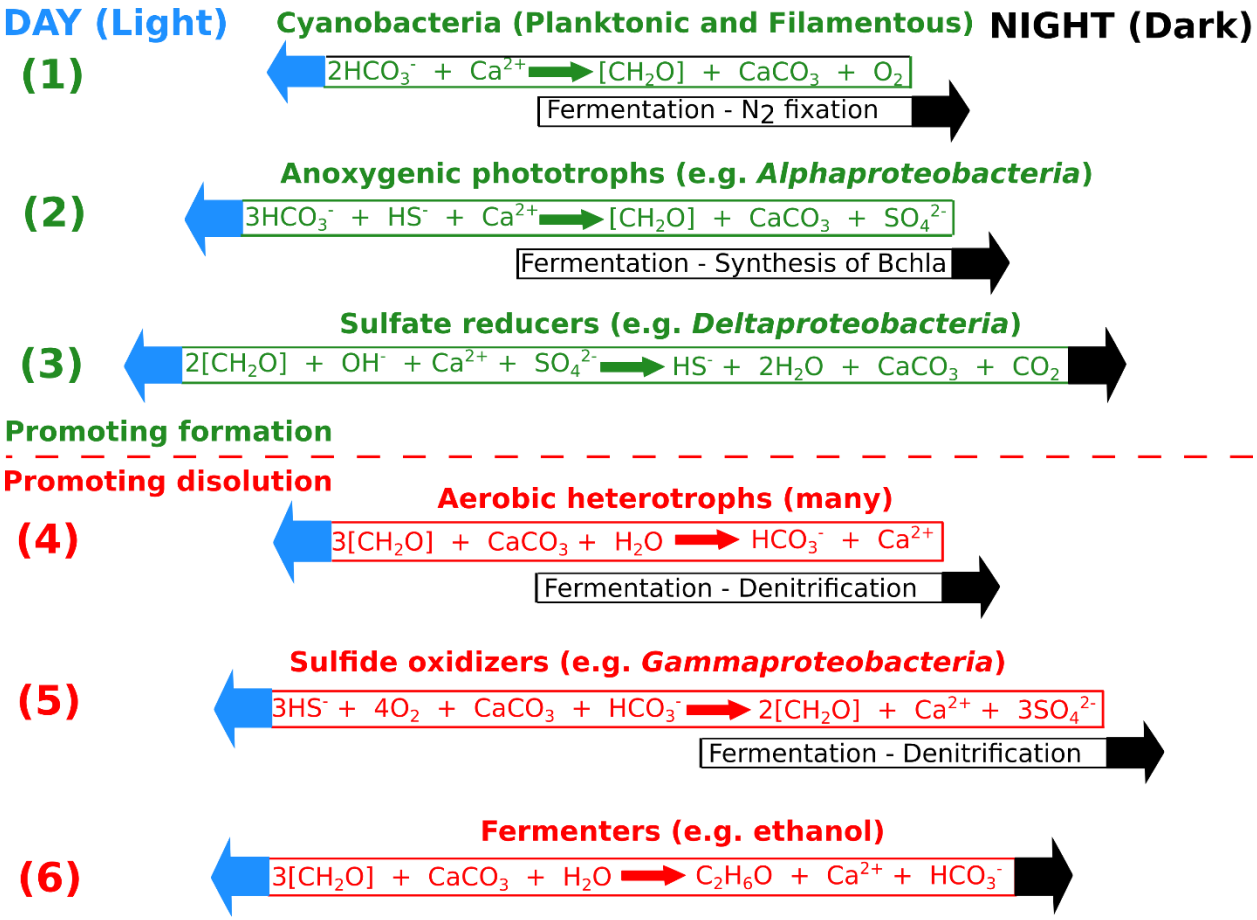

Figure 1.4: Generalized equations for microbialite formation and dissolution
Includes examples of key taxa involved or substrates (ethanol only) during light (day) and night (dark) cycles. Adapted from Dupraz and Visscher, 2005 and Dupraz *et al.*, 2009.

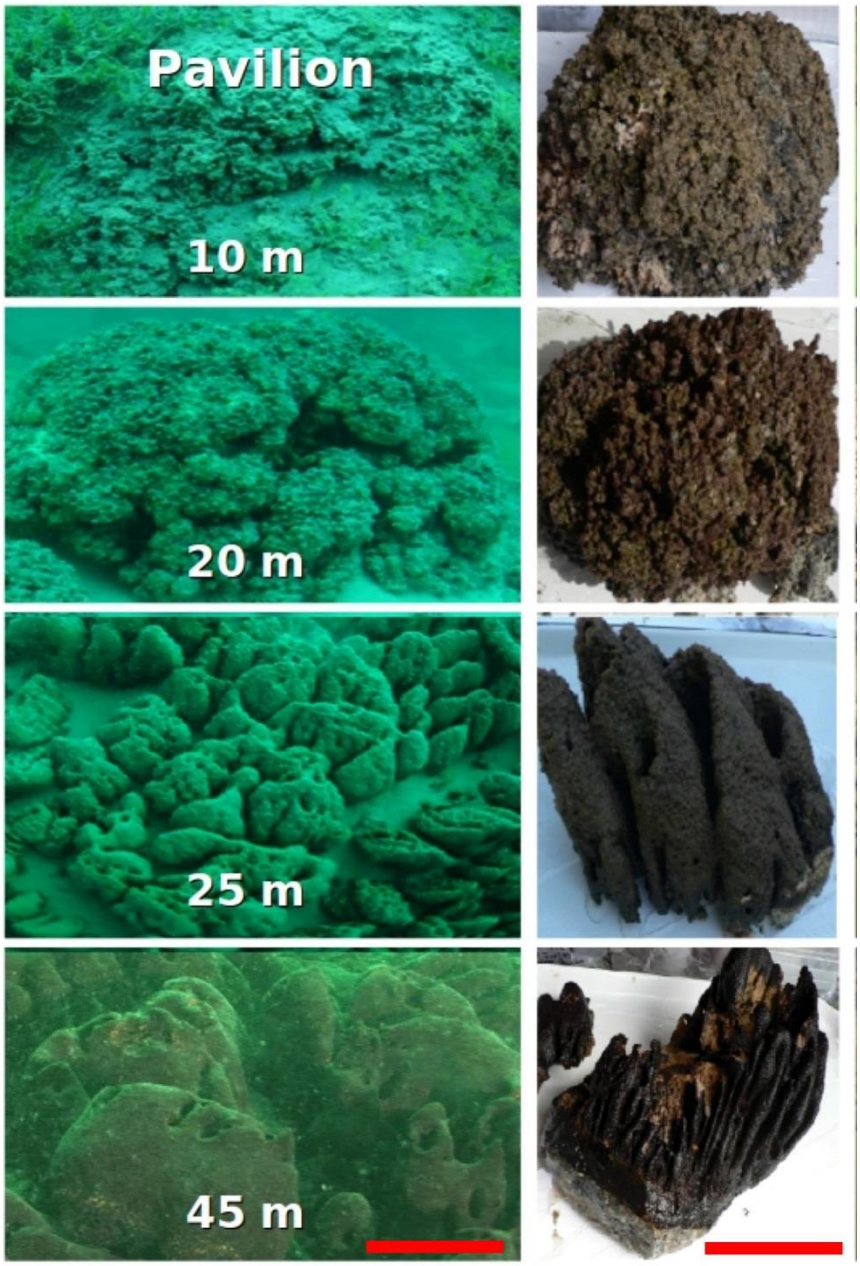

Figure 1.5: Pavilion microbialite morphologies
Red scale bar is ~10 cm across for both.
Photo courtesy of Donnie Reid (Nuytco reseach) and Tyler Mckay (UC Davis) with permission.

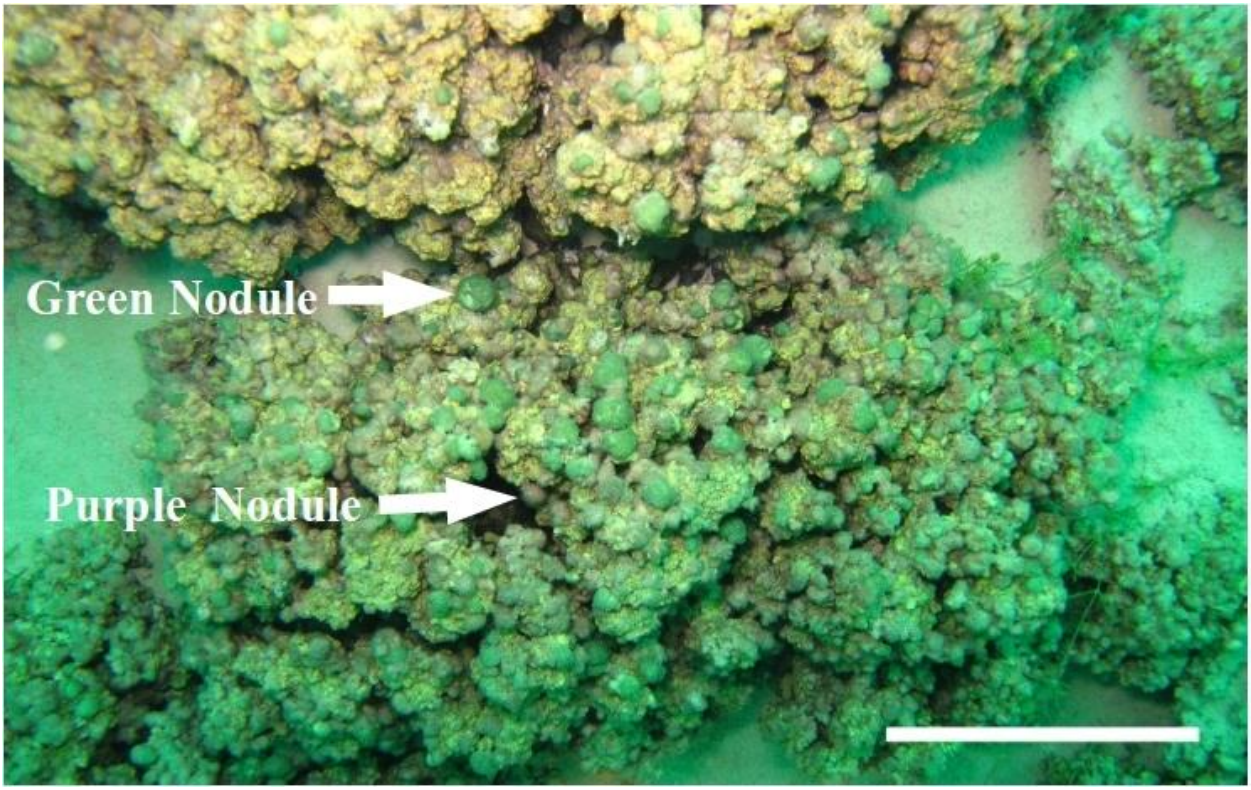

Figure 1.6: Pavilion Lake nodular cyanobacterial morphologies
Scale of the photo on the right at ~10 cm across.
Photo courtesy of Tyler Mckay (UC Davis) with permission.

Chapter 2:

Modern freshwater microbialite microbial community structure and metabolic potential is distinct from the surrounding environment

2.1 Introduction

Microbialites are thought to form through carbonate precipitation by a benthic microbial community and through trapping of detrital sediment (Burne and Moore, 1987: Dupraz and Visscher, 2005). This suggests that microbialites would comprise microbial communities from detrital sediments and surrounding water. Previous studies have not compared the microbial communities in microbialites with those of the sediments or water (Breitbart *et al.,* 2009; Khodadad and Foster, 2012; Mobberley *et al.* 2013). Determining the composition and metabolic potential of these microbial communities will allow the identification of microbialite-specific components.

Pavilion Lake is a temperate freshwater system that houses large diversity of microbialite structures (Laval *et al.,* 2000; Lim *et al.,* 2009). Isotopic data suggest that photosynthetic induced alkalinization is a major contributor to carbonate precipitation in Pavilion Lake microbialites. However, the metabolic potential, whether primarily photosynthetic or a mixture of heterotrophic and photosynthetic processes, is unknown (Brady *et al.,* 2009). Radiocarbon analysis shows that the microbialite-associated microbial community is using atmosphere-derived dissolved inorganic carbon (DIC) (Brady *et al.,* 2009). Moreover, elevated δ13C carbonate values within surface microbial mats and nodules from microbialites at < 20 m depth indicate photosynthetic carbonate precipitation (Brady *et al.,* 2010; Brady *et al.,* 2013). Although photosynthetic processes appear to be important in microbialite formation, the overall metabolic potential of microbialite communities in Pavilion Lake has not been investigated. In this contribution a metagenomic approach was used

to uncover the metabolic potential that is specifically associated with microbialite formation, and to distinguish it from that in microbial communities in the adjacent sediments and water.

As mentioned in Chapter 1, the only metagenomic data sets avaliable for freshwater microbialites are for a tropical system; other metagenomic studies on microbialites are marine (Breitbart *et al.,* 2009; Khodadad and Foster, 2012; Mobberley *et al.,* 2013). The freshwater microbialite metagenomic study of Cuatro Cienegás basin in Mexico (e.g. Pozas Azules II and Rios Mesquites) used multiple displacement amplification to obtain DNA, which can negatively affect quantitative results due to amplification bias (Abulencia *et al.,* 2006; Breitbart *et al.,* 2009; Yilmaz *et al.,* 2010; Abbai *et al.,* 2012). In this study, unamplified total genomic DNA from microbialites and their surrounding environments was sequenced, and used a metagenomic approach to identify constituent taxa and infer their metabolic potential. By examining taxonomic differences and representative genes across diverse metabolic pathways, we can explore the complex interface between microbialite communities and their environment.

2.2 Materials and methods

2.2.1 Sample collection

Triplicate representative microbialites (~10 kg), adjacent water (~100 L, at 10 m, 20 m and 45 m depths), and triplicate sediment samples (~20 g, at 10 m, 20 m, 25 m depths) were collected by divers and by pumping water from Pavilion Lake (50.86°N, 121.74°W) in 2010-11. The water was filtered in series through 120 µm pore-size Nitex screening to remove large plankton, and 1.2 µm pore-size glass-fiber, and 0.45 µm and 0.22 µm pore-size Durapore polyvinylidene difluoride (PVDF) filters (Millipore).

2.2.2 DNA extraction

A sterile razor blade was used to scrape off 3-10 mm (~5 g) from the surface of three morphologically similar microbialites collected at each depth, from which DNA was extracted on-site using a Powersoil Kit (Mobio, Carlsbad, CA). Samples were frozen on-site in liquid nitrogen and placed at -80 ºC when returned to the laboratory. Frozen samples were extracted with CTAB (Untergasser, 2008). For the filters, half of each glass-fiber and 0.22 µm pore-size filter was extracted using a PowerWater Kit (Mobio, Carlsbad, CA) and CTAB (Untergasser, 2008). Sediment samples were pelleted by centrifugation (5000 x *g*) and the DNA extracted from a ~5 g subsample using a PowerSoil Kit (Mobio, Carlsbad, CA) and CTAB (Untergasser, 2008). DNA concentrations were determined on-site using a Nanodrop-3300 (ThermoFisher, Wilmington, DE) with PicoGreen® reagent according to the manufacturer's instructions (Invitrogen, Carlsbad, CA). Purity was determined by absorbance (260/280 and 260/230) using a Nanodrop-1000 (ThermoFisher, Wilmington, DE). CTAB and MoBio DNA extractions were pooled (50:50) by equimolar DNA to reduce extraction bias and then used for library construction. Surface and 10 m water filter DNA was pooled for metagenomic library construction.

2.2.3 Metagenomic library preparation (454 FLX Titanium and Illumina)

Libraries for 454 FLX Titanium were constructed using random DNA shearing with a Bioruptor (Diagenode Denville, NJ). Fragments were polished and blunt-end ligated (NEBNext, DNA prep kit, Ipswich, MA) to in-house Multiplex Identifier barcode oligos (IDT, Coralville, Iowa), with small fragments removed by magnetic beads (Beckman Coulter, Danvers, MA). The libraries were quantified using a digital PCR quantified standard curve (White 3rd *et al.*, 2009), diluted, and pooled for 454 pyrosequencing with Titanium chemistry (Sick Kids Hospital, Toronto, Ontario).

For Illumina library construction, DNA was sheared by ultrasonication (Covaris M220 series, Woburn, MA), and the fragments end-paired, A-tailed (Lucigen NxSeq DNA prep kit, Middleton, WI) and ligated to TruSeq adapters (IDT, Coralville, Iowa); small fragments were removed twice using magnetic beads (Beckman Coulter, Danvers, MA). The resulting libraries were pooled, and both 250 bp and 100 bp paired-end sequenced on MiSeq (GenoSeq UCLA Los Angeles, CA) and HiSeq (McGill University/Génome Québec, CAN) platforms, respectively. Replicate samples were barcoded separately, then pooled for data analysis. The replicates were pooled based on data from tRFLP analysis that showed samples from a given depth had very similar taxonomic profiles. Pooling provide similar numbers of contigs across depths.

2.2.4 Metagenomic data assembly and analysis

The raw sequencing data were processed as follows: for the 454 data, the raw SFF files were converted to FASTQ format and binned by molecular barcode (MID) using a custom Perl script. Barcodes were removed by Tagcleaner (Schmieder *et al.*, 2010) and sequences cleaned for low quality and homopolymers using PRINSEQ (Schmider and Edwards, 2011). The Illumina data were extracted and demultiplexed using the CASAVA pipeline v1.8 (Illumina, San Diego, CA), and the PhiX spike-in used for sequencing quality control was screened using Bowtie2 (version 2.1.0) then removed using Picard tools (version 1.90) (White 3rd and Suttle, 2013c).

The resulting 454 FLX titanium reads, Illumina overlapping merged reads and Illumina non-overlapping reads from replicate libraries were combined and assembled (kmer size: 39) using the Ray DeNovo assembler (Boisvert *et al.*, 2010; 2012). Metagenomic rapid annotations using a subsystems technology (MG-RAST) server was used for contig annotation (Meyer *et al.*, 2008). MG-RAST annotation of the contigs used BLAT (BLAST-like alignment tool) annotations based on hierarchical classification against SEED subsystems and RefSeq databases with a minimum E-

value cutoff of 10^{-5}, a minimum percent identity cutoff of 60%, and a minimum alignment length cutoff of 15 base pairs.

Statistical analysis was completed using statistical analysis of metagenomic profiles (STAMP) and R (Parks *et al.*, 2010). STAMP and R were used to parse MG-RAST data for RefSeq (class level) and SEED subsystems (level I to function) results. The STAMP ANOVAs (including PCA) were completed using multiple groups, post-hoc tests (Tukey-Kramer at 0.95), an effect size (Eta-squared) and multiple test correction using Benjamini-Hochberg FDR (false discovery rate) procedure. SEED subsystems level III scatter plots for samples from microbialites, sediments and filters were constructed in STAMP using a one-sided Welch's t-test with Welch's inverted confidence interval (0.95), with Benjamini-Hochberg FDR. The top 25 RefSeq classifications were normalized for each sample using count-relative abundances. PCA analysis for the normalized top 25 RefSeq classifications used R libraries Ecodist (Dissimilarity-based functions for ecological analysis), and pvclust (Hierarchical Clustering with P-Values via Multiscale Bootstrap Resampling) using ward clustering and the Bray-Curtis distance metric at a thousand replicates (Suzuki and Shimodaira, 2006). The PCA for the normalized top 25 RefSeq classifications was plotted using R library ggplot2 and a dotplot was done using R libraries Reshape2 using the melt function, then plotted using ggplot2 (Wickham, 2009).

FragGeneScan was used to translate contigs into protein ORFs (Rho *et al.*, 2010) and ProPas was used to predict protein isoelectric points (pI) (Wu and Zhu 2012). These data were further analyzed with R (R development Core Team 2013) then visualized using the R library ggplot2 (Wickham, 2009).

2.2.5 **Recruitment analysis to draft genomes**

Metagenomic read recruitment from the Pavilion Lake 20 m microbialite metagenome to determine the abundance of *Agrococcus* sp. strain RW1 and *Exiguobacterium* sp. strain RW2 from their isolated environment (White 3rd *et al.*, 2013a-b). To determine genotypic-specific abundance we also recruited metagenomic reads to closely related genomes, which included *Agrococcus lahaulensis* strain DSM17612 (unpublished NCBI download), *Exiguobacterium* sp. strain S17 (Belfiore *et al.*, 2013; Ordoneza *et al.*, 2013), and *Exiguobacterium* sp. strain AT1b (Vishnivetkaya *et al.*, 2011). Metagenomic recruitment analysis used ~7.5 M reads pooled from HiSeq (~100 bp), MiSeq (~250 bp) and 454 FLX Titanium (~300 bp) sequencing platforms from 20 m Pavilion Lake microbialites only. EMBOSS union script was used to find overlapping contigs and merge contigs for draft genomes into a single scaffold that may not be contiguous; however, it yields a single genomic contig, which is required for metagenomic read recruitment (Rice *et al.*, 2000; Kunin *et al.*, 2008a). FR-hit program was used for metagenomic recruitment for the *Exiguobacterium* and *Agrococcus* genomes using default parameters with a minimum identity >70% and an E-value >$1e^{-5}$ (Nsiu *et al.*, 2011), the recuitments were then visualized with the R library ggplot2 (Wickham, 2009).

2.2.6 **Metagenomic data depositing**

All the data used in this study are publicly accessible from MG-RAST. From MG-RAST, it is listed in the project name Pavilion Lake surrounding environment under names PLsfcFil (ID 4532785.3), PL20Fil (ID 4532783.3), PL45Fil (ID 4532784.3), PLMB10 (ID 4532771.3), PLMB20 (ID 4532772.3), PLMB25 (ID 4532774.3), PLMB45 (ID 4532775.3), PL10Sed (ID 4526738.3), PL20Sed (ID 4526739.3) and PL25Sed (ID 4526740.3).

2.3 Results and discussion

2.3.1 Metagenomic assembly statistics

This study combined data from 454 FLX titanium pyrosequencing with Illumina MiSeq and HiSeq data, as Illumina sequencing compensates for the error-prone homopolymers of 454, while 454 compensates for Illumina's GC bias and substitution errors (Bentley *et al.,* 2008; Ross *et al.,* 2013). A total of 446 Mbp of assembled contigs from the microbialites and 17 Mbp of assembled contigs from the filters (Table 2.1) allowed differences in microbial structure and metabolic potential to be compared between the microbialites and surrounding water. The sediment metagenomes failed to assemble using Ray (Boisvert *et al.,* 2010; 2012), Velvet (Zerbino and Birney, 2008), MetaVelvet (Namiki *et al.,* 2012) or AbySS (Simpson *et al.,* 2009) (data not shown). Paired-end reads from the sediments only were extended for overlap and pooled with unextended reads for further analysis (Table 2.1). In the future, longer reads will allow for better assemblies of metagenomic data (Wommack *et al.,* 2008), aided by new sequencing technologies such as Pacific Biosciences (Rasko *et al*., 2011) or the Oxford nanopore, which promise reads as high as 50 kb (Loman *et al*., 2012).

2.3.2 Microbialites communities differ from the surrounding environment

The microbial community structure and metabolic potential of Pavilion Lake microbialites were distinct from the surrounding environment, based on GC content, RefSeq taxonomic classifications, including SEED and MetaCyc functional gene assignments. Across depths, the GC content in microbialites differed from that in adjacent waters and sediments; in constrast, predicted protein isoelectric content (pI) was not as useful a distinguishing metric. (Figure 2.1). The GC content across microbialites as a function of depth was very similar, implying that the microbial communities were similar.

Supporting the results from GC content analysis, the RefSeq classification also showed that the microbialite communities were collectively different from those in the water and sediments. STAMP ANOVA on the RefSeq classifications identified thirteen bacterial and seven archeal classes that were significantly enriched in microbialites over the surrounding environment (Table 2.2, $p < 0.01$). PCA based on RefSeq classifications also indicated that the metagenomes from microbialite was distinct from those in the water and sediment (Figure 2.2A). These analyses demonstrated that the microbialite communities are distinct from those of neighboring sediments and water.

The predicted metabolic potential based on SEED and MetaCyc functional gene assignments are also consistent with a microbialite community that is distinct from those in the. sediments and water. ANOVA using STAMP on the highest level classification (Level I) in the SEED database indicates that membrane transport, aromatic metabolism, motility, potassium metabolism, cell signaling and virulence genes are significantly enriched in microbialites over the neighboring environment (Table 2.3, $p < 0.05$). At the next level of metabolic organization within the SEED subsystems (Level II), ANOVA predicted more than 90 metabolic features that were overrepresented in the microbialite metagenomes; PCA using these data also indicates that the metabolic potential of the microbialites is distinct from that of the surrounding environment (Figure 2.3A). Welch's one sided t-test cluster analysis using >300 level III SEED subsystems indicates a weak correlation between the functional genes in the microbialites and sediments ($R^2 = 0.546$), but a stronger correlation between the microbialite and water as indicated by the data from the filters ($R^2 = 0.871$) (Figure 2.3C). PCA and NMDS analysis of MetaCyc features supports the SEED PCA, revealing that microbialites are distinct from the sediments and water (Figure 2.4).

Overall, the analyses of metagenomic data indicate that the microbialite communities and their metabolic potential are distinct from those in the surrounding environment.

The microbial communities and the metabolic potential of the surrounding environments differed significantly from those of the microbialites; the sediment metagenomes were predicted to have more sequences associated with *Betaproteobacteria* and *Spirochaetia* (Figure 2.5).The predicted metabolic potential of sediment metagenomes was associated with nitrogen metabolism (e.g. ammonification) and anaerobic fermentation (Figure 2.6). The water metagenomes had more phototrophic eukaryotes (e.g. *Chlorophyceae*) with a photosynthetic metabolic potential (e.g. carotenoid biosynthesis) (Figure 2.5 and 2.6). *Bacteroidetes* and *Chlorophyta* are low GC containing taxa which could explain the distinction between the water and microbialite metagenomes based on GC content (Figure 2.1). Thus, the surrounding environments had a microbial community and metabolic potential that was divergent from microbialites.

2.3.3 Pavilion Lake microbialite core microbial community and related pathways

The microbialites of Pavilion Lake were dominated by *Proteobacteria, Acidobacteria,* and *Cyanobacteria* (Figure 2.2B). Based on RefSeq taxonomic classification ANOVA using STAMP, the classes *Alphaproteobacteria*, *Deltaproteobacteria*, *Acidobacteriia* and *Gloeobacteria* were significantly more abundant in the microbialite metagenomes (Table 2.2; $p < 0.01$). The dominance of sequences associated with the members of the phyla *Proteobacteria* (mainly *Alphaproteobacteria* and *Deltaproteobacteria* classes), and *Cyanobacteria* is consistent with results from other marine and freshwater microbialite communities (Havemann and Foster 2008; Breitbart *et al.,* 2009; Goh *et al.*, 2009; Mobberley *et al.,* 2010; Khodadad and Foster 2012).

There were significantly more microbialite sequences classified as *Alphaproteobacteria* relative to the neighboring environment, which consisted of functional groups that were photoheterotrophic and heterotrophic (Figure 2.7; Table 2.2; $p<0.05$). Microbialite alphaproteobacterial specific contigs were assigned to genera of photoheterotrophic (e.g. *Rhodomicrobium*, *Rhodopseudomonas*, and *Rhodospirillum*), heterotrophic (e.g. *Sphingomonas*) and nitrogen-fixing (e.g. *Argobacterium*, *Bradyrhizobium*, and *Rhizobium*) bacteria (Figure 2.7; $p < 0.05$). Alphaproteobacterial-based nitrogen fixation complements cyanobacterial nitrogen fixation in microbialites likely because of cyanobacterial diel cycles (Havemann and Foster 2008).

Deltaproteobacterial-associated sequences within the microbialite metagenomes were assigned to genera of dissimilatory sulfate reducing (e.g. *Desulfobacterium* and *Desulfovibrio*) and heterotrophic carbonate precipitating (e.g. *Myxococcus*) bacteria (Jimenez-Lopez *et al.*, 2011), which were significantly more abundant in microbialites than in the neighboring environments (Figure 2.8). Sulfate-reducing deltaproteobacteria are often found where carbonates precipitate, and are important drivers of the "alkalinity engine," by pushing the saturation index higher via increasing alkalinity (Gallagher *et al.*, 2012). *Myxococcus* spp. are abundant in a variety of microbialite-forming systems and can directly precipitate carbonate through the release of ammonium (Ben Chekroun *et al.*, 2004; Jimenez-Lopez *et al.*, 2011). Analyses of the Pavilion Lake microbialite metagenomes confirmed prior investigations showing that members of the *Alphaproteobacteria* include photoheterotrophs and nitrogen-fixers, and the *Deltaproteobacteria* include sulfate-reducers (Havemann and Foster 2008; Breitbart *et al.*, 2009; Goh *et al.*, 2009; Mobberley *et al.*, 2010; Khodadad and Foster 2012).

Sequences associated with filamentous cyanobacterial mat-builders from the genera *Anabaena*, *Lyngbya*, *Microcoleus*, *Nostoc*, *Oscillatoria* and the planktonic *Cyanothece* and

Acrayochoris were enriched significantly in microbialites (Figure 2.9, $p < 0.05$). Pathways for synthesis of cyanoglobin and cyanophycin, as well as copper metabolism, which are associated with cyanobacterial mat-builders, were highly enriched in the microbialites over the surrounding environment. (Figure 2.10, $p < 0.05$). Cyanoglobin is a peripheral membrane protein that binds oxygen with high affinity, is highly expressed under low oxygen and could be restricted to some strains of *Nostoc* spp. and *Anabaena* spp. (Hill *et al.,* 1996). Cyanophycin is formed in filamentous cyanobacteria in response to low or changing DIC to O_2 ratios (Liang *et al.,* 2014). Copper homeostasis genes were abundant in microbialites, which is common for cyanobacterial derived mats, as copper is essential for growth (Varin *et al.,* 2012) but also toxic at levels ≥10 mM (Burnat *et al.,* 2009). The microbialite metagenome indicates that the metabolic potential of filamentous cyanobacterial mats is adaptive to metal homeostasis (e.g. copper), as well as carbon and oxygen limitation (e.g. cyanoglobin and cyanophycin).

Sequences associated with planktonic cyanobacteria (*Synechococcus* spp.) represented 40 to 60% of the cyanobacterial sequences in the water but <27% in microbialites based on RefSeq classification. This confirms the high abundances (8.3×10^4 cells ml^{-1}) of *Synechococcus* spp. reported by Laval *et al.* (2000). The low abundance of sequences associated with *Synechococcus* spp. in cyanobacterial mats is likely a reflection of their planktonic lifestyle. However, planktonic cyanobacteria are involved in "whiting events," during which photosynthetic alkalinization induces carbonate precipitation from the water (Thompson and Ferris, 1990; Thompson *et al.,* 1997). Measured sedimentation rates in Pavilion Lake are 0.07 g y^{-1} with 4.3% being carbonates (Lim *et al.,* 2009), indicating a minor contribution of whiting events to microbialite formation. This is consistent with phototrophic and heterotrophic processes in the cyanobacterial mats dominating microbialite formation (Omelon *et al.,* 2013).

More than 60% of the microbialite acidobacterial specific contigs were assigned to *Candidatus Solibacter* spp., and were more abundant in the microbialites than in the sediments or water (Table 2.2, p-value < 0.01). Representatives of the genus have been reported from other permanently cold environments, including Arctic tundra, and have cold-adapted glycoside hydrolases and transferases that breakdown diverse carbon sources and allow growth in cold oligotrophic conditions (Rawat *et al.,* 2012), such as found in Pavilion Lake (Lim *et al.,* 2009). These conditions are analogous to those in cyanobacterial mats on Pavilion Lake microbialites (Lim *et al.,* 2009). Solibacterial contigs in the microbialites contain both glycoside hydrolases and transferases that could degrade filamentous cyanobacterial mats, and reverse EPS-related calcium binding inhibiton (Dupraz and Visscher, 2005).

Recent studies have suggested that *Candidatus Chloracidobacterium thermophilum,* a novel photoheterotroph, could be present in microbialites (Couradeau *et al.,* 2011; Russell *et al.,* 2014). *Candidatus Chloracidobacterium thermophilum* was found at low abundance (<1% of contigs) in Pavilion Lake microbialites based on RefSeq classification. Despite low abundance of sequences for *Candidatus C. thermophilum,* evidence of functional genes in the microbialites included some for housekeeping (RecA, gyrB, tRNA synthetase), carotenoid biosynthesis, glycoside processing (hydrolases, transferases) and CRISPRs. While, no evidence for photosystems was found among the *Candidatus C. thermophilum* like sequences, there were many hypothetical genes that were unclassified.

Urealytic metabolism has been hypothesized to be involved in microbialite formation due to its carbonate preciptitating effects, but its detection in microbialites has remained elusive (Castanier *et al.,* 1999). *Gamma* and *Deltaproteobacteria* specific urease beta subunits and urease accessory proteins (UreD/F) were found only amongst the Pavilion Lake microbialite

metagenomes (Figure 2.10). The linkage of urease related genes to *Proteobacteria* was unexpected due to the strong experimental evidence supporting *Firmicutes* (mainly *Bacillus* spp.) as the dominant taxa contributing urease related genes (Boquet *et al.,* 1973; Hammes *et al.,* 2003; Lee, 2003; Dick *et al.,* 2006; Dhami *et al.,* 2013).

Two potential sources of urea in the microbialite are metazoans and bacteria. Crustaceans excrete urea as a by-product of heterotrophic metabolism (Weihrauch *et al.,* 2009). As well, some bacteria produce urea by the degradation of purines, arginine and allantoin (Jørgensen, 2006). Notably, gammaproteobacteria (e.g. *Pseudomonas* spp.) can produce urea without an external supply of organic nitrogen (Therkildsen *et al.,* 1997). Urea is likely produced locally in the microbialite mat and is degraded by urease as rapidly as it is produced, supporting the model that microbialites become progressively lithified as the photosynthetically derived carbonate becomes in-filled through subsequent carbonate precipitation by heterotrophic activity (Omelon *et al.,* 2013).

Antibiotic and heavy-metal resistance pathways were associated with *Proteobacteria* and by RefSeq classification were over-represented in the microbialites (Figure 2.11). These included antibiotic resistance pathways assigned to the *Alpha*, *Beta* and *Gamma* classes of *Proteobacteria* that include multidrug efflux transporter families (e.g. MexF and Bcr/CflA) and class A beta-lactamases (Figure 2.11). Genes related to antibiotic resistance in the Pavilion Lake microbialites could be in response to toxic organic molecules produced by cyanobacterial mats (Neilan *et al.,* 2013). Cobalt-zinc-cadmium resistance genes were also enriched in microbialites and assigned to *Alpha*, *Beta* and *Gamma* classes of *Proteobacteria* (Figure 2.11). Pavilion Lake has low levels of zinc (0.01 to 0.03 mg L^{-1}) and undetectable levels of cobalt, iron, arsenic and cadmium (Lim *et al.,* 2009). The presence of heavy metal resistance genes may be involved in resistance, homeostasis

or sequestration of metals. Conceivably, historical mining in the area (Stevenson, 1940) could have contaminated Pavilion Lake, and selected for resistance to heavy metals. Antibiotic resistance has also been linked to heavy-metal stress, suggesting that selection for resistance to one can lead to resistance to the other in complex bacterial communities (Nisanian *et al.*, 2014).

Primary alcohol fermentation related to genes associated with acetone, butanol and ethanol biosynthesis were assigned to *Alpha-* and *Beta-proteobacteria*, and were enriched in the microbialite metagenomes relative to the surrounding environment (Figure 2.11). Primary alcohol fermentation has been linked to microbialite dissolution; however, fermentation also provides substrates that fuel dissimilatory sulfate reduction, which can precipitate carbonate and thus could offset carbonate lost by fermentation (Dupraz and Visscher, 2005; Gallagher *et al.*, 2012). Members of the *Proteobacteria* appear to be major constituents of Pavilion Lake microbialites, and potentially provide important metabolic roles, such as resistance to antibiotics and heavy-metals, and primary alcohol fermentation, which have not previously been attributed to microbialites, and which suggest an important role for *Proteobacteria* in these systems.

2.3.4 Low abundance members of Pavilion Lake microbialite microbial community

Bacterial phyla such as *Gemmatimonadetes*, *Poribacteria* and *Chloroflexi* were in low abundance (<2% of the contigs) in the microbialite (Figure 2.2B). The ANOVA in STAMP using RefSeq classification found that *Chloroflexi* and *Gemmatimonadetes* were significantly more abundant in the microbialites than in the sediments or the water (Table 2.2, p-value <0.01). *Gemmatimonadetes* and *Chloroflexi* are likely part of the heterotrophic consortia in Pavilion Lake microbialites. Members of the *Gemmatimonadetes* synthesize carotenoids to protect against reactive oxygen species and possibly photo-oxidation, which would be useful to avoid photo-oxidation in the microbialite cyanobacterial mats (Takaichi *et al.*, 2010). *Porbacteria* are

associated with marine sponges (Fieseler *et al.*, 2004), and freshwater sponges are found throughout Pavilion Lake, even growing on microbialites.

Sequences assigned to *Archaea* in the microbialites were <1% of the contigs (Figure 2.2B). Little is known about the role of archaea in microbialites, but prior metagenomic evidence also suggests they are of minor importance (Mobberley *et al.*, 2010; Khodadad and Foster 2012). For example, in both nonlithifying and lithifying stromatolithic mats at Highbourne Cay there were no taxonomic or metabolic differences attributed to archaea (Mobberley *et al.*, 2010; Khodadad and Foster 2012).While the abundance of archaea is low, there are statistically significant differences in their occurrence between microbialites and the surrounding environments. RefSeq ANOVA assigned reads to the taxa *Halobacteria, Thermococci, Thermoplasmata, Methanopyri, Methanomicrobia,* and unclassified *Korarchaeota* (Table 2.2, $p < 0.01$), supporting the presence of archaea. Moreover, the SEED subsystem annotations found archaeal specific pathways in the microbialites for DNA replication, DNA recombination and tRNA modification, as well as tRNAs/rRNA methyltransferases and predicted archaeal chaperones associated with the Archease 2 pathway (Figure 2.12). However, given their low abundance and likely anerobic lifestyle, it is unlikely that archaea play a major functional role within the microbialites, although more study is warranted.

Exiguobacterium sp. strain RW2 was isolated from a microbialite collected from 20 m in Pavilion Lake; however, its abundance is unknown (White 3rd *et al.*, 2013b). Based on the taxonomic assignment of contigs from the metagenomic data, sequences most similar to those from *Exiguobacterium* spp. were more abundant in the microbialites than in the water or sediments (Figure 2.13a). Sequenced genomes from isolates of *Exiguobacterium* spp. (strains RW2, S17 and AT1b) were used to recruit against ~7.5M metagenomic reads from a 20 m microbialite to

determine which genotype recruited the most sequences. More reads (0.46% of total reads) recruited to the draft genome *Exiguobacterium* sp. strain RW2 than to the genomes of its closest relatives, including *Exiguobacterium* sp. strain AT1b (0.25% of total reads), and *Exiguobacterium* sp. strain S17 (0.33% of total reads) (Figure 2.13B). As well, *Exiguobacterium* sp. strain RW2 had the highest proportion of identical hits to metagenomic data, consistent with its presence in the system (Figure 2.13B). Members of the genus *Exiguobacterium* are associated with hard carbonate structures, calcium-rich springs, and alkaline environments (Vishnivetskaya *et al.,* 2011; Ordoñeza *et al.,* 2013; White *et al.,* 2013b). As well, isolates from modern microbialites, including *Exiguobacterium* sp. strain RW2 and *Exiguobacterium* sp. strain S17, appear to code for pathways involved in resistance to heavy metals (Belfiore *et al.,* 2013; Ordoñeza *et al.,* 2013; White *et al.,* 2013b). This is supported by analysis using tBLASTx ($1e^{-3}$) that showed reads recruited to *Exiguobacterium* sp. strain RW2 at 95 to 100% identity were heavy-metal resistance genes, which are relatively more abundant in the microbialites (Figure 2.11).

Agrococcus sp. strain RW1 was isolated from the same 20 m Pavilion Lake microbialite as *Exiguobacterium* sp. strain RW2 (White 3rd *et al.,* 2013a-b). However, like *Exiguobacterium* sp. strain RW2, the abundance of *Agrococcu*s sp. strain RW1 is unknown (White *et al.*, 2013a). In order to estimate the contribution of members of this genus to the microbialite community, the genomes of *Agrococcus* sp. strain RW1 and *A. lahaulensis* strain K22-21 were recruited against the ~7.5 M metagenomic reads from the 20 m microbialites. Both genomes recruited about 1.6% of the reads, indicating that *Agrococcus* spp. are significant members of this community. Although *A. lahaulensis* recruited a few hundred more reads, *Agrococcus* sp. strain RW1 had more reads that recruited at 95 to 100% identity (Figure 2.14). Similar to the *Exiguobacterium* sp. strain RW2

genome, these reads were confirmed by tBLASTx ($1e^{-3}$) to be heavy-metal resistance genes (Figure 2.11).

2.3.5 Metabolic potential relating to photosynthetic or heterotrophic processes

The metabolic potential of the microbialites is dominated by heterotrophic processes. Sequences related to photosynthesis including those encoding photosystems and electron transport proteins were ranked 28th out of 29 based on SEED subsystems (Figure 2.15). In contrast, pathways related to carbohydrate metabolism (carbon-related pathways) were ranked 2nd and accounted for ~9% of the contigs. Among the carbon-related pathways ~45% were related to central (TCA cycle) and one-carbon metabolism (e.g. serine-glyoxlate cycle), while another ~45% were related to degradation (e.g. fermentation, glycoside hydrolases and other hydrolytic enzymes) (Figure 2.16). Only ~10% of the microbialite-specific contigs were annotated as carbon-fixation related (e.g Calvin-Benson cycle) (Figure 2.16). Stable-isotope studies suggest that photosynthetic processes are linked to carbonate precipitation in the microbialites (Brady *et al.*, 2010, Omelon *et al.*, 2013), even though the metabolic potential is dominated by heterotrophic processes. Microbialite formation in Pavilion Lake appears to be localized carbonate precipitation associated with cyanobacterial photosynthesis and heterotrophic processes such as urealytic metabolism, dissimilatory sulfate reduction and heterotrophic mat degradation, which could reduce EPS related carbonate inhibition (Dupraz *et al.*, 2009). ^{13}C enrichment in microbialite carbonates may not only be a product of cyanobacterial photosynthesis, photoheterotrophs such as acidobacteria and proteobacteria may also contribute; however, this remains to be demonstrated.

2.3.6 Viral community and viral defense

Even though only the cellular fraction from the water was analyzed, viral sequences represented >1% of reads, whereas in total DNA extracted from microbialites they comprised

>0.05%. ANOVA in STAMP based on RefSeq classification further confirms that viruses from the water were significantly more abundant then in microbialites or sediments than water (Figure 2.17). Specifically, T4-like and large algal viruses (e.g. *Phycodnaviridae*) dominated the viral sequences in the water and were more abundant than in the microbialites and sediments (Figures 2.18). The low proportion of viral reads in the microbialite data may reflect the fact that in the RefSeq database there are many sequenced dsDNA viral genomes from water samples, but not from microbialites. Despite the limited data, viruses in the water appeared to have higher abundances of proteins related to phage structure (tail fibers), phage replication and DNA replication (Figure 2.18).

An active role for phages in the microbialites is suggested by the higher relative abundances of predicted genes involved with CRISPRs and phage excision (Figure 2.17 and 2.18). CRISPR *cas* genes were associated with the following taxonomic groups: *Chloroflexi* (e.g. *Dehalococcoides*), *Deltaproteobacteria* (e.g. *Myxococcus* and *Desulfuromonadales*), filamentous cyanobacteria (e.g. *Anabaena, Nostoc, Rivularia*) and *Firmicutes* (e.g. *Clostrida*) based on tBLASTx ($1e^{-3}$) analysis. As well, more putative genes involved in phage integration and excision occurred in the microbialites (Figure 2.17 and 2.18). Also, CRISPRs were predicted to be associated with key members involved in microbialite formation, such as filamentous cyanobacteria and *Myxococcus* spp., implying that the microbialite community is under continuous selective pressure from viral infection.

It is important to emphasize that the viral DNA was from the >0.22 µM cellular fraction captured on filters. Most free viral particles would have passed through the filters; hence, most viral sequences were likely from infected cells or from viruses attached to particles. It is not uncommon for filters with pore sizes much larger than viruses to contain many viral sequences

(Zeigler Allen *et al.,* 2012). The most abundant viral contigs in the water were for T4-like cyanophages and phycodnaviruses (Figure 2.18), although gene-specific primers failed to amplify DNA from either group from any of the samples, suggesting the viruses were divergent from those targeted by the primers (Chen and Suttle, 1995; Filée *et al.,* 2005).

Consistent with reports for other microbialites (Desnues *et al.,* 2008), relatively few viral sequences were recovered in this study. Yet, the occurrence of phage integration and CRISPR-*cas* sequences implies that the Pavilion Lake microbialites are under selection from viral infection. It is also likely that the lack of viral sequences from freshwater microbialites in databases compromised their identification.

2.4 Conclusion

Prior to this study, it was unknown if the microbial community profile and metabolic potential of microbialites was distinct from those in neighboring environments. Hypotheses on the formation of microbialites have suggested that material from the neighboring sediments is the source of the microbialite-associated microbial community (Burne and Moore, 1987). The data presented here clearly show that the two microbial communities differ markedly. Russell *et al.* (2014) also found taxonomically distinct microbial communities in non-lithifying soft-mat biofilms and microbialites in Pavilion Lake. As well, metagenomic analysis of marine microbialites in Highbourne Cay showed distinctly different communities associated with lithifying and non-lithifying microbial mats (Khodadad and Foster, 2012).

While differences among the Pavilion Lake metagenomes can be attributed to differing selection pressures among environments, the microbialite community is likely composed of taxa essential for microbialite growth, as well as opportunists taking advantage of nutrients and the matrix supplied by filamentous cyanobacterial mats. Isotopic data suggests that Pavilion Lake

microbialites are formed by photosynthetic influences (Brady *et al.*, 2010, 2013), however, our data suggest that photosynthetic gene presence is quite low. The microbialite community is dominated by filamentous cyanobacteria, proteobacteria and acidobacteria, all of which include phototrophs that may contribute to precipitation of carbonate.

Unlike other microbialites, those in Pavilion Lake are enriched for pathways that include heavy-metal and antibiotic resistance, as well as primary alcohol fermentation. These pathways are associated with members of the *Proteobacteria*, which are numerically dominant, likely convey resistance to toxins and heavy metals, and may influence carbonate formation through photosynthesis and urea metabolism. Omelon *et al.* (2013) suggested that heterotrophs contribute to the lifthification of thrombolites in Pavilion Lake by triggering additional carbonate precipitation, a hypothesis supported here by evidence for urealytic metabolism and dissimilatory sulfate reduction, which has not been reported previously in microbialites.

The prevalence of CRISPR-*cas* systems and phage excision genes imply that the microbialites are under continuous selective pressure from viral infection. In particular, the presence of CRISPRs assigned to taxa that precipitate carbonates (*Cyanobacteria*, *Deltaproteobacteria* and *Firmicutes*) suggest that viruses play an important role in the microbialite communities in Pavilion Lake.

2.5 **Tables and figures**

Table 2.1: Pavilion Lake metagenome assembly statistics

	Microbialites				Water			Sediments*		
Depth	10 m	20 m	25 m	45 m	Sfc**	20 m	25 m	10 m	20 m	25 m
# Contigs or Reads	510,415	881,449	499,134	179,215	43,909	19,977	32,086	120,680	544,185	94,150
Total Length (Bp)	115,196,707	178,186,326	111,159,198	41,483,863	8,537,385	3,836,213	5,930,888	12,560,841	61,059,259	10,421,166
N50 >500bp	647	752	717	668	649	734	608	(-)	(-)	(-)
Avg >500bp	721	783	760	736	776	753	644	(-)	(-)	(-)
Med >500bp	571	633	616	621	524	670	575	(-)	(-)	(-)
Largest (Bp)	3882	6079	2965	1964	7125	4003	1880	190	190	190
G+C%	60.8	57.9	60.1	60.3	47	52.8	52.6	59.6	57.7	52.2

*Not assembled reads only
**Sfc: surface water filter (1 to 10 m) (-) not available.

Table 2.2: Taxonomic classes (RefSeq) that are overrepresented in microbialites relative to the surrounding environment as determined by ANOVA using STAMP

Bacteria	p-val (corr)	Effect size	Water: Avg Rfreq (%)	Water: SD (%)	MB: Avg Rfreq. (%)	MB: SD (%)	Sed:Avg Rfreq. (%)	Sed: SD (%)
Acidobacteriia	1.96E-003	0.889	0.314	0.164	0.839	0.139	0.000	0.000
Acidobacteria (Unclass)	8.34E-005	0.972	0.096	0.053	0.849	0.094	0.000	0.000
Alphaproteobacteria	4.52E-004	0.947	7.078	0.266	19.768	2.196	2.679	2.008
Chloroflexi (class)	9.30E-005	0.973	0.449	0.142	1.481	0.116	0.000	0.000
Deferribacteres (class)	1.13E-003	0.917	0.059	0.014	0.117	0.020	0.000	0.000
Deinococci	1.82E-003	0.892	0.335	0.131	0.613	0.081	0.000	0.000
Deltaproteobacteria	1.81E-004	0.961	2.151	0.933	7.850	0.448	0.398	0.563
Gemmatimonadetes	1.39E-003	0.904	0.208	0.160	0.797	0.114	0.000	0.000
Gloeobacteria	7.68E-005	0.972	0.056	0.038	0.360	0.030	0.000	0.000
Ktedonobacteria	1.49E-003	0.900	0.076	0.042	0.310	0.062	0.000	0.000
Solibacteres	1.16E-004	0.973	0.386	0.279	3.346	0.331	0.000	0.000
Thermomicrobia (class)	1.44E-003	0.905	0.058	0.030	0.481	0.111	0.000	0.000
Thermotogae (class)	5.03E-003	0.845	0.044	0.023	0.138	0.006	0.023	0.033
Archaea	p-val (corr)	Effect size	Water: Avg Rfreq (%)	Water: SD (%)	MB: Avg Rfreq. (%)	MB: SD (%)	Sed: Avg Rfreq. (%)	Sed: SD (%)
Euryarchaeota (unclass)	8.67E-004	0.928	0.010	0.007	0.039	0.004	0.000	0.000
Halobacteria	8.11E-004	0.931	0.043	0.017	0.172	0.029	0.000	0.000
Korarchaeota (Unclass)	4.49E-004	0.945	0.000	0.000	0.009	0.002	0.000	0.000
Methanomicrobia	4.79E-004	0.943	0.062	0.036	0.312	0.044	0.000	0.000
Methanopyri	3.85E-003	0.860	0.000	0.000	0.005	0.002	0.000	0.000
Thermococci	2.64E-003	0.877	0.014	0.013	0.051	0.007	0.000	0.000
Thermoplasmata	3.70E-003	0.863	0.002	0.003	0.012	0.003	0.000	0.000

Avg Rfreq: Average relative frequency. SD: Standard Deviation. p-val corr: p-value ANOVA corrected by Benjamini-Hochberg FDR (false discovery rate).
Unclass: Unclassified. MB: Microbialite. Sed: Sediment.

Table 2.3: Functional annotations (SEED subsystem level I) that are overrepresented in microbialites relative to the surrounding environment as determined by ANOVA using STAMP

	P-val (corr)	Effect Size	Water:Avg Rfeq (%)	Water: SD (%)	MB:Avg Rfeq (%)	MB: SD (%)	Sed:Avg Rfeq (%)	Sed: SD (%)
Membrane Transport	8.12E-003	0.793	1.998	0.157	2.514	0.112	0.941	0.577
Metabolism of Aromatics	3.00E-004	0.934	1.270	0.074	1.775	0.111	0.872	0.109
Motility and Chemotaxis	3.60E-002	0.649	0.606	0.025	1.063	0.039	0.454	0.356
Potassium metabolism	6.40E-003	0.810	0.182	0.035	0.296	0.013	0.084	0.068
Regulation and Cell signaling	1.82E-003	0.874	1.090	0.028	1.506	0.079	0.978	0.133
Virulence, Disease and Defense	3.45E-004	0.928	2.069	0.195	2.997	0.057	1.167	0.327

Avg Rfreq: Average relative frequency. SD: Standard Deviation. p-val corr: p-value p-value ANOVA corrected by Benjamini-Hochberg FDR (false discovery rate).
MB: Microbialite. Sed: Sediment.

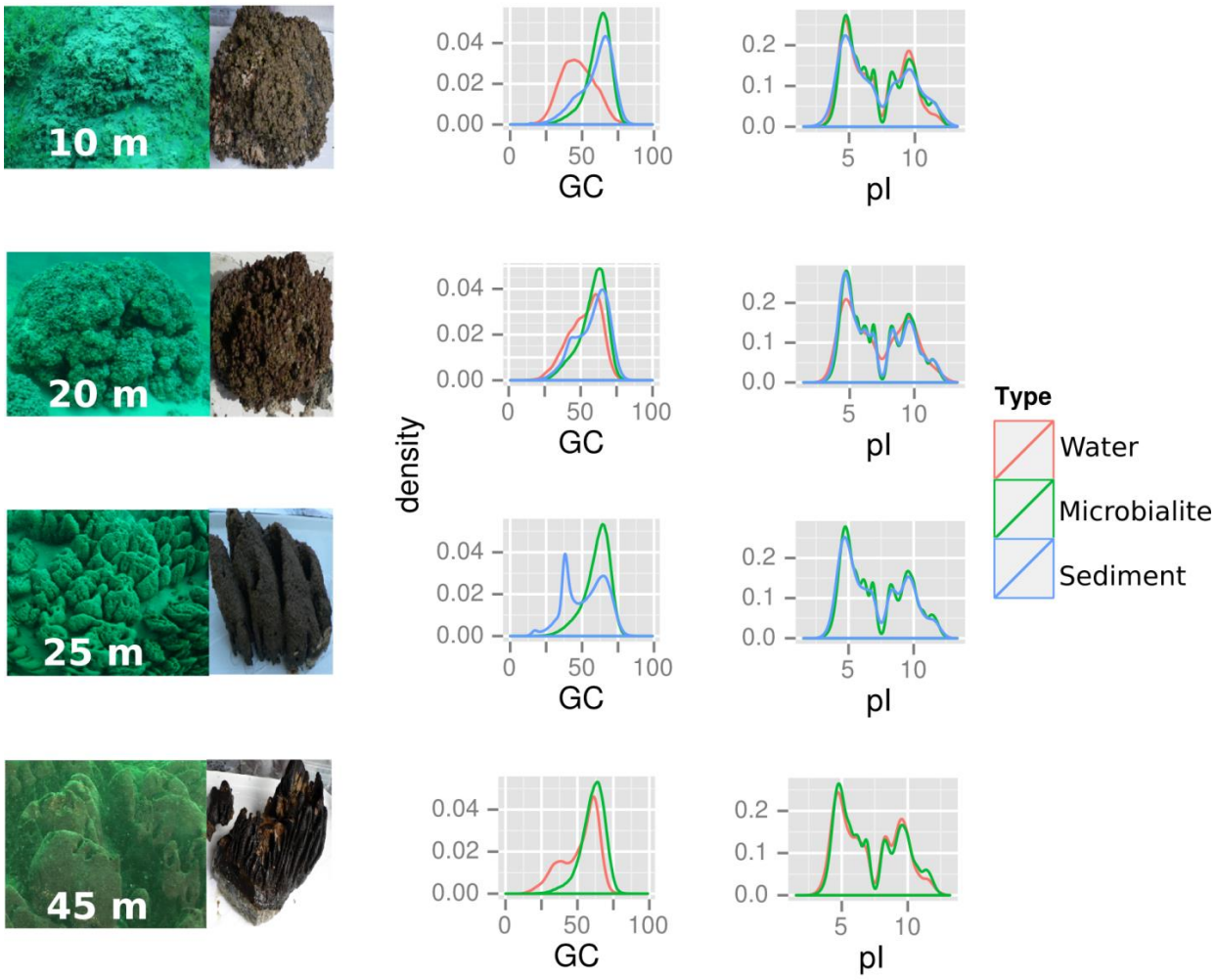

Figure 2.1: Pavilion Lake microbialite morphology with GC content and protein isoelectric points (pI)
Data for GC content and pI for water at 25 m and the sediment at 45 m were not available for comparison.

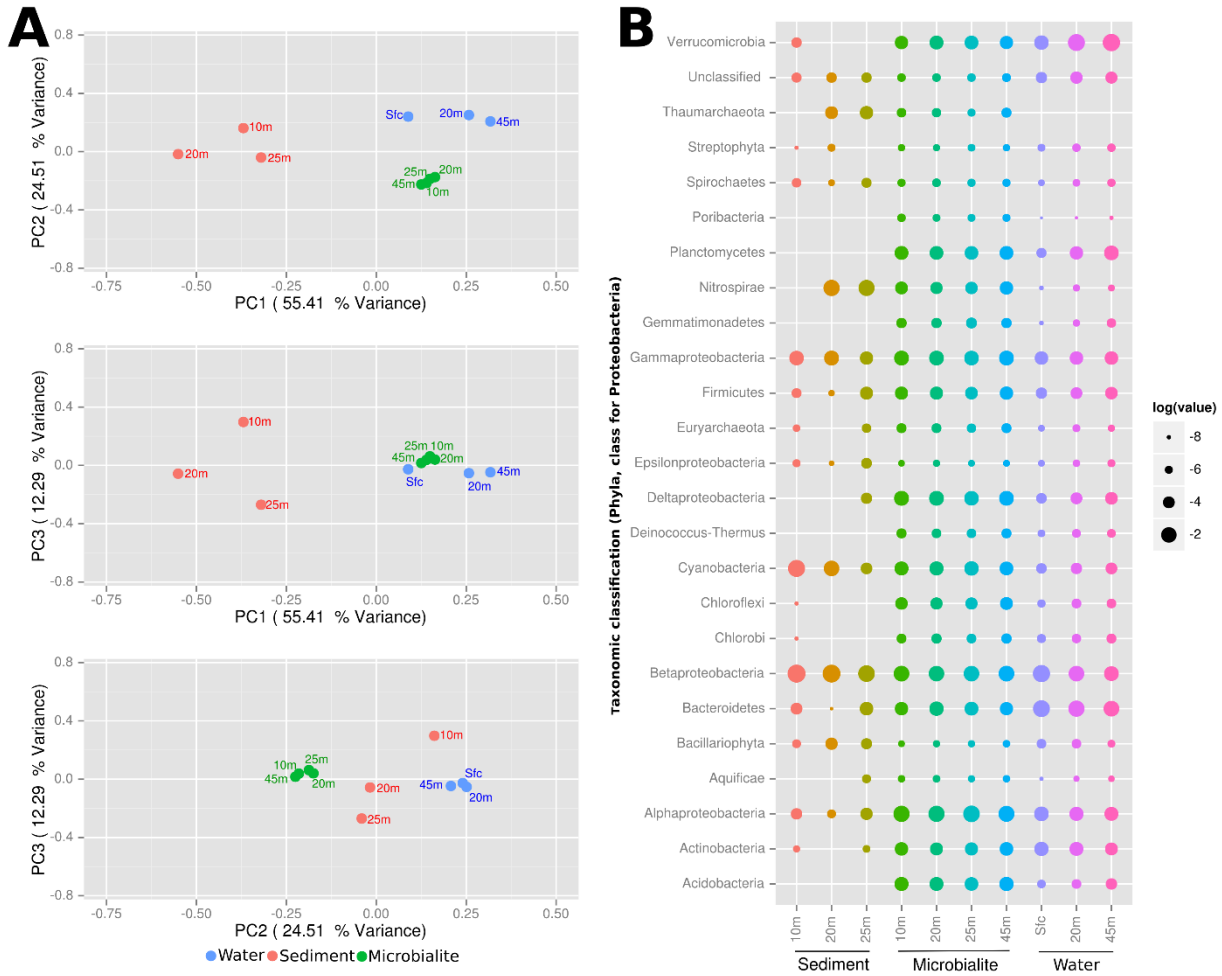

Figure 2.2: Pavilion Lake microbial community composition
(A) PCA plot of the normalized top 25 RefSeq classifications. Clustering was done using a ward matrix and Bray-Curtis distance cut-offs, bootstrapped with one thousand replicates.
(B) Dotplot of the normalized RefSeq classifications (top 25) in log relative abundances.

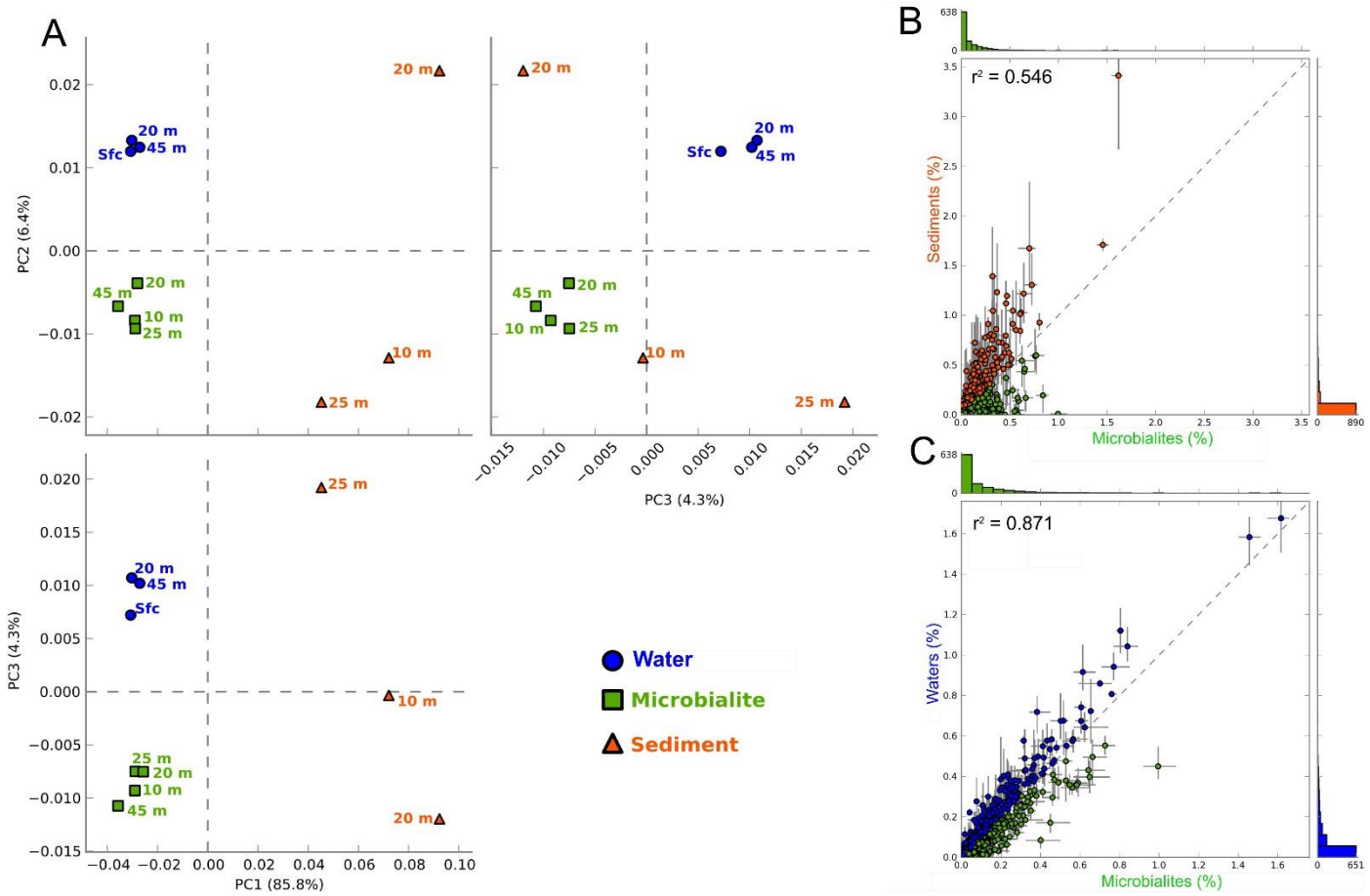

Figure 2.3: PCA and scatter plots using SEED subsystems based on ANOVA in STAMP for Pavilion Lake metagenomes
(A) PCA plot (multiple groups, subsystem level II)
(B) Scatter plot microbialites vs sediments (SEED subsystems level III).
(C) Scatter plot microbialites vs water filter (SEED subsystems level III).
For scatter plots only, each dot represents a single functional gene.

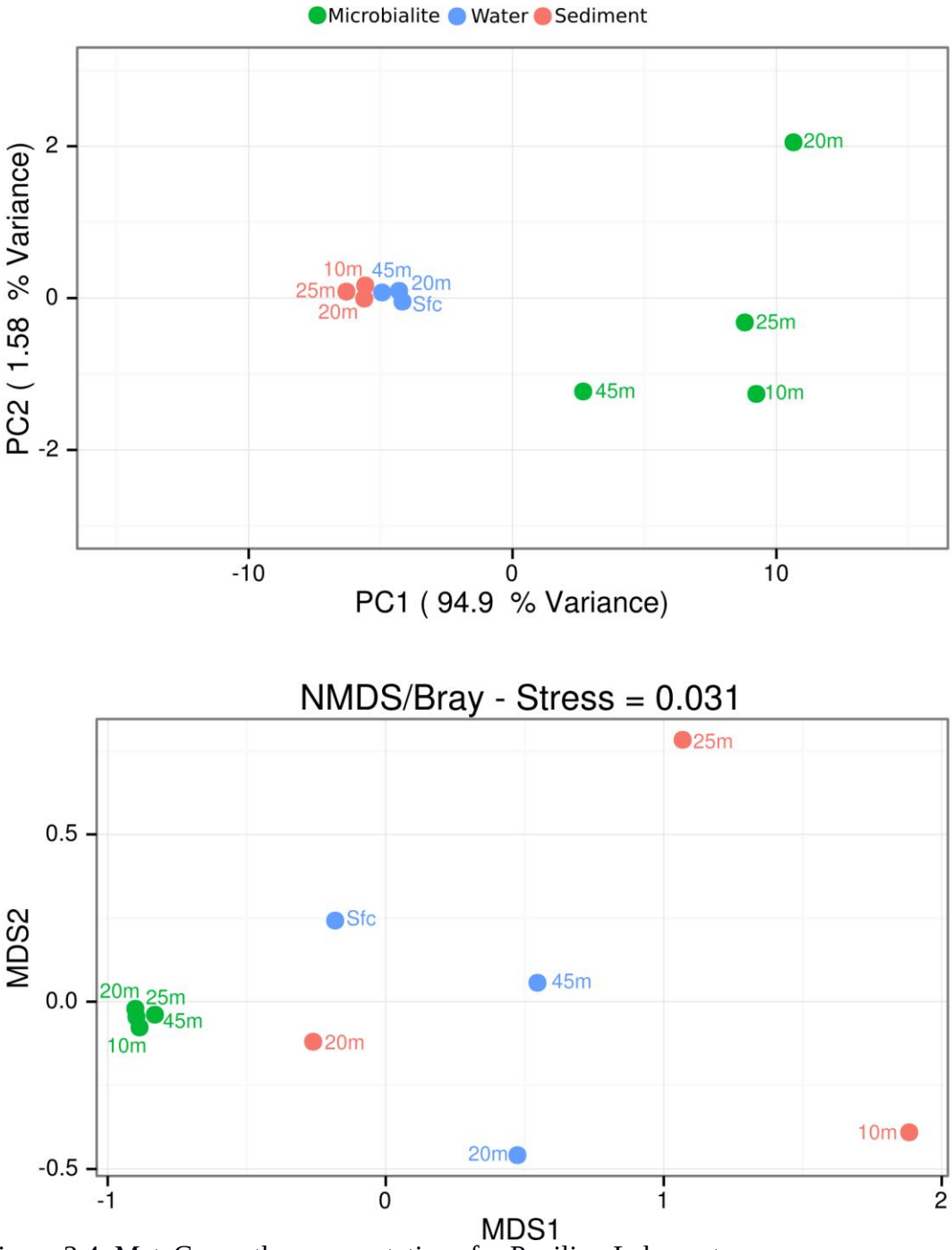

Figure 2.4: MetaCyc pathway annotations for Pavilion Lake metagenomes
(Top) PCA by ward clustering followed by bootstrapping of thousand replicates using Bray-Curtis distance metric.
(Bottom) NMDS by ward clustering followed by bootstrapping of thousand replicates using Bray-Curtis distance metric.

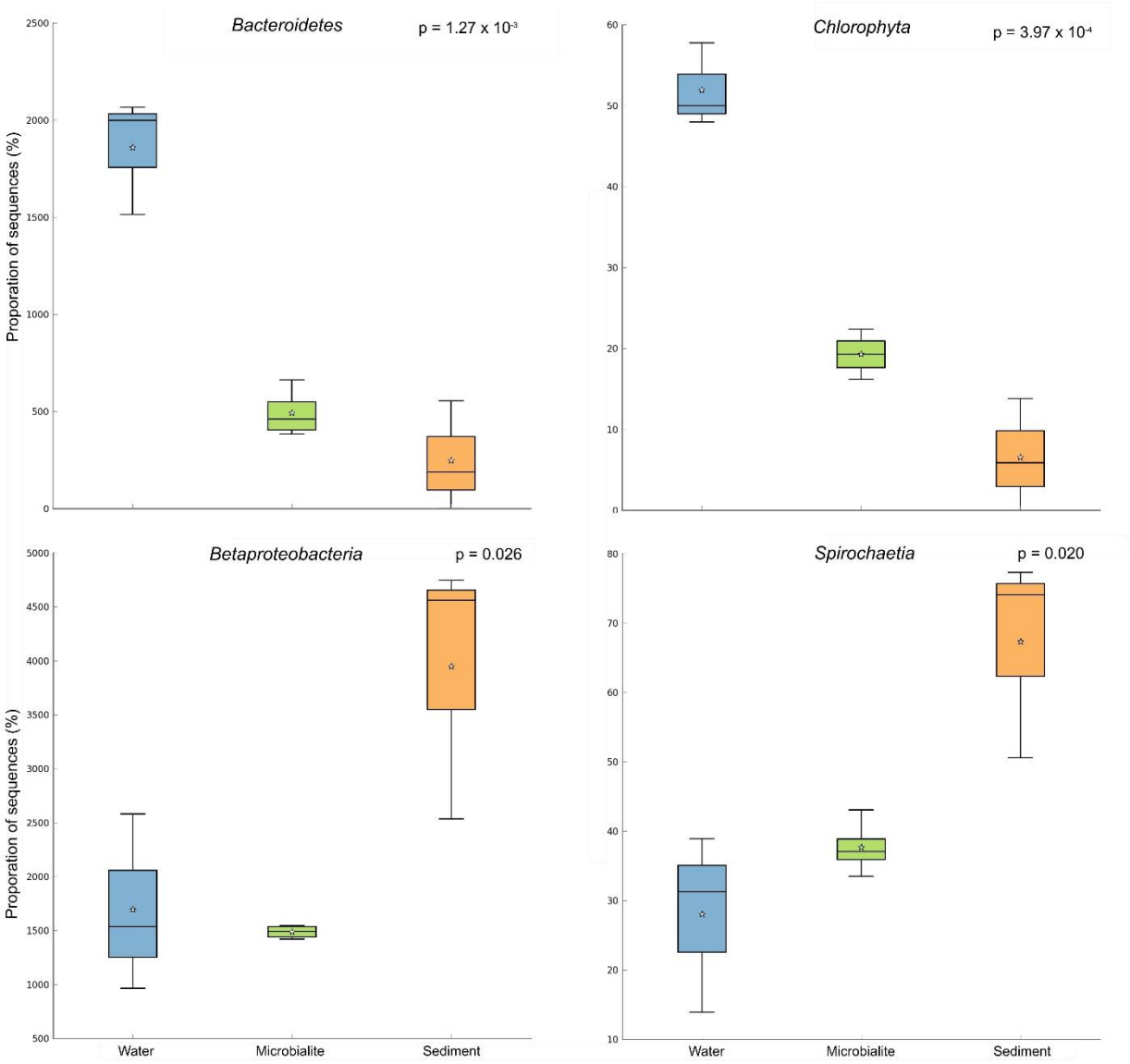

Figure 2.5: Box and whisker plots for significant taxa represented in water filters and sediments by RefSeq classification using ANOVA in STAMP based on multiple groups

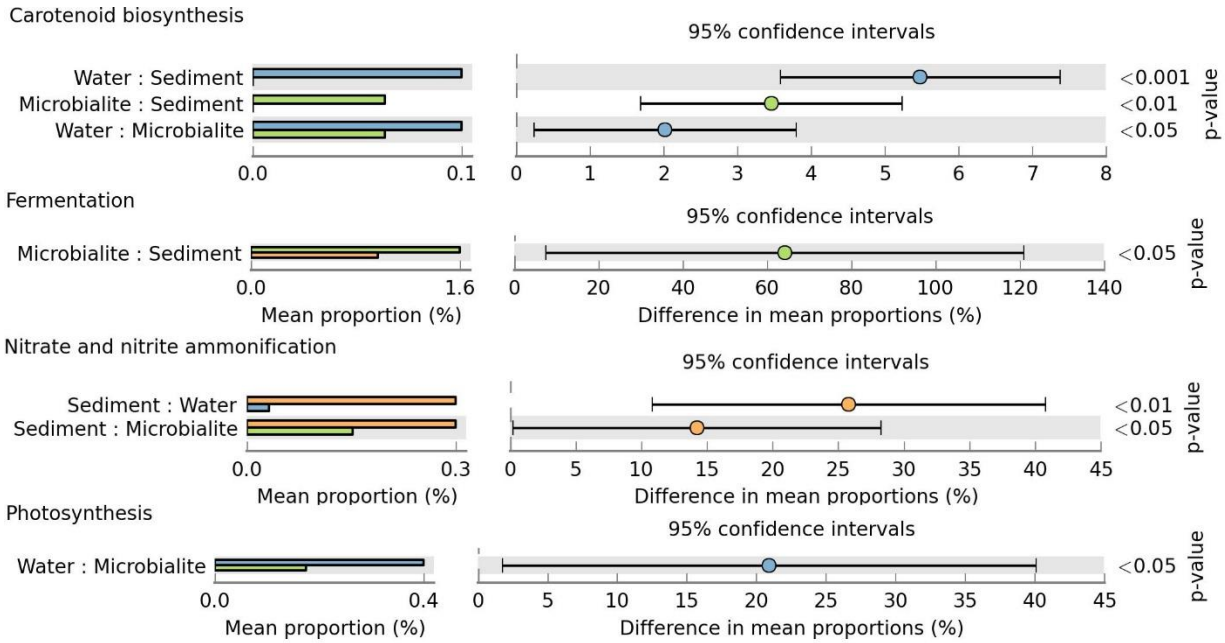

Figure 2.6: Post-havoc confidence interval plots functional classification for represented metabolic potential in surrounding environment (water filters and sediments)
SEED subsystems classifications are based on ANOVA in STAMP based on multiple groups. Microbialites are labeled in green, followed by sediments in orange and water in blue.

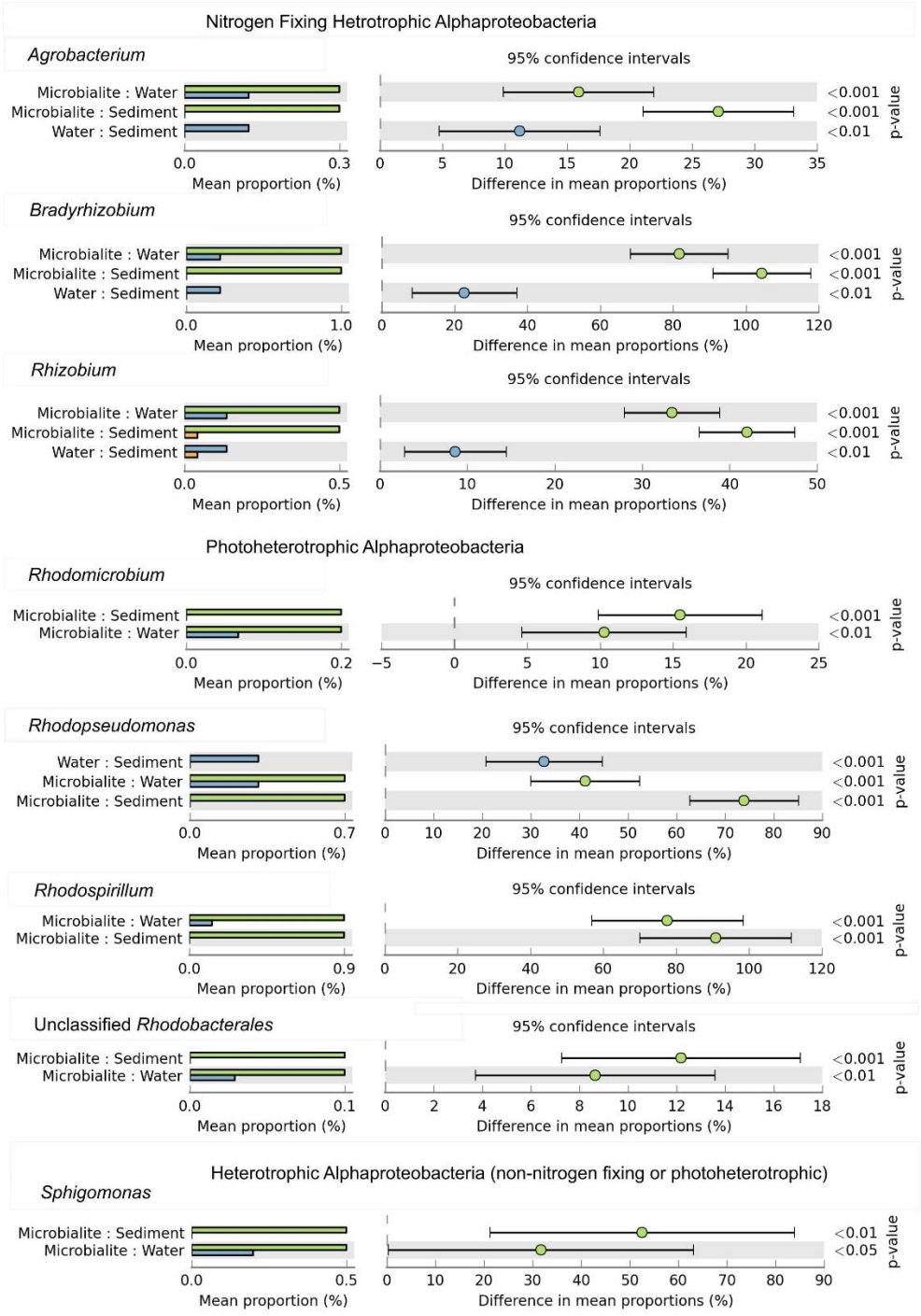

Figure 2.7: Post-havoc confidence interval plots for *Alphaproteobacteria* using RefSeq classification

Based on ANOVA in STAMP for significant genus-level members using multiple groups. Microbialites are labeled in green, followed by sediments in orange and water in blue.

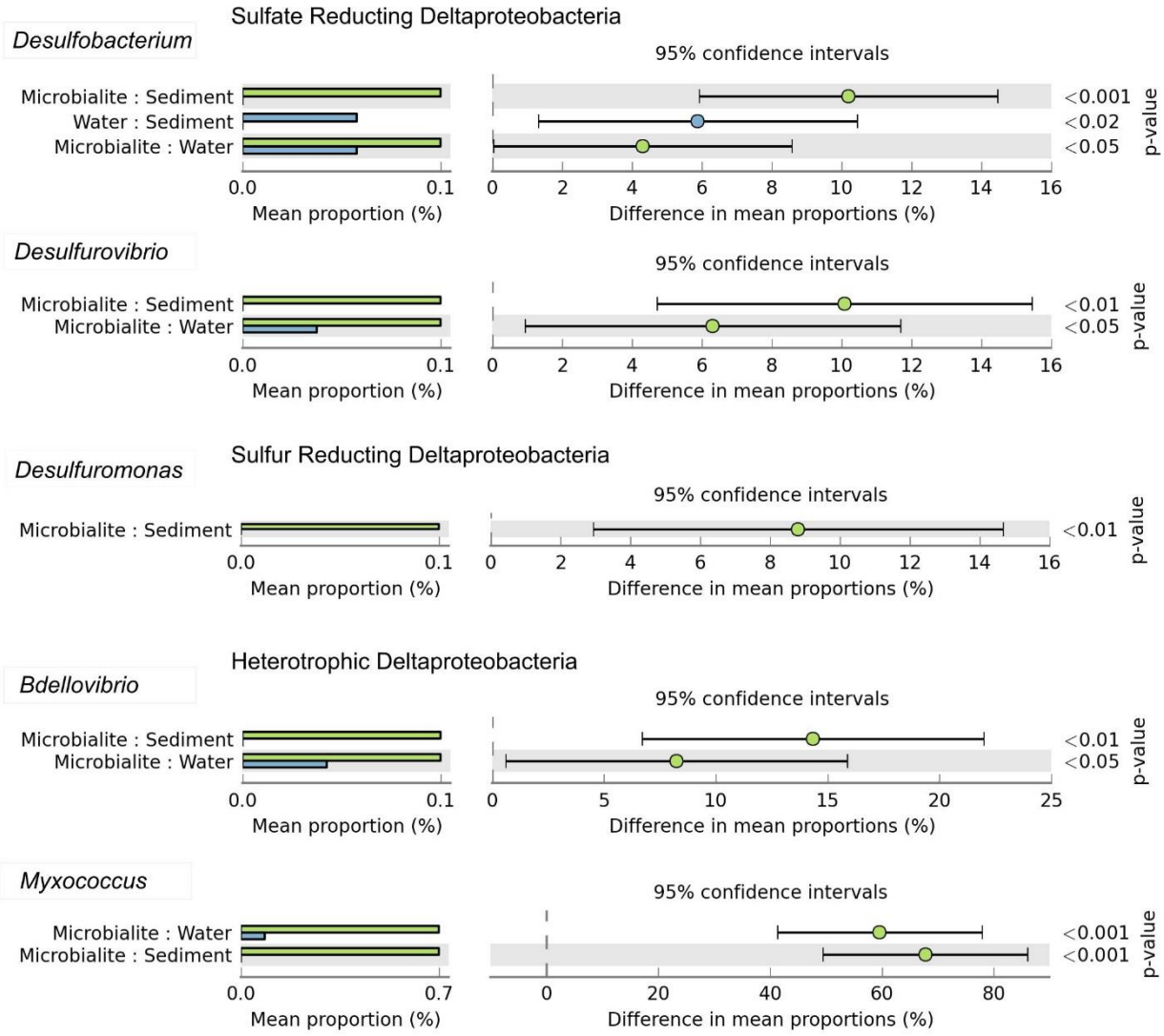

Figure 2.8: Post-havoc confidence interval plots for *Deltaproteobacteria* using RefSeq classification

Based on ANOVA in STAMP for significant genus-level members represented in Pavilion Lake metagenomes (microbialite, water filter and sediment) using multiple groups. Microbialites are labeled in green, followed by sediments in orange and water in blue.

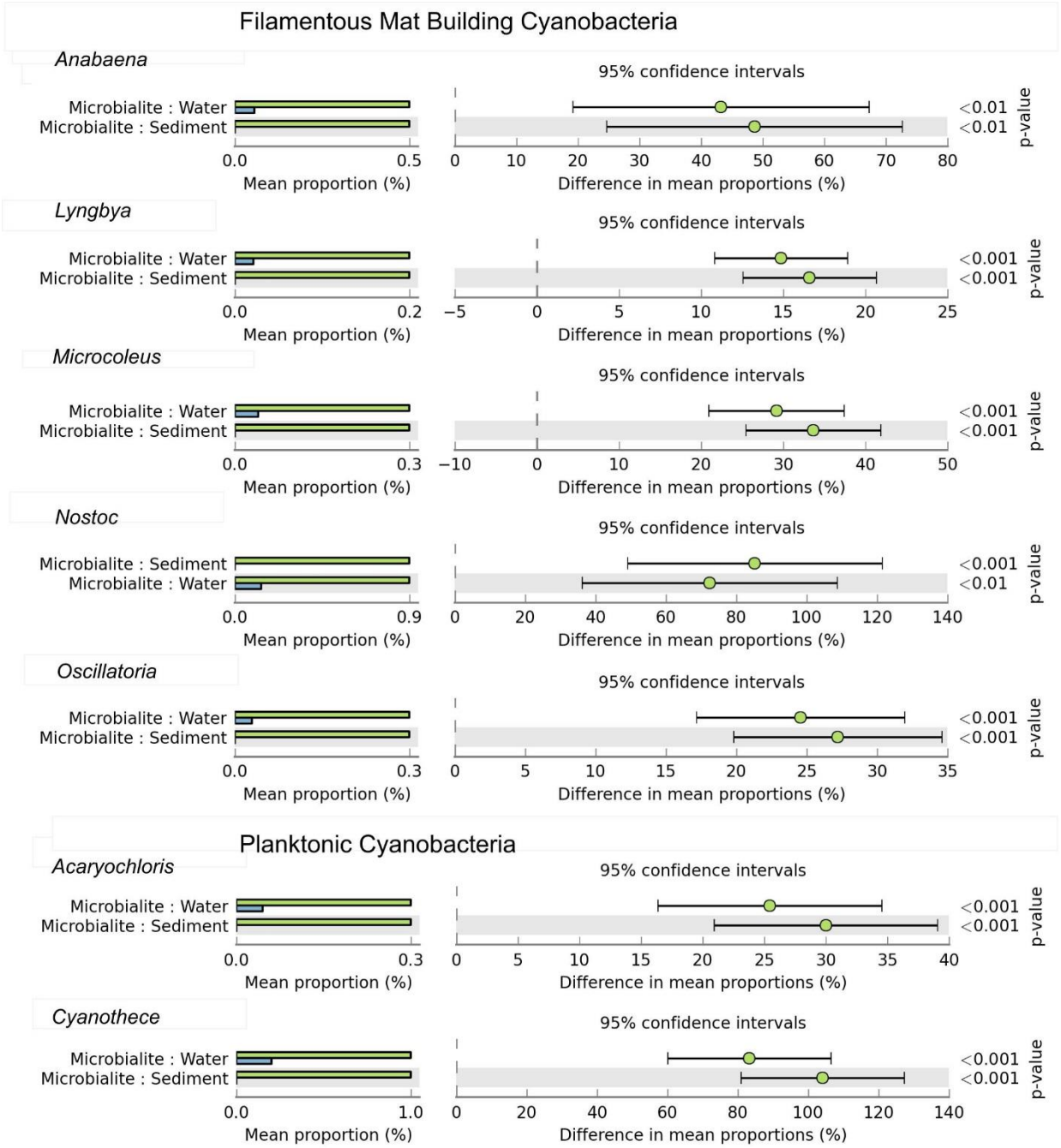

Figure 2.9: Post-havoc confidence interval plots for *Cyanobacteria* using RefSeq classification Based on ANOVA in STAMP for significant genus-level members represented in Pavilion Lake metagenomes (microbialite, water filter and sediment) using multiple groups. Microbialites are labeled in green, followed by sediments in orange and water in blue.

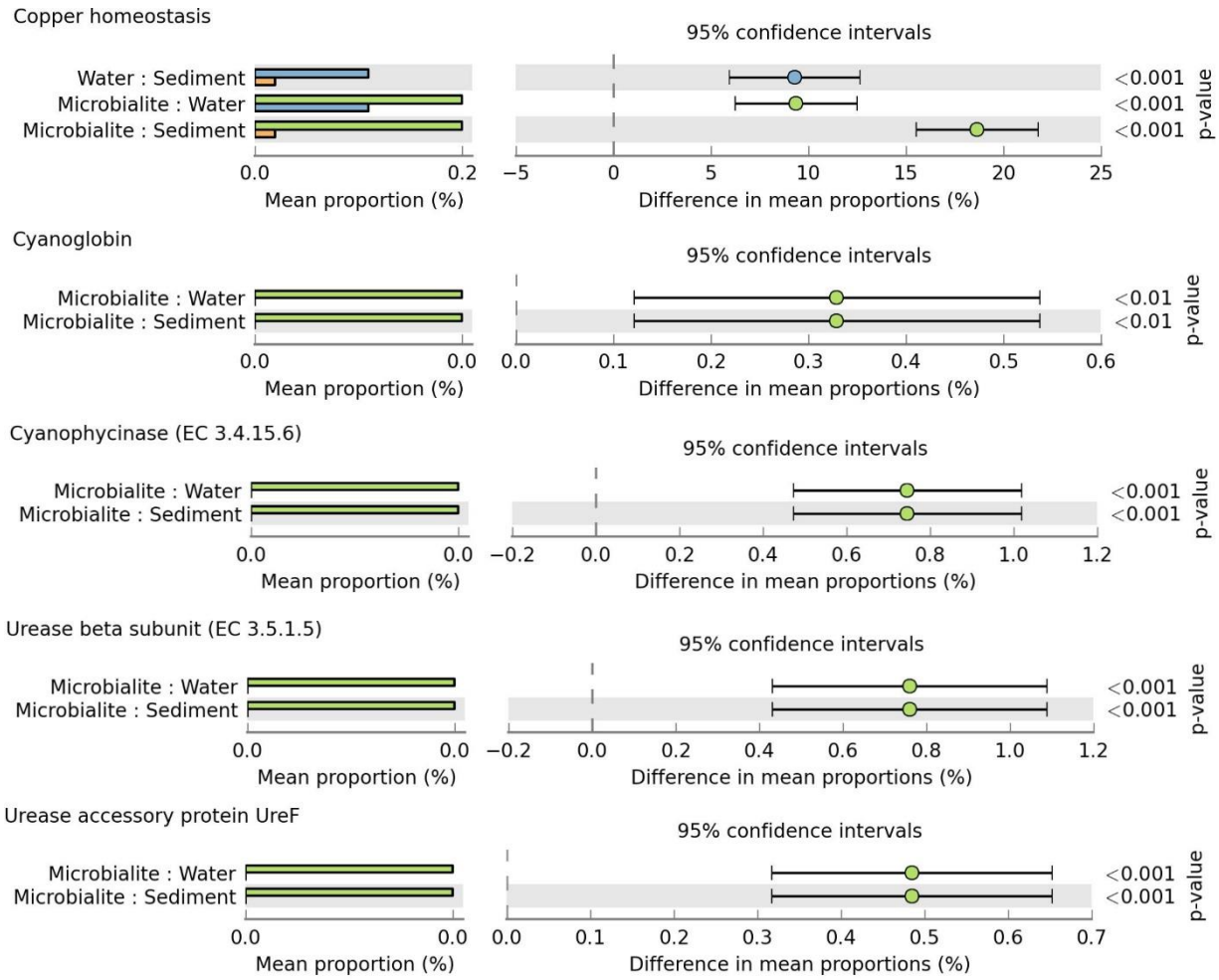

Figure 2.10: Post-havoc confidence interval plots for cyanobacterial based functional genes using SEED subsystem classification and urealytic pathways
Based on ANOVA in STAMP for significant functional classifications represented in Pavilion Lake metagenomes (microbialite, water filter and sediment) using multiple groups.
The urealytic genes are for general presence in the metagenomes and are not cyanobacterial specific. Microbialites are labeled in green, followed by sediments in orange and water in blue.

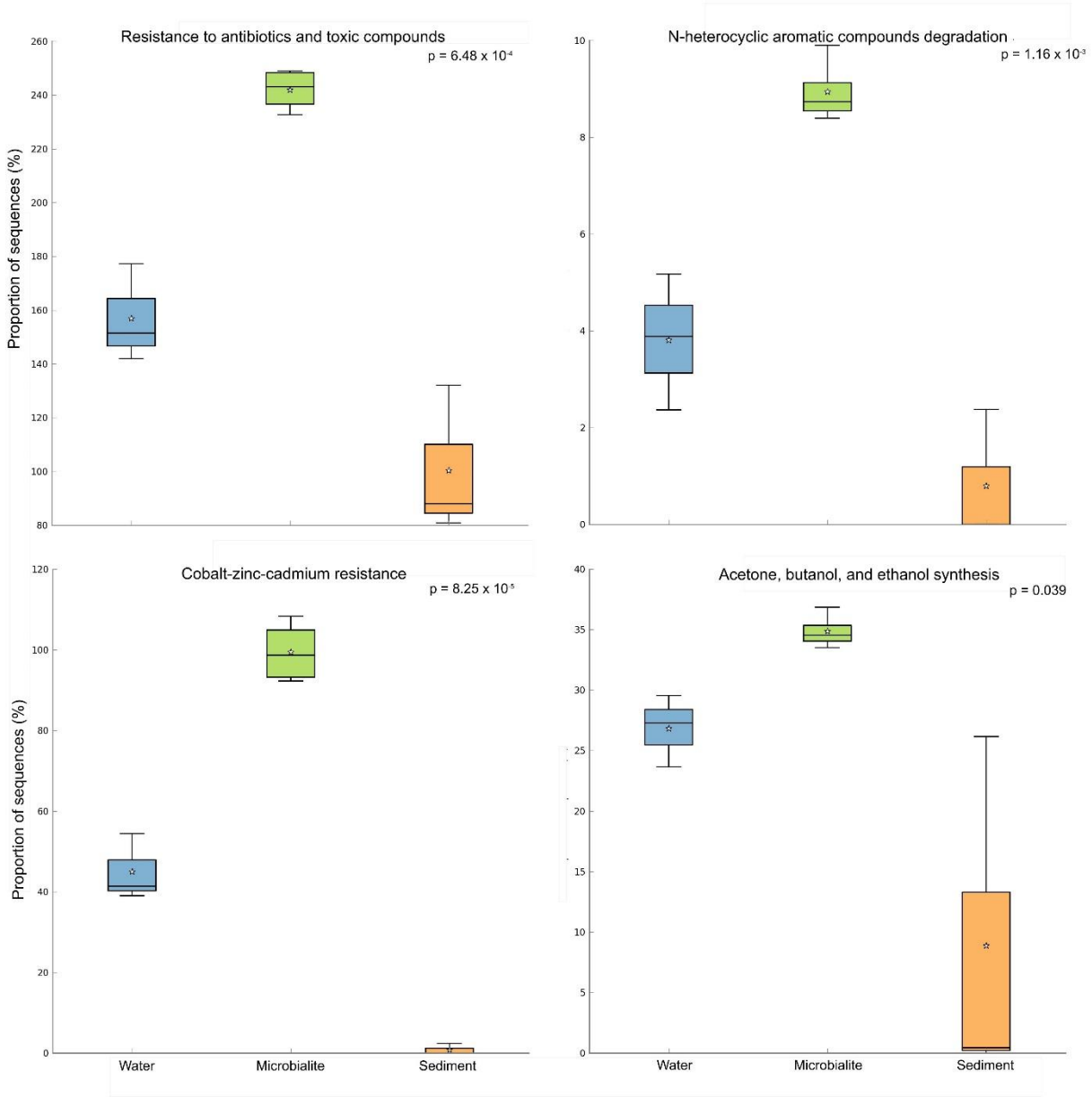

Figure 2.11: Box and whisker plots for novel functional classifications (SEED subsystem) represented in microbialites based on ANOVA in STAMP using multiple groups

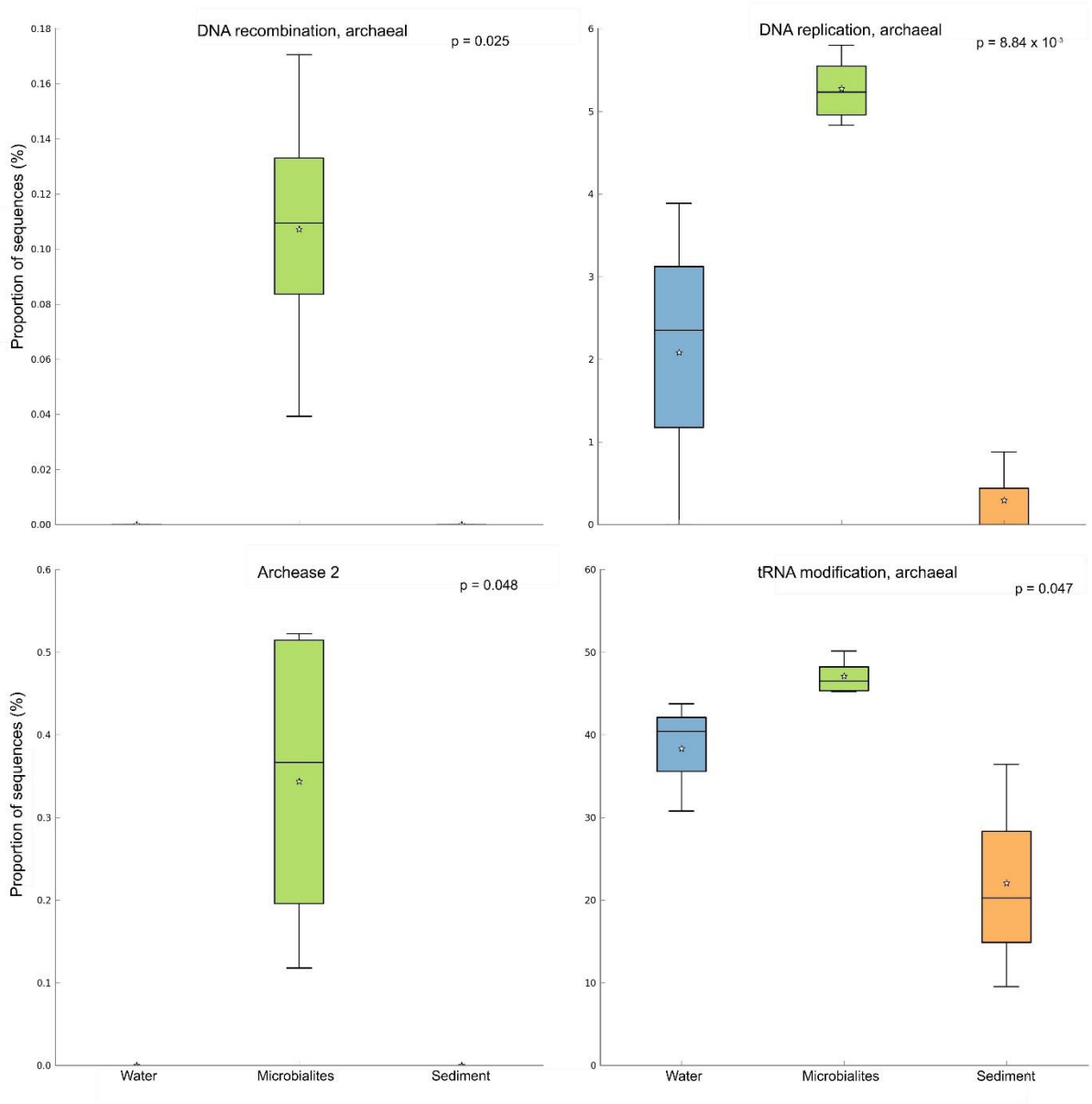

Figure 2.12: Box and whisker plots for novel Archael based functional classifications (SEED subsystem) represented in microbialites based ANOVA in STAMP using multiple groups

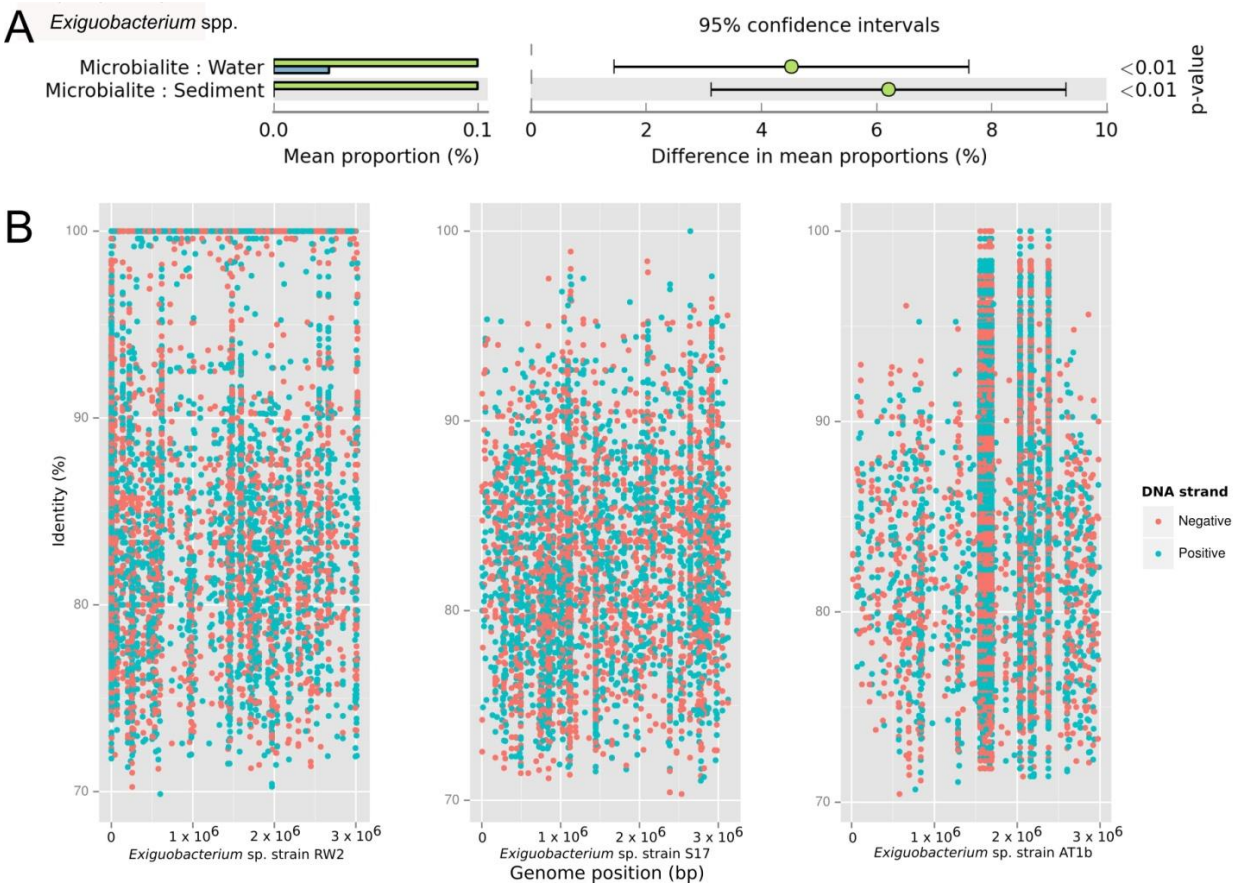

Figure 2.13: *Exiguobacterium* presence in Pavilion Lake microbialite metagenome

A) *Exiguobacterium* post-havoc confidence interval plots (0.95) based on ANOVA parameters for novel metabolic potential differences for microbialites and surrounding environment using multiple groups in STAMP.

B) Metagenomic recruitment plot of Pavilion lake 20 m microbialite reads (~7.5 Million) to three *Exiguobacterium* genetically related to *Exiguobacterium* sp. strain RW2 (minimum identity >70% and an E-value >$1e^{-5}$).

**Exiguobacterium* sp. strain RW2 was isolated from a microbialite at 20 m (White 3rd *et al.*, 2013b).

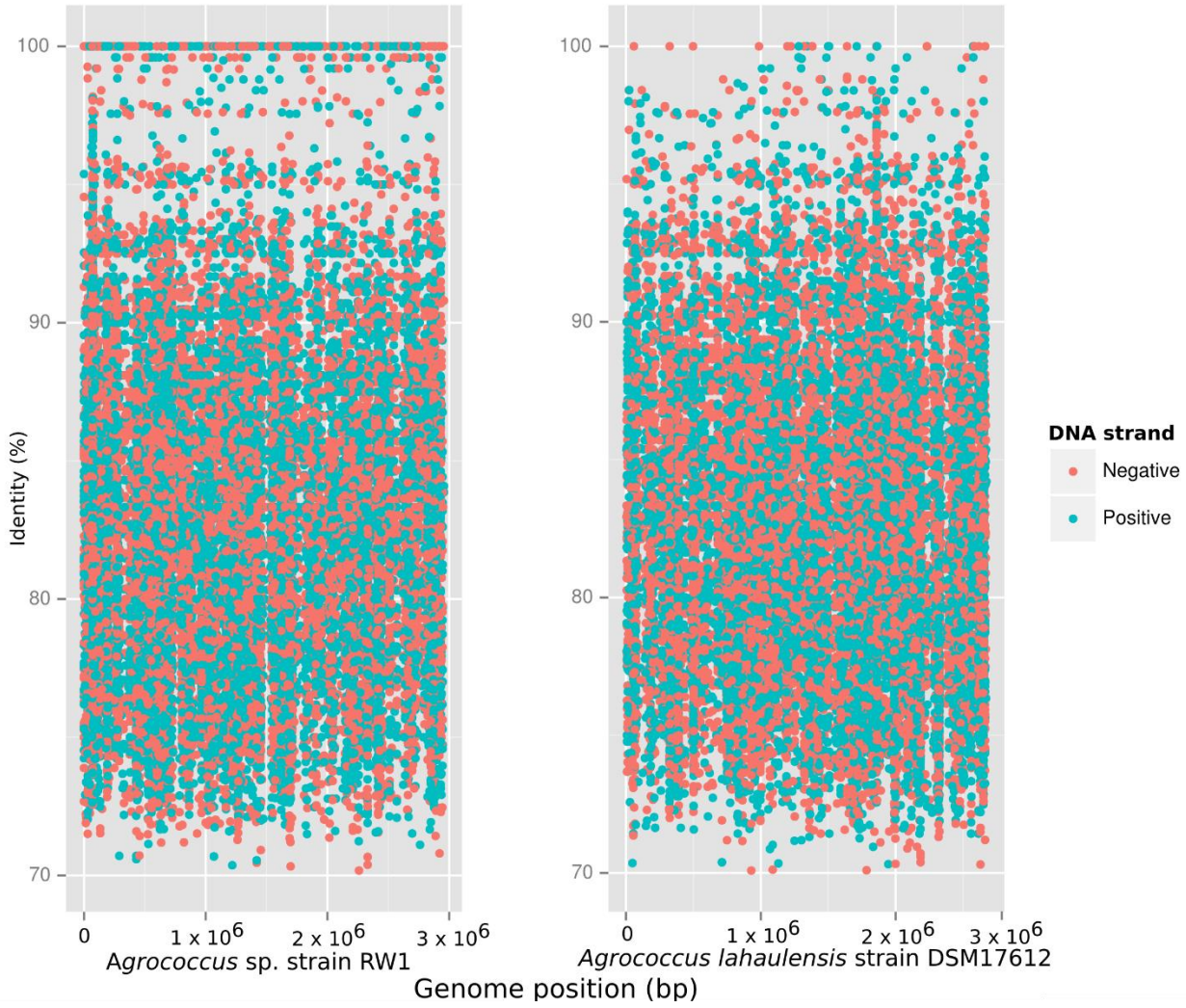

Figure 2.14: Metagenomic recruitment plot for Pavilion Lake microbialite against *Agrococcus*

FR-Hit recruitment plot of Pavilion lake 20 m microbialite reads (~7.5 Million) to *Agrococcus* sp. strain RW1 and to *Agrococcus lahaulensis* strain DSM17612 (Minimum identity >70% and an E-value >$1e^{-5}$).

* *Agro*coccus sp. strain RW1 was isolated from a microbialite at 20 m (White 3rd *et al.*, 2013a).

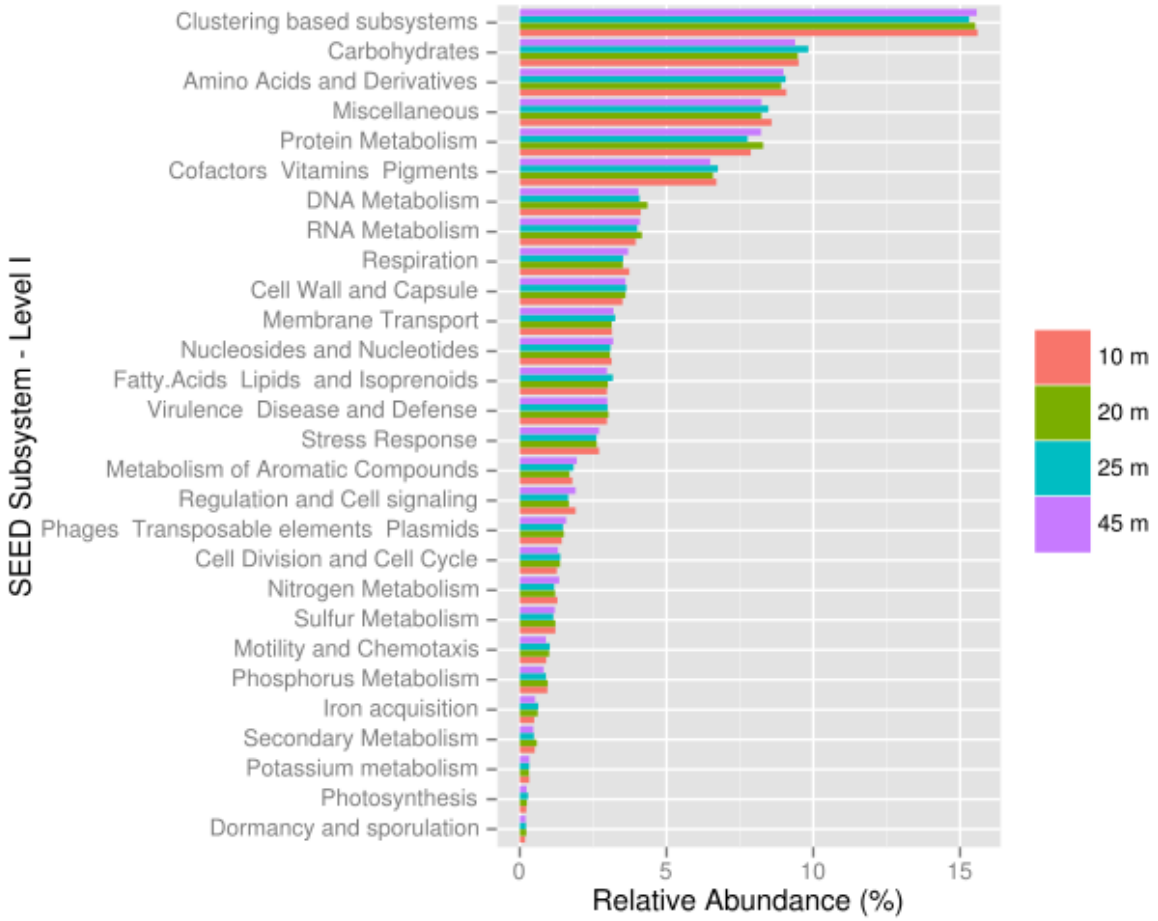

Figure 2.15: Microbialite metagenome functional annotation ranking using SEED subsystem (Level I)
Microbialite metagenomes are listed as a function of depth (m).

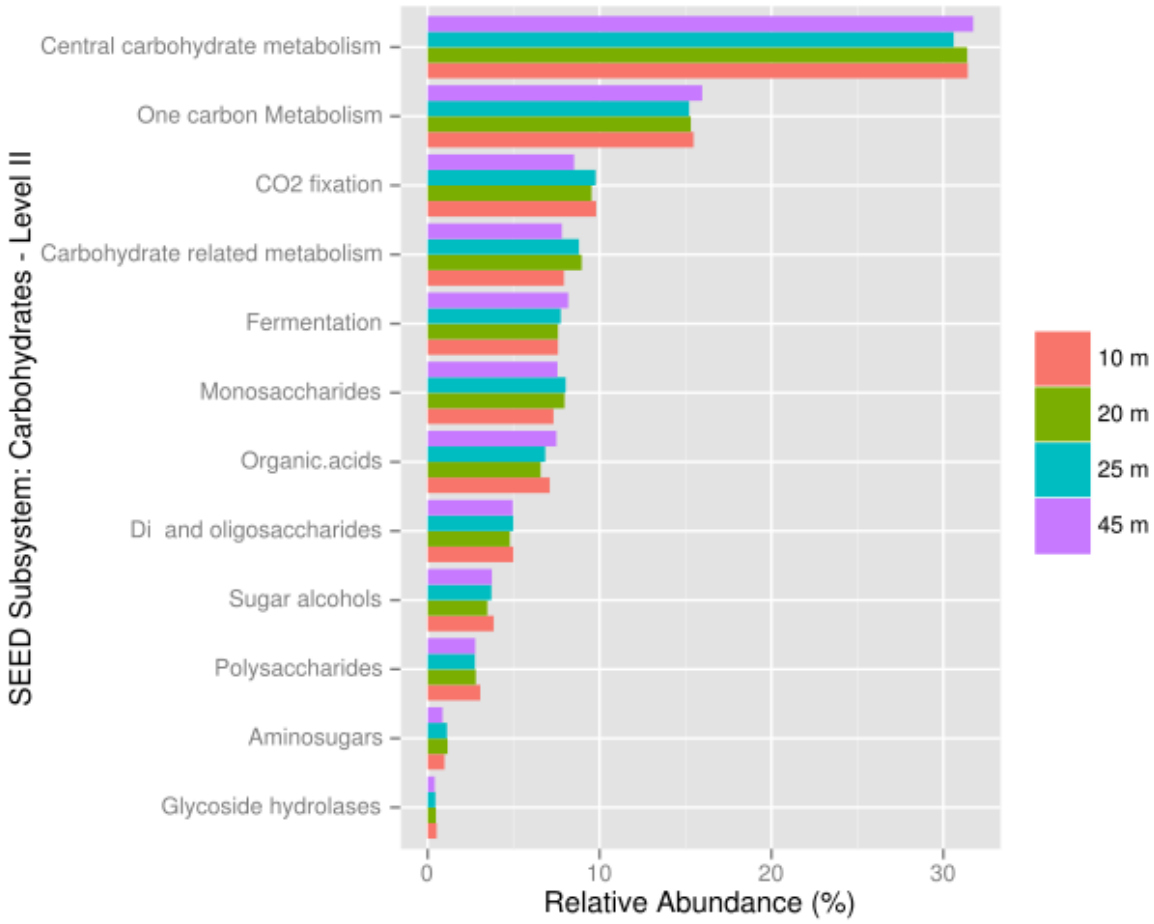

Figure 2.16: Microbialite metagenome carbohydrate related SEED subsystem (Level II) functional annotations
Microbialite metagenomes are listed as a function of depth (m).

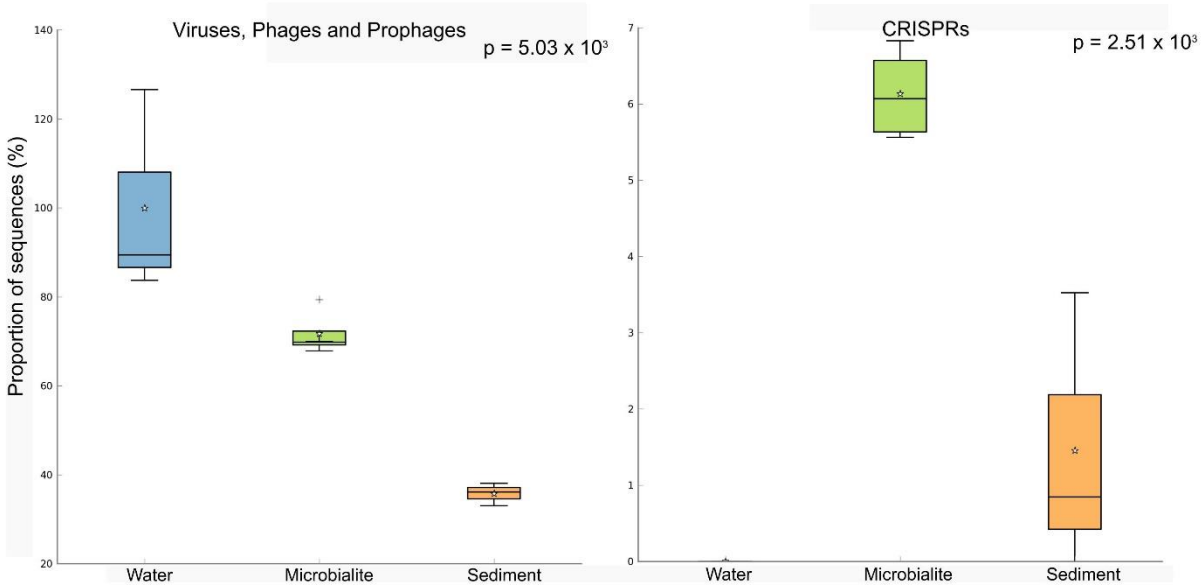

Figure 2.17: Box and whisker plots for viruses and CRISPRs in Pavilion Lake RefSeq and SEED subsystem represented in microbialites based on ANOVA in STAMP using multiple groups

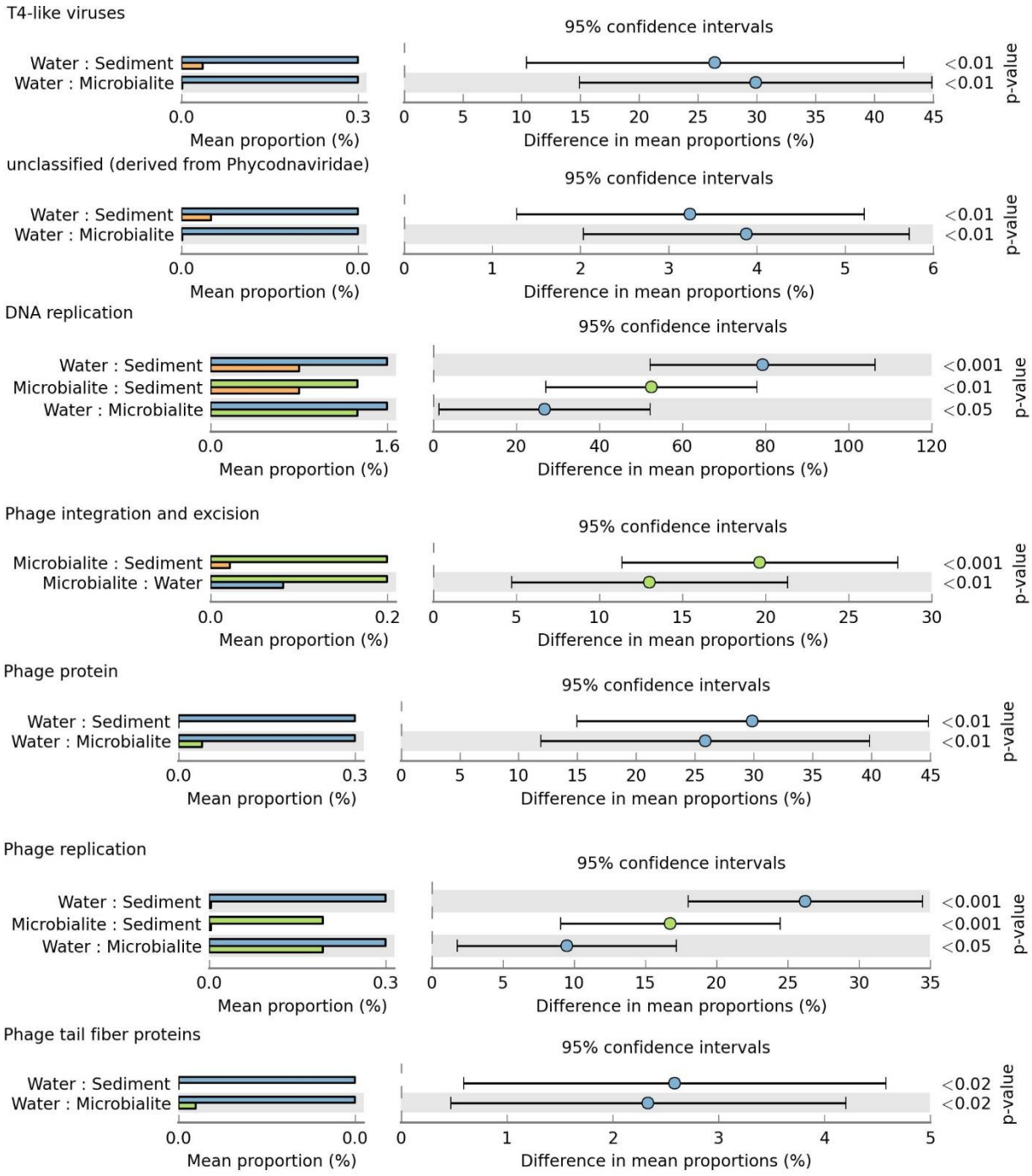

Figure 2.18: Post-havoc confidence interval plots for viral taxa using RefSeq and viral specific functional genes in SEED
Based on ANOVA in STAMP for genus-level and functional gene-level classifications that were statistically significant by analysis using multiple groups.

Chapter 3:

Comparative analysis of microbiome of rapidly forming modern microbialites from the Canadian Yukon

3.1 Introduction

The extent to which microbialite communities are similar or different from surrounding sediments and waters remains unresolved due to a limited number of comparative sampling efforts. Sampling surrounding sediments and waters provide the environmental context needed to better constrain the study of common and unique aspects of microbialite community structure and function. This information may be used to uncover conserved patterns of microbial community assembly and the metabolic pathways mediating microbialate formation under different environmental conditions.

Freshwater microbialites from the Clinton Creek mine tailings pond located in Yukon Territory manifest a rapid growth rate allowing study of the interplay between the biotic and abiotic factors driving microbialite formation on a human time-scale. Clinton Creek microbialites have an estimated maximum accretion rate of ~5 mm per year (Power *et al.*, 2011a), more than ten times faster than other modern microbialite-forming ecosystems, including Highbourne Cay (~0.33 mm per year) (Planavsky and Ginsburg, 2009) and Pavilion Lake (0.05 mm per year) (Brady *et al.*, 2009).

Here we use a metagenomic approach to explore the community structure and metabolic potential of Clinton Creek microbialites in relation to those in the adjacent sediments in an effort to better understand the metabolic drivers of rapid growth in this freshwater ecosystem. We focus

on describing metabolic pathways mediating photosynthetic or heterotrophic carbonate precipitation and the taxonomic distribution of these pathways. We then compare the metagenomic sequence information from Clinton Creek microbialites and sediments to those in diverse non-lithifying mats, sediments, microbialites and corals, to explore whether a core community and associated functional potential can be defined for microbialites.

3.2 Materials and methods

3.2.1 Site description and water chemistry

Clinton Creek (64°26'42"N and 140°43'25"W) is a flooded and abandoned open-pit asbestos mine located in the subarctic ~77 km northwest of Dawson City, Yukon, Canada (Power *et al.,* 2011a; Figure 3.1A to B). The mine was active for eleven years until closing in 1978 (Power *et al.,* 2011a). Microbialites presumably began to form soon after the mine closed and the open-pit flooded. The photic zone likely occupies the full depth of the open-pit pond and there is minimal nutrient input, due to the lack of surrounding soil (Power *et al.,* 2011a). Sediments in the open pit are composed of quartz, muscovite, kaolinite, chrysotile, and minor amounts of aragonite and trace calcite (Power *et al.,* 2011a). The microbialites are columnar, up to 15 cm in height, and are primarily composed of aragonite with spherulitic fabric (Power *et al.,* 2011a; Figure 3.1D). The open pit water is subsaline (>3.0 g L^{-1}), oligotrophic (undetectable phosphate), and alkaline in pH (8.4); the distribution of cation concentrations are Mg^{2+} >> Ca^{2+} >> Na^{+} > K^{+} > Si^{4+}, while anions concentrations are SO_4^{2-} >> dissolved inorganic carbon (DIC) > Cl^{-} (Power *et al.,* 2011a). The iron concentration in the water is very low, and phosphate is undetectable, indicating that the pond is oligotrophic, which is common in microbialite forming systems (Dupraz *et al.,* 2009; Lim

et al., 2009). The water is supersaturated with aragonite (saturation index = 0.6), the dominant mineral in the microbialites, as well as calcite [$CaCO_3$] (Power *et al.*, 2011). Aragonite will preferentially precipitate, as calcite crystal growth is inhibited at high magnesium to calcium ratios, as is the case in Clinton Creek (Power *et al.*, 2011a).

3.2.2 Sampling, DNA extraction, purity and concentration measurements

Microbialites and sediment samples and sediment samples were obtained in July 2011 and were stored at 4ºC prior to DNA extraction. Community genomic DNA was extracted from ~10 g of each of the triplicate microbialites and sediment samples using the PowerMax soil DNA isolation kit (MoBio Laboratories, Inc., Carlsbad, CA, USA), following the manufacturer's instructions. DNA concentrations were determined using a Nanodrop-3300 (ThermoFisher, Nandrop Wilmington, DE) with PicoGreen® reagent used according to the manufacturer's instructions (Invitrogen, Carlsbad, CA). The purity of extracted DNA and samples was determined by absorbance (260/280 and 260/230 ratios) using a Nanodrop-1000 (ThermoFisher, Nandrop Wilmington, DE). Genomic DNA from each replicate was pooled prior to Illumina library construction.

3.2.3 Illumina HiSeq/MiSeq library construction quality control and quantification

For Illumina library construction, DNA was sheared by ultrasonication (Covaris M220 series, Woburn, MA), and the fragments end-paired, A-tailed (Lucigen NxSeq DNA prep kit, Middleton, WI) and ligated to TruSeq adapters (IDT, Coralville, Iowa); small fragments were removed twice using magnetic beads (Beckman Coulter, Danvers, MA) (White 3rd *et al.*, 2013a-c). No PCR enrichment was used to amplify libraries to avoid PCR duplication bias.

Libraries were checked for size and adapter-dimers using a Bioanalyzer HighSens DNAchip (Agilent). Libraries were quantified using Qubit (Invitrogen, Carlsbad, CA), according to the manufacturer's instructions, by qPCR using a microfluidic digital PCR quantified standard curve (White 3rd *et al.,* 2009). The resulting libraries were pooled, and sequenced using both 250 bp and 100 bp paired-end sequencing on the Illumina MiSeq at GenoSeq UCLA Los Angeles, CA and HiSeq at McGill University/Génome Québec, CAN platforms, respectively.

3.2.4 **Analysis of Illumina sequencing data**

Raw Illumina sequencing data were screened for PhiX spike-in contaminants using Bowtie2 (version 2.1.0) which were removed using Picard tools (verison 1.90) (White 3rd and Suttle, 2013c). Reads were quality checked using FastQC, then paired-end reads were merged by FLASH (version 1.2.5) and assembled with the Ray assembler (kmer size: 39 and 55) (Boisvert *et al.,* 2010; 2012, White 3rd and Suttle, 2013c), FragGeneScan was used to predict and translate open reading frames (ORFs) of the contigs (Rho *et al.,* 2010) and ProPas (Wu e*t al.,* 2012) was used to calculate predicted protein isoelectric points (pI).

The assemblies were annotated using Metagenomic Rapid Annotations using Subsystems Technology (MG-RAST) (Meyer *et al.,* 2008). MG-RAST analysis of the contigs, used BLAT (BLAST-like Alignment Tool) annotations based on hierarchical classification against M5RNA (MG-RAST ribosomal specific database), SEED subsystems and RefSeq databases with a minimum e-value cutoff of 10^{-5}, a minimum percent identity cutoff of 60%, and a minimum alignment length cutoff of 15 base pairs. The SEED, RefSeq and M5RNA (MG-RAST rRNA database) classifications were normalized using relative count abundances for each sample. PCA

analysis for the normalized RefSeq classifications (top 25) used R libraries Ecodist (dissimilarity-based functions for ecological analysis), and pvclust (hierarchical clustering with p-values via multiscale bootstrap resampling) using ward clustering and the Bray-Curtis distance metric, with a thousand replicates (Suzuki and Shimodaira, 2006). Principal component analysis (PCA) for the normalized RefSeq classifications was plotted using R library ggplot2 (Wickham, 2009). A dotplot of the top 25 normalized RefSeq classifications was completed using R libraries Reshape2, using the melt function, and then plotted using ggplot2 (Wickham, 2009). The annotations were parsed analyzed using statistical analysis of metagenomic profiles (STAMP) (Parks and Beiko, 2010). MG-RAST annotations using SEED subsystems for Clinton Creek microbialite and sediment contigs were loaded into STAMP and compared for metabolic potential using the one-sided G-test (with Yates' + Fishers') alternative to the chi-square test, with asymptomatic confidence intervals (0.95), using the Benjamini-Hochberg FDR procedure (Parks *et al.*, 2010).

In addition to MG-RAST, metabolic pathways were predicted using MetaPathways, a modular pipeline for gene prediction and annotation that uses pathway tools and the MetaCyc database to construct environmental pathway/genome databases (ePGBDs) (Paley and Karp, 2006; Konwar *et al*., 2013; Caspi *et al.*, 2014). Metapathways uses the seed-and-extend homology search algorithm LAST (local alignment search tool) for annotations of ORFs with a minimum of 180 bp and minimum alignment length cutoff of 50 bp (Kiełbasa *et al.*, 2011). Venn diagrams were constructed from predicted MetaCyc pathways based on normalized pathway size, and the number of ORFs associated with each pathway were examined using R, and then plotted using ggplot2 (Wickham, 2009).

3.2.5 **Comparative metagenomics**

MG-RAST annotations for Clinton Creek microbialite (ID 4532705.3) and sediment (ID 4532704.3) metagenomes were loaded into STAMPS and compared against arctic mats and sediments (Ward Hunt Ice Shelf mat (ID 4532782.3), MarkHam Ice Shelf (ID 4532781.3), and Lost Hammer Sediments (ID 4532786.3), mats from Yellowstone (Octopus Springs Mat (ID 4443749.3), and Mushroom Springs Mat (ID 4443762.3) and Antarctica mats, marine-derived lakes, freshwater lakes and marine (McMurdo ice shelf mat (ID 4532780.3), Marine Lake 1 (ID 4443683.3), Marine Lake 5 (ID 4443682.3), Marine 8 (ID 4443686.3), Marine 9 (ID 4443687.3), and Ace Lake (ID 4443684.3) using a multiple group ANOVA in STAMP with SEED subsystems (Level III) annotations by post-hoc tests (Tukey-Kramer at 0.95), an effect size (Eta-squared) and multiple test correction using the Benjamini-Hochberg FDR procedure. Clinton Creek microbialites were further examined against polar mats, Cuarto Ciénegas microbialites (IDs 4440060.4, 4440067.3) and marine stromatolites from Highbourne Cay (ID 4440061.3) in STAMP by the one-sided G-test (with Yates' + Fisher's) alternative to chi-squared, with asymptomatic confidence intervals (0.95), using Benjamini-Hochberg FDR procedure. Corals (IDs 4445755.3, 4445756.3) and Whale fall (IDs 4441619.3, 4441620.3 44416564.4) metagenomes were comparing with SEED subsystem III in STAMP using a one-sided Welch's t-test with Welch's confidence interval (0.95), and Storey’s FDR multiple correction test.

3.2.6 Metagenomic data depositing

The data used in this study are freely available from the MG-RAST metagenomics analysis server under the project name; Yukon microbialites' under the names Clinton Creek microbialite (ID 4532705.3) and Clinton Creek sediment (ID 4532704.3).

3.3 Results and discussion

3.3.1 Metagenomic assembly and contig properties

The assemblies were selected based on the number of contigs (>100bp), N50/N90 values, longest contig, and total length (bp) of the assembly (Table 3.1). Based on these analyses, a kmer size of 39 was used for all further analysis (Table 3.1). A kmer size of 55 generally yielded longer but fewer contigs, which would not allow for a comparable differential analysis between microbialites and sediments (Table 3.1). Nevertheless, only 0.64% and 1.74% of the reads from the sediment and microbialite metagenomes, respectively, assembled into contigs, indicating that both environments had complex microbial communities

The GC content differed in the microbialite compared to the sediment, whereas protein isoelectric points (pI) were similar (Figure 3.2). The lower GC content in the sediments was likely due to more representatives from low GC containing phyla such as *Bacteroides* and *Firmicutes*. The higher GC content in the microbialite data is likely due to the high relative abundance of sequences assigned to anoxic photoheterotrophic *Alphaproteobacteria,* including *Rhodobacterales* (59 to 65% GC content) and *Rhodomicrobium* (62.2% GC content). GC content across bacterial genomes can be highly variable amongst microbial taxa, although amino-acid usage is typically

similar (Lightfield *et al.,* 2011), which is consistent with our metagenomic data that GC is more variable then pI content (Figure 3.2).

3.3.2 Community composition

The microbialite and sediment microbial communities were dominated by bacteria with low abundances of eukaryotes and archaeal sequences (Table 3.2). From RefSeq annotations, <1% of the microbialite and sediment contigs were of archaeal origin (Table 3.2, RefSeq), and no archaeal ribosomal genes were detected in either the sediment or microbialite contigs (Table 3.2, M5RNA). Clinton Creek microbialites, similar to Highbourne Cay marine microbialites and the freshwater microbialites from Cuarto Cienegás, had low abundances (<1%) of archaea and eukaryotes (Breitbart *et al.,* 2009; Khodadad *et al.,* 2012; Mobberley *et al.,* 2013). Eukaryotes were rare, as they made up <1% of the sediment and microbialite contigs of Clinton Creek (Table 3.2), although common taxa such as diatoms, dinoflagellates, cryptomonas, chlamydomonades and fungi were detected, which support microscopy data (Power *et al.,* 2011a). Diatoms and other protists have been observed by microscopy and detected in the metagenomic data from Clinton Creek, but their contribution to the formation of microbialite structures requires further study (Power *et al.,* 2011a). Diatoms may influence carbonate precipitation through photosynthetic alkalinization, akin to processes found in cyanobacteria, or through the ammonification of amino acids and the metabolism of urea (Tesson *et al.,* 2008; Allen *et al.*, 2011).

Sequences from metazoans represented a small proportion of those from the eukaryotes, and were <0.1% of the total assigned reads in the Clinton Creek microbialites. The sequences included representatives from the taxa *Nematoda, Platyhelminthes, Microsporidia*, *Cnidaria* (e.g.

Hydra spp.) and *Arthropoda* (e.g. insects). Our data supports microscopic observations showing low abundances of metazoans (Power *et al.*, 2011a). Metazoan grazing has been a prime suspect in the global decline of microbialites as it removes cyanobacterial mats, thereby reducing microbialite formation by removing the main carbon source and structural components (Awramik, 1971; Garrett 1970). The low abundance of metazoans in Clinton Creek suggests that there grazing impact on the microbialites is quite low.

The *Proteobacteria* dominated the taxonomic groups in the Clinton Creek sediments and microbialites, with >50% of the predicted ORFs and >35% of the ribosomal sequences being assigned to this taxon (Figure 3.3A). The microbialite contigs were dominated by anoxic photoheterotrophic *Alphaproteobacteria* (e.g. *Rhodobacterales*), while sediment contigs had more nitrogen-fixing *Gammaproteobacteria* (e.g. *Pseudomonas* spp.) (Figure 3.3A). *Alphaproteobacteria* are commonly found among microbialite-forming microbial consortia and likely play an important role as nitrogen fixers during darkness, when heterocystous cyanobacteria are not active (Havemann and Foster, 2008).

Sequences assigned to the *Deltaproteobacteria* represented ~10% of the predicted *Proteobacterial* ORFs (based on RefSeq) from the sediments and microbialites (Figure 3.3A). The microbialite Deltaproteobacterial contigs consisted mainly of *Myxococcus* spp.; whereas, members of the *Desulfuromonadales* dominated in the sediments. *Myxococcus* spp. are abundant in a variety of microbialite-forming systems and can directly precipitate carbonate through the release of ammonium (Ben Chekroun *et al.*, 2004; Jimenez-Lopez *et al.*, 2011). The microbialites and sediments had similar abundances of *Desulfurovibrionales*, *Desulfobacterales* and

Syntrophobacterales, the major orders of dissimilatory sulfate reducers. The dissimilatory sulfate-reducers in the *Deltaproteobacteria* may be critical drivers of the alkalinity engine and thereby induce carbonate precipitation (Gallagher *et al.*, 2012). The occurrence of the major groups of dissimilatory sulfate-reducing bacteria (*Desulfurovibrionales*, *Desulfobacterales* and *Syntrophobacterales*) in Clinton Creek microbialites is not surprising; however, the proportion of sequences assigned to these taxa, including genes involved in dissimilatory sulfate-reduction, were similar in the sediments. Thus, the sediments and ground water could be sources of these dissimilatory sulfate-reducing bacteria in microbialites, or the bacteria may be dispersed as spores from other environments.

Sequences assigned to *Cyanobacteria* were the fourth most abundant (Figure 3.3A). The microbialites had 4-fold more protein-coding ORFs that were classified as *Cyanobacteria* than the sediments (Figure 3.3A). The cyanobacterial ribosomal sequences (based on the M5RNA database) recovered from the microbialites were assigned to filamentous cyanobacteria from the genera *Tolypothrix* and *Leptolyngbya*, and unclassified Antarctic *Cyanobacteria.* In contrast, no ribosomal sequences were recovered from the sediments that were assigned to the *Cyanobacteria* (Figure 3.3A; M5RNA). Based on RefSeq classification, in the microbialites there were more contigs assigned to filamentous genera including *Microcoleus, Lyngbya, Nodularia,* and *Anabaena*, and more unicellular calcifying *Synechococcus,* than in the sediments. The sediments had fewer sequences assigned to genera of filamentous and unicellular *Cyanobacteria* (e.g. *Synechococcus*). Cyanbacterial carbon fixation produces the nutrient-rich EPS that likely supports the growth of the heterotrophic microbial consortium, and fuels microbialite formation by

increasing the saturation index to favor carbonate precipitation (Dupraz and Visscher 2005; Dupraz *et al.*, 2009).

Contigs assigned to the phylum *Gemmatimonadetes* comprised 7 to 8% of the protein-coding ORFs in the sediments and microbialites (Figure 3.3A). To our knowledge, this is the first report of protein-coding sequences in metagenomic data from microbialites that have been assigned to the *Gemmatimonadetes*, although they were also found in other environments. The contigs annotated mainly as hypothetical proteins, although threre were annotations to ATPases, Zn-dependent peptidases and glucose/sorbosone dehydrogenase-like genes. Glucose/sorbosone dehydrogenases transform various sugar moieties into vitamins, including L-ascorbic acid (vitamin C). Gemmatimonadetes can also make D-glucono-1,5-lactone from D-glucose, which can acidify the extracellular environment and lead to dissolution of carbonate (Dupraz and Visscher, 2005; Miyazaki *et al.*, 2006; Fender *et al.*, 2012). Whether they are involved in microbialite formation or dissolution, or are just opportunists, needs to be elucidated.

3.3.3 Metabolic potential

The metagenomic data predicts that the metabolic potential of the Clinton Creek microbialites relating to carbonate precipitation is dominated by photosynthesis; whereas, the sediment metagenomes indicated more heterotrophic metabolism (e.g. respiration) (Figure 3.4A). SEED subsystem level I (i.e. the highest functional classification) annotations indicated that carbohydrate metabolism relating to carbon fixation, DNA metabolism and photosynthesis pathways were more abundant in the microbialites than sediments (Figure 3.4A, FDR p-value < 0.01). Lower level SEED subsystem predictions (level III) also revealed more photosynthetic

pathways (e.g. photosystem II reaction centers, and carotenoid and chlorophyll biosynthesis) in microbialites than sediments (Figure 3.4B, FDR p-value < 0.01). These photosynthetic pathways in microbialites were assigned to genera of filamentous cyanobacteria such as *Microcoleus*, *Lyngbya*, *Nodularia*, and *Anabaena*, which were not found in the sediments.

Power *et al.* (2011a) found that aragonite-associated biomass within the Clinton Creek microbialites was modestly enriched in ^{13}C by 0.8‰, relative to aragonite not associated with biomass, consistent with carbonate precipitation by phototrophs. Electron microscopy of the microbialites confirmed that phototrophs were associated with carbonate enriched in ^{13}C (Power *et al.*, 2011a). The isotopic data and high abundance of sequences associated with photosynthetic pathways support the model that carbonate precipitation is mediated through photosynthetic-induced alkalinization. Heterotrophic processes may also contribute to carbonate precipitation, as it is hypothesized that microbialites become progressively lithified as the photosynthetically derived carbonate becomes in-filled through subsequent carbonate precipitation by heterotrophic activity (Omelon *et al.*, 2013).

The metapathway pipeline was used for MetaCyc pathway annotations to complement the SEED functional gene annotations. MetaCyc predicted that pathways revealed that most pathways were shared between microbialites and sediments (Figure 3.5A). Only 13 pathways were restricted to the sediments, while 240 were unique to the microbialites; 358 pathways were shared (Figure 3.5A). The forty most abundant shared pathways were housekeeping genes with functions such as protein, nucleic-acid, lipid and carbohydrate biosynthesis and degradation (Figure 3.5B). In the microbialites, MetaCyc annotations predicted higher levels of glutamine degradation I, which

results in the donation of nitrogen in the form of ammonium, while glutamine biosynthesis appeared to be higher in the sediments (Figure 3.5B). Both the sediments and the microbialites were predicted to recycle ammonium through the ammonium assimilation cycle I-II (Figure 3.5B), which would supply nitrogen, and support primary production of the filamentous cyanobacterial mats in microbialites, thus leading to further carbonate precipitation.

3.3.4 **Comparative metagenomic analysis**

The metagenomic data are consistent with the Clinton Creek microbialites and sediments being functionally more related to polar mats than marine or tropical freshwater microbialites. Using SEED subsystem level III, PCA indicates better clustering to polar mats and sediments from the Arctic and Antarctica (Figure 3.6). The Clinton creek data cluster closest to data from Markham and Ward Hunt ice-shelf mats from the Canadian High Arctic (Figure 3.6; Vanin *et al.*, 2012). Functionally, the Markham mats and Clinton Creek microbialites are most strongly correlated based on SEED subsystem level III annotations (Figure 3.7, $R^2 = 0.952$). Overall, based on functional pathways in SEED, the polar mats (e.g. Markham, Ward Hunt, and Mcmurdo) were strongly correlated with the Clinton Creek microbialites. Markham mats, like the microbialites of Clinton Creek, are dominated by members of the *Proteobacteria*, and *Gemmatimonadetes* also comprise 3% of the 16S rDNA sequences (Bottos *et al.*, 2008). Polar mats, whether on microbialites or ice shelves, appear to have functional similarities; this likely relates to shifts in temperature, including temperatures well below freezing (Varin *et al.*, 2012).

SEED-based functional annotations for metagenomic data from the Clinton Creek microbialites were also compared with those from tropical freshwater microbialites from Cuarto

Cienegás and Highbourne Cay marine stromatolites (Figure 3.7). The Clinton Creek microbialite metagenome had weak correlations with microbialites from two locations in Cuarto Cienegás, including Pozas Azules II (Figure 3.7, $r^2 = 0.702$), Rio Mesquites (Figure 3.7, $r^2 = 0.633$), and Highbourne Cay marine stromatolites (Figure 3.7, $r^2 = 0.018$). Arctic polar mats had stronger correlations for SEED pathways than Cuarto Cienegás microbialites and Highbourne Cay stromatolite metagenomes (Figure 3.7, $r^2 > 0.900$). Cuarto Cienegás microbialites and Highbourne Cay are tropical; hence, many pathways related to cold-adaptation that are present in the Clinton Creek micobialites and polar mats (Varin et al., 2012) are absent. The SEED functional gene classifications for Highbourne Cay stromatolite were the least correlated with those from the Clinton Creek microbialites, consistent with marine and freshwater microbialite communities being quite different.

The Clinton Creek microbialite metagenomic data were distinct from non-lithifying mats or biofilms from Octopus and Mushroom Springs in Yellowstone (Figure 3.6), whale fall and corals (Figure 3.8 to 3.9). These data reveal that Clinton Creek microbialites are closely related to polar mats, due possibly to cold-adaptation, and differ greatly from tropical microbialites. This reveals that under the correct chemistry (e.g. alkaline pH, high DIC, and dissolved Ca^{2+} or Mg^{2+}), polar mats on ice shelves could have at least the metabolic potential to make microbialites.

3.4 Conclusion

The northernmost and fastest growing microbialites known are located at subarctic Clinton Creek (Yukon, Canada). DNA from representative microbialites was extracted and directly sequenced, without bias from DNA amplification, and used to produce the largest set of assembled

metagenomic data for a freshwater microbialite-forming ecosystem. The microbialite metagenomes revealed a high proportion of photosynthetic genes, implying that microbialite formation is driven by photosynthesis-induced alkalinization, which is consistent with data from ^{13}C isotopic enrichment (Power *et al.*, 2011a). Predicted metabolic pathways overlapped extensively between microbialite and sediment communities, particularly with respect to housekeeping genes; however, they have distinct core communities with microbialites dominated by *Alphaproteobacteria* (mainly anoxic phototrophs like *Rhodobacterales*) and sediments dominated by *Gammaproteobacteria* (mainly heterotrophic nitrogen-fixing *Pseudomonas* spp.).

The microbiome of the Clinton Creek microbialites was distinct from that of mats and biofilms from corals, whale fall, Yellowstone hot springs, and marine stromatolites. While Clinton Creek microbialites shared some functional potential with microbialites from Cuarto Cienegás, the Arctic mats (e.g. Markham and Ward Hunt) shared greater functional potential, possibly because of cold-adaptation. The shared metabolic potential between Clinton Creek microbialites and the polar ice-shelf Markham, Ward Hunt and McMurdo mats suggests that under favorable chemical conditions (e.g. alkaline pH, high DIC, and dissolved Ca^{2+} or Mg^{2+}), Arctic mats have the metabolic potential to make microbialites.

At Clinton Creek, precipitation of carbonate minerals within the mine tailings has been shown to be a significant sink for atmospheric CO_2 (Wilson *et al.*, 2009). This study supports the view that cyanobacteria generate alkalinity and sustain heterotrophic communities, which together drive the fast formation of microbialites at Clinton Creek.

3.5 Tables and figures

Table 3.1: Assembly statistics for Clinton Creek metagenomes

	Microbialite (k = 39)	Microbialite (k = 55)	Sediment (k = 39)	Sediment (k = 55)
No. Contigs >100bp	109722	689	59928	171
Total length (Bp) >100bp	27180461	219687	12690391	151415
Mean >100bp	247	318	211	885
N50 >100bp	248	289	200	1307
N90 >100bp	184	231	160	383
Med Length >100bp	240	269	186	582
No. Contigs >500bp	371	46	557	99
Total length (bp) >500bp	230702	37861	508559	127068
Mean >500bp	621	823	913	1283
N50 >500bp	588	611	849	1591
Med >500bp	574	566	608	916
Largest	9491	9752	33503	5896
Total GC count	16801673	135459	7329632	82490
GC%	61.82	61.66	57.76	54.48

k = kmer size (bp)

Table 3.2: Domain classification of the microbial community in Clinton Creek (%)

Domains*	Microbialite (RefSeq)	Microbialite (M5RNA)	Sediment (RefSeq)	Sediment (M5RNA)
Bacteria	99.05	73.91	98.22	92.50
Eukaryotes	0.60	25.00	1.16	7.50
Archaea	0.32	0.00	0.45	0.00
Viruses	0.02	0.00	0.13	0.00
Unassigned	0.01	1.09	0.04	0.00

*Based on MG-RAST annotations. RefSeq: Protein coding ORFs. M5RNA: Ribosomal rRNA genes.

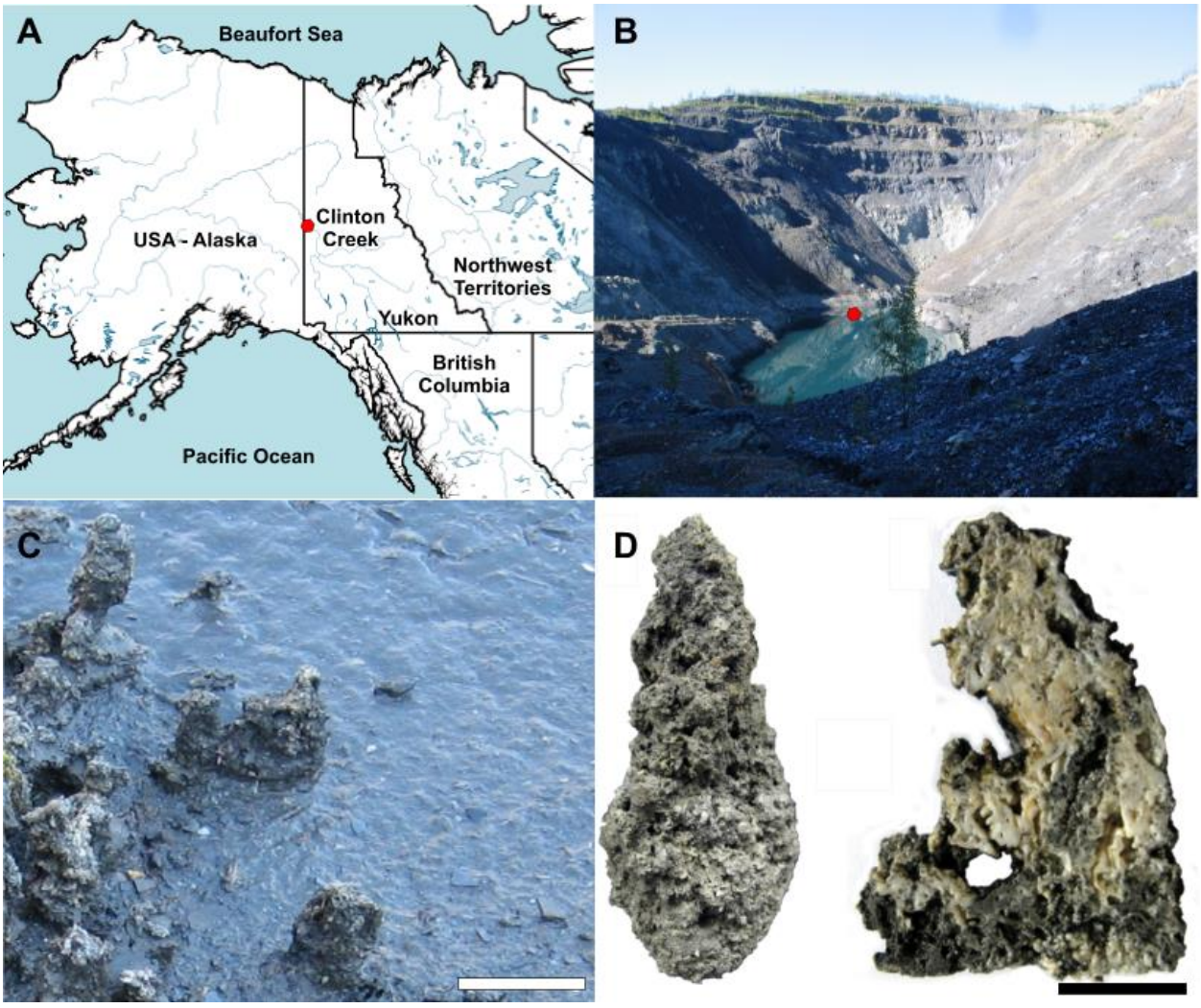

Figure 3.1: Clinton Creek sample site and examples of microbialite morphology
A) Map of northwestern North America illustrating the location of Clinton Creek Yukon, Canada.
B) Photograph of the Clinton Creek open pit-pond; the red dot indicates the sampling location.
C) Photograph of the microbialites along the periphery of the open pit pond
Scale bar equals ~100cm.
D) Complete microbialite and cross-section of a microbialite. Scale bar represents ~10cm.

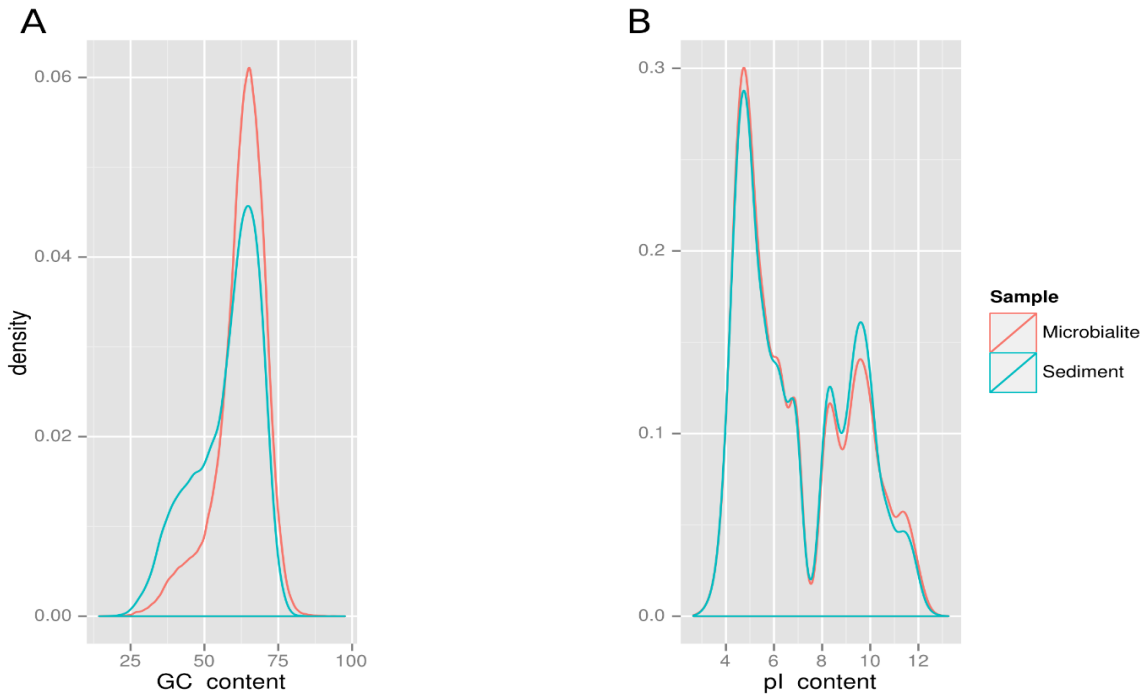

Figure 3.2: Molecular properties of the Clinton Creek microbialite and sediment contigs A) GC content (%) B) Predicted protein isoelectric (pI) content (%)

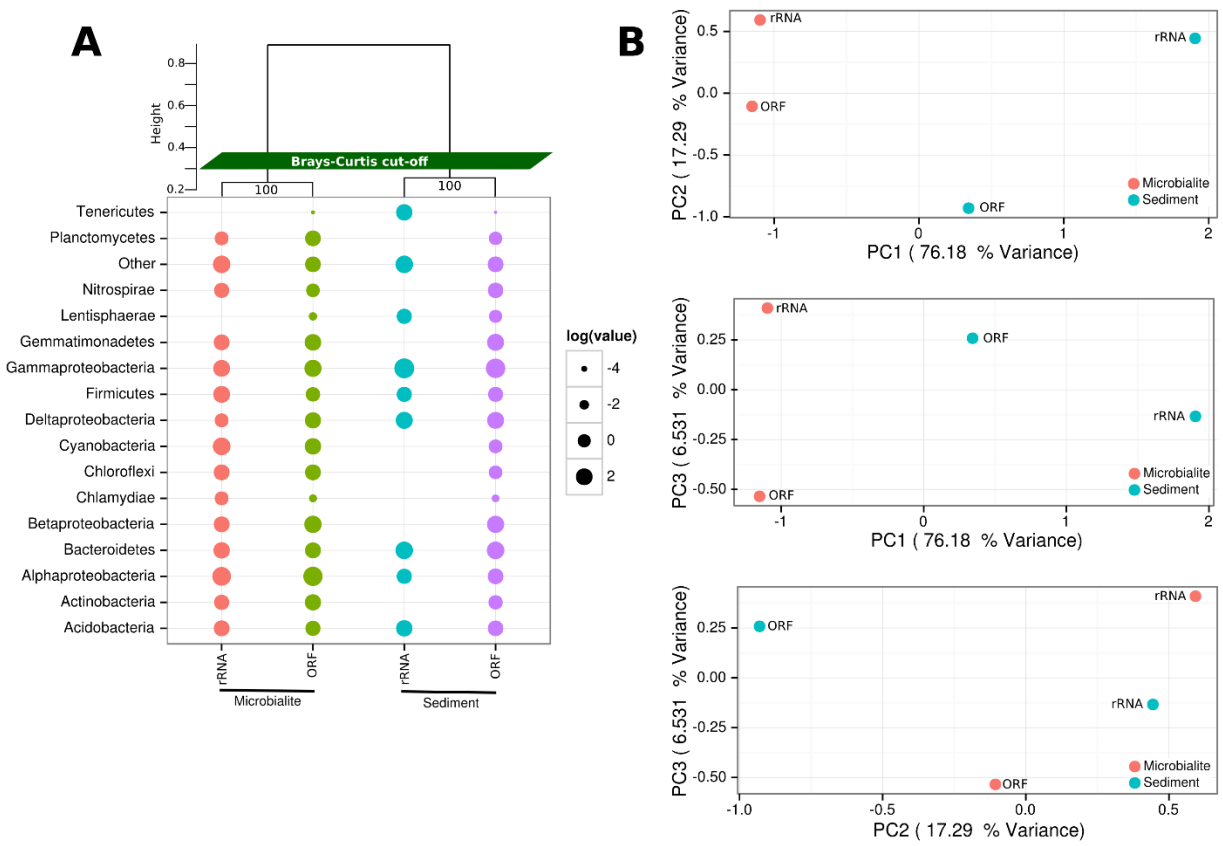

Figure 3.3: Microbial community structure of Clinton Creek metagenomes

A) Dot pot of representative taxonomic groups from Clinton Creek sediments and microbialites using RefSeq (protein coding ORFs) and M5RNA (rRNA, MG-RAST rRNA database) in log relative abundances. “Other” denotes low abundance taxa that were <1% of the total ORF or rRNA, individually, but were all combined here into one point.

B) PCAs of top 25 taxonomic groups from Clinton Creek sediments and microbialites by RefSeq (ORFs) and M5RNA (rRNA, MG-RAST rRNA database) classification.

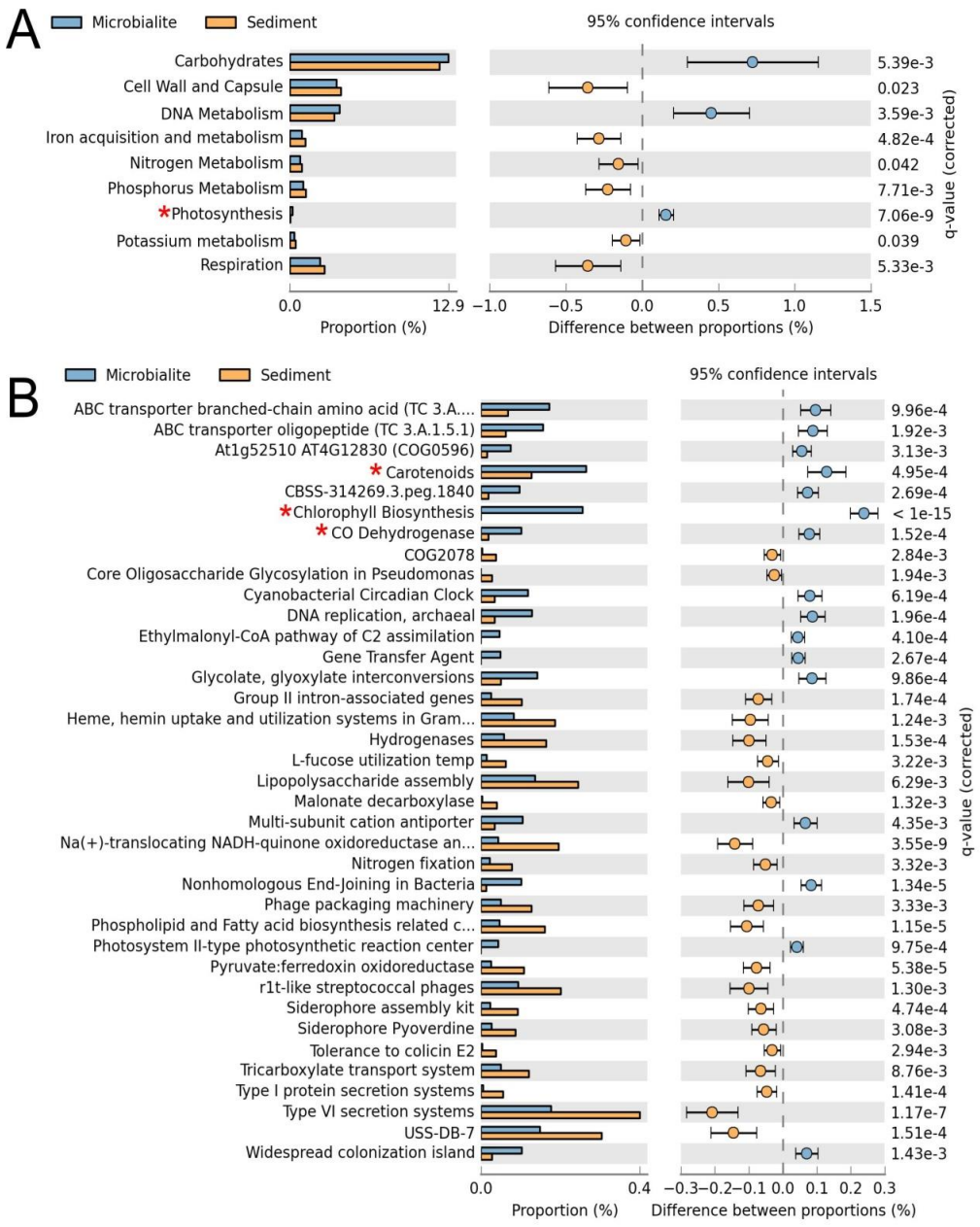

Figure 3.4: Extended error plots for functional gene annotations for Clinton Creek metagenomes in STAMP using SEED subsystems
A) SEED subsystem level I (highest level classification in SEED).
B) SEED subsystem level III (3rd lowest classification in SEED out of four levels).
Extended error plots used a one sided G-test (w/Yates' + Fisher's) with asymptomatic confidence intervals (0.95) using Benjamini-Hochberg FDR procedure.
*Red asterisks are significant photosynthetic pathways.

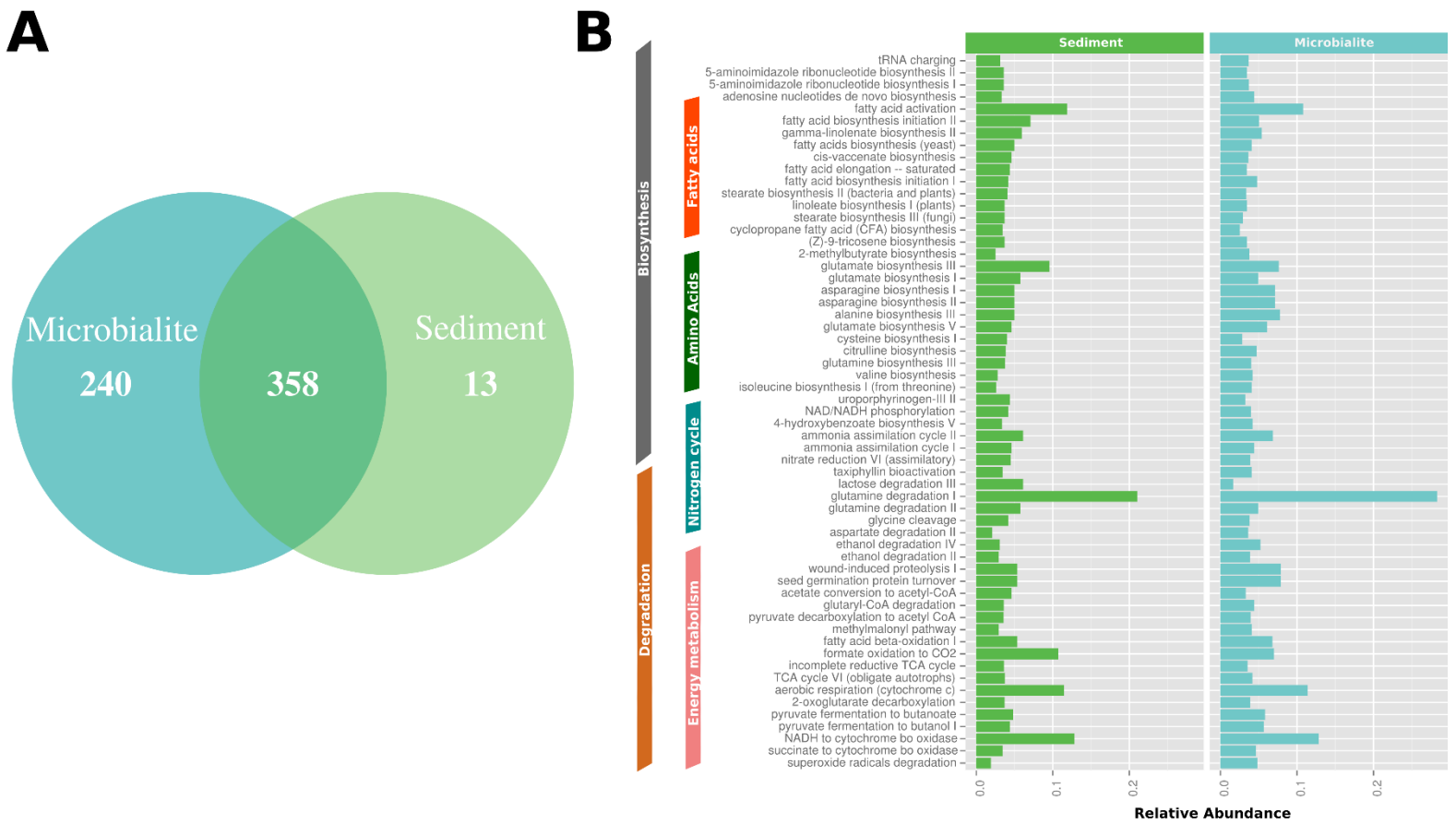

Figure 3.5: MetaCyc pathway annotations for Clinton Creek metagenomes
A) Venn diagram of MetaCyc pathways
B) The top 40 shared MetaCyc pathways from Venn diagram.

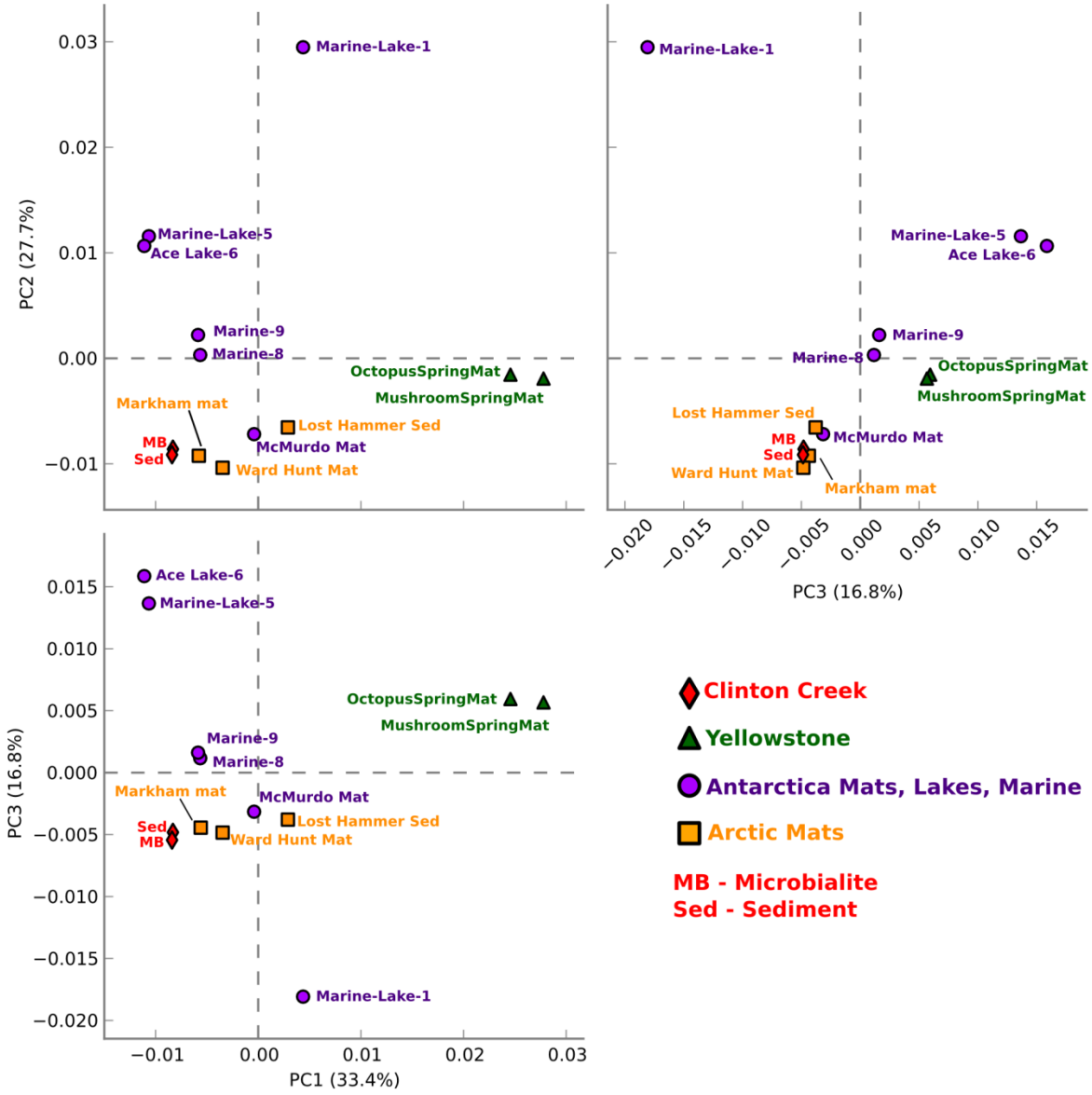

Figure 3.6: Functional gene comparative PCA plot for Clinton Creek metagenomes Based on ANOVA for multiple groups using SEED subsystem level III in STAMP.

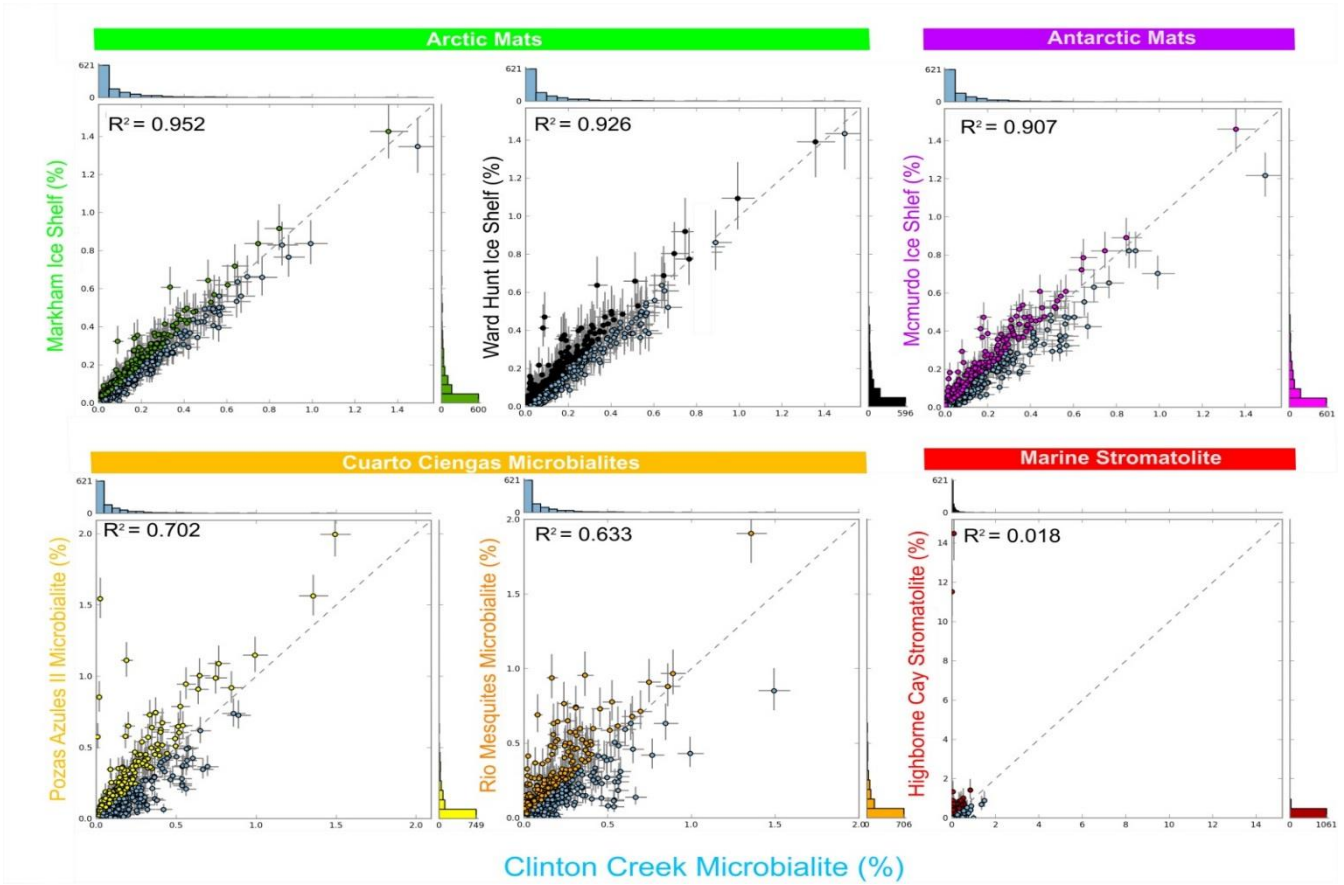

Figure 3.7: Scatter plots of functional gene annotations using SEED subsystem level III
One sided G-test (w/Yates' + Fisher's) with asymptomatic confidence intervals (0.95) using Benjamini-Hochberg FDR procedure in STAMP.
Each dot represents a unique functional classification gene.

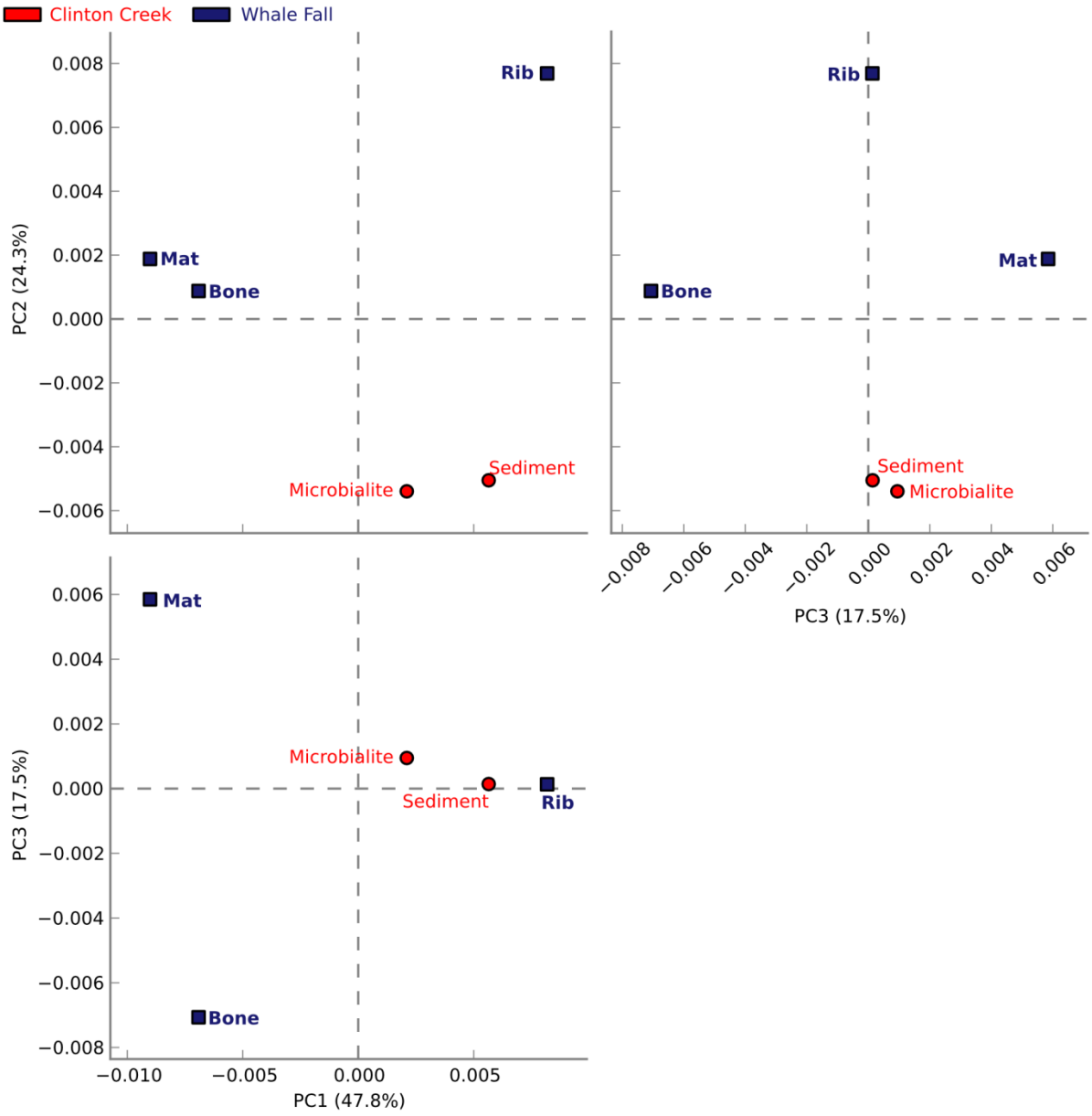

Figure 3.8: Comparative functional gene PCA plot for Clinton Creek against whale fall metagenomes
In STAMP, a one-sided Welch's t-test with Welch's confidence interval (0.95), and Storey's FDR multiple correction test.

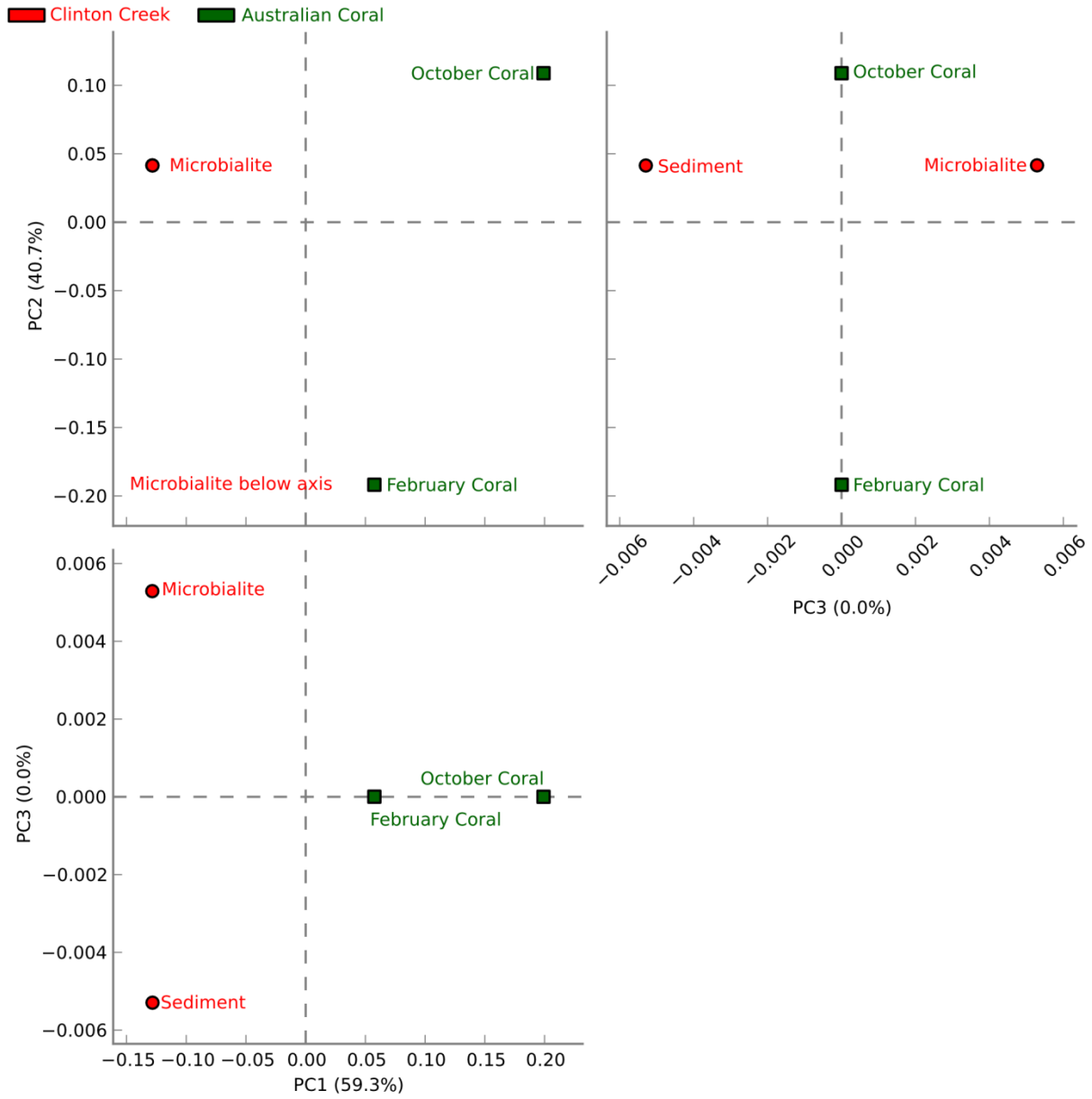

Figure 3.9: Comparative functional gene PCA plot for Clinton Creek against coral metagenomes In STAMP, a one-sided Welch's t-test with Welch's confidence interval (0.95), and Storey's FDR multiple correction test.

Chapter 4:

The genome of *Agrococcus* sp. strain RW1 isolated from modern microbialites reveals genetic promiscuity and elements responsive to environmental stresses

4.1 Introduction

Little is known about non-photosynthetic pigmented bacteria in modern microbialite mats. We screened over one hundred isolates from Pavilion Lake for bacteria that were pigmented but non-photosynthetic using a culture-dependent method, to supplement our culture-independent metagenomic approach. As part of this screen we isolated yellow *Agrococcus* sp. strain RW1 described here and orange *Exiguobacterium* sp. strain RW2 described in Chapter 5 pigmented bacteria from a microbialite collected at 20 m depth in Pavilion Lake (White 3rd *et al.*, 2013a-b). To date, there are no completed genomes for the genus *Agrococcus*, making inferences on the abundance, distribution, and metabolic potential of this genus intractable. Additionally, the pathway responsible for the yellow pigmentation in the genus *Agrococcus* has not been described.

The genus *Agrococcus* was described based on two strains of *Agrococcus jenensis* isolated from soil and the surface of sandstone (Groth *et al.* 1996). The genus is classified within the family *Microbacteriaceae*, members of which have diaminobutyric acid within the cell wall, which could impart the distinctive lemon-yellow color, although whether diaminobutyric acid is involved in the pigmentation is unknown (Groth *et al.*, 1996). *Agrococcus* spp. have been isolated from a wide range of environments, including air (Zlamala *et al.*, 2002), a coal mine (Dhanjal *et al.*, 2011),

cheese (Bora *et al.*, 2007), cold-desert soil (Mayilraj *et al.*, 2006), forest soil (Zhang *et al.*, 2010), a medieval wall painting (Wieser *et al.*, 1999), dried seaweed (Lee, 2008), and the phyllosphere of potato plants (Behrendt *et al.*, 2008). There are eight described species of *Agrococcus* as follows: *A. jenensis* (Groth *et al.*, 1996), *A. baldri* (Ziamala *et al.*, 2002), *A. carbonis* (Dhanjal *et al.*, 2011), *A. casei* (Bora *et al.*, 2007), *A. citreus* (Wieser *et al.*, 1999), *A. jejuensis* (Lee 2008), *A. lahaulensis* (Mayilraj *et al.*, 2006), *A. terreus* (Zhang *et al.*, 2010), and *A. versicolor* (Behrendt *et al.*, 2008). However, little is known about the metabolism, genetic richness and diversity of this genus.

Here, we present the polyphasic characterization of a new species of *Agrococcus* isolated from modern microbialites, including the first complete reference genome. Genomic analysis revealed signatures of environmental adaption to the cold oligotrophic conditions of Pavilion Lake. Promiscuous mobile elements were found in two plasmids involved in heavy metal resistance and DNA transposition. The genomes of *Agrococcus* sp. RW1 and *A. lahaulensis* K22-21 both encode a carotenogenic gene cluster that could be responsible for producing the characteristic lemon-yellow pigmentation found in *Agrococcus.*

4.2 Materials and methods

4.2.1 Isolation, growth conditions, phage induction, biochemical and antibiotic susceptibility tests

Agrococcus sp. strain RW1 was isolated by plating 0.5 g of a thrombolitic microbialite, collected from 20 m in Pavilion Lake, British Columbia (50.86677 °N, 121.74191 °W), on Luria - Bertani medium [1% (w/v) tryptone, 0.5% (w/v) yeast extract, 1% (w/v) NaCl, pH 7] solidified with 1.5% (w/v) agar, and incubated at 30 °C for 3 days. Solidified LB was also used for assessing

growth at various temperatures (4, 11, 16, 20, 25, 30, 35, 42, 50 °C), at pH 7 and 1% (w/v) NaCl. To assess growth at various pH (5, 6, 6.5, 7, 7.5, 8, 8.5, 9, 10, 10.5, 11), standard solidified LB was used at 30 °C and 1% (w/v) NaCl. Growth at different salinities was tested using solidified LB (pH 7) spiked with various amounts of NaCl (0-6%, 9, 12, 13, 16%) at 30 °C. Cultures were maintained in LB broth or on agar at 1% NaCl, pH 7 and at 30 °C. M-agar medium [0.5% (w/v) tryptone, 0.25% (w/v) yeast extract, 1% (w/v) NaCl, 1.5% (w/v) agar, pH 7], a diluted version of LB-agar medium, was used to determine filamentous growth under carbon-limitation. Strain characteristics, including colony and cell morphologies were determined by standard methods (Murry *et al.,* 1994). Oxidase tests, biochemical enzyme assays, and carbohydrate utilization tests were completed using API20E (BioMérieux) test strips according to the manufacturer's instructions. Antibiotic susceptibility of strain RW1 was determined by the Kirby-Bauer method using antibiotic discs on solidified LB (Collee *et al.,* 1996). Prophage induction assays were done either by adding 0.2 μg ml^{-1} of mitomycin C, or by heating cultures to 45 °C , incubating at 30 °C for 3-10 h and monitoring changes in turbidity until a decrease of OD_{600} to 0.1 or less was observed (starting OD_{600} = 0.6). At several time points, cells were pelleted at 3,250 x *g* and the supernatent filter-sterilized twice through a 0.22 μm pore-size Millex Durapore PVDF membrane (Millipore) filters before plating using a double-agar overlay plaque assay (Kropinski *et al.,* 2009).

4.2.2 **Phospholipid fatty acid analysis**

Phospholipid fatty acids (PLFAs) were extracted from cultures grown in 25 ml LB broth for 4 d at 22 °C. Cultures were transferred into pre-combusted vials for an overnight solvent extraction in a 1:2:0.8 ratio solution of dichloromethane (DMC), methanol (MeOH), phosphate-

buffered saline (PBS) [137 mM NaCl, 2.7 mM KCL, 10 mM Na_2HPO_4 $2H_2O$, 2 mM KH_2PO_4, pH 7.4] (Bligh and Dyer, 1959). The extract was filtered through a separatory funnel where DCM and water were added to achieve a mixture of MeOH:DCM:water of 1:1:0.9 (Bligh and Dyer, 1959). The lower organic phase was removed and purified into polar, neutral, and non-polar fractions using liquid chromatography through silica-gel. Phospholipids in the polar fraction were subjected to mild alkaline methanolysis to produce fatty-acid methyl esters (FAMEs) (Guckert *et al*., 1985). FAMEs were separated, identified, and quantified using gas chromatography mass spectrometry (GC/MS) (Agilent Technologies Inc., Santa Clara, CA, USA) with a DB-5MS capillary column (30 m x 0.32 mm I.D. x 0.25 µm film thickness) at a temperature regime of 50 °C (1 min), 20 °C min^{-1} to 130 °C, 4 °C min^{-1} to 160 °C, and 8 °C min^{-1} to 300 °C (5 min). PLFAs were identified by retention time and mass spectra relative to those of reference standards (Bacterial Acid Methyl Ester Mix, Matreya Inc., Pleasant Gap, PA, USA; and Supelco 37 Component FAME Mix, Sigma-Aldrich Co., Bellefonte, PA, USA). A modified picolinyl ester derivatization was used to determine the branching point in unknown compounds (Destaillats and Angers, 2002; Dowd, 2012). Dimethyl disulphide adducts derivatives were prepared to determine the double bond position in unsaturated fatty acids (Nichols *et al.*, 1986).

4.2.3 Light and scanning electron microscopy (SEM)

Exponentially growing cells were harvested after 48 h of growth in LB-medium and then viewed by light microscopy under oil immersion at 100x. For SEM, a culture in stationary phase (~72 h), was pelleted at 3,250 x *g* for 10 min, and the LB medium was then exchanged and cells were fixed in 2.5% glutaraldehyde spiked phosphate-buffered saline (PBS) [137 mM NaCl,

2.7 mM KCL, 10 mM Na_2HPO_4 $2H_2O$, 2 mM KH_2PO_4, pH 7.4] solution for 30 min on ice. The fixed culture was filtered onto a 0.2 µm pore-size Supor polycarbonate membrane (Pall Port Washington, NY). The filter was washed with PBS and post-fixed in 1% OsO_4 for 1 h. The stained filter was passed through a graded ethanol series (25, 50, 70, 95, 100%) at 10 min intervals, and at 100% EtOH, were critical-point dried. A sputter coater applied 5 nm of gold/palladium alloy onto the cells prior to imaging by SEM using a Hitachi S4700 microscope.

4.2.4 DNA extraction, PCR and Illumina library construction

DNA was extracted using QIAamp followed by MinElute cleanup columns (Qiagen Germantown, MD). Full length 16S rDNA was amplified using the universal primers 27f and 1492r (Lane *et al.*, 1991). To ensure coverage of the full length 16S rDNA sequence, another PCR amplification was completed using primers 341f and 907r (Muyzer *et al.*, 1993; 1998). PCR products were sequenced using the standard Sanger method on an ABI3730 (Applied Biosystems Foster City, Ca). The Illumina MiSeq library was constructed using the NxSeq library prep kit (Lucigen Middleton, WI) without the final 14-cycle PCR enrichment to avoid PCR bias, and quality control of the resulting library was completed using Agilent high-sensitivity DNA chips and digital droplet PCR (Hindson *et al.*, 2011; White 3rd *et al.*, 2013 a). The library was sequenced using 250 bp paired-end sequencing on the Illumina MiSeq at GenoSeq UCLA Los Angeles, CA.

4.2.5 Phylogenetic analysis

Sanger sequences obtained from the 27f-1492r and 341f-907r PCR products were merged into full-length 16S rDNA sequence using Consed (Gordon *et al.*, 1998) with manual editing. The phylogenetic position of *Agrococcus* sp. strain RW1 was assessed using the error-corrected whole-

genome assembled 16S rDNA (~99% similar to PCR amplified) rather than the PCR amplified sequence, due to a lower chance of PCR based substitution errors and greater sequence length (1409 bp vs. 1354 bp). MLST (multiple locus sequencing typing) marker analysis was completed by extracting inferred amino-acid sequences for rpoB (β subunit of bacterial RNA polymerase, ~1156 aa), RecA (recombination protein A, ~352 aa), gyrB (DNA gyrase subunit B, ~679 aa), and ppK (Polyphosphatkinase, ~752 aa) from draft and completed genomes by BLASTP analysis or from prior MLST analysis (*A. jenensis* strain DSM9580 only, Stackebrandt *et al.,* 2007), and then concatenated them into a ~2939 aa sequence. All phylogenetic analyses were aligned and trimmed using MUSCLE (parameters: -400 gap open with zero gap extended) and clustered using UPGMB. Trees were constructed in MEGA using Maximum likelihood followed by bootstrapping (1000 replicates) and the Jukes-Cantor substitution model (Edgar 2004; version 5.10, Tamura *et al.,* 2011).

4.2.6 **Whole genome assembly and genome finishing**

Raw Illumina sequencing data were screened for PhiX spike-in contaminants using Bowtie2 (version 2.1.0), removed using Picard tools (version 1.90) (White 3rd and Suttle, 2013c). For the draft genome assembly, read-error correction using AllPaths-LG (version 44837), Celera assembly (version 7.0, including plasmid pHC-CG425: listed in the paper as a 1,427 bp single contig), and read partitioning using Jellyfish (version 1.1.10), were done as described (White 3rd *et al.,* 2013a). Ray genome assembly for *Agrococcus* sp. RW1 was completed using the error-corrected reads (from AllPath-LG, version 44837) with a k-mer size of 55 bp (Boisvert *et al.,* 2010).

Progressive Mauve was used to find the best representative assembly and contig order, and to complete the genome (Darling *et al.,* 2010). Contigs from Celera and Ray assemblies were pooled, and the remaining gaps were closed by recursive alignments in Mauve. The draft *A. lahaulensis* K22-21 genome from NCBI (version ASM42510v1) was used for genome ordering. The ordered and aligned overlapping contigs were merged using the EMBOSS union script, yielding three circular contigs (Rice *et al.,* 2000).

To confirm the three circular contigs as separate circular genomes, read mapping was used. Error-corrected, phiX-removed reads were mapped back to the genome and plasmids using Bowtie2 with the very sensitive local option (Langmead and Salzberg, 2012). The Bowtie2 readmapping output file (Sam file) was visually inspected using the Tablet program (Milne *et al.,* 2013).

Annotation was completed on RAST using SEED (Aziz *et al.,* 2008). RAST server parameters used SEED subsystems with FigFam under the Glimmer 3 option (Meyer *et al.,* 2009). In addition to RAST, metabolic pathways were predicted using MetaPathways, a modular pipeline for gene prediction and annotation that uses pathway tools and the MetaCyc database to construct environmental pathway/genome databases (ePGBDs) (Paley and Karp, 2006; Konwar *et al*., 2013; Caspi *et al.,* 2014). Metapathways uses the seed-and-extend homology search algorithm LAST (local alignment search tool) for annotations of ORFs with a minimum of 180 bp and minimum alignment length cutoff of 50 bp (Kiełbasa *et al.*, 2011).

Annotations were further analyzed for comparison to the genome of *A. lahaulensis* strain K22-21, for genome synteny, average amino acid identity, and phage lifestyle prediction.

The genome circular plot was constructed using CGviewer (Grant and Stothard, 2008); Celera (k0-k1250) and Ray (k0-k1250v2) assemblies of the *A. lahaulensis* strain K22-21 genome were mapped to the *Agrococcus* sp. strain RW1 genome using tBLASTx at an e-value of $1e^{-3}$ with 50% identity and 25 bp overlap, and then displayed in the CGviewer genome plot. Synteny plots were completed in the RAST server module using a BLAST based dot-plot format (Aziz *et al.*, 2008). Average amino-acid identity (AAIr) analysis and functional gene similarities were calculated on the RAST server module and then parsed with a web-based tool called AAIr (Aziz *et al.*, 2008; Krebs *et al.*, 2013). RAST server annotation predicted a prophage element in the genome, which was analyzed for lytic or lysogenic lifestyle using the phage classification tool set (PHACTS) (McNair *et al.*, 2012).

4.3 Results and discussion

4.3.1 Morphology and growth characteristics

The morphology of *Agrococcus* sp. strain RW1 shared features with other members of the genus but had a novel phenotype of mycelial-like growth. *Agrococcus* sp. strain RW1 cells were coccoid during logarithmic growth, and were irregular rod-like or coccoid in stationary phase (Figure 4.1/Table 4.1). Cells of strain RW1 were 0.5 to 0.7 μm in diameter, similar to other described members of the genus (Zhang *et al.*, 2010; Table 4.1). On solidified LB, the colonies were bright lemon-yellow, smooth and circular, and were 0.5 to 2 mm in diameter after ~72 h of growth at 30ºC. After one week of growth at 25ºC on diluted LB or M-agar, colonies were pale-yellow to white with mycelial-like branched irregular filaments. Mycelial-like growth morphology is common among actinobacteria, including isolates of *Streptomyces* spp.; however, this phenotype

has not been reported for other members of the *Microbacteriaceae* (Doroghazi and Metcalf, 2013). While branched mycelial-like growth has not been reported for members of the genus, they are known to live on surfaces (e.g. sandstone or seaweed) (Groth *et al.,* 1996). Possibly, mycelial-like growth may favor nutrient acquisition during growth on solid substrates.

Agrococcus sp. strain RW1 grew under a wide range of conditions. Growth occurred from pH 6 to 10, at 0 to 6% added NaCl, and over a temperature range of 11 to 42˚C (Table 4.1). A close relative of strain RW1, *A. lahaulensis* strain K22-21, has a narrower temperature range of growth between 25 and 37ºC, but can grow at salt concentrations as high as 7% (Mayilraj *et al.,* 2006; Table 4.1). Strain RW1 had the highest reported growth temperature for the genus at 42˚C, but had no observed growth at <4˚C (Zhang *et al.,* 2010; Table 4.1). Although growth of strain RW1 was not observed at 4 ˚C, the temperature of the permanently cold hypolimnion of Pavilion Lake suggests that strain RW1 may find warmer regions of the microbialite mat or that warmer excursions in temperature occasionally occur (Lim *et al.,* 2009).

4.3.2 PLFA characterization and comparative analysis

The PLFA composition of *Agrococcus* sp. RW1 was distinct from that of other characterized strains of *Agrococcus* spp., including its close relative *A. lahaulensis. Agrococcus* sp. RW1 had half the amount of iC16:0 but three times as much C16:0, compared to *A. lahaulensis* (Mayilraj *et al.,* 2006, Table 4.2). The branched unsaturated PLFA iC15:1Δ^4 was 3.5% of the total PLFAs found in *Agrococcus* sp. RW1; it has only been found in trace amounts (<1%) in *A. versicolor* strain K 114/01^T (Behrendt *et al.,* 2008; Table 4.2). Branched monoenoic PLFAs such as iC15:1Δ^4 are typically used as biomarkers for anaerobic sulfate reducing bacteria (Kohring *et*

al., 1994); however, *Agrococcus* sp. RW1 grows aerobically and does not reduce sulfate. Although the PLFA profiles between *Agrococcus* sp. RW1 and *A. lahaulensis* K22-21 are quite similar, these differences suggest that the two isolates are from different taxonomic groups.

4.3.3 Evolutionary placement of *Agrococcus* sp. RW1 within the genus

Phylogenetic analysis of the 16S rDNA gene indicates that *Agrococcus* sp. RW1 is a close relative of *A. lahaulensis*, in the same clade but evolutionarily distinct (Figure 4.2). In support of this, *Agrococcus lahaulensis* K22-21 is more closely related to an isolate from human skin than to *Agrococcus* sp. RW1 (Figure 4.2). However, full-length 16S rDNA sequence alone was unable to resolve whether *Agrococcus* sp. RW1 and *A. lahaulensis* are different species.

MLST analysis also supports the argument that *Agrococcus* sp. strain RW1 and *A. lahaulensis* are in the same clade, but was unable to resolve whether they are separate species (Figure 4.3). MLST needs a minimum of seven loci to assign species-level classification of closely related bacterial taxa and only four loci are available for the genus *Agrococcus*; hence, species classification using MLST is currently not tractable (Maiden *et al.,* 2013). Due to low amounts of protein-coding sequences from related isolates, MLST alone was unable to determine whether *Agrococcus* sp. RW1 and *A. lahaulensis* are different species.

Agrococcus sp. RW1 and *A. lahaulensis* are distinct species based on whole genome analysis based on gaps in genomic synteny and functional gene annotations. *Agrococcus* sp. strain RW1 was the first published draft genome (White 3rd *et al.*, 2013a); subsequently, the genome of *A. lahaulensis* strain K22-21 was released on NCBI. We mapped the assemblies of *A. lahaulensis* and *Agrococcus* sp. RW1 (both Ray and Celera) against the final circular chromosome of

Agrococcus sp. RW1 using tBLASTx, and only the *A. lahaulensis* assembly showed gaps (Figure 4.4/Table 4.3). Synteny plots revealed 12 large gaps between the genomes of *Agrococcus* sp. RW1 and *A. lahaulensis*, along with 1752 non-conserved intergenic regions in *A. lahaulensis* (Figure 4.5). A comparison of functional gene annotations for *Agrococcus* sp. RW1 and *A. lahaulensis* K22-21, using both SEED (RAST-based) and MetaCyc (MetaPathways-based), revealed >200 conserved genes, suggesting high genomic plasticity, and that few genes are shared between the isolates (Figure 4.5). The whole genomic comparison between *Agrococcus* sp. RW1 and *A. lahaulensis* K22-21 also indicates the isolates are close relatives, but the differences between the genomes suggests high genomic plasticity within the group.

Average amino-acid identity score between the two genomes supports classifying *Agrococcus* sp. RW1 and *A. lahaulensis* K22-21 as different species (Figure 4.5). Average amino-acid identity is a robust measure for bacterial species classification that is based on whole-genome sequences, and that is comparable to DNA-DNA hybridization (Konstantinidis and Tiedje, 2005). The standard cut-off to distinguish bacterial isolates as different species is <70% similarity by DNA-DNA hybridization; this corresponds to <95% average amino-acid identity (Konstantinidis and Tiedje, 2005). The average amino-acid identity score for *Agrococcus* sp. RW1 and *A. lahaulensis* K22-21 was only 86.2% based on bidirectional whole-genome best-hit protein analysis using RAST annotation, supporting the classification of the isolates as different species (Konstantinidis and Tiedje, 2005; Krebs *et al.*, 2013; Figure 4.5)

4.3.4 **Biochemical properties and antibiotic susceptibility**

Agrococcus sp. strain RW1 shared many biochemical properties with other members of the genus, except for β-galactosidase activity. *Agrococcus* spp. strain RW1, like other members of the genus, is Gram positive, negative for oxidase, arginine dihydrolase, lysine decarboxylase, ornithine decarboxylase, citrate utilization, hydrogen sulfide production, urease, indole production, inositol/myo-inositol utilization and acetoin production, but positive for catalase (Behrendt *et al.,* 2008). However, strain RW1 was positive for β-galactosidase activity; whereas, other isolates have only weak or no activity (Behrendt *et al.,* 2008; Table 4.4). In *A. lahaulensis* there is no reported β-galactosidase activity or predicted gene in the genome (Mayilraj *et al.,* 2006, Table 4.4). β-galactosidase activity in strain RW1 may be a response to living in microbialite mats, and allow for the degradation of filamentous cyanobacterial mats containing complex exopolysaccharides with β-galactoside moieties.

Tests for antibiotic sensitivity in strain RW1 indicate that sensitivity to penicillin, tetracycline and streptomycin, as well as rifampin is shared with other *Agrococcus* spp. (Weiser *et al.,* 1999; Table 4.5). *Agrococcus* sp. RW1 was sensitive to tobramycin, vancomycin and clindamycin, but resistant to cefixime, sulfisoxazole, oxacillin, trimethoprim and a mixture of sulfamethoxazole/trimethoprim. *Agrococcus* c*itreus* DSM 12453T and *A.* j*enensis* strains DSM9580^{T} and DSM9996 are sensitive to oxacillin at 5 μg and weakly sensitive to polymyxin (Weiser *et al.,* 1999); whereas, strain RW1 was resistant to oxacillin at 1 μg and sensitive to polymyxin (Table 4.5). The resistance of *Agrococcus* sp. RW1 to 1 μg of oxacillin, given that other *Agrococcus* spp. are sensitive to doses of 5 μg (Wieser *et al.,* 1999), suggests that *Agrococcus* sp.

RW1 could be sensitive to higher oxacillin concentrations. β-lactamase is commonly involved in oxacillin resistance, but evidence for its occurrence was not found in the genomes of either *Agrococcus* sp. RW1 or *A. lahaulensis* K22-21 (Hou *et al.*, 2007). Although there were no putative antibiotic resistance genes predicted within the genome of *Agrococcus* sp. RW1, there were predicted pathways for aromatic compound degradation, including salicylate and gentisate catabolism, which may be involved in resistance. The antibiotic resistance in strain RW1 may have evolved from exposure to toxic organic molecules produced by cyanobacterial mats (Neilan *et al.*, 2013).

4.3.5 Mobile DNA and viral elements in *Agrococcus* sp. RW1

Mobile DNA elements, which are plasmid encoded in *Agrococcus* sp. RW1, are involved in integration, transposition, and heavy-metal resistance. Two plasmids were discovered in strain RW1, named pHCCG425 and pLC-RRW783. The 1,427-bp plasmid pHC-CG425 had a GC content of 67.8% (4.7% lower than the main chromosome) and encoded a putative integrase and a hypothetical protein of unknown function. However, pHC-CG425 shares strong similarities to gene clusters in other *Actinobacteria* including *Brevibacterium linens* and *Mycobacterium* spp. Plasmid pLC-RRW783 was 31,975 bp with a GC content of 70.6% (2% lower than the main chromosome) and 36 ORFs (Figure 4.6). Plasmid pLC-RRW783 contained ORFs annotated for mercuric reduction, arsenic resistance, various metal-dependent proteases, peptidases and ATPases, cadmium and unknown transporters, and an unclassified oxidoreductase. There were also three putative transposases, as well as DNA processing/binding proteins with a suggested role

in DNA transposition and/or integration. Seven ORFs in pLC-RRW783 had no predicted function and are annotated as hypothetical proteins.

Plasmids such as pLC-RRW783 that carry genes associated with heavy-metal resistance could be common in Gram-positive bacteria from cold alkali environments. The plasmid pGIAK1 was found in *Bacillus* sp. isolated from the Antarctic and is similar to pLC-RRW783 (Guo and Mahillon, 2013). Both plasmids pGIAK1 and pLC-RRW783 encode arsenic (including *arsR*) and cadmium resistance genes (Guo and Mahillon, 2013). pGIAK1 has been transferred from an isolate of *Bacillus* sp. to isolates of *Staphylococcus* spp., so it is possible that pLC-RRW783 could have been transferred by conjugation, phage transduction or transposition (Guo and Mahillon, 2013). The copy number of pLC-RRW783 is unknown, as is whether it can be transferred, or if its genes are expressed.

Annotation of the *Agrococcus* sp. RW1 genome revealed a putative prophage-like element. The 34,174 bp region on the genome resembled *Siphoviridae* prophages found in Actinobacteria, and had 43 predicted ORFs and a GC content of 70.1%, which was ~2% less than the GC content of the genome. The phage classification tool set (PHACTS) predicted that the lifestyle of this prophage would be temperate (52% of the trees voting for temperate lifestyle at standard deviation of 0.040) (McNair *et al.*, 2012). Temperate phages are not previously known to be found in the genus *Agrococcus*. The addition of heat and mitomycin C did not result in induction; hence it is unknown if the prophage can enter the lytic cycle. No prophage or phage genes are predicted in the genome of *A. lahaulensis*. The prophage in *Agrococcus* sp. RW1, has conserved genes for a phage tape-measure protein and protease that are related to other *Streptomyces* phages including

VWB, phi-c31, phi-BT1, as well as the *Mycobacterium* phage Brujita. These phages belong to the *Siphoviridae* and have a temperate lifestyle, which is consistent with predictions using PHACTS (Gregory *et al.,* 2003; Van Dessel *et al.,* 2005).

4.3.6 *Agrococcus* sp. RW1 life in a cold microbialite mat

Pavilion Lake microbialites exist in permanently cold (4 ° to 8 °C) water (Lim *et al.,* 2009), and the genome of *Agrococcus* sp. RW1 has signatures of cold adaptation. The *Agrococcus* sp. RW1 genome encoded a single copy of *cspA* gene (cold shock protein A), which is consistent with growth under the *in situ* cold conditions of Pavilion Lake**.** CspA is induced and essential for growth at <10 ˚C, and functions as a molecular chaperone that binds mRNA, preventing secondary structure formation and ensures translation at low temperatures (Yamanka and Inouye, 1997). CspA is essential and expressed during subzero temperature growth in the genus *Exiguobacterium* (Rodrigues *et al.,* 2008). In *Agrococcus* sp. RW1, CspA function under cold stress has not been confirmed, nor has growth at <10˚C, although analysis of the genome predicts the ability to grow under colder conditions.

Heavy-metal resistance gene clusters were also located on the main chromosome of *Agrococcus* sp. RW1. A mercury resistance operon spans positions 501 to 8136 bp, and includes a transposase, mercuric ion reductase, FAD dependent oxidoreductase, thiol oxidoreductase, and arsenic resistance protein are gene duplications presumably from a prior pLC-RRW783 plasmid transposition. Pavilion Lake has very low levels of zinc (0.01 to 0.03 mg L^{-1}) and undetectable levels of cobalt, copper, chromium, arsenic and cadmium (Lim *et al.,* 2009); hence, it is unclear why an organism from Pavilion Lake would carry gene clusters for heavy-metal resistance.

However, mercury was actively mined near Pavilion Lake in the 1940s (Stevenson, 1940), indicating that mercury could have been at a higher concentration in the lake, making these heavy-metal resistance genes a possible remnant of this event. *Agrococcus* sp. RW1 is a limited component of the Pavilion Lake microbialite community (<1% metagenomic recruitment) (unpublished data, Thesis Chapter 2). Sequences in the metagenome that recruited with high similarity (>95%) by confirmatory tBLASTx ($1e^{-3}$) to the *Agrococcus* sp. RW1 genome were predicted heavy-metal resistance genes (unpublished data, Thesis Chapter 2). This suggests that *Agrococcus* sp. RW1 contributes heavy-metal resistance genes, thereby adding new capabilities for metal metabolism to the Pavilion Lake microbialite community

The *Agrococcus* sp. RW1 genome encodes a phosphate (Pho) regulon for the high-affinity uptake of phosphate, which could be an adaption to the low concentration of total phosphorus (3.3 µg L^{-1}) present in Pavilion Lake (Lim *et al.,* 2009). Phosphate (Pho) regulon encoded by *Agrococcus* sp. RW1 included the phosphate permease protein (PstA), phosphate regulon sensor protein (PhoR) and the phosphate regulon transcriptional regulatory protein (PhoB). The phosphate regulon proteins (PhoR/PhoB) and PstA are not predicted within the *A. lahaulensis* genome. Genes associated with phosphorus scavenging have been found in other freshwater microbialites as well (Breitbart *et al.,* 2009). The response of the Pho regulon in *Agrococcus* sp. RW1 under phosphorus limitation remains to be tested; however, it may be a footprint of living in an oligotrophic environment.

Agrococcus sp. RW1 is able to metabolize a wide range of carbon compounds, including amygdalin (Table 4.3). The ability of *Agrococcus* sp. RW1 to use amygdalin was surprising,

because has not been reported for other *Agrococcus* spp., and amygdalin-specific glycosylases were not predicted in the genome. The ability to use amygdalin is found in the distant relative, *Rhodococcus kunmingensis*, an actinobacterium isolated from soil (Wang *et al.,* 2008). Analysis of the *Agrococcus* sp. RW1 genome predicts carbohydrate utilization pathways for mannose, fructose, D-gluconate, trehalose, D-ribose, and glycogen, as well as for chitin, lactate, glycerate, deoxyribose and deoxynucleoside catabolism. Carbohydrate utilization tests of D-glucose, D-mannitol and D-sucrose validated the putative metabolic potential observed in the *Agrococcus* sp. RW1 genome (Table 4.3). *Agrococcus* sp. RW1 was able to grow on many more single carbon sources compared to other members of the genus, possibly allowing access to carbon provided by cyanobacterial mats (Breitbart *et al.,* 2009; Table 4.3).

4.3.7 Carotenoid biosynthesis

The pathway responsible for the yellow pigmentation in the genus *Agrococcus* has not been described, although it has been suggested that diaminobutyric acid within the cell wall could impart the distinctive lemon-yellow colony color (Groth *et al.,* 1996). However, it is unlikely that diaminobutyric acid is completely responsible for the yellow pigmentation in *Agrococcus* spp., as diaminobutyric acid is a quite rare. And, many other bacteria (e.g. *Cronobacter sakazakii*) have yellow colonies in the absence of diaminobutyric acid (Zhang *et al.,* 2014). As well, actinobacteria, which form yellow colonies, produce C_{40} carotenoids (e.g. canthaxanthin and echinenone) and C_{50} carotenoids (e.g. flavuxanthin) (Tao *et al.,* 2007; Klassen, 2010).

Cronobacter sakazakii strain BAA894 is a *Gammaproteobacteria* that also produces yellow pigmented colonies (Zhang *et al.,* 2014). The carotenoid biosynthetic pathway from *C.*

sakazakii strain BAA894, when reconstructed in *E. coli*, produced lycopene, β-carotene, cryptoxanthin or zeaxanthin (Zhang *et al.,* 2014). The production of zeaxanthin or zeaxanthin glycoside from *C. sakazakii* strain BAA894 pathways in *E. coli* changed the colony pigmentation from white to yellow (Zhang *et al.,* 2014).

We therefore screened *Agrococcus* sp. RW1 and *A. lahaulensis* K22-21 genomes for genes involved in the production of carotenoids, and based on these results, propose a C_{40}/C_{50} carotenoid biosynthetic pathway (Figure 4.7). Both *Agrococcus* sp. RW1 and *A. lahaulensis* K22-21 have the genetic potential to produce lycopene, β-carotene, canthaxanthin, echinenone, and/or zeaxanthin or astaxanthin (Figure 4.7). In both *Agrococcus* sp. RW1 and *A. lahaulensis* K22-21 the carotenoid biosynthetic pathway includes predicted genes for phytoene synthase, phytoene dehydrogenase, beta-carotene ketolase, and a second beta-carotene-like ketolase that likely converts echinenone to canthaxanthin, which are characteristic of C_{40}/C_{50} carotenoid pathway (Tao *et al.,* 2007; Figure 4.7). Genes within the carotenogenic gene cluster of *Agrococcus* sp. RW1 and *A. lahaulensis* K22-21 shared similarity to *Brevibacterium linens,* a C_{50} carotenoid producer (Krubasik *et al.,* 2000).

The proposed carotenoid biosynthetic pathways in both *Agrococcus* sp. RW1 and *A. lahaulensis* K22-21 are similar to the pathway described in *Cronobacter sakazaki,* which produces yellow pigmented colonies (Zhang *et al.,* 2014). While we predict that zeaxanthin is responsible for the yellow pigmentation in *Agrococcus*, astaxanthin, another yellow-pigmented carotenoid, could alternatively be responsible (Figure 4.7). No hydrolases are predicted by either the *Agrococcus* sp. RW1 or *A. lahaulensis* genome, which is the only enzyme known to convert β-carotene to zeaxanthin or canthaxanthin to astaxanthin (Klassen, 2010; Zhang *et al.,* 2014). It is

also possible that a hypothetical gene within the genome is functioning as a hydrolase to convert β-carotene to zeaxanthin or canthaxanthin to astaxanthin. Prelimary HPLC data suggests that the yellow pigment is carotenoid like however, we were unable to determine its structure.

The function of yellow pigmentation within *Agrococcus* sp. RW1 remains unclear. Low dissolved organic carbon (DOC) in Pavilion Lake allows for high penetration of solar UV radiation, which benthic microbial mats partially protect against with carotenoids (Lim *et al.*, 2009; Lionard *et al.*, 2012). Similarly, the yellow pigment may help protect *Agrococcus* sp. RW1 from photo-damage in Pavilion Lake.

4.4 Conclusions

Agrococcus sp. strain RW1 was isolated from a modern microbialite, and has a number of features that distinguish it from previously characterized members of this genus. These include the presence of PLFA iC15:1Δ^4, β-galactosidase activity, the amygdalin utilization, and filamentous growth in diluted medium. Phylogenetic analysis using either 16S rDNA or MLST could not resolve *Agrococcus* sp. RW1 and *A. lahaulensis* as different species, but placed them consistently in the same clade. However, whole genome analysis indicates that *Agrococcus* sp. RW1 and *A. lahaulensis* K22-21 are separate species, based on relatively low functional gene conservation, less than 95% amino-acid identity, and the presence of many non-conserved intergenic regions within the *A. lahaulensis* genome. We suggest the renaming of *Agrococcus* sp. RW1 to *Agrococcus pavilionensis* RW1 based on our polyphasic analysis.

The genome of *Agrococcus* sp. RW1 suggests genetic promiscuity due to mobile elements, plasmids and predicted prophage. The plasmids could act as mobile elements through replicative

transposition leading to high genomic plasticity between *Agrococcus* sp. RW1 and *A. lahaulensis*. The LC-RRW783 plasmid and chromosome encodes genes related to heavy-metal resistance, which could contribute to the heavy metal-resistance genes found in the metagenome. Although the predicted prophage in *Agrococcus* sp. RW1 could not be induced to enter the lytic phase, such a lysogen may also act as a moble element in the genome.

The presence of cold-shock proteins, a low phosphrous response regulon (Pho), heavy-metal resistance, and carotenogenic gene clusters that are likely responsible for the yellow pigmentation, are features that are likely highly condusive to living in Pavilion Lake. These results will provide a blueprint for future studies of members of this genus including their distribution, stress response, pigment synthesis, and phage interactions.

4.5 **Tables and figures**

Table 4.1: Comparison of physiological properties of *Agrococcus* selected strains

	Strain RW1	*A.lahaulensis*[1] K22-21	*A.baldri*[1] V-108	*A.citreus*[1] D-1/1a	*A.jenensis*[1] 2002-39/1	*A.terreus*[1] DNG5
Habitat of isolation	microbialite	desert soil	air	painting	sandstone	forest soil
Cell size (µm)						
Length	0.5 - 0.7	1.0 - 1.5	1.1 - 1.7	1.1 - 1.7	0.7 - 1.7	0.8 - 1.0
width	0.3 - 0.5	0.6 - 1.0	0.7 - 1.0	0.7 - 1.0	0.7 - 1.0	0.4 - 0.5
Growth temp range(˚C)						
11	+	NA	NA	NA	NA	NA
30	+	+	+	+	+	+
37	+	+	W	+	V	+
42	+	-	-	NA	-	NA
pH growth range						
6	+	+	NA	NA	NA	+
7	+	+	+	+	+	+
10	+	+	NA	NA	NA	-
NaCl tolerance (%)						
0	+	NA	NA	NA	NA	+
6	+	+	+	+	NA	-
7	-	+	NA	+	NA	-

- Negative, + Positive, W: Weak growth, V: Variable growth, NA: not available, Temp: Temperature
All growth measurements for strain RW1 were taken after 3 d.
[1]Groth *et al.*, 1996; Wieser *et al.*, 1999; Zlamala *et al.*, 2002; Zhang *et al.*, 2010.

Table 4.2: Selected cellular phospholipid fatty acids of *Agrococcus* selected strains (%)

	Strain RW1	*A.lahaulensis*[1] K22-21	*A. baldri*[1] V-108	*A. citreus*[1] D-1/1a	*A. jenensis*[1] 2002-39/1
$C_{14:0}$	ND	ND	ND	tr	tr
$iC_{14:0}$	ND	ND	ND	tr	tr
$C_{15:0}$	ND	ND	ND	tr	ND
$iC_{15:1\Delta4}$	3.5	ND	ND	ND	ND
$iC_{15:1}$	ND	ND	ND	ND	1.9
$aiC_{15:1}$	ND	tr	ND	ND	0
$iC_{15:0}$	8.8	9.9	5.7	10	12.2
$aiC_{15:0}$	46.6	48.4	44.9	53.1	57.8
$C_{16:0}$	5.5	1.8	3.0	1.7	2
$iC_{16:0}$	2.8	5.8	7.5	12.0	12.6
$iC_{17:0}$	3.1	4.8	1.5	1.7	1.9
$aiC_{17:0}$	29.7	27.6	24.3	13.2	9.3
$aiC_{17:1}$	ND	ND	ND	ND	ND
$C_{18:0}$	ND	ND	ND	tr	tr

Values are percentages of total phospholipid fatty acids. ND: not detected, tr: traces (<1%). Strain RW1: *Agrococcus* sp.
[1]Mayilraj *et al.*, 2006.

Table 4.3: *Agrococcus* spp. final assembly statistics

	Strain RW1		*A. lahaulensis* K22-21
Assembler	Celera*	Ray	Unknown
Assembly Name	k0-k1250	k0-k1250v2	ASM42510v1
No. Contigs	50	36	18
No. Scaffold	NA	NA	13
Genome Size (bp)	2,878,403	2,658,972	2,677,837
N50	133,224	113,826	659,136
N90	31,609	51,815	75,009
Largest Contig (bp)	308,429	206,548	851,024
G+C%	72.53	72.65	72.5

*Published in White 3rd *et al.*, 2013a.

Table 4.4: Biochemical properties of *Agrococcus* spp. selected strains

	Strain RW1	*A. lahaulensis*[1] K22-21	*A. baldri*[1] V-108	*A. citreus*[1] *D-1/1a*	*A. jenensis*[1] 2002-39/1	*A. versicolor*[1] K114/01(T)
Activity of:						
Gelatinase	-	+	-	-	-	ND
β-galactosidase	+	-	-	-	-	W
Assimilation of:						
D-glucose	+	-	+	-	+	+
D-mannitol	+	+	+	+	+	W
D-sorbitol	+	-	+	-	-	-
L-Rhamnose	+	+	-	-	-	-
D-sucrose	+	-	-	-	-	+
Amygdalin	+	-	-	-	-	-
L-arabinose	-	+	+	+	+	+

ND: Not detected, W: Weakly positive, Strain RW1: *Agrococcus* sp.
[1]Behrendt *et al.*, 2008.

Table 4.5: Antibiotic susceptibility of *Agrococcus* spp. selected strains

Antibiotic	Disc content	Strain RW1	*A. citreus*[1] D1/1a^T	*A. jenensis*[1] DSM9580^T	*A. jenensis*[1] DSM9996
Sulfamethoxazole + Trimethoprim	23.75 + 1.25 µg	+	ND	ND	ND
Penicillin	10 IU	-	-	-	-
Clindamycin	2 µg	-	ND	ND	ND
Rifampin*	5 / 30 µg	-	-	-	-
Polymyxin	300 IU	-	W	W	W
Cefixime	5 µg	+	ND	ND	ND
Sulfisoxazole	300 µg	+	ND	ND	ND
Oxacillin**	1 / 5 µg	+	-	-	-
Tetracycline	30 µg	-	-	-	-
Trimethoprim	5 µg	+	ND	ND	ND
Tobramycin	10 µg	-	ND	ND	ND
Vancomycin	30 µg	-	ND	ND	ND
Streptomycin	10 µg	-	-	-	-

+ Resistant, - Sensitive, W: Weakly Sensitive, ND: No Data
*Strain RW1 was sensitive to 5 µg, whereas the other strains were sensitive at 30 µg.
**Strain RW1 was resistant to 1 µg, whereas the other strains were sensitive at 5 µg.
Strain RW1 was not tested at 5 µg Oxacillin, only at 1 µg.
[1]Wieser *et al.*, 1999.

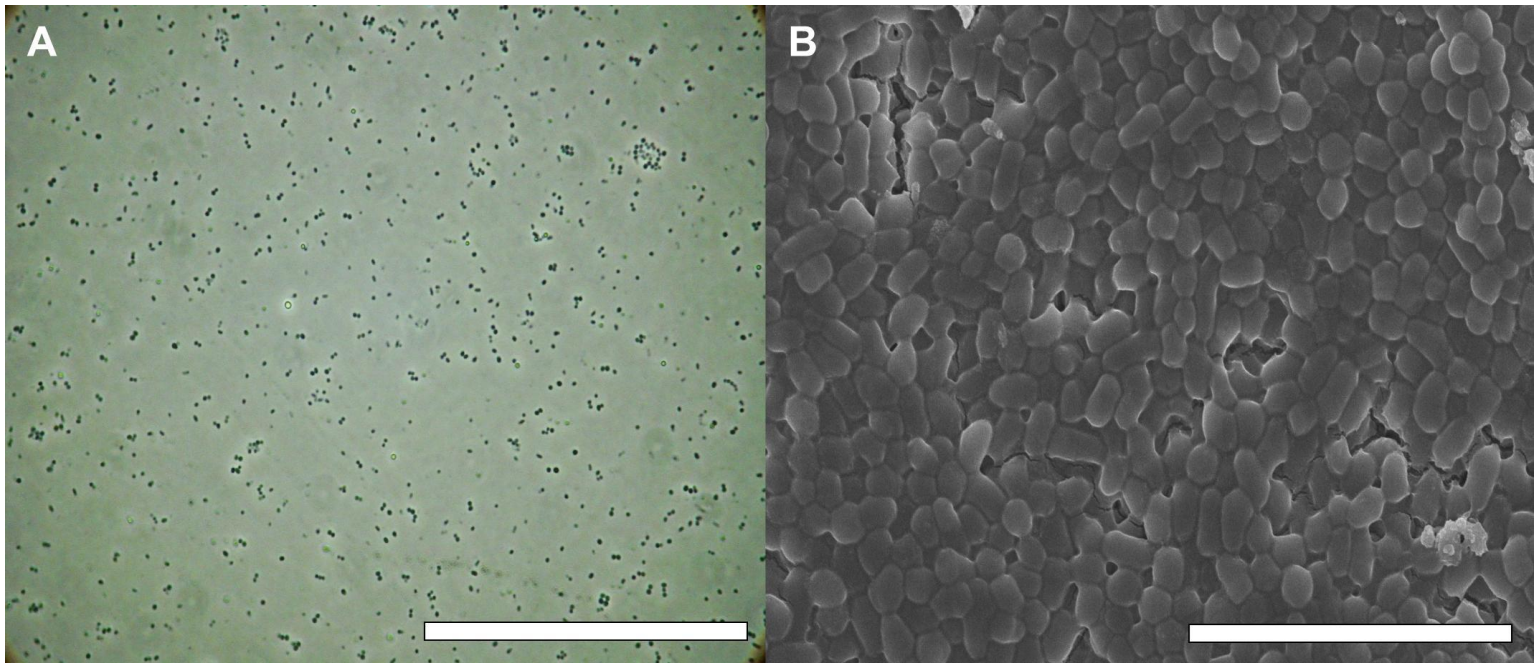

Figure 4.1: *Agrococcus* sp. strain RW1 microscopy
A) Light microscopy image during logarithmic phase of growth (48 h). Scale bar: ~100 µm.
B) SEM image during stationary phase of growth (72 h). Scale bar: ~10 µm.
Observed here at standard growth conditions in LB medium at 30ºC.

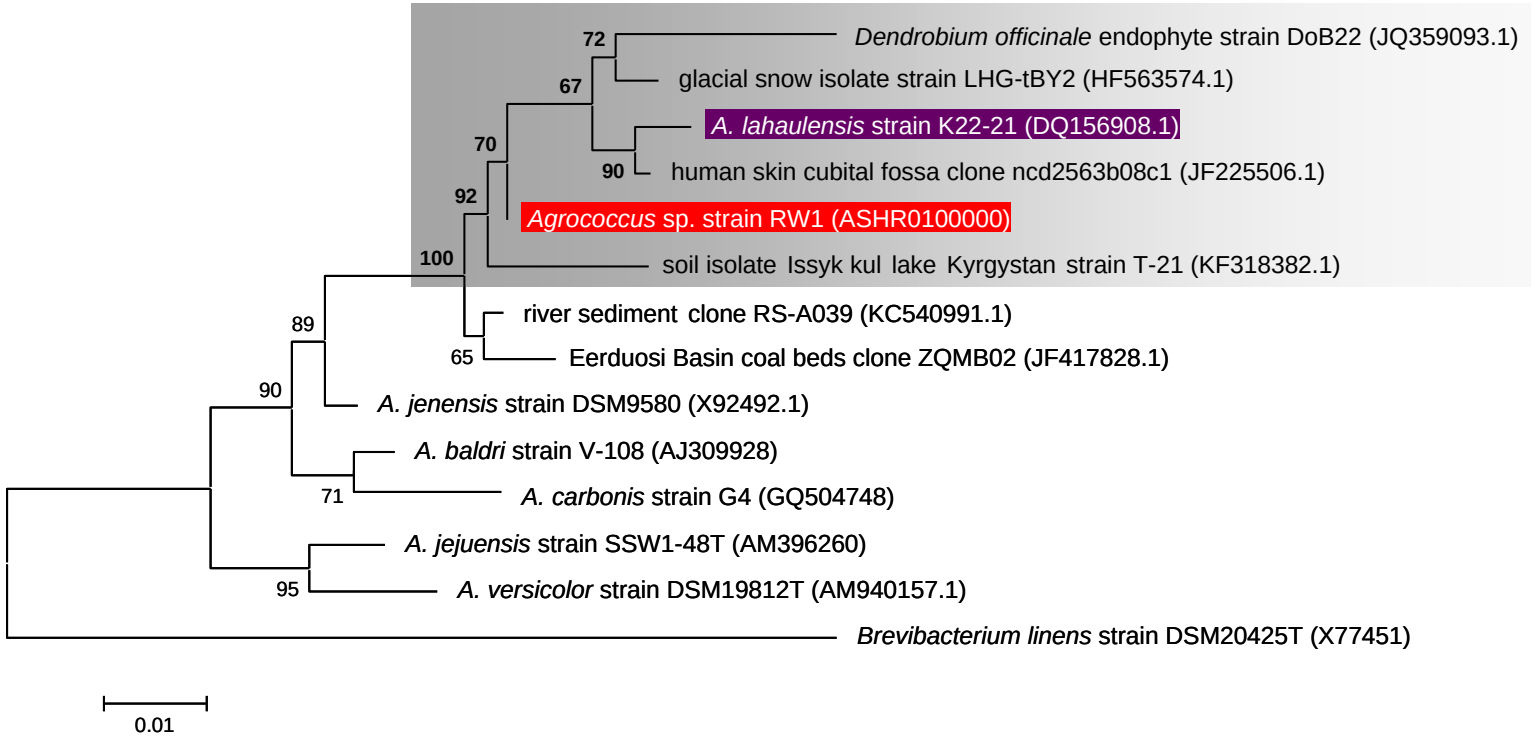

Figure 4.2: Maximum-likelihood tree of 16S rRNA gene sequences for *Agrococcus* spp. and related taxa (~1409 bp) Bootstrap values greater than 50% at given branches.

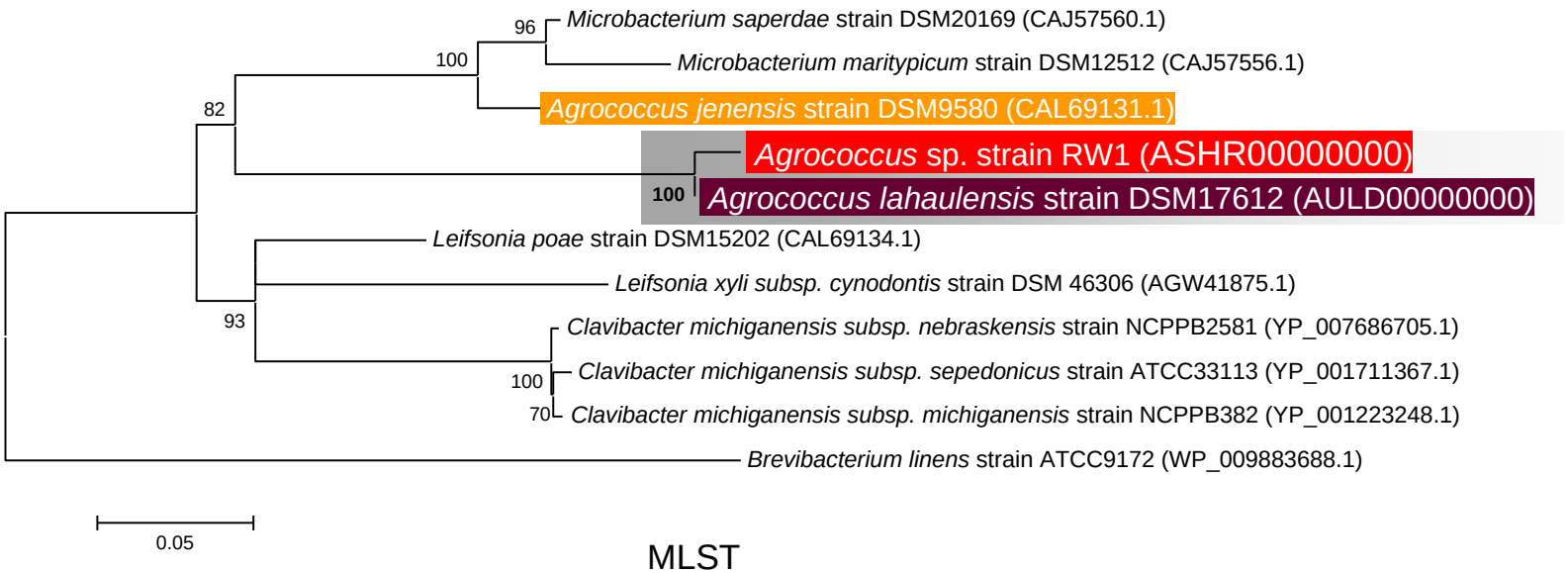

Figure 4.3: MLST (multiple locus sequence typing) maximum-likelihood tree of *Microbacteriaceae* (~2939 amino acids) Bootstrap values greater than 50% at given branches.

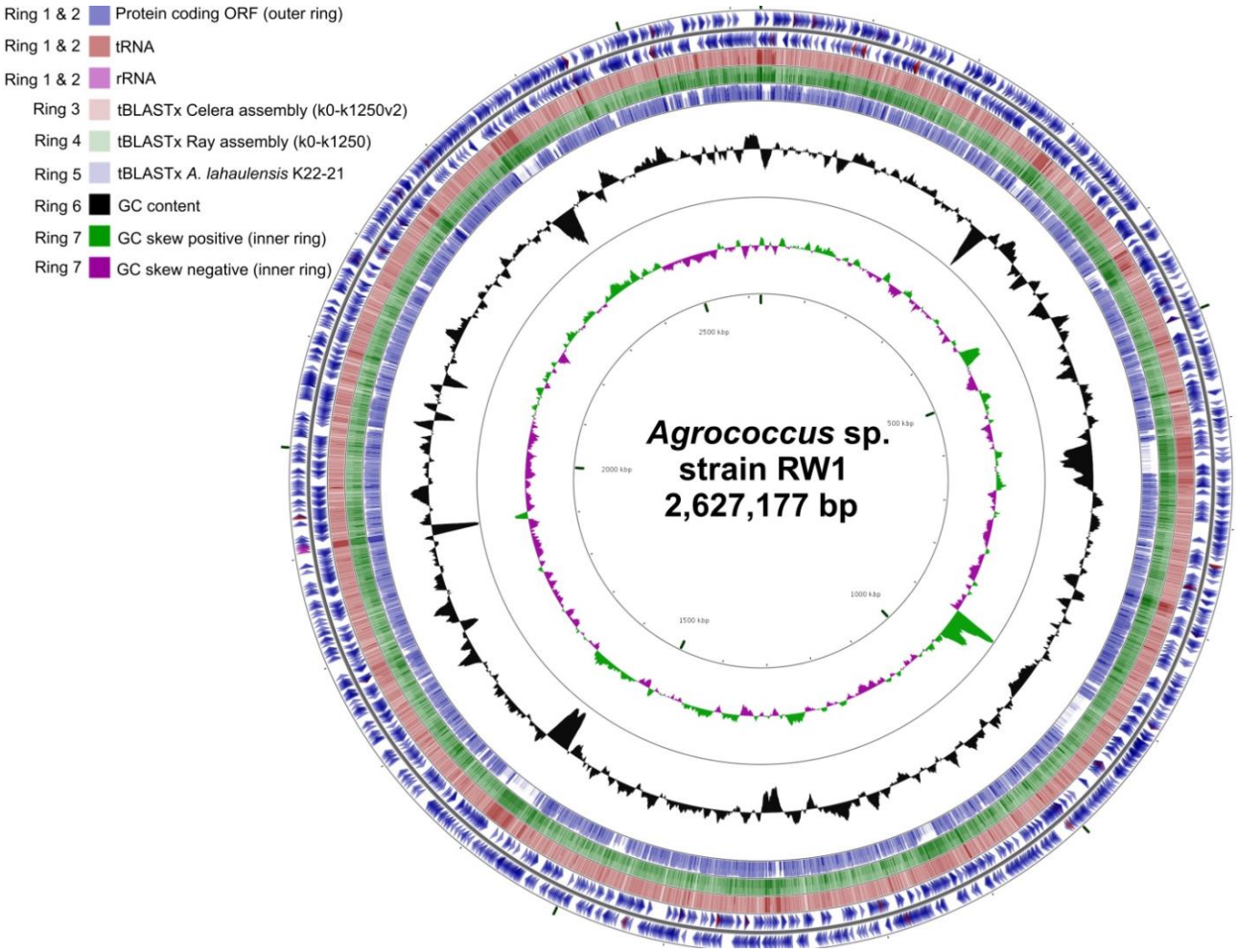

Figure 4.4: Genome plot (~2.6Mb) of *Agrococcus* sp. strain RW1
Genome key (left corner): starts with inner most ring which is a genome ruler followed by GC skew (purple/green) and ends with two outer rings which contain protein-coding ORFs, tRNAs and rRNAs.

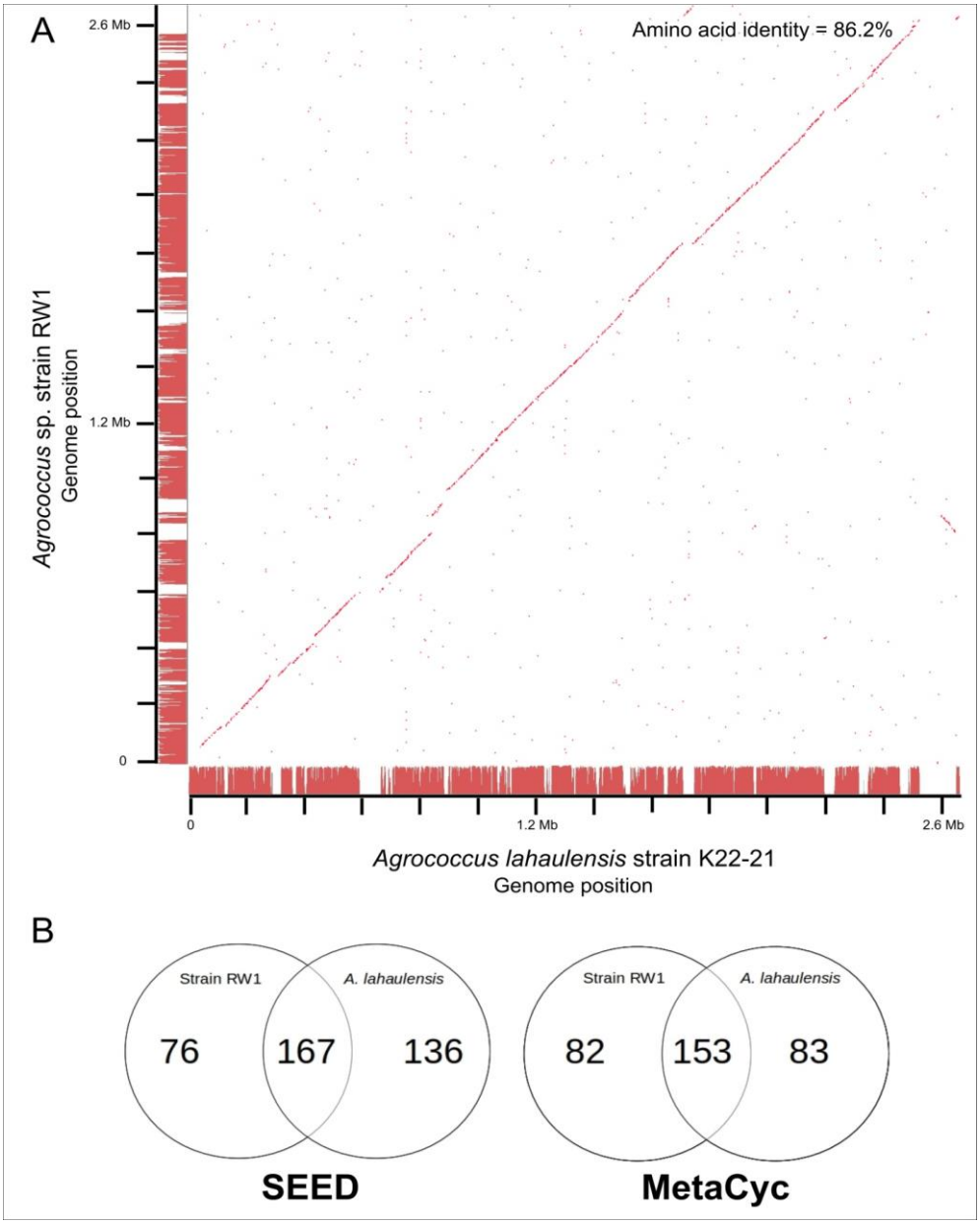

Figure 4.5: Genome synteny and Venn diagrams of *Agrococcus* sp. RW1 vs. *A. lahaulensis* K22-21

A) RAST bidirection blast genome synteny dot-plot with Progressive Mauve alignments as axes. Red dots are positive blast hits based on RAST genome comparision module. Red line regions at the axes are regions of synteny based on Progressive Mauve. Average amino-acid identity was calculated by RAST functional module with web based tool AAIr (Krebs *et al.*, 2013).

B) Venn Diagrams based on RAST SEED/Figfams and Metapathways MetaCyc annotations.

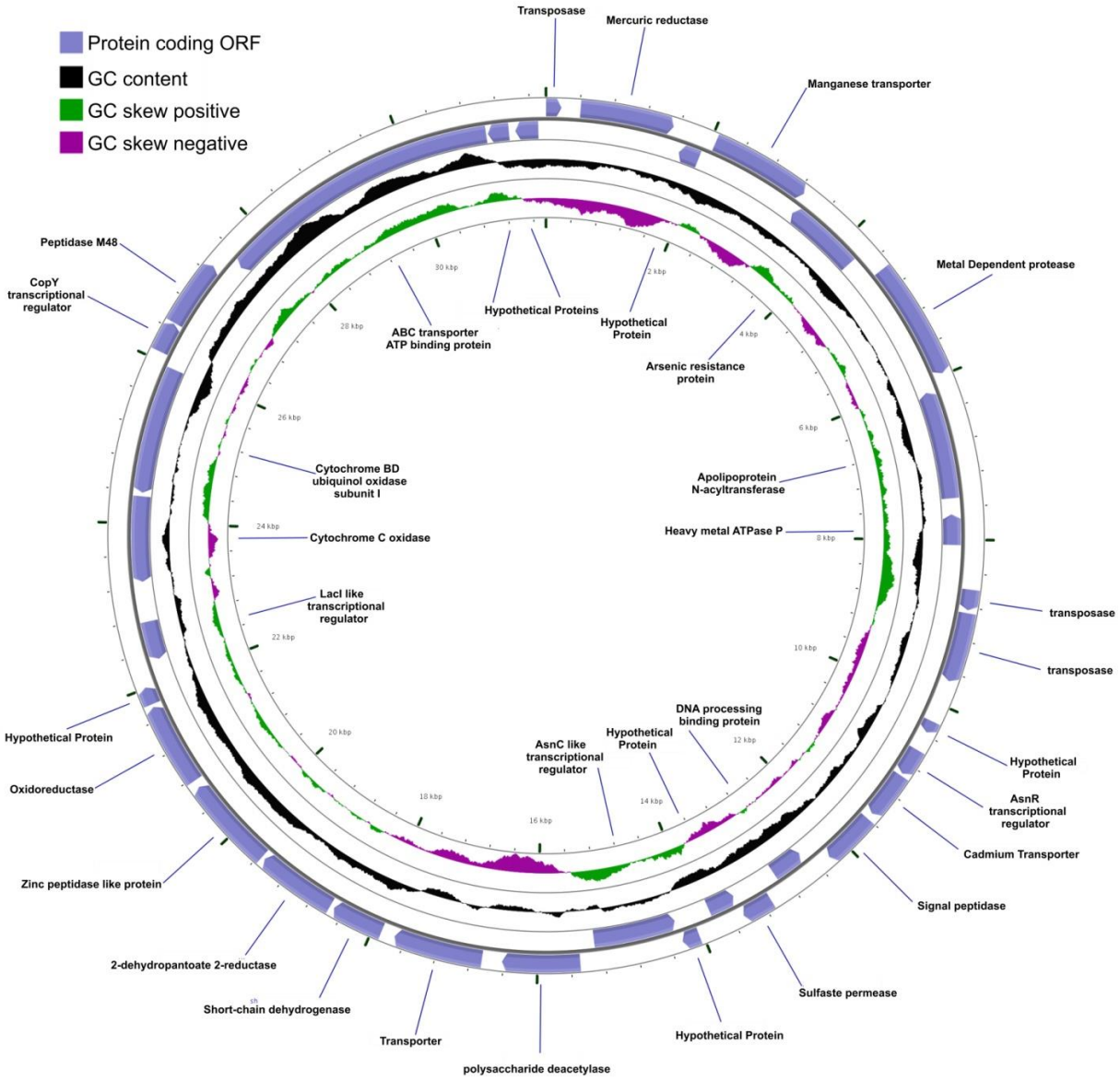

Figure 4.6: *Agrococcus* sp. RW1 LC-RRW783 plasmid genomic plot

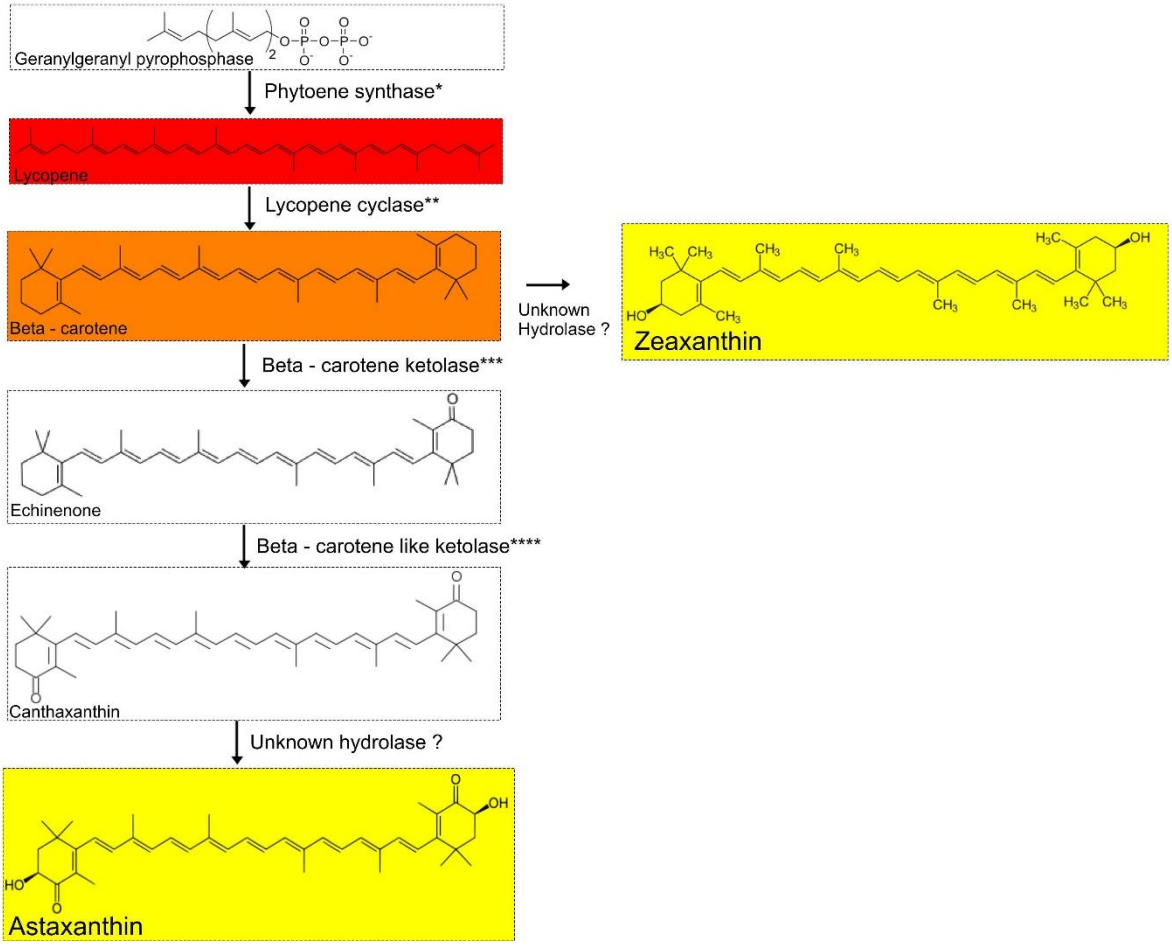

Figure 4.7: Proposed carotenoid biosynthetic pathway for *Agrococcus*

Agrococcus has the genetic potential to accumulate C_{40} carotenoids (canthaxanthin and echinenone). Hydrolases are not predicted in the genomes of *Agrococcus* sp. RW1 or *A. lahaulensis* K22-21.

*Phytoene synthase, **lycopene cyclase, ***beta - carotene ketolase, ****beta - carotene like ketolase are predicted in the genomes of *Agrococcus* sp. RW1 or *A. lahaulensis* K22-21.

Chapter 5:

Illumination of an *Exiguobacterium* through the comparative lenses of classical characterization and modern genomic analysis

5.1 Introduction

Here we describe a second non-photosynthetic pigmented isolate from a 20 m Pavilion Lake microbialite, *Exiguobacterium* sp. strain RW2. The pathway responsible for the orange colony pigmentation in the genus *Exiguobacterium* has not been described.

The genus *Exiguobacterium* is found in many environments due to its tolerance of a wide range of conditions, including pH (5 to 11), salinity (NaCl: 0 to 16%), heavy metals, and temperature (-12°C to 55°C), which is rooted in its diverse metabolic capabilities (Kim *et al.*, 2005; Vishnivetskaya *et al.,* 2009; Belfiore *et al*., 2013; White 3rd *et al.,* 2013b). The first described member of the genus, *E. aurantiacum* DSM6208^{T}, was isolated from a potato processing plant (Collins *et al.,* 1983). The genus *Exiguobacterium* has fifteen named species, which were isolated from diverse environments, including permafrost (Rodrigues *et al.,* 2006), deep-sea vents (Crapart *et al.,* 2007) and hot springs (Vishnivetskaya *et al.,* 2009, 2011; Table 5.1 and Table 5.2).

The distribution of *Exiguobacterium* spp. across many different environments is related to their growth under a wide range of conditions. Consequently, isolates of *Exiguobacterium* have been used as model organisms for understanding thermal adaptation (Rodrigues *et al.,* 2008), heavy metal stress (Belfiore *et al*., 2013), and the function of non-marine proteorhodopsin (Gushchin *et al.,* 2013). Their metabolic capabilities have industrial and

biotechnological applications, including production of biofuels (Vijayalaxmi *et al.,* 2013), cheese (Lusk *et al.,* 2012) and L-lactate (Jiang *et al.,* 2013a-b), removal of chemicals associated with the textile industry, including chloronitrophenols (CNPs) and N-methylated diaminotriphenylmethane (Arora *et al.,* 2012; Wang *et al.,* 2012), use as biodetergents (Anbu *et al.,* 2013), and for degrading shrimp biowaste (Anil and Suresh, 2013). Further insights into the genetic potential of these microbes may yield a greater understanding of their metabolic capabilities in nature and possibly reveal other industrial applications.

Seven genomes from the genus *Exiguobacterium* have been completed as either drafts (many contigs) or complete genomes (as a single chromosome with plasmids). These include draft genomes of *Exiguobacterium* sp. strain S17 from a stromatolithic microbialite (Ordoñez *et al.,* 2013), strain 8-11-1 from lake sediments (Jiang *et al.,* 2013), strain OS77 from a Japanese hot-spring (Nonaka *et al.,* 2014), and complete genomes for *E. sibiricum* strain 255-15 from permafrost (Rodrigues *et al.,* 2008), *E. antarcticum* strain B7 from a microbial mat in Antarctica (Azevedo *et al.,* 2012), *Exiguobacterium* sp. strain MH3 from the rhizosphere of duckweeds (complete genome, Tang *et al.,* 2013), and *Exiguobacterium* sp. strain AT1b from Mammoth Terrace hot spring, Yellowstone National Park (Vishnivetskaya *et al.,* 2011). Eleven other ongoing genome sequencing projects through the Joint Genome Institute include *E. acetylicum* strain DSM20416 (Farrow *et al.,* 1994), *E. aurantiacum* strain DSM6208 (Collins *et al.,* 1983), *E. marinum* strain DSM16307 (Kim *et al.,* 2005), *E. oxidotolerans* strain JCM12280 (Yumoto *et al.,* 2004) and *E. sibiricum* strain 7-3 (Vishnivetskaya *et al.,* 2009).

In this contribution, classical and modern genomic analyses are used to characterize the pigmented bacterium *Exiguobacterium* sp. strain RW2, an isolate from a modern freshwater microbialite. The genome encodes many putative proteins, potentially involved in the adaptive physiological response to ranges of salinity, pH, temperatures and heavy-metal stress. As well, a putative carotenoid biosynthetic pathway is likely related to the characteristic orange pigmentation found in the genus. These results provide further insight into the potential of this genus to exploit such a wide range of environmental conditions.

5.2 Materials and methods

5.2.1 Isolation, growth conditions, biochemical and antibiotic susceptibility tests

Exiguobacterium sp. strain RW2 was isolated by plating 0.5 g of a thrombolitic microbialite, collected from 20 m depth in Pavilion Lake, British Columbia (50.86 °N, 121.74 °W), onto M-agar medium [0.5% (w/v) tryptone, 0.25% (w/v) yeast extract, 1% (w/v) NaCl, 1.5% (w/v) agar, pH 7], followed by incubation at 30 °C for 3 d (White 3rd *et al.*, 2013b). M-agar was also used for maintenance (at 30 °C) and for assessing growth with respect to temperature (4, 5, 11, 16, 20, 25, 30, 37, 42, 45, 50, 55 °C at pH 7 and 1% NaCl), pH (4, 5, 6, 6.5, 7, 7.5, 8, 10, 10.5, 11, 12 at 30 °C) and salinity (0, 1, 3, 6, 9, 12, 13, 16 % NaCl at 30 °C) for 3 d. Strain characteristics, including colony and cell morphologies were determined by standard methods (Murry *et al.*, 1994). Oxidase tests and biochemical enzyme assays and carbohydrate utilization were done using API20E (BioMérieux) test strips on cultures re-suspended in sterile water. Antibiotic susceptibility was determined by the Kirby-Bauer method using antibiotic discs on M agar (Collee *et al.*, 1996). Prophage induction assays were done either by adding 0.2 μg ml^{-1} of

mitomycin C, or heating cultures to 45 °C , incubating at 30 °C for 3-10 h and monitoring changes in turbidity until a decrease of OD_{600} to 0.1 or less was observed (starting OD_{600} 0.6). At several time points cells were pelleted at 3,250 x *g* for 10 mins and the supernatent filter-sterilized twice through a 0.22 µm pore-size Millex Durapore PVDF membrane (Millipore) filter before plating using a double agar overlay plaque assay (Kropinski *et al.,* 2009).

5.2.2 **Phospholipid fatty acid analysis (PLFA)**

Phospholipid fatty acids were extracted from cultures grown in 25 ml M broth for 4 d at 22 °C. Cultures were transferred into pre-combusted vials for an overnight solvent extraction in a 1:2:0.8 ratio of dichloromethane (DMC), methanol (MeOH) and phosphate-buffered saline (PBS) [137 mM NaCl, 2.7 mM KCL, 10 mM Na_2HPO_4 $2H_2O$, 2 mM KH_2PO_4, pH 7.4] (Bligh and Dyer, 1959). The extract was filtered through a separatory funnel where DCM and water were added to achieve a mixture of MeOH:DCM:water of 1:1:0.9 (Bligh and Dyer, 1959). The lower organic phase was removed and purified into polar, neutral, and non-polar fractions using liquid chromatography through silica-gel. Phospholipids present in the polar fraction were subjected to mild alkaline methanolysis to produce fatty-acid methyl esters (FAMEs) (Guckert *et al*., 1985). FAMEs were separated, identified, and quantified using gas chromatography mass spectrometry (GC/MS) (Agilent Technologies Inc., Santa Clara, CA, USA) with a DB-5MS capillary column (30 m x 0.32 mm I.D. x 0.25 µm film thickness) under a temperature regime of 50 °C (1 min), 20 °C min^{-1} to 130 °C, 4 °C min^{-1} to 160 °C, and 8 °C min^{-1} to 300 °C (5 min). PLFAs were identified by retention time and mass spectra relative to those of reference standards (Bacterial Acid Methyl Ester Mix, Matreya Inc., Pleasant Gap, PA, USA; and Supelco 37

Component FAME Mix, Sigma-Aldrich Co., Bellefonte, PA, USA). A modified picolinyl ester derivatization was used to determine the branching point in unknown compounds (Destaillats and Angers, 2002; Dowd, 2012). Dimethyl disulphide adducts derivatives were prepared to determine the double bond position in unsaturated fatty acids (Nichols *et al.*, 1986).

5.2.3 Light and scanning electron microscopy (SEM)

Exponentially growing cells harvested 26 h after being transferred to liquid M-medium were viewed by light microscopy under oil immersion at 100x. For SEM, a culture in mid-stationary phase 72 h after being transferred to liquid M-medium was pelleted at 3,250 x *g* for 10 min, then the M medium was exchanged and cells were fixed in 2.5% glutaraldehyde spiked phosphate-buffered saline (PBS) [137 mM NaCl, 2.7 mM KCL, 10 mM Na_2HPO_4 $2H_2O$, 2 mM KH_2PO_4, pH 7.4] solution for 30 min on ice. The fixed culture was filtered onto a 0.2 µm pore-size Supor polycarbonate membrane (Pall Port Washington, NY). Cells on the filter were washed with PBS and post-fixed in 1% OsO_4 for 1 h. The fixed culture was filtered onto a 0.2 µm pore-size Supor polycarbonate membrane (Pall Port Washington, NY). The filter was washed with PBS and post-fixed in 1% OsO_4 for 1 h. The stained filter was passed through a graded ethanol series (25, 50, 70, 95, 100%) at 10 min intervals, and at 100% EtOH, was critical-point dried. A sputter coater applied 5 nm of gold/palladium alloy onto the cells prior to imaging by SEM using a Hitachi S4700 microscope.

5.2.4 DNA extraction, PCR and Illumina library construction

DNA was extracted using QIAamp followed by MinElute cleanup columns (Qiagen Germantown, MD). Full length 16S rDNA was amplified using the universal primers 27f and

1492r (Lane *et al.,* 1991). To ensure coverage of the full length 16S rDNA sequence, another PCR amplification was completed subsequently using primers 341f and 907r (Muyzer *et al.*, 1993; 1998). PCR products were sequenced using the Sanger method on an ABI3730 (Applied Biosystems Foster City, Ca). The Illumina MiSeq library was constructed using the Lucigen NxSeq library prep kit (Lucigen Middleton, WI) without the final 14-cycle PCR enrichment to avoid PCR bias; quality control of the resulting library was completed using Agilent high-sensitivity DNA chips and digital droplet PCR (Hindson *et al.,* 2011; White 3rd *et al.*, 2013 a-c). The library was sequenced using 250 bp paired-end sequencing on the Illumina MiSeq at GenoSeq UCLA Los Angeles, CA.

5.2.5 **Whole genome assembly, assembler comparison, genome finishing and annotation**

Raw Illumina sequencing data was screened for PhiX spike-in contaminants using Bowtie2 (version 2.1.0) then removed using Picard tools (version 1.90) (White 3rd and Suttle, 2013c). The draft genome assembly was completed using Ray (version 2.2.0) using the error-corrected reads (from AllPath-LG, version 44837) using a k-mer size of 55 bp (Boisvert *et al.*, 2010; White 3rd *et al.,* 2013b). The genome of *Exiguobacterium* sp. strain AT1b was downloaded from NCBI for comparison, scaffolding and contig ordering. Progressive Mauve was used to find the best representative assembly, contig order among the various assemblies, and for scaffolding (Darling *et al.,* 2010). The *Exiguobacterium* sp. strain RW2 contigs were ordered and aligned in Progressive Mauve to *Exiguobacterium* sp. strain AT1b to visualize genome order (Vishnivetskaya *et al.,* 2011). The remaining gaps between contigs were closed by recursive

alignments using Mauve. The ordered contigs with overlaps were merged into a singular circular contig using the EMBOSS union script (Rice *et al.*, 2000).

Error-corrected, phiX-removed reads used in the *Exiguobacterium* sp. strain RW2 Ray assembly were mapped back to the final singular circular genome using Bowtie2 with the very sensitive local option (Langmead and Salzberg, 2012). The Bowtie2 read mapping output file (Sam file) was visually inspected by the Tablet program (Milne *et al.*, 2013). The contigs that were screened for overlaps and read mapping depth (>10x) were then merged manually.

Annotations were further analyzed by comparison to other genomes, genome synteny, and average amino-acid identity. A genome circular plot of *Exiguobacterium* sp. strain RW2 was constructed using CGviewer (Grant and Stothard, 2008), and compared to the genomes of *E. sibiricum* strain 255-15, *Exiguobacterium* sp. strain AT1b and *Exiguobacterium* sp. strain MH3 using tBLASTx at an e-value of $1e^{-3}$ with 50% identity and 25 bp overlap, and then displayed in the CGviewer genome plot (Grant and Stothard, 2008). Synteny plots were completed in the RAST server module using a BLAST based dot plot format (Aziz *et al.*, 2008). Average amino-acid identity (AAIr) analysis and functional gene similarities were calculated on the RAST server module and then parsed with a web-based tool AAIr (Aziz *et al.*, 2008; Krebs *et al.*, 2013).

5.2.6 **Phylogenetic analysis and multiple locus sequence typing (MLST) analysis**

Sanger sequences obtained from 27f-1492r and 341f-907r PCR products were merged into a full length 16S rDNA reference sequence using Consed (Gordon *et al.*, 1998) with manual editing. The phylogenetic position of *Exiguobacterium* sp. strain RW2 was assessed using the error-corrected whole-genome assembled 16S rDNA (~99% similar to PCR amplified) rather

than the PCR amplified sequence, due to a lower chance of PCR based substitution errors and having greater total sequence (1353 bp vs. 1276 bp). All sequences for phylogenetic analysis were aligned, trimmed using MUSCLE parameters (-400 gap open with zero gap extended), and then clustered using UPGMB (Edgar 2004). MLST (multiple locus sequencing typing) marker analysis was completed by extracting amino-acid sequences for RpoB (β subunit of bacterial RNA polymerase, ~1180 aa), RecA (recombination protein A, ~349 aa), GyrB (DNA gyrase subunit B, ~643 aa), DnaK (Heat shock protein 70, ~614 aa), IDH (isocitrate dehydrogenase ~422 aa), and IleS (isoleucyl-tRNA synthetase, ~ 921 aa) from *Exiguobacterium* spp. genomes by BLASTP analysis. The MLST protein marker genes (RpoB, RecA, GyrB, DnaK, IDH and IleS) were then concatenated based on strain into ~3856 aa sequences. Maximum-Likelihood trees were constructed using the trimmed 16S rRNA gene sequences (~1353 bp), 5S-16S-23S combined sequences (~4350 bp), and the concatenated MLST sequences (~3856 aa) with bootstrapping (1000 replicates), using the Jukes-Cantor substitution model in MEGA (version 5.10, Tamura *et al.*, 2011).

5.3 Results and discussion

5.3.1 Morphology and growth characteristics

Exiguobacterium sp. strain RW2 is a Gram-positive facilitative anaerobe. After 48 h growth at 30°C on M-agar, it forms bright orange, smooth, circular colonies that are typically 3 to 4 mm in diameter (Table 5.2). In liquid M-medium at 30 ºC, the cells are coccoid in logarithmic growth phase after 24 to 48 h, and irregular shaped after ~72 h in late stationary phase, coincident with the beginning of biofilm formation (Figure 5.1). Biofilm formation could facilitate

association with the microbial mats found on microbialites in Pavilion Lake, and may be a survival mechanism in nutrient-poor or starvation states (Shao *et al.,* 2013). Hence, biofilm formation could be a survival strategy for *Exiguobacterium* sp. strain RW2 in the cold oligotrophic conditions of Pavilion Lake (Lim *et al.,* 2009), and is consistent with the isolation of *Exiguobacterium antarcticum* strain DSM14480 and *E. antarcticum* strain B7 from a cold microbial mat and biofilm (Vishnivetskaya *et al.,* 2009).

Exiguobacterium sp. strain RW2 grows under a wide range of temperatures, from 4 to 50 ˚C, which is the largest temperature range for growth reported for the genus (Table 5.2). Other isolates from Antarctica and permafrost can grow at even lower temperatures, with *E. antarcticum* strain DSM 14480, and *E. sibiricum* strains 255-15, 7-3, and 190-11 growing at -2.5 ˚C (Vishnivetskaya *et al.,* 2009). Temperatures at which Pavilion Lake microbialites are stably 4˚C throughout the year (Lim *et al.,* 2009), (Lim *et al.,* 2009), removing the selective pressure for growth at lower temperatures. At the other end of the temperature range, *Exiguobacterium* sp. strain RW2 grows at 50˚C, and is the first member of this genus that has been isolated from a permanently cold environment that has been demonstrated to grow at such a high temperature. Although growth at temperatures as high as 55˚C is not uncommon among isolates of *Exiguobacterium* spp., strains that grow at 50˚C or above have previously only been isolated from hot springs and deep-sea hydrothermal vents (Crapart *et al.,* 2007; Vishnivetskaya *et al.,* 2009). Growth at such high temperatures is not a requirement for life in Pavilion Lake; however, *Exiguobacterium* sp. RW2 is adapted for higher temperatures, suggesting that its distribution is not restricted to cold oligotrophic environments.

Exiguobacterium sp. strain RW2 grows in acidic (pH 5) and alkaline (pH 11) media; whereas, other isolates of *Exiguobacterium* spp. only grow between pH 6 and 10 (Vishnivetskaya *et al.*, 2009, Table 5.2). Growth at a pH range of 5 to 11 has not been reported for other typed strains of *Exiguobacterium* spp. (Table 5.2); however the marine isolates *E. profundum* (Crapart *et al.*, 2007), *E. aestuarii* and *E. marinum* (Kim *et al.*, 2005) grow at pH 5.5 and are unable to grow at pH 10.

The growth of *Exiguobacterium* sp. strain RW2 at NaCl concentrations between 0 and 7% is different from most strains of *Exiguobacterium* spp, although some marine strains can grow in the presence of 19% NaCl (Kim *et al.*, 2005; Lopez-Cortes *et al.*, 2006; Table 5.2). Strain RW2 is the first non-marine strain able to grow in the presence of 7% NaCl (Table 5.2). Growth over such wide ranges of temperature, pH, and salinity makes *Exiguobacterium* sp. strain RW2 unique among isolates of the genus.

5.3.2 Biochemical properties and antibiotic susceptibility

Exiguobacterium sp. strain RW2 differed from other typed strains as it has urease function, no oxidase activity, and cannot produce acetoin (Table 5.3). Even though the genome of *Exiguobacterium* sp. strain RW2 encodes putative cytochrome oxidases (including types B and C), out of fifteen strains of *Exiguobacterium* spp., only strain RW2, *E. aestuarii, E. marinum* and *E. aurantiacum* lack demonstrated oxidase function (Fruhling *et al.*, 2002). Additionally, within the genus, urease activity has only been found in *Exiguobacterium* sp. strain RW2 (Table 5.3), although a gene encoding urease was not found in the genome, suggesting that it may be plasmid encoded. Urease can induce carbonate precipitation and is found in carbonate

precipitating members of *Bacillus* spp. (Hammes *et al.,* 2003), which is a distant relative of strain RW2. Finding an active urease in strain RW2 would set the stage for further experimentation relating to urease mediated carbonate precipitation.

Little is known about antibiotic sensitivity in *Exiguobacterium* spp. With the exception of *E. indicum* and *E. acetylicum*, isolates of *Exiguobacterium* spp. are sensitive to clindamycin (Chaturvedi *et al.,* 2008), although not all isolates have been tested and the concentrations have not been uniform (Table 5.4). Homologs of genes such as *ermB*, *ermTR*, and *mefA/E* that are typically associated with clindamycin resistance were not found in genomic data for *Exiguobacteriu*m spp. (Gygax *et al.,* 2006). Additionally, *Exiguobacterium* sp. strain RW2 was tested against eleven other antibiotics (Table 5.4); resistance was only found for sulfisoxazole (300 μg). Sensitivity was shown for sulfamethoxazole and trimethoprim in combination, consistent with observations that some strains of *Exiguobacterium* spp. are sensitive to sulfamethoxazole (Chaturvedi and Shivaji, 2006). Sulfamethoxazole and sulfisoxazole resistance genes such as *sul*1, *sul*2 and *dhfr* are carried on plasmids (Barman *et al.,* 2010; Toleman *et al.,* 2007; Sherley *et al.,* 2004), as are resistance genes for trimethoprim. Plasmid pMC1 in *Exiguobacterium* sp. strain S3-2 carries resistance genes for tetracycline, trimethoprim, florfenicol and erythromycin (Yang *et al.,* 2014). There was no evidence for the presence of *sul*1, *sul*2 or *dhfr* genes in strain RW2; hence the sulfisoxazole resistance mechanism is unknown. A vancomycin resistance type B protein was predicted by the strain RW2 genome, although strain RW2 is not resistant to vancomycin (Table 5.4) suggesting that the pathway is incomplete or that the protein serves another function.

5.3.3 PLFA characterization and comparative analysis

The PLFA profiles of strain RW2 were dominated by branched fatty acids, with minor contributions from saturated and monounsaturated PLFA (Table 5.5). The major phospholipids in strain RW2 are Iso-C13:0 (15.7%), anteiso-C13:0 (15.4%), and iso-C17:0 (25.6%), which is similar to the profiles from *E. himgiriensis* K22-26^T and *E. marinum* MTCC 7751^T (Singh *et al.*, 2012). The percentages of iso-C17:0 and C17:0, at 25.6% and 1.3%, respectively, are the highest reported percentages of these PLFAs for any characterized strain of *Exiguobacterium* spp. (Table 5.5). In strain RW2, the fourth most abundant phospholipid at 7.6% is Iso-C17:1Δ^5, which is not found in any other *Exiguobacterium* isolate (Table 5.5). Iso-17:1Δ^5 occurs in *Bacillus alvei*, a distant relative of strain RW2 (Moss and Daneshvar, 1992). The high proportion of PLFA Iso-17:1Δ^5 is consistent with strain RW2 being assigned as a new species within the genus *Exiguobacterium*.

5.3.4 Evolutionary placement of *Exiguobacterium* sp. RW2 within the genus

Phylogenetic analysis of 16S rDNA places *Exiguobacterium* sp. strain RW2 in a strongly supported clade with other isolates of *Exiguobacterium* spp. (Figure 5.2), with the closest relative being *Exiguobacterium* sp. strain GIC31, an isolate from glacial ice in Greenland (Vishnivetskaya *et al.*, 2009). However, the 16S rDNA sequence similarity between strains RW2 and GIC31 is <97%, suggesting that they are separate species.

Analysis of the combined ribosomal 5S-16S-23S operon also indicates that *Exiguobacterium* sp. strain RW2 is phylogenetically distinct but in a strongly supported clade related to *Exiguobacterium* sp. strain AT1b (Figure 5.3). The combined ribosomal operon of

Exiguobacterium sp. strain RW2 shares the highest sequence similarity to *Exiguobacterium* sp. strain S17 and *Exiguobacterium* sp. strain 8-11-1 (Figure 5.3). No strains related to *Exiguobacterium* sp. strain RW2 based on combined ribosomal operon have been officially named species (Figure 5.3). We suggest that *Exiguobacterium* sp. strain RW2 is a distinct species based on sequences for the 16S rDNA and combined ribosomal operon. Both strain RW2 and strain S17 were isolated from modern microbialites, and are in a clade with *Exiguobacterium* sp. strain AT1b (based on ribosomal 5S-16S-23S operon) suggesting that they could share a distant ancestor from a high temperature environment (Vishnivetskaya *et al.*, 2011; Belfiore *et al.*, 2013; Ordoñez *et al.*, 2013; White 3rd *et al.*, 2013b).

MLST analysis is consistent with combined ribosomal operon and 16S rDNA gene analysis that *Exiguobacterium* sp. strain RW2 is phylogenetically distinct but in a strongly supported clade related to *Exiguobacterium* sp. strain AT1b (Figure 5.4). MLST analysis needs a minimum of seven loci with regions containing conservation across the genus, but also containing variable regions (Rebollar *et al.*, 2012; Maiden *et al.*, 2013). RecA, RpoB, GyrB, DnaK, IDH, and IleS amino-acid sequences were combined for MLST marker sequence analysis because they are conserved across *Exiguobacterium* spp., as well as in the order *Firmicutes* (Rebollar *et al.*, 2012; Maiden *et al.*, 2013). MLST analysis suggests that *Exiguobacterium* sp. strain RW2 is sister species to *E. aurantiacum* strain DSM14480 (Figure 5.4). This suggests that *Exiguobacterium* sp. strain RW2 is a new species based on MLST analysis. Isolates of *Exiguobacterium* spp. from Cuatro Cienegás form distinct genetic clusters based on whether they were isolated from water or sediment (Rebollar *et al.*, 2012). Our MLST analysis support combined ribosomal operon

analysis that microbialite-isolated strains RW2 and S17 are genetically similar and may share a distant ancestor from a high temperature environment (Vishnivetskaya *et al.,* 2011; Belfiore *et al.,* 2013; Ordoñez *et al.,* 2013; White 3rd *et al.,* 2013b).

5.3.5 Comparative genome analysis

The draft and completed genomes of *Exiguobacterium* spp. were similar in terms of genome size, GC content, and number of protein-coding genes. As a genus, the sizes of sequenced genomes ranges from 2.82 to 3.16 Mb, with 47.5% to 53% GC content, and 2,941 to 3,323 genes that encode a potential of 2,772 to 3,203 predicted proteins (Table 5.6). Some genomes were larger than the initial estimates from pulse-field gel electrophoresis (PFGE), which ranged from 2.4 to 2.7 Mb (Vishnivetskay *et al.*, 2009, Table 5.6). All completed genomes have a GC skew; whereby, about half of the chromosomes have a positive skew, while the other half have a negative skew (Figure 5.5, Vishnivetskaya *et al.,* 2011). Strain RW2 had a lower number of rRNA gene operons compared to other members of the genus based on the RAST annotation (Table 5.6).

Whole genome analysis supports the phylogenetic analysis and is consistent with strain RW2 being assigned to a new species. tBLASTX analysis of *E. sibiricum* strain 255-15, *Exiguobacterium* sp. strain AT1b, and *Exiguobacterium* sp strain MH3 against the genome of RW2 showed many gaps, indicating low similarity (Figure 5.5). Whole genome based average amino acid analysis is a robust measure for bacterial species classification that is comparable to DNA-DNA hybridization; with this analysis, <95% average amino acid identity cut-off allows for assignment of a new species (Konstantinidis and Tiedje, 2005; Richter *et al.,* 2009). Among

the completed genomes, strain RW2 had the highest genome synteny to strain AT1b (Figure 5.6). The high genome synteny between strain RW2 and AT1b were consistent with their close phylogenetic placement (section 5.3.4). Strain RW2 has the highest overall amino-acid identity to *Exiguobacterium* sp. strain S17 (87.76%, Figure 5.6), but low gene synteny due to the high number of contigs in the assembly of strain S17 (Figure 5.6 and Table 5.6). Since <95% of its genome is shared with other sequenced representatives of the genus and genomic synteny is general low (except with its near relative, strain AT1b), strain RW2 can be considered a new species within the genus.

Exiguobacterium sp. strain RW2 shared >50% of its protein coding genes with other members of the genus and more distant relatives in the phylum *Firmicutes* (e.g *Planococcus halocryophilus* and *Bacillus halodurans*) based on SEED annotations (Figure 5.6 to 5.8). Among isolates with >80% amino-acid identity scores, strain RW2 shares 1659 to 1743 protein-coding genes (average, 1705 of 3092), while 106 to 135 (average, 115) are not shared with *Exiguobacterium* strains S17, AT1b, and 8-11-1) (Figure 5.6 and Table 5.6). Strain RW2 shares 1455 to 1775 of its protein coding genes (average, 1641 out of 3092) with isolates that have <65% amino acid identity, with 86 to 254 (average, 170) not found in *Exiguobacterium* spp. strains B7, OS-77, MH3, 255-15, *Planococcus halocryophilus* and *Bacillus halodurans* (Figure 5.7 to 5.8 and Table 5.6). *Exiguobacterium* sp. strain RW2 shared 1455 out of 3092, of its protein-coding genes with *Planococcus halocryophilus*; however, 254 protein-coding genes are unique to *Exiguobacterium* sp. strain RW2 (Figure 5.8 and Table 5.6). *Planococcus halocryophilus* is a distant relative of stain RW2 that is adapted for drastic shifts in temperature and salinity

(Mykytczuk *et al.,* 2013). The high percentage of shared protein-coding genes between *Exiguobacterium* sp. strain RW2 and other members of the genus suggests a large core genome with low genomic plasticity.

Comparisons of MetaCyc pathway annotations among strain RW2 and representative genomes of *Exiguobacterium* spp. with high (>80%) and low (<65%) amino-acid identity revealed many pathways that were shared within the genus and few that were specific to strain RW2. When compared to genomes with high amino-acid identity, there were only six pathways that were specific to strain RW2 (Figure 5.9A), and only eighteen were specific when compared to genomes with low amino-acid identity (Figure 5.9B). Strain RW2 shared 240 MetaCyc pathways with strains that had high amino-acid identity (Figure 5.9A), and 222 with strains that had low amino-acid identity (Figure 5.9B). Even genomes with <65% amino-acid identity shared >200 pathways with strain RW2, indicating that there are many shared metabolic pathways within the genus (Figure 5.9B). The MetaCyc pathway annotations are consistent with the SEED annotations, and suggest low genomic plasticity within the genus.

5.3.6 **Carbohydrate metabolism**

The biochemical tests indicated that strain RW2 uses monosaccharides, polysaccharides, and sugars as carbohydrate sources, unlike other members of the genus (Table 5.3). Strain RW2 has the metabolic potential to use a wide variety of monosaccharides, polysaccharides, sugar alcohols, and amino sugars, but cannot use D-glucose or D-sucrose, unlike other members of the genus (Table 5.3). Although sucrose use was not observed, the genome of strain RW2 predicts a complete sucrose utilization pathway, suggesting that it was not functional or that only

fermentation occurs (Table 5.3). Pathways for lactose uptake and use were present, but only a LacZ (β-galactosidase) for lactose utilization appeared to be present and functional (Table 5.3). Strain RW2 could not use D-mannitol, D-inositol, D-sorbitol, L-rhamnose, D-melibiose, and L-arabinose as sole carbon sources (Table 5.3). D-mannitol utilization was predicted by the genome, but was not used, suggesting that only fermentation occurs (Table 5.3). Amygdalin was used, as is the case for several members of the genus, although is not predicted by the genome (Table 5.3).

The genome of strain RW2 suggests the metabolic potential to perform various forms of fermentation including mixed acid, lactate, and acetyl-CoA fermentation to butyrate. The genome of strain RW2 also suggests that chitin, N-acetylglucosamine, maltose, maltodextrin, trehalose, glycerol, glycerol-3-phosphate, glycogen, fructose, gluconate, ribose, fructooligosaccharides (FOS), raffinose and deoxyribose can be used, although none were tested as growth substrates here. Further growth substrates should be tested to better understand carbohydrate utilization in strain RW2.

5.3.7 **Amino acid biosynthesis and catabolism**

Strain RW2, like other members of the genus, appears unable to make branched-chain amino acids, but has the metabolic potential for the ammonification of amino acids, which is linked to carbonate precipitation (Castanier *et al.,* 1999; Rodrigues *et al.,* 2008; Vishnivetskaya *et al.,* 2011). Whether *Exiguobacterium* spp. are auxotrophic for branched-chain amino acids is unknown, as there is no experimental evidence, and >30% of the ORFs are for hypothetical proteins. Pathways for the complete degradation of branched-chain amino acids were predicted by the genome of strain RW2, including full isoleucine, leucine and valine degradation pathways.

Moreover, arginine dihydrolase was functional in strain RW2; whereas, tryptophan deaminase, lysine and ornithine decarboxylases were not (Table 5.3). L-asparagine was not an essential amino acid for strain RW2, but the genome encodes aspartate aminotransferase, aspartate-ammonia ligase and L-asparaginase in an L-asparagine biosynthetic pathway. If L-asparaginase is active in strain RW2, it could generate alkalinity through the conversion of L-asparagine to ammonia by the ammonification of amino acids (Castanier *et al.*, 1999). Further experimentation is needed to confirm the metabolic potential of ammonification of amino acids in strain RW2 and whether it is functionally involved in carbonate precipitation.

5.3.8 Motility and flagellum biosynthesis

While flagella were not observed by SEM or light microscopy (Figure 5.1), strain RW2 has complete flagellum biosynthesis pathways (including the *fih, fli, fig* operons), as does strain AT1b (Vishnivetskaya *et al.*, 2011) and *E. sibiricum* strain 255-15 (Rodrigues *et al.*, 2008). Under low temperature, *E. sibiricum* strain 255-15 loses its flagellum (-2.5 ˚C), and expression of flagellum synthesis operons are downregulated (Rodrigues *et al.*, 2008). Rodrigues *et al.* (2008) suggested that at lower temperatures, aqueous media becomes more viscous, rendering flagella impractical. Under these prohibitively cold conditions, considerable energy could be saved by repressing flagellar assembly. While RW2 did not exhibit visible flagella, our proteomic survey data suggests that flagellar proteins are expressed at 10 ˚C but not at 4 ˚C (data not shown). Hence, strain RW2 appears to downregulate flagellar pathways at a much warmer temperature than the permafrost-dwelling *E. sibiricum* strain 255-15 (4 ˚C vs. -2.5 ˚C).

5.3.9 **Stress response temperature, heavy-metals and salinity**

Exiguobacterium sp. strain RW2 is unlikely grow at subzero temperatures due to the lack of the *cspA* gene (cold-shock protein A). Cold-shock protein A is induced at temperatures <11 ˚C, where it functions as a molecular chaperone, binding mRNA to prevent secondary structure formation and ensure efficient translation at low temperatures (Yamanka and Inouye, 1997). *Exiguobacterium sibiricum* strain 255-15 grows at -2.5 ˚C and has four copies of *cspA* (Rodrigues *et al.*, 2008). Strain AT1b cannot grow below 10 ˚C; whereas, strain RW2 grows at 4 ºC (White 3rd *et al.*, 2013b; Table 5.2). Strain AT1b, RW2 and S17 do not encode *cspA*, and hence would not be expected to grow at subzero temperatures.

Strain AT1b and RW2 were able to grow at temperatures as high as 50 ˚C (Vishnivetskaya *et al.*, 2011: Table 5.2). Both strains contain copies of genes (*dnaJ*, *dnaK* and *grpE*) encoding heat-shock related proteins, and a repressor of the heat-shock cascade, *hrcA*. However, unlike strain AT1b, strain RW2 does not encode *hspR*, the transcriptional repressor of the heat-shock protein operon (Schmid *et al.*, 2005). In *Deinococcus radiodurans*, the Δ*hspR* mutant has a lower survival rate at >48 ˚C; however, this didn't occur in strain RW2, which survived at over 48 ˚C (White 3rd *et al.*, 2013b; Table 5.2). Further experimentation is needed to confirm the essential genes required by strain RW2 to grow at 50 ˚C.

Cold-stress responses may confer protection to high salinity in a cross-protective manner (Tsuzuki *et al* 2011, Mykyczuk *et al.*, 2013). Strain RW2, grows at 0 to 7% NaCl and can grow at temperatures <11 ˚C (White 3rd *et al.*, 2013b; Table 5.2). Transcriptome analysis of *Rhodobacter sphaeroides* under salt stress showed significant upregulation of genes encoding

cold-shock DNA-binding proteins (Tsuzuki *et al.,* 2011). Genome and transcriptome analysis of the hypercryophile *Planococcus halocryophilus* strain Or1 suggests that adaptation to osmotic stress (mainly NaCl stress) may allow for synergistic adaptation to cold stress, as strain Or1 is able to grow in both high salt (~18%) and subzero temperatures (-15˚C) (Mykyczuk e*t al.,* 2013). *OpuA* and *opuD* are essential genes found in *P. halocryophilus* (Mykyczuk e*t al.,* 2013) that provide osmoprotection using glycine-betaine uptake systems, and are upregulated under NaCl stress (Hahne *et al.,* 2010). Unlike *P. halocryophilus*, strain RW2 does not encode *opuA* or *opuD*. The lack of the Opu proteins may be why strain RW2 did not grow in media with >7% NaCl. Strain RW2 was able to grow in 0% added NaCl, but little is known about cellular functions contributing to low salt survival.

The occurrence of heavy-metal resistance genes in strain RW2 was unexpected, given the low levels of zinc (0.01 to 0.03 mg L^{-1}) and undetectable levels of cobalt, copper, chromium, arsenic and cadmium in Pavilion Lake (Lim *et al.,* 2009). *Agrococcus* sp. strain RW1, which was isolated from the same microbialite as strain RW2, also carried genes for heavy-metal resistance (Thesis Chapter 3; White 3rd *et al.,* 2013b). Other members of the genus *Exiguobacterium*, such as the closely-related strain S17, have similar heavy-metal resistance gene clusters, and display high resistance to arsenic (Belfiore *et al.,* 2013). However, the gene encoding the ACR3 arsenite efflux pump is only found in strain S17 (Ordoñez *et al.,* 2013). Lake Socompa, where strain S17 was isolated, differs from Pavilion Lake in having high levels of arsenic (18.5 mg L^{-1}) and iron (1 mg L^{-1}) (Farías *et al.,* 2013). Historical mining in the Pavilion Lake region (Stevenson, 1940) suggests that higher metal content occurred in the past. Alternatively, heavy metal genes may

have a secondary role, as in *Rhodobacter sphaeroides* in which it upregulates arsenic resistance genes under high salt stress (Tsuzuki *et al.,* 2011).

The Pavilion Lake microbialite metagenomes had a number of heavy metal resistance genes which could be contributed by strain RW2 (unpublished data, Thesis Chapter 2). The abundance of strain RW2 in Pavilion lake microbialites was <0.5% by metagenomic recruitment analysis (unpublished data, Thesis Chapter 2). We suggest that strain RW2, like strain RW1, contributes heavy-metal resistance genes to the Pavilion Lake microbialite metabolic potential (confirmed by tBLASTx $1e^{-3}$); however, further experimentation is needed to determine whether these genes function under heavy-metal stress (unpublished data, Thesis Chapter 2).

5.3.10 **Carotenoid biosynthesis**

The characteristic orange pigmentation of colonies in *Exiguobacterium* spp. is distinct from other members of the phylum *Firmicutes*. However, the phylum has carotenoid biosynthesis, including the C_{30} pathway that is responsible for colony pigmentation (Pelz *et al.*, 2005; Köcher *et al.,* 2009; Klassen, 2010). Genes from the 4-4' diapocarotenoids C_{30} carotenoid pathway were present in all the published *Exiguobacterium* spp. genomes, including diapophytoene synthase (*crtM,* annotated as phytoene synthase), diapophytoene desaturase (*crtN,* annotated as phytoene desaturase), and diapophytoene desaturase (*crtNb,* annotated as second copy of phytoene desaturase) (Pelz *et al.,* 2005; Köcher *et al.,* 2009; Klassen, 2010; Figure 5.10; Table 5.7). In *Exiguobacterium* sp. strain RW2 the phytoene-based C_{30} carotenoid pathway is located on the same genetic locus between 1521530 to 1527203 on the genome. These genomic predictions suggest that diaponeurosporene-4-oic acid through the C_{30} carotenoid pathway could

be responsible for the orange colony pigmentation in *Exiguobacterium* spp. (Köcher *et al.,* 2009; Klassen, 2010). *Halobacillus halophilus* DSM2266 loss-of-function mutants for diapophytoene desaturase (*ΔcrtNb/Nc*) accumulate diaponeurosporene-4-oic acid which causes orange colony pigmentation (Köcher *et al.,* 2009).

To our knowledge, a hypothesis has not been advanced to explain the function of pigments in *Exiguobacterium* spp. Low concentration of dissolved organic carbon (DOC) in Pavilion Lake allows for high penetration of solar UV radiation, which benthic microbial mats may partially protect against using carotenoids (Lim *et al.,* 2009; Lionard *et al.,* 2012). *Agrococcus* sp. strain RW1, was also isolated from the same Pavilion Lake microbialite, and is also bright yellow (unpublished data, Thesis Chapter 4), suggesting that the pigments may serve in photo-protection.

5.4 Conclusions

Polyphasic analysis, using chemotaxonomic markers, and sequences for 16S rDNA, the combined ribosomal operon, MLST analysis and whole genome amino-acid identity is consistent with *Exiguobacterium* sp. strain RW2 being assigned as a new member of the genus. As well, novel chemotaxonomic markers including urease function, amygdalin utilization, and the presence of 7.6% iC17:1Δ5 (Table 5.3 and Table 5.5) are consistent the designation of a new species, and we suggest the name *Exiguobacterium pavilionensis* strain RW2.

Exiguobacterium sp. RW2 is able to grow over wide ranges of temperature, salinity and pH. Phylogenetic trees constructed from MLST, 16S rDNA and combined ribosomal operon analyses, as well as high genome synteny and whole-genome amino-acid identity (>80%) indicate that *Exiguobacterium* sp. strains RW2 and AT1b are close relatives; yet, AT1b was

isolated from Mammoth Terrace hot spring in Yellowstone National Park (Vishnivetskaya *et al.*, 2011). These results are consistent with the wide geographically and environmental range where *Exiguobacterium* spp. can be found.

We suggest that diaponeurosporene-4-oic acid, may be responsible for the orange pigmentation through the C_{30} carotenoid biosynthesis pathway. This pathway is universally conserved in all currently available *Exiguobacterium* genomes. These carotenoids may function in *Exiguobacterium* as photo-protection, and further experimentation is needed to validate the pathway and to demonstrate this functional relationship.

Exiguobacterium spp. are highly adaptable and thrive under a variety of conditions, including wide ranges of pH, temperature, salinity and heavy metals. Consequently, *Exiguobacterium* spp. colonize a wide range of systems and are useful models for understanding adaptation to a wide variety of environmental stresses

5.5 **Tables and figures**

Table 5.1: Names and isolation location of *Exiguobacterium* species

Officially named species

Species Name	*Environment of isolation*	*Reference*	*Isolation Notes*
E. acetylicum	Creamery waste	Farrow *et al.*, 1994	Levine and Soppeland, 1926 classified "*Flavobacterium acetylicum*" renamed "*Brevibacterium acetylicum*" then reclassified by Farrow *et al.*, 1994
E. antarcticum	Microbial mat/biofilm	Fruhling *et al.*, 2002	Lake Fryxell mat in Antactica
E. aestuarii	Marine tidal flat	Kim *et al.*, 2005	Daepo beach in yellow sea near Mokpo City, Korea,
E. alkaliphilum	Wastewater drained sludge	Kulshreshtha *et al.*, 2013	Beverage industry facility New Delhi, India
E. aquaticum	Freshwater lake	Raichand *et al.*, 2012	Tikkar Tal Lake, Haryana, India
E. aurantiacum	Potato processing plant	Collins *et al.*, 1983	Type species for the genus
E. himgiriensis	Soil	Singh *et al.*, 2013	Lahaul-Spiti valley, Indian Himalayas
E. indicum	Glacial melt water	Chaturvedi and Shivaji 2006	Hamta glacier (4270 m above sea level), Himalayans
E. martemiae	Brine shrimp cysts	Lopez-Cortes *et al.*, 2006	*Artemia franciscana* cysts
E. mexicanum	Brine shrimp cysts	Lopez-Cortes *et al.* 2006	*Artemia franciscana* cysts
E. oxidotolerans	Fish processing plant	Yumoto *et al.*, 2004	Hokkaido, Japan

Species Name	*Environment of isolation*	*Reference*	*Isolation Notes*
E. profundum	Hydrothermal Vent	Crapart *et al.*, 2007	Northeast Pacific rise at ~ 2600m
E. sibiricum	Permafrost	Rodrigues *et al.*, 2006	Siberian permafrost (3 Mya old)
E. soli	Glacial moraine	Chaturvedi *et al.*, 2008	McMurdo dry valleys, Antarctica
E. undae	Garden pond water	Fruhling *et al.*, 2002	Wolfenbüttel, Lower Saxon Germany
Published strains in NCBI			
Species Name	*Environment of isolation*	*Reference*	*Isolation Notes*
Strain RW2	Thromatolithic microbialite	White 3rd *et al.*, 2013b	Pavilion lake 20 m microbialites
Strain AT1B	Alkaline hot spring	Vishnivetskaya *et al.*, 2011	Mammoth Terrace hot spring ($CaCO_3$ rich), Yellowstone National Park Wyoming, USA
Strain MH3	Rhizosphere of duckweeds	Tang *et al.*, 2013	*Lemna minor* duckweed from Shenzhen, China
Strain OS77	Alkaline hot spring	Nonaka *et al.*, 2014	Tepid spring (41 °C, pH 7.9) Oguni-tyo, Kumamoto, Japan.
Strain S17	Stromatolithic microbialite	Ordoñez et al., 2013	Polyextremophile strain tolerate heavy metals (As)

Officially named species are published species: these names are recognized by IJSEM (international journal of systematic and evolutionary microbiology) or other journals.

Isolates published in NCBI as genome announcements that are unnamed, not classically described, or not characterized by IJSEM or other journal, are listed as an *Exiguobacterium* sp.

Table 5.2: Properties of *Exiguobacterium* selected strains

	Strain RW2	*E. soli*[1] DVS 3Y	*E. antarcticum*[1] DSM14480	*E. sibiricum*[1] DSM17290	*E. undae*[1] DSM14481	*E. indicum*[1] DSM15368	*E. oxidotolerans*[1] JCM12280	*E. acetylicum*[1] DSM20416
Habitat of isolation	Microbialite	Morine	Microbial Mat	Permafrost	Garden Pond	Glacial Water	Fish processing Plant	Creamery
Colony size (mm)	2 – 4	2 – 3	2 – 3	2 – 3	2 – 4	2 – 4	1 – 5	2 – 5
Colony shape	Round	Round	Round	Round	Round	Round	Round	Irregular
Colony color	Orange	Orange	Orange	Orange	Orange	Yellow-orange	Orange	Yellow-orange
Growth temp range (ºC)								
-2.5	NA	+	+	+	+	w	w	-
5	+	+	+	+	+	+	+	-
37	+	+	+	+	+	-	+	w
40	+	-	+	+	+	-	+	-
45	+	-	-	-	-	-	-	-
50	+	-	-	-	-	-	-	-
Max growth temp (ºC)	**50**	30	41	40	41	30	40	37
pH growth range								
4	-	-	-	-	-	-	-	-
5	+	-	-	-	-	-	-	-
11	+	-	-	-	-	-	-	-
NaCl growth range								
5.8%	+	+	+	+	+	+	+	+
7.0%	+	-	-	-	-	-	-	-

- Negative, + Positive, W: Weak growth, NA: Not available, Temp: temperature. All growth measurements for strain RW2 were taken after 2 d, except 5 °C which took 10 d to grow.

[1]Chaturvedi *et al.*, 2008

Table 5.3: Biochemical tests for selected strains of *Exiguobacterium* spp.

	Strain RW2	*E. soli*[1] DVS 3Y	*E.antarcticum*[1] DSM14480	*E.sibiricum*[1] DSM17290	*E. undae*[1] DSM14481	*E. indicum*[1] DSM15368	*E.oxidotolerans*[1] JCM12280	*E.acetylicum*[1] DSM20416
Activity for:								
Catalase	+	+	+	+	+	+	+	+
Oxidase	-	+	+	+	+	+	+	+
β-galactosidase	+	+	+	+	+	+	+	+
Arginine dihydrolase	+	+	+	+	+	+	+	+
Lysine decarboxylase	-	+	-	+	+	+	-	-
Ornithine decarboxylase	-	+	+	+	+	+	+	+
Urease	+	-	-	-	-	-	-	-
Tryptophan deaminase	-	-	+	+	-	-	+	+
Citrate utilization	+	-	-	+	-	+	+	+
Gelatinase	+	+	+	+	+	-	+	+
Production of:								
H_2S	-	-	-	-	-	-	-	-
Indole	-	-	-	-	-	-	-	-
Acetoin	-	+	+	+	+	+	+	+
Assimilation of:								
D-mannitol	-	-	-	-	+	-	+	+
Inositol	-	+	-	-	-	+	-	-
D-sorbitol	-	+	-	+	-	+	-	-
L-Rhamnose	-	+	-	-	-	+	-	-
D-Melibiose	-	-	-	+	-	-	-	-
Amygdalin	+	+	+	+	+	-	+	-
L-arabinose	-	+	-	+	-	-	-	-
D-glucose	-	+	+	+	+	+	+	+
D-sucrose	-	+	+	+	+	+	+	+

All growth measurements for strain RW2 were taken after 24 h.
[1]Chaturvedi *et al.*, 2008.

Table 5.4: Antibiotic susceptibility for selected strains *Exiguobacterium* spp.

Antibiotic	Disc Content	Strain RW2	*E.antarcticum*[1] DSM14480	*E.sibiricum*[1] DSM17290	*E. undae*[1] DSM14481	*E.indicum*[1] DSM15368	*E.acetylicum*[1] DSM20416
Sulfamethoxazole/ Trimethoprim	23.75 µg /1.25µg	-	ND	ND	ND	ND	ND
Sulfamethoxazole	50 µg	ND	-	+	+	+	-
Clindamycin*	2 / 25 µg	-	-	-	-	+	+
Penicillin	10 IU	-	ND	ND	ND	ND	ND
Rifampin	5 µg	-	ND	ND	ND	ND	ND
Polymyxin	300 IU	-	ND	ND	ND	ND	ND
Cefixime	5 µg	-	ND	ND	ND	ND	ND
Sulfisoxazole	300 µg	+	ND	ND	ND	ND	ND
Oxacillin	1 µg	-	ND	ND	ND	ND	ND
Tetracycline	30 µg	-	ND	ND	ND	ND	ND
Trimethoprim	5 µg	-	ND	ND	ND	ND	ND
Tobramycin	10 µg	-	ND	ND	ND	ND	ND
Vancomycin	30 µg	-	ND	ND	ND	ND	ND
Streptomycin	10 µg	-	ND	ND	ND	ND	ND

+ Resistant, - Sensitive, ND: No data
All growth measurements for strain RW2 were taken after 24 h.
[1]Chaturvedi *et al*., 2008.

Table 5.5: Selected phospholipid fatty acids from *Exiguobacterium* spp. strains (%)

	Strain RW2	*E. antarcticum* DSM14481[a]	*E. aurantiacum* DSM6208[a]	*E. sibiricum* 7-3[a]	*E. himgiriensis* K22-24[b]	*E. marium* MTCC7751[b]
$iC_{13:0}$	15.7	12	18	9	12.2	1
$aC_{13:0}$	15.4	11	12	11	16.4	16.8
$iC_{15:0}$	5.6	11	4	13	14.2	14.1
$aC_{15:0}$	2.1	2	ND	3	5.8	2.2
$C_{16:1\Delta5}$	2.7	18	10	8	2.4	3.6
$iC_{16:0}$	1.8	ND	ND	2	3.8	6.9
$brC_{16:1}$	1.2	ND	ND	ND	ND	ND
$C_{16:0}$	3.9	13	27	17	2.8	4.7
$iC_{17:1\Delta5}$	7.6	ND	ND	ND	ND	ND
$iC_{17:0}$	25.6	5	6	9	16.1	16.8
$C_{17:0}$	1.3	ND	ND	ND	tr	tr
$aC_{17:0}$	5.7	ND	ND	3	4.8	3.6
$C_{18:1\Delta5}$	1.9	ND	ND	ND	ND	ND
$C_{18:0}$	2.3	5	5	4	tr	tr
$iC_{18:0}$	2.3	ND	ND	ND	1.6	tr

ND: Not detected, tr: traces (<1%)

[a]Rodrigues *et al.*, 2006, [b]Singh *et al.*, 2012.

Table 5.6: *Exiguobacterium* spp. assembly and annotation statistics

	Draft Genomes					Completed Genomes			
	Strain RW2	Strain S17	Strain OS-77	Strain 8-11-1	Strain RW2	Strain AT1b	Strain MH3	*E. antarcticum* B7	*E. sibiricum* 255-15
Sequencing Method	Illumina MiSeq	454 GS FLX	454 GS FLX	Illumina HiSeq	Illumina MiSeq	454 Sanger	Illumina HiSeq	SOLiD	454 Sanger
Assembler	Ray	Newbler	Newbler	Velvet	Ray	Phred Phrap	SOAP denovo	Velvet Edena	Phred Phrap
Assembly Name	r23 K55	Exi S17_1.0	ASM 41419v1	V1	r23 K55	ASM 2304v1	ASM 49663v1	ASM 29943v1	ASM 1990v1
Genome coverage	300x	63x	45x	300x	>100x	20x	140x	>400x	-
No. Contigs	23	163	23	31	1	1	1	1	3
Scaffolds	-	-	5	-	-	-	-	-	-
Genome Size (bp)	3,019,504	3,127,363	3,151,479	2,906,962	3,019,504	2,999,895	3,164,195	2,815,863	3,040,786
N50	705,844	34,407	349,882	340,222	-	-	-	-	-
Largest Contig (bp)	947,149	122,784	929,170	663,994	-	-	-	-	-
G+C%	52.1	53.1	47.1	52.8	52.1	49	47.2	47.5	47.7
Annotation Method	RAST	RAST	RAST	RAST	RAST	NCBI	NCBI	NCBI	NCBI
Gene No.	-	-	-	-	-	3,141	3,332	2,941	3,155
Protein coding	3,079	3,215	3,265	2,926	3,092	3,020	3,203	2,772	3,015
Pseudo genes	0	-	-	-	-	23	41	76	-
rRNAs operons	2	2	2	2	2	9	9	9	9
tRNAs	48	47	49	14	46	68	60	66	69
Plasmids	-	-	-	-	0	0	0	0	2
SEED subsystems	370	370	388	373	395	372	398	-	430

- Not available, Draft genome contains many contigs (>20), whereas a completed genome contains a usually a single chromosome with plasmids..

Table 5.7: *Exiguobacterium* spp. carotenoid biosynthesis genes

	Strain RW2	Strain S17	Strain 8-11-1	Strain AT1b	*E. antarcticum* B7	Strain MH3	Strain OS-77	*E. sibiricum* 255-15
Phytoene synthase	1	1	1	1	1	1	1	2
Phytoene desaturase	3	2	3	4	3	4	2	4

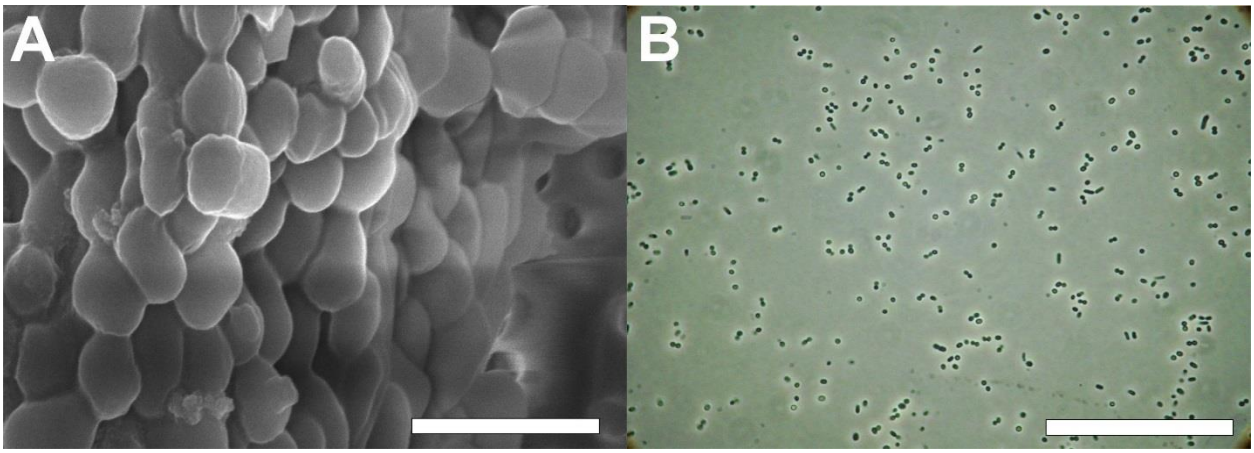

Figure 5.1: *Exiguobacterium* sp. strain RW2 microscopy
A) SEM image of biofilm during late-stationary phase of growth (72 h). Scale bar: ~10 μm.
B) Light microscopy image during logarithmic phase of growth (24 h). Scale bar: ~100 μm.
Observed here at standard growth conditions in liquid M medium at 30ºC

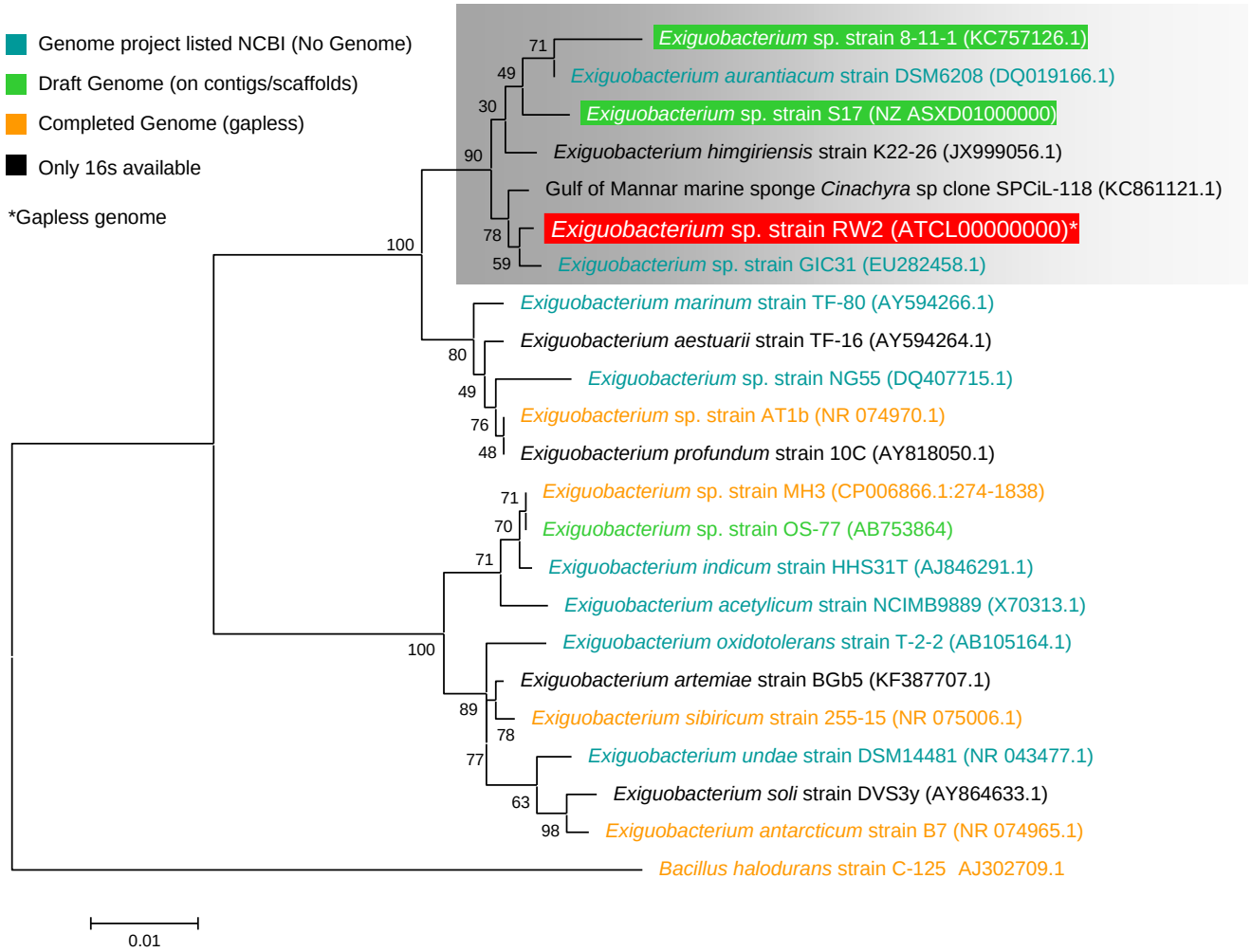

Figure 5.2: *Exiguobacterium* maximum-likelihood tree based on 16S rDNA gene sequences (~1353 bp) Bootstrap values greater than 40% at the given branches.

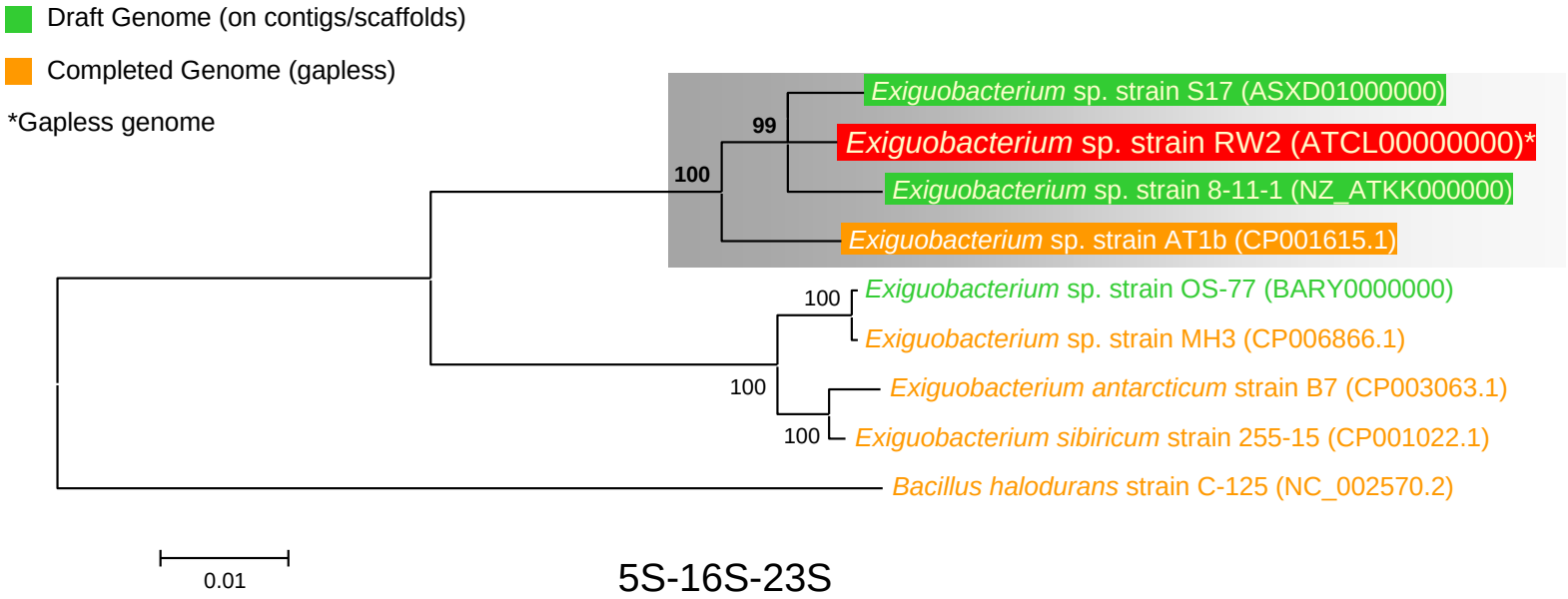

Figure 5.3: *Exiguobacterium* combined ribosomal operon maximum-likelihood tree
Bootstrap values greater than 50% at the given branches.

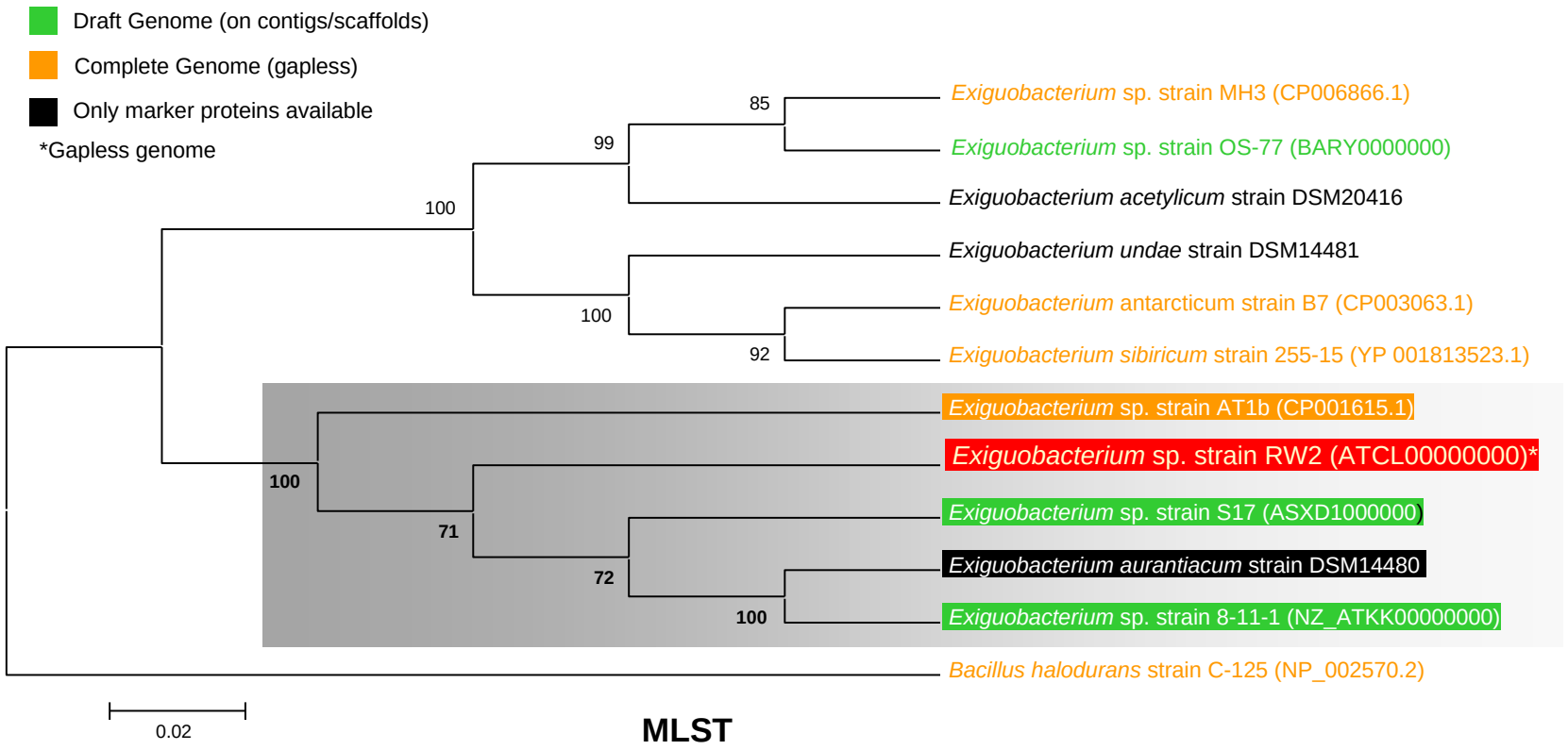

Figure 5.4: MLST maximum-likelihood phylogenetic tree
MLST based on concatenated rpoB, RecA, gyrB, DnaK, IDH and IARS protein sequence (~3856 amino acids).
Bootstrap values greater than 50% at the given branches.

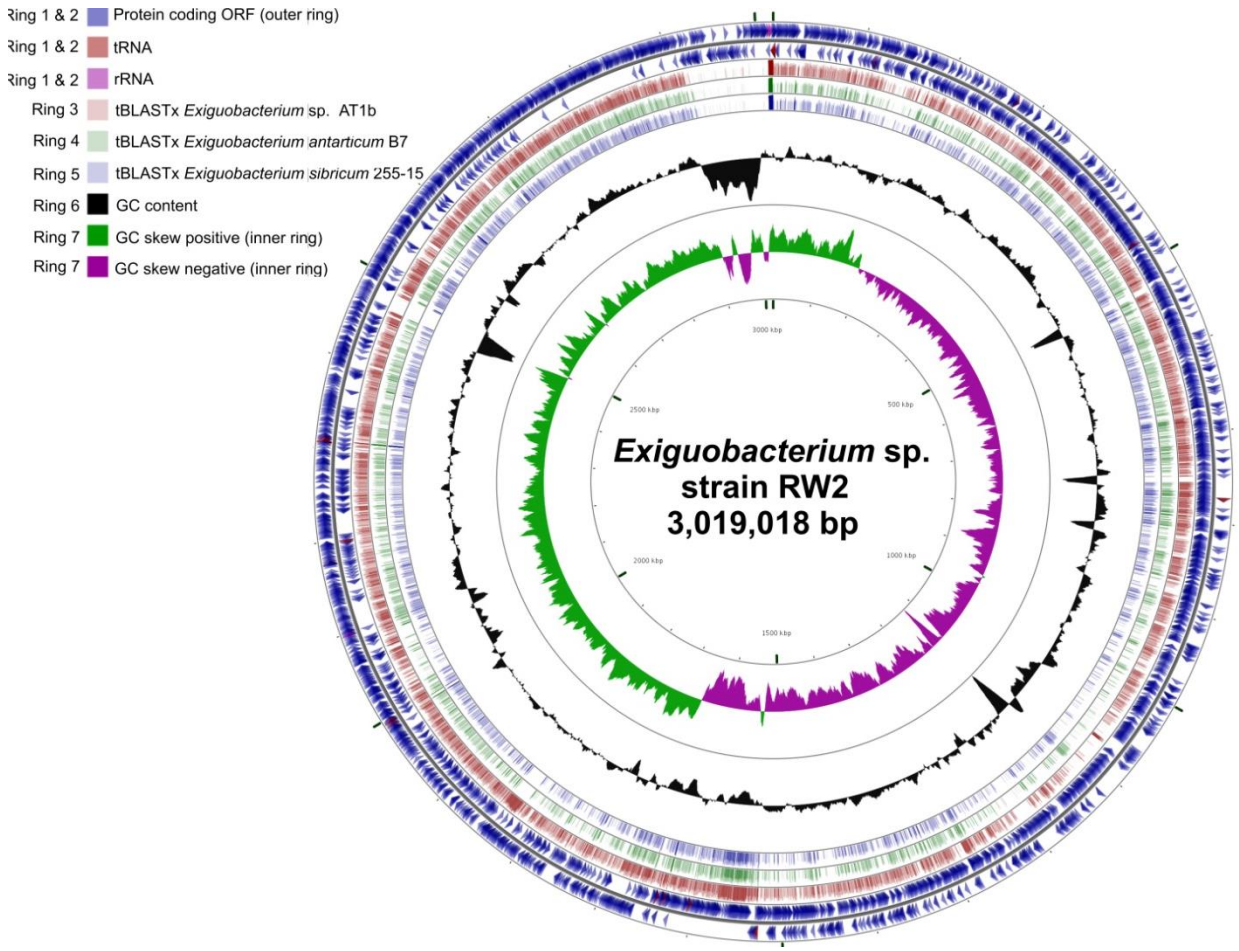

Figure 5.5: Genome plot (~3 Mb) of *Exiguobacterium* sp. strain RW2
Genome key (left corner): starts with inner most ring which is a genome ruler, followed by GC skew (purple/green) and ends with two outer rings, which contain protein-coding ORFs, tRNAs and rRNAs genes.

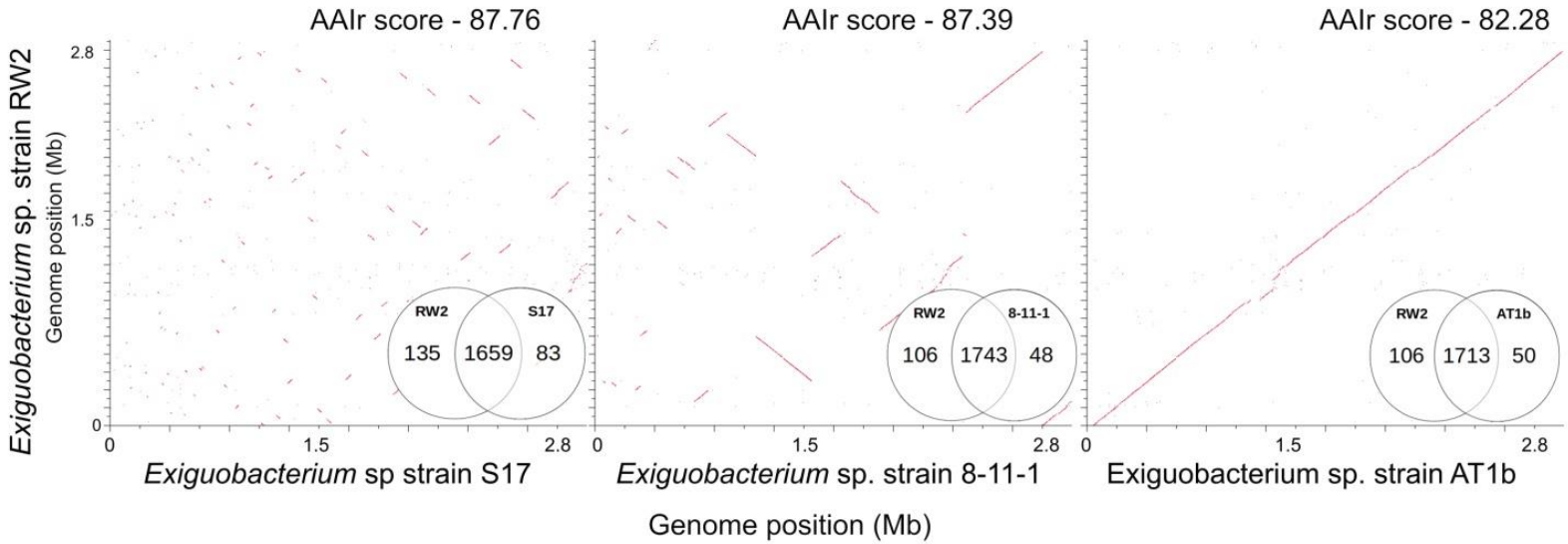

Figure 5.6: Genome synteny and functional Venn diagrams (SEED) with high amino acid identities (AAIr >80%) to *Exiguobacterium* sp. RW2

Genomes are listed in megabase pairs (Mb). Red dots are positive BLAST hits based on RAST genome comparision module. Amino acid identity (AAIr) was calculated by the RAST functional module with web based tool AAIr (Krebs *et al.*, 2013). Venn diagrams are listed by strain name based on RAST functional annotations (SEED/FigFams).

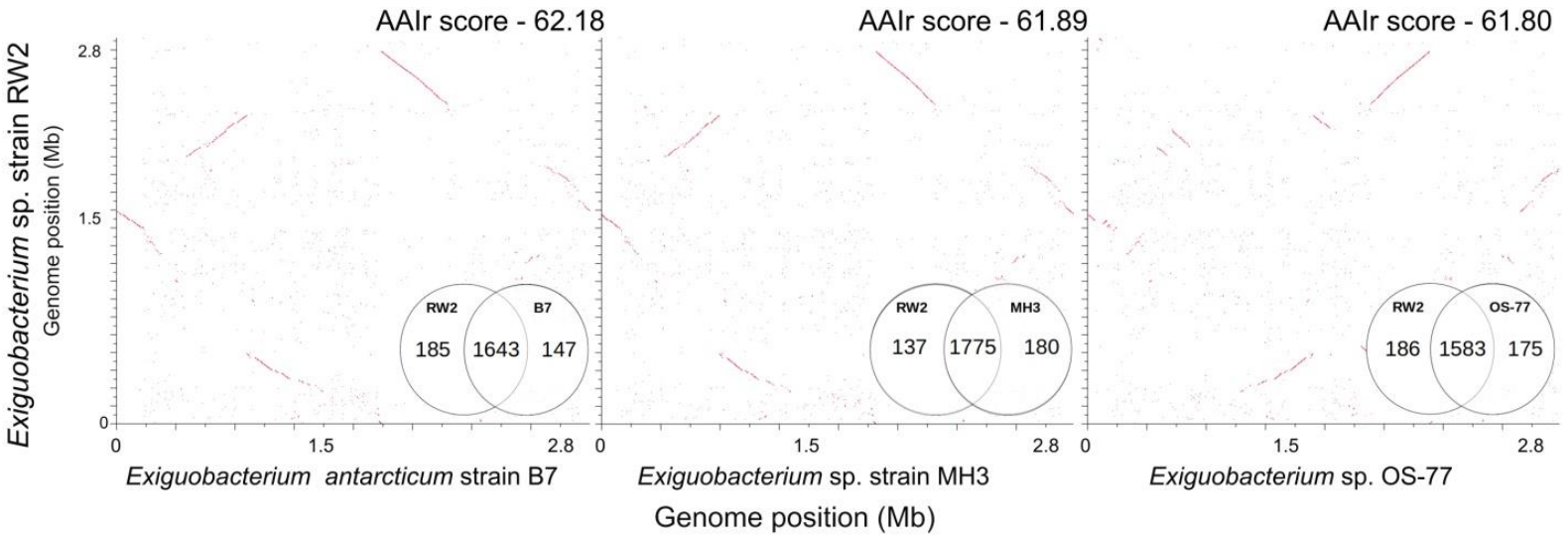

Figure 5.7: Genome synteny and functional Venn diagrams (SEED) with low amino acid identities (AAIr <65%) to *Exiguobacterium* sp. RW2

Genomes are listed in megabase pairs (Mb). Red dots are positive BLAST hits based on RAST genome comparision module. Amino acid identity (AAIr) was calculated by the RAST functional module with web based tool AAIr (Krebs *et al.*, 2013). Venn diagrams are listed by strain name based on RAST functional annotations (SEED/FigFams).

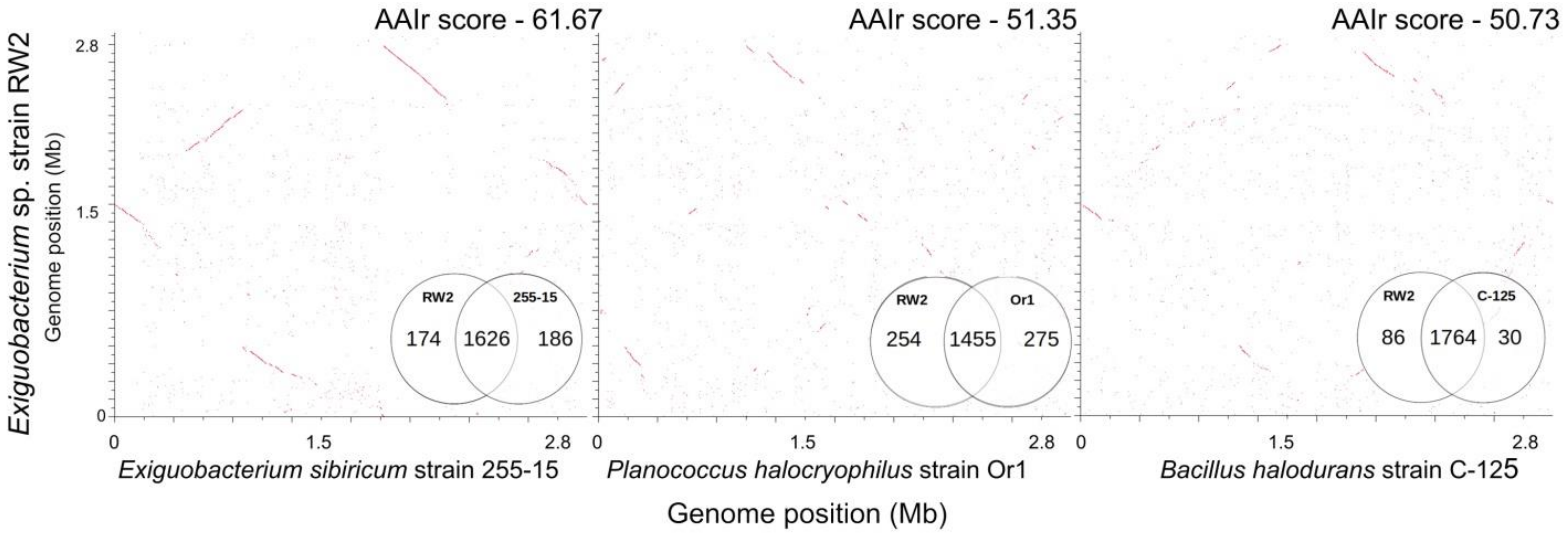

Figure 5.8: Genome synteny and functional Venn diagrams (SEED) with low amino acid identities (AAIr <65%) to *Exiguobacterium* sp. RW2

Genomes are listed in megabase pairs (Mb). Red dots are positive BLAST hits based on RAST genome comparision module. Amino acid identity (AAIr) was calculated by the RAST functional module with web based tool AAIr (Krebs *et al.*, 2013). Venn diagrams are listed by strain name based on RAST functional annotations (SEED/FigFams).

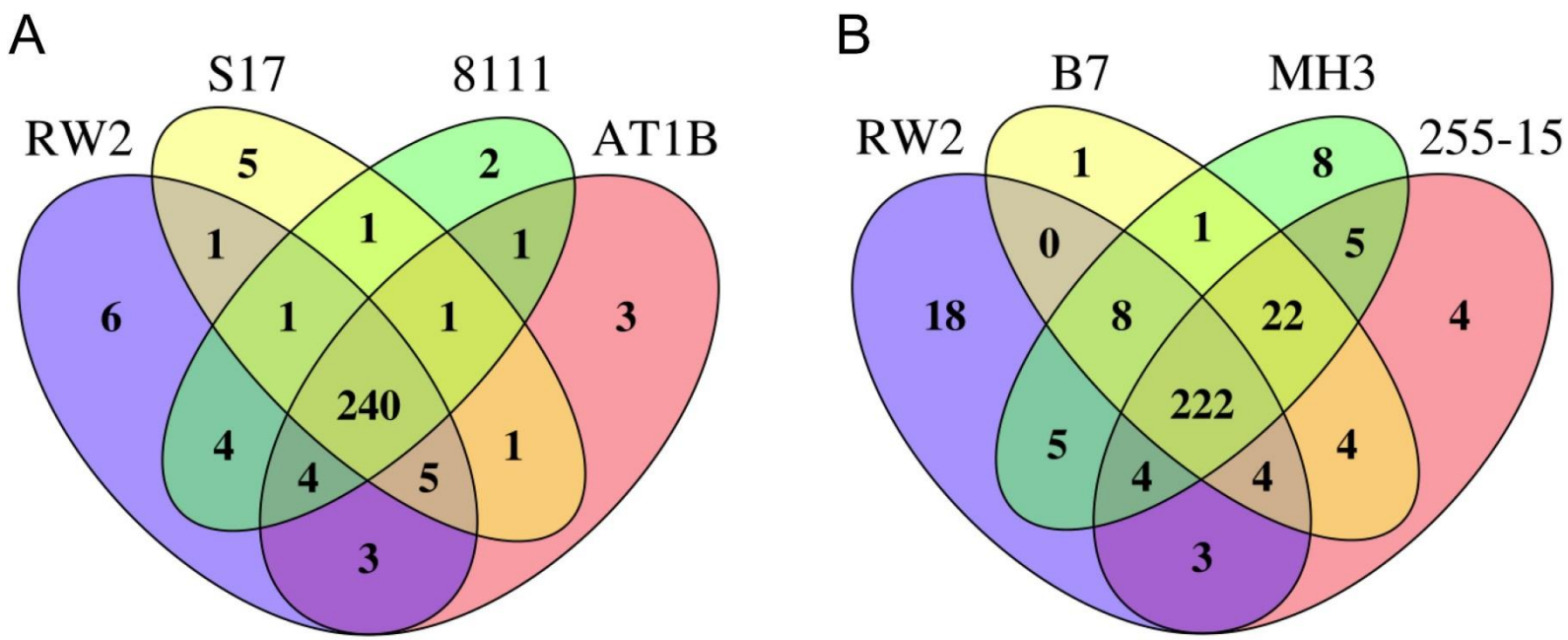

Figure 5.9: MetaCyc pathway annotations for *Exiguobacterium* genomes
A) Venn diagram comparing isolates with >80% amino acid identity (AAIr) to strain RW2
B) Venn diagram comparing isolates with <62% amino acid identity (AAIr) to strain RW2
Labels on Venn diagrams are listed by strain name with strains of *Exiguobacterium* spp. (8111, AT1b, MH3, RW2 and S17) and *E. sibiricum* (255-15) and *E. antarcticum* (B7) shown.

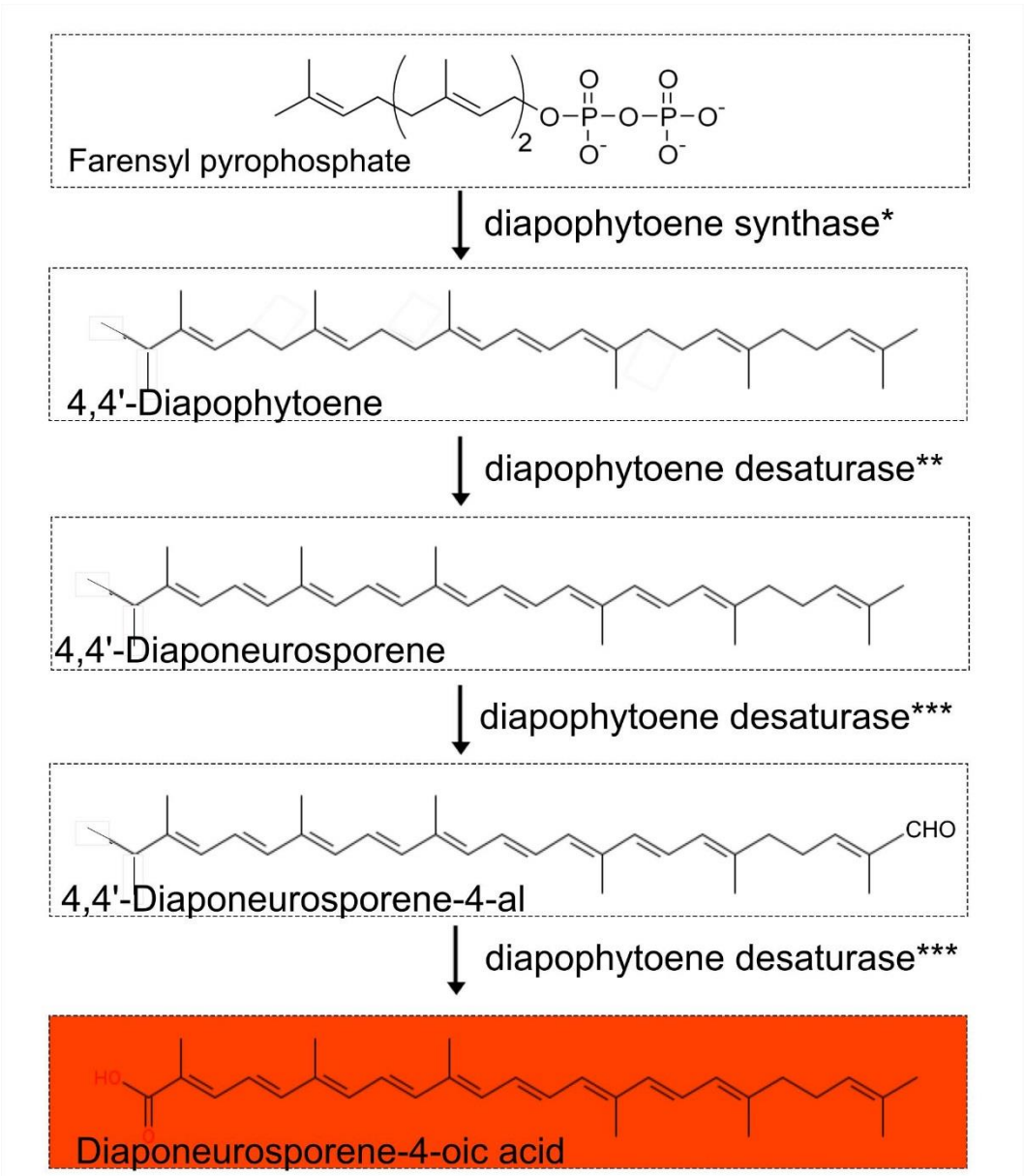

Figure 5.10: Proposed carotenoid biosynthesis pathway in the genus *Exiguobacterium*
*Diapophytoene synthase (*crtM*) annotated as phyotene synthase.
**Dipophytoene desaturase (*crtN*) annotated as phyotene desaturase.
***Dipophytoene desaturase (*crtNb*) annotated as phyotene desaturase.
All genes are found in all *Exiguobacterium* spp. genomes listed in Table 5.7.

Chapter 6: Conclusion

6.1 Summary

This thesis presents an in-depth metagenomic analysis of two freshwater microbialite-forming ecosystems (Pavilion Lake and Clinton Creek). The microbial community structure and metabolic potential of the microbialites and adjacent environment are described. While there are specific features to both systems, there are also many similarities between them, and with other freshwater and marine microbialite-forming ecosystems. In particular, the microbialite communities were dominated by *Proteobacteria* and filamentous *Cyanobacteria*, as has been found in other investigations (Havemann and Foster, 2008; Papineau *et al.,* 2005; Allen *et al.,* 2009; Baumgartner *et al.,* 2009; Myshrall *et al.,* 2010; Couradeau *et al.,* 2011; Farías *et al.,* 2013; Russell *et al.,* 2014).

Pavilion Lake microbialite communities were distinct from those in the surrounding environment in relation to GC content, community composition and metabolic potential. The microbialites had significantly higher abundances of sequences assigned to metabolic pathways related to heavy metals, antibiotic resistance, urea metabolism, and primary alcohol fermentation that are associated with members of the *Proteobacteria*. These pathways, and hence the proteobacteria, likely play an important role in these microbialite systems by protecting against heavy metals and toxins, influencing microbialite formation through photosynthetic and urealytic pathways, and stimulating primary and heterotrophic production by liberating nutrients through the degradation of the EPS rich cyanobacterial mats, which would also remove EPS-related inhibition of carbonate precipitation. Therefore, although isotopic data support photosynthesis-

related processes as being the drivers of carbonate precipitation (Brady *et al.,* 2009; Omelon *et al.,* 2013), our data imply that heterotrophic processes dominate microbialite metabolism, and also likely play an important role. Moreover, the isotopic data do not disguish between photosynthesis-related carbonate-induced precipitation by cyanobacteria, or by more abundant microbial taxa, including *Acidobacteria* and *Proteobacteria.* We suggest that *Acidobacteria* and *Proteobacteria* play a role in photosynthesis-related carbonate-induced precipitation in microbialites. Pavilion Lake microbialite formation is likely a localized event in the cyanobacterial mat, caused by a combination of heterotrophic and photosynthetic processes. This is consistent with observations that sedimentation rates in Pavilion Lake are quite low, suggesting that photosynthetically induced water-based whiting events are not a major factor in Pavilion Lake microbialite formation (Lim *et al.,* 2009; Omelon *et al.,* 2013).

Genetic signitures of viruses were evident in water from Pavilion Lake, and the presence of CRISPR-cas systems in the microbialites indicates that viruses are interacting with the microbialite community. CRISPRs were abundant in genomes associated with carbonate precipitators, including members of the *Deltaproteobacteria* (e.g. *Myxococcus* and *Desulfuromonadales*), *Cyanobacteria* (e.g. *Anabaena, Nostoc, Rivularia*) and *Firmicutes* (e.g. *Clostrida*). This suggests that viral infection may influence the microbialite-forming community.

Subarctic Clinton Creek (Yukon, Canada) houses the northernmost and fastest growing microbialites known (Power *et al.,* 2011a). Microbialite contigs had a high proportion of photosynthetic genes, implying that microbialite formation is driven by photosynthesis-induced alkalinization. Predicted metabolic pathways overlapped extensively between microbialite and

sediment communities, particularly with respect to housekeeping genes; however, they have distinct core communities, with microbialites dominated by *Alphaproteobacteria* (mainly anoxic phototrophs like *Rhodobacterales*), and sediments dominated by *Gammaproteobacteria* (mainly heterotrophic nitrogen-fixing *Pseudomonas* spp.).

The Clinton Creek microbialite communities were distinct from microbialites from marine and tropical freshwater systems and microbial mats on corals, whale fall and hot springs. While Clinton Creek and Cuarto Ciengás microbialites shared some functional potential, the functional potential of the Arctic mats was the most similar with those from Clinton Creek, likely because of cold-adaptation. This suggests that given the correct abiotic conditions, polar mats on ice shelves could have the metabolic potential to make microbialites. The microbialites in Clinton Creek appear to be primarily formed as the result of cyanobacterial photosynthetic alkalinization in the mat.

To complement the metagenomic study in Pavilion Lake, a culture-based study was completed, resulting in two isolates, *Exiguobacterium* spp. and an *Agrococcus* spp. from a microbialite collected at 20m from Pavilion Lake. Polyphasic characterization of the isolates included growth studies, biochemical testing, lipid analysis, microscopy, antibiotic testing, phylogenetic analysis and whole-genome comperative analysis. Based on these analyses, the isolates were proposed as new species, *Agrococcus pavilionensis* strain RW1 and *Exiguobacterium pavilionensis* strain RW2. Genome sequencing and comparative genome and phylogenetic analyses studies were performed to find the evolutionary placement and metabolic potential of the isolates in relation to other members of the genera. Although both isolates appear to be at relatively

low abundance in the Pavilion Lake microbialites, they contribute heavy-metal resistance genes that account for stress response metabolism. *Exiguobacterium pavilionensis* strain RW2 had a functional urease gene, which may contribute to carbonate precipitation through urealytic pathways. In addition, hypothetical carotenoid pathways were discovered that may be responsible for the coloration in *Agrococcus* spp. and *Exiguobacterium* spp., and it is hypothesized that the pigments may contribute to photo-protection.

6.2 Future directions

The characterization of a Pavilion Lake microbialite has set the stage for further comparative metagenomic studies of microbialites from neighboring Kelly Lake. The microbialites in Kelly Lake have no visible cyanobacterial mats; however, like Pavilion Lake, microbialite formation is suspected to be driven by photosynthetic alkalization. There are no reports on the microbial communities or metabolic potential of microbialites from Kelly Lake.

While bacterial communities and their metabolic potential were the focus of this thesis, eukaryotic communities and viruses need to be examined in greater detail to determine their roles in freshwater microbialite systems. Preliminary analysis of metagenomic data from Pavilion Lake suggests that the abundance of eukaryotes is low; however, the metagenomic data from the water were significantly enriched with sequences assigned to photosynthetic eukaryotes. The viral communities in Pavilion Lake suggest that interactions occur between viruses in the water and the bacterial community in the microbialite, as evidenced by the presence of CRISPR-cas sequences. A viral metagenomic study of water from both Pavilion and Kelly Lakes could be used to link viral CRISPR spacers to members of the microbialite bacterial community.

The nodule-associated cyanobacteria of Pavilion Lake have elevated δ13C carbonate values, suggesting they influence carbonate precipitation by photosynthetic alkalinization resulting in the formation of microstromatolithic structures (Brady *et al.,* 2010). A metaproteomic analysis of the nodules could provide insight into how the carbonates in these structures are formed and by which metabolic pathways.

Finally, a global study comparing all of the metagenomic data for microbialites and microbial mats in relation to the environments in which they occur could help to solve questions relating to microbialite-specific metabolic potential and microbial community structure. While a comprehensive metagenomic analysis has not been conducted on many microbialites, a small comparison of freshwater microbialites (Clinton Creek, Kelly and Pavilion Lakes) and marine microbialites (Highbourne Cay and Shark Bay) can now be pursued.

References

Abbai NS, Govender A, Shaik R, Pillay B. (2012). Pyrosequence analysis of unamplified and whole genome amplified DNA from hydrocarbon-contaminated groundwater. Mol Biotechnol. 50, 39-48.

Abulencia CB, Wyborski DL, Garcia JA, Podar M, Chen W, Chang SH. (2006). Environmental whole-genome amplification to access microbial populations in contaminated sediments. Appl Environ Microbiol. 72, 3291-330.

Achtman M and Wagner M. (2008). Microbial diversity and the genetic nature of microbial species. Nat. Rev. Microbiol. 6, 431-440

Aitken JD. (1967). Classification and environmental significance of cryptalgal limestones and dolomites, with illustrations from the Cambrian and Ordovician of southwestern Alberta. J Sed. Petro. 37, 1163-1178.

Allen AE, Dupont CL, Oborník M, Horák A, Nunes-Nesi A, McCrow JP, Zheng H, Johnson DA, Hu H, Fernie AR, Bowler C. (2011). Evolution and metabolic significance of the urea cycle in photosynthetic diatoms. Nature. 473, 203-7.

Allen MA, Goh F, Burns BP, Neilan BA. (2009). Bacterial, archaeal and eukaryotic diversity of smooth and pustular microbial mat communities in the hypersaline lagoon of Shark Bay. Geobiology 7, 82-96.

Allwood AC, Walter MR, Kamber BS, Marshall CP, Burch IW. (2006). Stromatolite reef from the early Archaean era of Australia. Nature. 441, 714-718.

Anbu P, Hur BK, Gyun Lee C. (2013). Isolation and characterization of a novel oxidant- and surfactant-stable extracellular alkaline protease from *Exiguobacterium profundum* BK-P23. Biotechnol Appl Biochem. 60, 155-61.

Andersen DT, Sumner DY, Hawes I, Webster-Brown J, McKay CP. (2011). Discovery of large conical stromatolites in Lake Untersee, Antarctica. Geobiology. 9, 280-93.

Andres MS, Sumner, DY, Reid RP, Swart PK. (2006). Isotopic fingerprints of microbial respiration in aragonite from Bahamian stromatolites. Geology 34, 973-976.

Anil Kumar PK, Suresh PV. (2013). Biodegradation of shrimp biowaste by marine *Exiguobacterium* sp. CFR26M and concomitant production of extracellular protease and

antioxidant materials: production and process optimization by response surface methodology. Mar Biotechnol (NY).

Aris-Brosou S, Yang Z. (2003). Bayesian models of episodic evolution support a late Precambrian explosive diversification of the Metazoa. Mol Biol Evol. 20, 1947-54.

Arora PK, Sharma A, Mehta R, Shenoy BD, Srivastava A, Singh VP. (2012). Metabolism of 4-chloro-2-nitrophenol in a gram-positive bacterium, *Exiguobacterium sp.* PMA. Microb Cell Fact. 11, 150

Arp G, Thiel V, Reimer A, Michaelis W, Reitner J. (1999). Biofilm exopolymers control microbialite formation at thermal springs discharging into the alkaline Pyramid Lake, Nevada, USA. Sedimentary Geology 126, 159-176.

Arp G, Reimer A, Reitner J. (2001). Photosynthesis-induced biofilm calcification and calcium concentrations in Phanerozoic oceans. Science 292, 1701-1704.

Arp G, Reimer A, Reitner J (2004). Microbialite formation in seawater of increased alkalinity, Satonda Crater Lake, Indonesia. J Sediment Res 74, 318-325.

Aury JM, Cruaud C, Barbe V, Rogier O, Mangenot S, Samson G, Poulain J, Anthouard V, Scarpelli C, Artiguenave F. (2008). High quality draft sequences for prokaryotic genomes using a mix of new sequencing technologies. BMC Genomics 9, 603.

Awramik SM. (1971). Precambrian columnar stromatolite diversity: reflection of metazoan appearance. Science. 174, 825-7.

Awramik SM, and Margulis L. (1974). Definition of stromatolite. Stromatolite Newsletter 2, 5.

Aziz RK, Bartels D, Best AA, DeJongh M, Disz T, Edwards RA, Formsma K, Gerdes S, Glass EM, Kubal M, et al. (2008). The RAST server: rapid annotations using subsystems technology. BMC Genomics 9, 75.

Barabesi CA, Galizzi G, Mastromei M, Rossi E, Tamburini B, Perito, B. (2007). *Bacillus subtilis* gene cluster involved in calcium carbonate biomineralization. J. Bacteriol. 189, 228-235.

Barman S, Chatterjee S, Koley H. (2010). Plasmid-mediated streptomycin and sulfamethoxazole resistance in *Shigella flexneri* 3a. Int J Antimicrob Agents 36, 348-351

Baumgartner LK, Reid RP, Dupraz C, Decho AW, Buckley DH, Spear JR, Przekop KM, Visscher PT. (2006). Sulfate reducing bacteria in microbial mats: changing paradigms, new discoveries. Sediment Geol 185, 131-145.

Baumgartner LK, Spear JR, Buckley DH, Pace NR, Reid RP, Dupraz C, Visscher PT. (2009). Microbial diversity in modern marine stromatolites, Highborne Cay, Bahamas. Environ Microbiol 11, 2710-2719.

Belfiore C, Ordonez OF, Farías ME. (2013). Proteomic approach of adaptive response to arsenic stress in *Exiguobacterium* sp. S17, an extremophile strain isolated from a high-altitude Andean Lake stromatolite. Extremophiles 17, 421-431.

Ben Chekroun K, Rodriguez-Navarro C, Gonzalez-Muñoz MT, Arias JM, Cultrone G, Rodriguez–Gallego M. (2004). Precipitation and growth morphology of calcium carbonate induced by *Myxococcus xanthus*: implications for regognition of bacterial carbonates. J. Sedimentary Res. 74, 868-876.

Ben-Shem A, Frolow F, Nelson N. (2004). Evolution of photosystem I from symmetry through pseudosymmetry to asymmetry. FEBS Letters 564, 274-280.

Bentley DR, Balasubramanian S, Swerdlow HP, Smith GP, Milton J, Brown CG, Hall KP, Evers DJ, Barnes CL, et al. (2008). Accurate whole human genome sequencing using reversible terminator chemistry. Nature 6, 53-9.

Bernhard JM, Edgcomb VP, Visscher PT, McIntyre-Wressnig A, Summons RE, Bouxsein ML, Louis L, Jeglinski M. (2013). Insights into foraminiferal influences on microfabrics of microbialites at HighbourneCay, Bahamas. PNAS 110, 9830-9834.

Berrendero E, Perona E, Mateo P. (2011). Phenotypic variability and phylogenetic relationships of the genera *Tolypothrix* and *Calothrix* (Nostocales, Cyanobacteria) from running water. Int J Syst Evol Microbiol 61, 3039-51.

Bischoffa LJ, Alcantarab II, Garduno-Monroyb HV, Shanks III, CW. (2004). The springs of Lake Patzcuaro: chemistry, salt-balance, and implications for the water balance of the lake. Applied Geochemistry 19, 1827-1835.

Bligh EG, Dyer WJ. (1959). A rapid method of total lipid extraction and purification. Canadian Journal of Biochemistry and Physiology 37, 911-917.

Boisvert S, Laviolette F, Corbeil J. (2010). Ray: simultaneous assembly of reads from a mix of high-throughput sequencing technologies. J. Comput. Biol. 11, 1519-33

Boisvert S, Raymond F, Godzaridis E, Laviolette F, Corbeil J. (2012). Ray Meta: scalable de novo metagenome assembly and profiling. Genome Biol. 13, R122.

Bontognali TR, Sessions AL, Allwood AC, Fischer WW, Grotzinger JP, Summons RE, Eiler JM. (2012). Sulfur isotopes of organic matter preserved in 3.45-billion-year-old stromatolites reveal microbial metabolism. PNAS 109, 15146-51.

Boquet E, Boronat A, Ramos-Cormenzana A. (1973). Production of calcite (calcium carbonate) crystals by soil bacteria is a general phenomenon. Nature 246, 527-29.

Bosak T, Greene SE, Newman DK. (2007). A likely role for anoxygenic photosynthetic microbes in the formation of ancient stromatolites. PNAS 5, 119-126.

Bosak T, Liang B, Wu TD, Templer SP, Evans A, Vali H, Guerquin-Kern JL, Klepac-Ceraj V, Sim MS, Mui J. (2012). Cyanobacterial diversity and activity in modern conical microbialites. Geobiology. 10, 384-401.

Bottos EM, Vincent WF, Greer CW, Whyte LG. (2008). Prokaryotic diversity of arctic ice shelf microbial mats. Environ Microbiol. 10, 950-66.

Brady AL, Slater G, Laval B, Lim DS. (2009). Constraining carbon sources and growth rates of freshwater microbialites in Pavilion Lake using (14)C analysis. Geobiology. 7, 544-55.

Brady AL, Slater GF, Omelon CR, Southam G, Druschel G, Andersen DT, Hawes I, Laval B, Lim DSS (2010). Photosynthetic isotope biosignatures in laminated micro-stromatolitic and non-laminated nodules associated with modern, freshwater microbialites in Pavilion Lake, BC. Chemical Geology 274, 56 – 67.

Brady AL, Laval B, Lim DSS, Slater GF (2013). Autotrophic and heterotrophic associated biosignatures in modern freshwater microbialites over seasonal and spatial gradients Org Geochem. 0146-6380.

Braithwaite CJR, Zedefa V. (1994). Living hydromagnesite stromatolites from Turkey. Sed. Geology. 92, 1-5

Brehm U, Palinska KA, Krumbein WE. (2004). Laboratory cultures of calcifying biomicrospheres generate ooids - A contribution to the origin of oolites. Notebooks on Geology: Letter 2004/03 (CG2004_L03)

Breitbart M, Hoare A, Nitti A, Siefert J, Haynes M, Dinsdale E, Edwards R, Souza V, Rohwer F, Hollander D. (2009). Metagenomic and stable isotopic analyses of modern freshwater microbialites in Cuatro Cienegas, Mexico. Environ Microbiol. 11, 16-34.

Bridgwater DN, Holmes AJ, O'Hara LS. (1999). Complex controls on the trace-element chemistry of non-marine ostracods: an example from Lake Patzcuaro, central Mexico. Palaeogeogr Palaeoclimatol Palaeoecol. 148, 117-131

Brocks JJ, Logan GA, Buick R, Summons RE. (1999). Archean molecular fossils and the early rise of eukaryotes. Science. 285, 1033-6.

Buick R, Groves DI, Dunlop JS. (1995). Abiologial origin of described stromatolites older than 3.2 Ga. Geology. 23, 191.

Burnat M, Diestra E, Esteve I, Solé A. (2009). In situ determination of the effects of lead and copper on cyanobacterial populations in microcosms. PLoS One. 4, e6204.

Burne RV, Moore LS. (1987). Microbialites: organosedimentary deposits of benthic microbial communities. Palaios 2, 241-254.

Burns BP, Goh F, Allen M, Neilan BA. (2004). Microbial diversity of extant stromatolites in the hypersaline marine environment of Shark Bay, Australia. Environ Microbiol. 6, 1096-101.

Burns BP, Gudhka RK, Neilan BA. (2012). Genome sequence of the halophilic archaeon *Halococcus hamelinensis*. J Bacteriol. 194, 2100-1.

Canfield DE, Abicht K, Thamdrup B. (2000). The archaean sulfur cycle and the early history of atmospheric oxygen. Science 288, 658-661.

Canfield DE. (2005). The early history of atmospheric oxygen: homage to Robert A. Garrels. Annu. Rev. Earth Planet. Sci. 33, 1–36

Carneiro AR, Ramos RT, Dall'Agnol H, Pinto AC, de Castro Soares S, Santos AR, Guimarães LC, Almeida SS, Baraúna RA, et al. (2012). Genome sequence of *Exiguobacterium antarcticum* B7, isolated from a biofilm in Ginger Lake, King George Island, Antarctica. J. Bacteriol. 23, 6689-6690.

Caspi R, Altman T, Billington R, Dreher K, Foerster H, Fulcher CA, Holland TA, Keseler IM, et al. (2014). The MetaCyc database of metabolic pathways and enzymes and the BioCyc collection of Pathway/Genome Databases. Nucleic Acids Res. 42, 459-71.

Castanier S, Le Metayer-Levrel G, and Perthuisot JP. (1999). Ca-carbonates precipitation and limestone genesis the microbiogeologist point of view: Sedimentary Geology 126, 9-23.

Centeno CM, Legendre P, Beltrán Y, Alcántara-Hernández RJ, Lidström UE, Ashby MN, Falcón LI. (2012). Microbialite genetic diversity and composition relate to environmental variables. FEMS Microbiol Ecol. 82, 724-35.

Challacombe J, Kuske C. (2012). Mobile genetic elements in the bacterial phylum *Acidobacteria*. Mob Genet Elements 2, 179-183.

Chaturvedi P, Shivaji S. (2006). *Exiguobacterium indicum* sp. nov. a psychrophilic bacterium from the Hamta glacier of the Himalayan mountain ranges of India. Int. J. Syst. Evol. Microbiol. 56, 2765-2770.

Chaturvedi P, Prabahar V, Manorama R, Pindi PK, Bhadra B, Begum Z, Shivaji S. (2008). *Exiguobacterium soli* sp. nov. a psychrophilic bacterium from the McMurdo dry valleys, Antarctica. Int. J. Syst. Evol. Microbiol. 58, 2447-2453.

Chen F, Suttle CA. (1995). Amplification of DNA polymerase gene fragments from viruses infecting microalgae. Appl Environ Microbiol. 61, 1274-1278.

Chen PH, Liu HL, Chen YJ, Cheng H, Lin WL, Yeh CH, Chang CH. (2012). Enhancing CO_2 bio-mitigation by genetic engineering of cyanobacteria. Energy and Environmental Science 5, 8318-8327.

Clokie M, Clokie JR, Millard DA, Mann HN. (2010). T4 genes in the marine ecosystem: studies of the T4-like cyanophages and their role in marine ecology. Virology Journal 7, 291.

Collee JG, Miles RS, Watt B. (1996). Tests for the identification of bacteria, In Collee JG, Fraser AG, Marmion BP, Simmons A, editors. (ed), Mackie and McCartney practical medical microbiology, 14th ed Churchill Livingstone, London, United Kingdom. 131-149

Collins MD, Lund BM, Farrow JAE, Schleifer KH. (1983). Chemotaxonomic study of an alkaliphilic bacterium, *Exiguobacterium aurantiacum* gen nov., sp. nov. J. Gen. Microbiol. 129, 2037-2042.

Couradeau E, Benzerara K, Moreira D, Gérard E, Kaźmierczak J, Tavera R, López-García P. (2011). Prokaryotic and eukaryotic community structure in field and cultured microbialites from the alkaline Lake Alchichica (Mexico). PLoS One. 6, e28767.

Couradeau E, Benzerara K, Gérard E, Moreira D, Bernard S, Brown GE Jr, López-García P (2012). A nearly-branching microbialite cyanobacterium forms intracellular carbonates. Science 336, 459-62.

Crapart S, Fardeau ML, Cayol JL, Thomas P, Sery C, Ollivier B,Combet-Blanc Y. (2007). *Exiguobacterium profundum* sp nov., a moderately thermophilic, lactic acid-producing bacterium isolated from a deep-sea hydrothermal vent. Int. J. Syst. Bacteriol. 57, 287-292.

Crowe SA, Døssing LN, Beukes NJ, Bau M, Kruger SJ, Frei R, Canfield DE. (2013). Atmospheric oxygenation three billion years ago. Nature. 501, 535-8.

Cuerno R, Escudero C, García-Ruiz JM, Herrero MA. (2012). Pattern formation in stromatolites: insights from mathematical modelling. J R Soc Interface. 9, 1051-62.

Darling AE, Mau B, Perna NT. (2010). ProgressiveMauve: multiple genome alignment with gene gain, loss and rearrangement. PLoS One 5, e11147.

Desnues C, Rodriguez-Brito B, Rayhawk S, Kelley S, Tran T, Haynes M, Liu H, Furlan M, Wegley L, Chau B, Ruan Y, et al. (2008). Biodiversity and biogeography of phages in modern stromatolites and thrombolites. Nature 452, 340-3.

Destaillats F, Anger P. (2002). One-step methodology for the synthesis of FA picolinyl esters from intact lipids. JAOCS 3, 253-256.

Dhami NK, Reddy MS, Mukherjee A. (2013). Biomineralization of calcium carbonate polymorphs by the bacterial strains isolated from calcareous sites. J Microbiol Biotechnol. 23, 707-14.

Dhami NK, Reddy MS, Mukherjee A. (2014). Synergistic role of bacterial urease and carbonic anhydrase in carbonate mineralization. Appl Biochem Biotechnol. 172, 2552-61.

Dick J, De Windt W, De Graef B, Saveyn H, Van der Meeren P, De Belie N, Verstraete W. (2006). Bio-deposition of a calcium carbonate layer on degraded limestone by *Bacillus* species. Biodegradation 17, 357-367.

Dittricha M, Müllera B, Mavrocordatosb D, Wehrlia B. (2003). Induced Calcite Precipitation by Cyanobacterium Synechococcus. Acta hydrochim hydrobiol. 31, 162-169.

Doroghazi JR, Metcalf WW. (2013). Comparative genomics of actinomycetes with a focus on natural product biosynthetic genes. BMC Genomics. 14, 611.

Dowd M. (1998). Identification of the unsaturated heptadecyl fatty acids in the seed oils of *Thespesia populnea* and *Gossypium hirstum.* J Amer Oil Chem Soc. 89, 1599-1609.

Dupraz C, Visscher PT. (2005). Microbial lithification in marine stromatolites and hypersaline mats. Trends in Microbiol. 13, 429-438

Dupraz C, Reid RP, Braissant O, Decho AW, Norman RS, Visscher PT (2009). Processes of carbonate precipitation in modern microbial mats. Earth Sci Rev. 96, 141-162.

Edgar RC. (2004). MUSCLE: multiple sequence alignment with high accuracy and high throughput. Nucleic Acids Res 32, 1792-1797

Edgcomb VP, Bernhard JM, Summons RE, Orsi W, Beaudoin D, Visscher PT. (2013). Active eukaryotes in microbialites from HighbourneCay, Bahamas, and Hamelin Pool (Shark Bay), Australia. ISME J. (Epub ahead of print)

Elser JJ, Schampel JH, García-Pichel F, Wade BD, Souza V, Eguiarte L, Escalante A Farmer JD. (2005). Effects of phosphorous enrichment and grazing snails on modern stromatolitic microbial communities. Freshw Biol. 50, 1808-25.

Elser JJ, Watts J, Schampel JH, Farmer J. (2006). Early Cambrian food webs on a trophic knife-edge? A hypothesis and preliminary data from a modern stromatolite-based ecosystem. Ecol Lett. 9, 295-303.

Ercole C, Cacchio P, Botta AL, Centi V, Lepidi A. (2007). Bacterially induced mineralization of calcium carbonate: the role of exopolysaccharides and capsular polysaccharides. Microsc Microanal. 13. 42-50.

Falkowski P, Scholes RJ, Boyle E, Canadell J, Canfield D, Elser J, Gruber N, Hibbard K, Högberg P, Linder S, Mackenzie FT, Moore B 3rd, Pedersen T, Rosenthal Y, Seitzinger S, Smetacek V, Steffen W. (2000). The global carbon cycle: a test of our knowledge of earth as a system. Science 290, 291-6.

Farías ME, Rascovan N, Toneatti DM, Albarracın VH, Flores MR, Poire DG, Collavino MM, Aguilar OM, Vazquez MP, Polerecky L. (2012). The discovery of stromatolites developing at 3570 m above sea level in a high-altitude volcanic lake Socompa, Argentinean Andes. PLoS One 8, e53497

Farrow JAE, Wallbanks S, Collins MD. (1994). Phylogenetic interrelationships of round-spore forming bacilli containing cell walls based on lysine and the non-spore-forming genera *Caryophanon, Exiguobacterium, Kurthia and Planococcus*. Int J Syst Bacteriol 44, 74-82

Fender JE, Bender CM, Stella NA, Lahr RM, Kalivoda EJ, Shanks RM. (2012). *Serratia marcescens* quinoprotein glucose dehydrogenase activity mediates medium acidification and inhibition of prodigiosin production by glucose. Appl Environ Microbiol. 78, 6225-35.

Ferris FG, Thompson JB, Beveridge TJ. (1997). Modern freshwater microbialites from Kelly Lake, British Columbia, Canada. Palaios 12, 213-219.

Fieseler L, Horn M, Wagner M, Hentschel U (2004). Discovery of the novel candidate phylum "*Poribacteria*" in marine sponges. Appl Environ Microb 70, 3724-3732.

Filée J, Tétart F, Suttle CA, Krisch HM. (2005). Marine T4-type bacteriophages, a ubiquitous component of the dark matter of the biosphere. PNAS. 102, 12471-6.

Fox GE, Wisotzkey JD, Jurtshuk Jr P. (1992). How close is close: 16S rRNA sequence identity may not be sufficient to guarantee species identity. Int. J. Syst. Bacteriol. 42, 166-170.

Friedrich CG, Bardischewsky F, Rother D, Quentmeier A, Fischer J. (2005). Prokaryotic sulfur oxidation. Curr Opin Microbiol. 8, 253-9.

Fruhling A, Schumann P, Hippe H, Straubler B, Stackebrandt E. (2002). *Exiguobacterium undae* sp nov. and *Exiguobacterium antarcticum* sp. nov. Int. J. Syst. Evol. Microbiol. 52, 1171-1176.

Gallagher KL, Kading TJ, Braissant O, Dupraz C, Visscher PT. (2012). Inside the alkalinity engine: the role of electron donors in the organomineralization potential of sulfate-reducing bacteria. Geobiology 10, 518-30.

Garrett P. (1970). Phanerozoic stromatolites: noncompetitive ecologic restriction by grazing and burrowing animals. Science 169, 171-3.

Gischler E, Gibson MA, Oschmann W. (2008). Giant Holocene freshwater microbialites, Laguna Bacalar, Quintana Roo, Mexico. Sedimentology 55, 1293-1309.

Goh F, Allen MA, Leuko S, Kawaguchi T, Decho AW, Burns BP, Neilan BA. (2009). Determining the specific microbial populations and their spatial distribution within the stromatolite ecosystem of Shark Bay. ISME J 3, 383-96.

Gordon DC, Abajian C, and Green P. (1998). Consed: A Graphical Tool for Sequence Finishing. Genome Research. 8, 195-202

Graham LE, Knack JJ, Piotrowski MJ, Wilcox LE, Cook ME, Wellman CH, Taylor W, Lewis LA, Arancibia-Avila P. (2014). Lacustrine *Nostoc* (*Nostocale*s) and associated microbiome generate a new type of modern clotted microbialite. J Phycol. 50, 280-291.

Grey K, Moore LS, Burne RV, Pierson BK, Bauld J. (1990). Lake Thetis, Western Australia:an example of saline sedimentation dominated by benthic microbial processes: Australian J Mar. Freshw. Res. 41, 275-300.

Groth I, Schumann P, Weiss N, Martin K, Rainey FA. (1996). *Agrococcus jenensis* gen. nov., sp. nov., a new genus of actinomycetes with diaminobutyric acid in the cell wall. Int J Syst Bacteriol. 46, 234-239.

Grotzinger JP, Rothman DR. (1996). An abiotic model for stromatolite morphogenesis. Nature 383, 423-425.

Grotzinger JP, Knoll AH (1999). Stromatolites in Precambrian carbonates: evolutionary mileposts or environmental dipsticks? Annu Rev Earth Planet Sci. 27, 313-358.

Gushchin I, Chervakov P, Kuzmichev P, Popov AN, Round E, Borshchevskiy V, Ishchenko A, Petrovskaya L, Chupin V, Dolgikh DA, Arseniev AS, Kirpichnikov M, Gordeliy V. Structural insights into the proton pumping by unusual proteorhodopsin from nonmarine bacteria. (2013). PNAS 110, 12631-6

Guckert JB, Antworth CP, Nichols PD, White DC. (1985). Phospholipid, ester-linked fatty acid profiles as reproducible assays for changes in prokaryotic community structure of estuarine sediments. FEMS Microbiology Ecology 31, 147-158.

Gygax SE, Schuyler JA, Kimmel LE, Trama JP, Mordechai E, Adelson ME. (2006). Erythromycin and clindamycin resistance in group B *Streptococcal* clinical isolates. Antimicrob Agents Chemother 50, 1875-1877.

Hahne H, Mäder U, Otto A, Bonn F, Steil L, Bremer E, Hecker M, Becher D. (2010). A comprehensive proteomics and transcriptomics analysis of *Bacillus subtilis* salt stress adaptation. J Bacteriol. 92, 870–882.

Hammes F, Boon N, de Villiers J, Verstraete W, Siciliano SD. (2003). Strain-specific ureolytic microbial calcium carbonate precipitation. Appl Environ Microbiol. 69, 4901-9

Havemann SA, Foster JS. (2008). Comparative characterization of the microbial diversities of an artificial microbialite model and a natural stromatolite. Appl Environ Microbiol. 74, 7410-21.

Hawes I, Sumner DY, Andersen DT, Mackey TJ. (2011). Legacies of recent environmental change in the benthic communities of Lake Joyce, a perennially ice-covered Antarctic lake. Geobiology. 9, 394-410.

Hill DR, Belbin TJ, Thorsteinsson MV, Bassam D, Brass S, Ernst A, Böger P, Paerl H, Mulligan ME, Potts M. (1996). GlbN (cyanoglobin) is a peripheral membrane protein that is restricted to certain *Nostoc* spp. J Bacteriol. 178, 6587-98.

Hindson BJ, Ness KD, Masquelier DA, Belgrader P, Heredia NJ, Makarewicz AJ, Bright IJ, Lucero MY, Hiddessen AL, Legler TC, Kitano TK, et al. (2011). High-throughput droplet digital PCR system for absolute quantitation of DNA copy number. Anal. Chem. 83, 8604-8610.

Jackson DJ, Thiel V, Wörheide G. (2010). An evolutionary fast-track to biocalcification. Geobiology. 8, 191-196.

Jansson C, Northen T. (2010). Calcifying cyanobacteria-the potential of biomineralization for carbon capture and storage. Current Opinion in Biotechnology 21, 365-371.

Jiang X, Xue Y, Wang A, Wang L, Zhang G, Zeng Q, Yu B, Ma Y. (2013). (a) Efficient production of polymer-grade L-lactate by an alkaliphilic *Exiguobacterium* sp. strain under nonsterile open fermentation conditions. Bioresour Technol. 143, 665-8.

Jiang X, Xue Y, Wang L, Yu B, Ma Y. (2013). (b) Genome sequence of a novel polymer-grade l-lactate-producing alkaliphile, *Exiguobacterium* sp. strain 8-11-1. Genome Announc. 1, e00616-13.

Jimenez-Lopez C, Chekroun KB, Jroundi F, Rodríguez-Gallego M, Arias JM, González-Muñoz MT. (2011). *Myxococcus xanthus* colony calcification: an study to better understand the processes involved in the formation of this stromatolite-Like structure. Advances in Stromatolite Geobiology 131, 161-181.

Jørgensen NOG. (2006). Uptake of urea by estuarine bacteria. Aquatic Microb. Ecol. 42, 227-242.

Kalkowsky E. (1908). Oolith und Stromatolith im norddeutschen Buntsandstein. Zeitschrift Deutschen geol. Gesellschaft 60, 68-125. (Article in German).

Kazmierczak J, Kempe S. (2006). Genuine modern analogues of Precambrian stromatolites from caldera lakes of Niuafo'ou Island, Tonga. Naturwissenschaften 93, 119–126.

Kempe S, Kazmierczak J, Landmann G, Konuk T, Reimer A, Lipp A. (1991). Largest known microbialites discovered in Lake Van, Turkey. Nature 349, 605-8

Kennard JM and James NP. (1986). Thrombolites and stromatolites; two distinct types of microbial structures. Palaios 1, 492-503.

Khodadad CL, Foster JS. (2012). Metagenomic and metabolic profiling of nonlithifying and lithifying stromatolitic mats of HighbourneCay, The Bahamas. PLoS One.7, e38229.

Kiełbasa SM, Wan R, Sato K, Horton P, Frith MC. (2011). Adaptive seeds tame genomic sequence comparison. Genome Res. 3, 487-93.

Kim IJ, Lee MH, Jung SY, Song JJ, Oh TK, Yoon JH. (2005). *Exiguobacterium aestuarii* sp. nov. and *E. marinum* sp. nov. isolated from tidal flat of the yellow sea in Korea. Int. J. Syst. Evol. Microbiol. 55, 885-889.

Klassen JL. (2010). Phylogenetic and evolutionary patterns in microbial carotenoid biosynthesis are revealed by comparative genomics. PLoS One. 5, e11257.

Köcher S, Jurgen B, Müller V, Sandmann G. (2009). Structure, function and biosynthesis of carotenoids in the moderately halophilic bacterium *Halobacillus halophilus*. Arch. Microbiol. 191, 95-104.

Konishi Y, Prince, J and Knott B (2001). The fauna of thrombolitic microbialites, Lake Clifton, Western Australia. Hydrobiologia. 457, 39-47

Konwar KM, Hanson NW, Pagé AP, Hallam SJ. (2013). MetaPathways: a modular pipeline for constructing pathway/genome databases from environmental sequence information. BMC Bioinformatics 14, 202.

Krebs JE, Gale AN, Sontag TC, Keyser VK, Peluso EM, and Newman JD. (2013). A web-based method to calculate average amino acid identity (AAI) between prokaryotic Genomes. BioTechniques submitted August, 2013. http://lycofs01.lycoming.edu/~newman/AAI/

Kropinski AM, Mazzocco A, Waddell TE, Lingohr E, Johnson RP. (2009). Enumeration of bacteriophages by double agar overlay plaque assay. Methods Mol Biol. 501, 69-76.

Kulshreshtha NM, Kumar R, Begum Z, Shivaji S, Kumar A. (2013). *Exiguobacterium alkaliphilum* sp. nov. isolated from alkaline wastewater drained sludge of a beverage industry located in India. Int J Syst Evol Microbiol. 63, 4374-9.

Kunin V, Copeland A, Lapidus A, Mavromatis K, Hugenholtz P. (2008). (a) A bioinformatician's guide to metagenomics. Microbiol Mol Biol Rev. 72, 557-78

Kunin V, Raes J, Harris JK, Spear JR, Walker JJ, Ivanova N, von Mering C, Bebout BM, Pace NR, Bork P, Hugenholtz P. (2008). (b) Millimeter-scale genetic gradients and community-level molecular convergence in a hypersaline microbial mat. Mol Syst Biol. 4, 198.

Lane DJ. 1991. 16S/23S rRNA sequencing. In: Nucleic acid techniques in bacterial systematics. Stackebrandt, E., and Goodfellow, M., eds., John Wiley and Sons, New York, NY, pp. 115-175.

Langmead B, Salzberg S. 2012. Fast gapped-read alignment with Bowtie 2. Nat. Methods 9, 357-359

Laval B, Cady SL, Pollack JC, McKay CP, Bird JS, Grotzinger JP, Ford DC, Bohm HR. (2000). Modern freshwater microbialite analogues for ancient dendritic reef structures. Nature 407, 626-629.

Lee SH, Cho JC (2009). Distribution patterns of the members of phylum *Acidobacteria* in global soil samples. J Microbiol Biotechnol. 19, 1281-1287.

Lee SW, Park SB, Jeong SK, Lim KS, Lee SH, Trachtenberg MC. (2010). On carbon dioxide storage based on biomineralization strategies. Micron 41, 273-282.

Lee YN. (2003). Calcite production by *Bacillus amyloliquefaciens* CMB01. J Microbiol. 41, 345 - 48.

Lenz G, Ron EZ. (2014). Novel interaction between the major bacterial heat shock chaperone (GroESL) and an RNA chaperone (CspC). J Mol Biol. 426, 460-6.

Leuko S, Goh F, Allen MA, Burns BP, Walter MR, Neilan BA. (2007). Analysis of intergenic spacer region length polymorphisms to investigate the halophilic archaeal diversity of stromatolites and microbial mats. Extremophiles. 11, 203-10.

Liang B, Wu TD, Sun HJ, Vali H, Guerquin-Kern JL, Wang CH, Bosak T. (2014). Cyanophycin mediates the accumulation and storage of fixed carbon in non-heterocystous filamentous cyanobacteria from coniform mats. PLoS One. 9, e88142.

Lightfield J, Fram NR, Ely B. (2011). Across bacterial phyla, distantly-related genomes with similar genomic GC content have similar patterns of amino acid usage. PLoS ONE 6, e17677.

Lim DSS, Laval BE, Slater G, Antoniades D, Forrest AL, Pike W, Pieters R, Saffari M, Reid D, Schulze-Makuch D, Andersen D, McKay CP. (2009). Limnology of Pavilion Lake B.C. - Characterization of a microbialite-forming environment. Fundamental and Applied Limnology 173, 329-351.

Lionard M, Péquin B, Lovejoy C, Vincent WF. (2012). Benthic cyanobacterial mats in the high arctic: multi-layer structure and fluorescence responses to osmotic stress. Front Microbiol. 3, 140.

Logan BW, Rezak R, Ginsburg RN. (1964). Classification and environmental significance of algal stromatolites Jour. Geology 72, 68-83.

Loman NJ, Constantinidou C, Chan JZ, Halachev M, Sergeant M, Penn CW, Robinson ER, Pallen MJ. (2012). High-throughput bacterial genome sequencing: an embarrassment of choice, a world of opportunity. Nat Rev Microbiol. 10, 599-606.

López-Cortes A, Schumann P, Pukall R, Stackebrandt E. (2006). *Exiguobacterium mexicanum* sp nov. and *Exiguobacterium artemiae* sp. nov., isolated from the brine shrimp *Artemia franciscana*. Syst. Appl. Microbiol. 29, 183-190.

López-García P, Kazmierczak J, Benzerara K, Kempe S, Guyot F, Moreira D. (2005). Bacterial diversity and carbonate precipitation in the giant microbialites from the highly alkaline Lake Van, Turkey. Extremophiles. 9, 263-74.

Lowe DR. (1994). Abiological origin of described stromatolites older than 3.2 Ga. Geology. 22, 387-90.

Lozano RP, Rossi C. (2012). Exceptional preservation of Mn-oxidizing microbes in cave stromatolites (El Soplao, Spain). 256, 42-55.

Lundberg J, Mcfalane D. (2011). Subaerial freshwater phosphatic stromatolites in Deer Cave, Sarawak A unique geobiological cave formation. Geomorphology 128, 57-72.

Luo R, Liu B, Xie Y, Li Z, Huang W, Yuan J, He G, Chen Y, Pan Q, et al. (2012). SOAPdenovo2: an empirically improved memory-efficient short-read de novo assembler. Gigascience. 1, 18.

Lusk TS, Ottesen AR, White JR, Allard MW, Brown EW, Kase JA. (2012). Characterization of microflora in Latin-style cheeses by next-generation sequencing technology. BMC Microbiol. 12, 254

Lynch EA, Langille MG, Darling A, Wilbanks EG, Haltiner C, Shao KS, Starr MO, Teiling C, Harkins TT, Edwards RA, Eisen JA, Facciotti MT. Sequencing of seven haloarchaeal genomes reveals patterns of genomic flux. PLoS One. 7, e41389.

Lyons TW, Reinhard CT, Planavsky NJ. (2014). The rise of oxygen in Earth's early ocean and atmosphere. Nature 506, 307-315.

Maliva GR, Missimer, MT, Leo CK, Statom AR, Dupraz C, Lynn M, Dickson JAD. (2000). Unusual calcite stromatolites and pisoids from a landfill leachate collection system. Geology 28, 931-934.

Margulies M, Egholm M, Altman WE, Attiya S, Bader JS, et al. (2005). Genome sequencing in microfabricated high-density picolitre reactors. Nature 437, 376-380.

Mareš J, Hrouzek P, Kaňa R, Ventura S, Strunecký O, Komárek J. (2013). The primitive thylakoid-Less cyanobacterium gloeobacter is a common rock-dwelling organism. PLoS One. 8, e66323.

Mayilraj S, Suresh K, Schumann P, Kroppenstedt RM, Saini, HS. (2006). *Agrococcus lahaulensis* sp. nov., isolated from a cold desert of the Indian Himalayas. Int J Syst Evol Microbiol. 56, 1807-1810.

McLoughlin N, Wilson LA, Brasier MD. (2008). Growth of synthetic stromatolites and wrinkle structures in the absence of microbes - implications for the early fossil record. Geobiology. 6, 95-105.

Meyer FD, Paarmann M, D'Souza R, Olson EM, Glass M, Kubal T, Paczian A, Rodriguez R, Wilke A, Wilkening J, Edwards RA. (2008). The Metagenomics RAST server – A public resource for the automatic phylogenetic and functional analysis of metagenomes BMC Bioinformatics 9, 386.

Meyer F, Overbeek R, Rodriguez A. (2009). FIGfams: yet another set of protein families. Nucleic Acids Res. 37, 6643-54.

Milne I, Stephen G, Bayer M, Cock PJA, Pritchard L, Cardle L, Shaw PD and Marshall D. (2013). Using Tablet for visual exploration of second-generation sequencing data. Briefings in Bioinformatics 14, 193-202.

Mitchell AC, Dideriksen K, Spangler LH, Cunningham AB, Gerlach R. (2010). Microbially Enhanced Carbon Capture and Storage by Mineral-Trapping and Solubility-Trapping. Environmental Science and Technology. 44, 5270-5276.

Miyazaki T, Sugisawa T, Hoshino T. (2006). Pyrroloquinoline quinone-dependent dehydrogenases from *Ketogulonicigenium vulgare* catalyze the direct conversion of L-sorbosone to L-ascorbic acid. Appl Environ Microbiol. 72, 1487-95.

Mobberley JM, Khodadad CL, Foster JS. (2013). Metabolic potential of lithifying cyanobacteria-dominated thrombolitic mats. Photosynth Res. 118, 125-40.

Mojzsis SJ, Arrhenius G, McKeegan KD, Harrison TM, Nutman AP, Friend CR. (1996). Evidence for life on Earth before 3,800 million years ago. Nature 384, 55-9.

Moss CW, Daneshvar MI. (1992). Identification of some uncommon monounsaturated fatty acids of bacteria. J Clin Microbiol. 30, 2511-2.

Muga A, Moro F. (2008). Thermal adaptation of heat shock proteins. Curr Protein Pept Sci. 9, 552-66.

Muyzer G, Brinkhoff T, Nübel U, Santegoeds C, Schäfer H, Waver C. (1998). Denaturing gradient gel electrophoresis (DGGE) in microbial ecology. In: Akkermans ADL, van Elsas JD, de Bruijn

FJ (eds). Molecular Microbial Ecology Manual. Kluwer Academic Publishers: Dordrecht, The Netherlands. 1-27.

Muyzer G, De Waal EC, Uitterlinden AG. (1993). Profiling of complex microbial populations by denaturing gradient gel electrophoresis analysis of polymerase chain reaction-amplified genes coding for 16S rRNA. Appl Environ Microbiol 59, 695-700.

Mykytczuk NC, Foote SJ, Omelon CR, Southam G, Greer CW, Whyte LG. (2013). Bacterial growth at -15 °C; molecular insights from the permafrost bacterium Planococcus halocryophilus Or1. ISME J. 7, 1211-26.

Myshrall KL, Mobberley JM, Green SJ, Visscher PT, Havemann SA, Reid RP, Foster JS. (2010). Biogeochemical cycling and microbial diversity in the thrombolitic microbialites of Highbourne Cay, Bahamas. Geobiology. 8, 337-54.

Namiki T, Hachiya T, Tanaka H, Sakakibara Y. (2012). MetaVelvet: an extension of Velvet assembler to de novo metagenome assembly from short sequence reads. Nucleic Acids Res. 40, e155

Neilan BA, Pearson LA, Muenchhoff J, Moffitt MC, Dittmann E. (2013). Environmental conditions that influence toxin biosynthesis in cyanobacteria. Environ Microbiol. 5, 1239-53.

Nichols PD, Gukert JB, White DC. (1986). Determination of monounsaturated fatty acid double bond position and geometry for microbial monocultures and complex consortia by capillary GC-MS of their dimethyl disulphide adducts. Journal of Microbial Methods 5, 49-55.

Nisanian M, Holladay SD, Karpuzoglu E, Kerr RP, Williams SM, Stabler L, McArthur JV, Tuckfield RC, Gogal RM Jr. (2014). Exposure of juvenile Leghorn chickens to lead acetate enhances antibiotic resistance in enteric bacterial flora. Poult Sci. 93, 891-7.

Niu B, Zhu Z, Fu L, Wu S, Li W. (2011). FR-HIT, a Very Fast Program to Recruit Metagenomic Reads to Homologous Reference Genomes. Bioinformatics. 27, 1704-1705.

Noble RRP, Stalker L, Wakelin SA, Pejcic B, Leybourne MI, Hortle AL, Michael, K. (2012). Biological monitoring for carbon capture and storage - A review and potential future developments. Int. J. Greenh. Gas Control 10, 520-535.

Nübel U, Garcia-Pichel F, Kühl M, Muyzer G. (1999). Quantifying microbial diversity: morphotypes, 16S rRNA genes, and carotenoids of oxygenic phototrophs in microbial mats. Appl Environ Microbiol. 65, 422-30.

Obst M, Wehrli B, Dittrich M. (2009). CaCO3 nucleation by cyanobacteria: laboratory evidence for a passive, surface-induced mechanism. Geobiology 7, 324-347.

Olson JM, Pierson BK. (1986). Photosynthesis 3.5 thousand million years ago. Photosynth Res. 9, 251-259.

Omelon CR, Brady AL, Slater GF, Laval B, Lim DSS, Southam G. (2013). Microstructure variability in freshwater microbialites, Pavilion Lake, Canada. Palaeogeography, Palaeoclimatology, Palaeoecology 392, 62-70.

Ordoñez OF, Lanzarotti E, Kurth D, Gorriti MF, Revale S, Cortez N, Vazquez MP, Farías ME, Turjanski AG. 2013. Draft genome sequence of the polyextremophilic *Exiguobacterium* sp. strain S17, isolated from hyperarsenic lakes in the Argentinian Puna. Genome Announc. 1(4):e00480-13. doi:10.1128/genomeA.00480-13.

Paerl HW, Steppe TF, Reid RP. (2001). Bacterially mediated precipitation in marine stromatolites. Environ Microbiol. 3, 123-30.

Paley SM, Karp PD. (2006). The Pathway Tools cellular overview diagram and omics viewer. Nucleic Acids Res. 34, 3771-8.

Papineau D, Walker JJ, Mojzsis SJ, Pace NR. (2005). Composition and structure of microbial communities from stromatolites of Hamelin Pool in Shark Bay, Western Australia. Appl Environ Microbiol. 71, 4822-32.

Parks DH, Beiko RG. (2010). Identifying biologically relevant differences between metagenomic communities. Bioinformatics 26, 715-21.

Patterson CC. (1956). Age of meteorites and the Earth. Geochim. Cosmochim. Acta 10, 230-7

Pelz A, Wieland K-P, Putzbach K, Hentschel P, Albert K, Götz F .2005. Structure and biosynthesis of staphyloxanthin from *Staphylococcus aureus*. J Biol Chem. 280, 32493-98.

Perry RS, Mcloughlin N, Lynne BY, Sephton MA, Oliver JD, Perry CC, Campbell K, Engel MH, Farme, JD, Brasier MD, Staley JT. (2007). Defining biominerals and organominerals: direct and indirect indicators of life. Sedimentary Geology 201, 157-179.

Pia J. (1933). Die Rezenten Kalkesteine: Zeitschr. fiir Kristallographle, Mineralogie und Petrographic, Abt. B, 1-420 (In German).

Planavsky N, Ginsburg RN. (2009). Taphonomy of modern marine Bahamian microbialites. Palaios 24, 5-17.

Planavsky NJ, Asael D, Hofmann A, Reinhard CT, Lalonde SV, Knudsen A,Wang X, Ossa FO, Pecoits E, et al. (2014). Evidence for oxygenic photosynthesis half a billion years before the Great Oxidation Event. Nat Geosci. 7, 283–286

Ponder MA, Gilmour SJ, Bergholz PW, Mindock CA, Hollingsworth R, Thomashow MF, Tiedje JM. (2005). Characterization of potential stress responses in ancient Siberian permafrost psychroactive bacteria. FEMS Microbiol Ecol. 53, 103-115.

Power IM, Wilson SA, Thom JM, Dipple GM, Southam G. (2007). Biologically induced mineralization of dypingite by cyanobacteria from an alkaline wetland near Atlin, British Columbia, Canada. Geochem Trans. 8, 13.

Power IM, Wilson SA, Dipple GM, Southam G. (2011). (a) Modern carbonate microbialites from an asbestos open pit pond, Yukon, Canada. Geobiology. 9, 180-95.

Power IM, Wilson SA, Small DP, Dipple GM, Wan W, Southam G. (2011). (b) Microbially mediated mineral carbonation: roles of phototrophy and heterotrophy. Environ Sci Technol. 45, 9061-8.

Raichand R, Pareek S, Singh NK, Mayilraj S. (2012). *Exiguobacterium aquaticum* sp. nov. a new member of the genus *Exiguobacterium.* Int. J. Syst. Evol. Microbiol. 62, 2150-2155.

Rasko DA, Webster DR, Sahl JW, Bashir A, Boisen N, Scheutz F, Paxinos EE, Sebra R, Chin CS, Iliopoulos D, Klammer A, et al. (2011). Origins of the *E. coli* strain causing an outbreak of hemolytic-uremic syndrome in Germany. N Engl J Med. 365, 709-717.

Rath D, Jawali N. 2006. Loss of Expression of cspC, a Cold Shock Family Gene, Confers a Gain of Fitness in Escherichia coli K-12 Strains J. Bacteriol. 188, 6780-85.

Rawat SR, Männistö MK, Bromberg Y, Häggblom MM. (2012). Comparative genomic and physiological analysis provides insights into the role of *Acidobacteria* in organic carbon utilization in Arctic tundra soils. FEMS Microbiol Ecol. 82, 341-55

Rebollar EA, Avitia M, Eguiarte LE, González-González A, Mora L, Bonilla-Rosso G, and Souza V. (2012). Water-sediment niche differentiation in ancient marine lineages of *Exiguobacterium* endemic to the Cuatro Cienegas Basin. Environ Microbiol. 14, 2323-2333.

Reid RP, Visscher PT, Decho AW, Stolz JF, Bebout BM, Dupraz C, Macintyre IG, Paerl HW, Pinckney JL, Prufert-Bebout L, Steppe TF, DesMarais DJ. (2000). The role of microbes in accretion, lamination and early lithification of modern marine stromatolites. Nature 406, 989-99.

Rice P, Longden I, and Bleasby A. (2000). EMBOSS: The European Molecular Biology Open Software Suite Trends in Genetics 16, 276-277.

Rho M, Tang H, Ye Y. (2010). FragGeneScan: predicting genes in short and error-prone reads. Nucleic Acids Res. 38, e191.

Rodrigues DF, Goris J, Vishnivetskaya T, Gilichinsky D, Thomashow MF, Tiedje JM. (2006). Characterization of *Exiguobacterium* isolates from the Siberian permafrost Description of *Exiguobacterium sibiricum* sp. nov. Extremophiles 10, 285-294.

Rodrigues DF, Ivanova N, He Z, Huebner M, Zhou J, Tiedje JM. (2008). Architecture of thermal adaptation in an *Exiguobacterium sibiricum* strain isolated from 3 million year old permafrost: a genome and transcriptome approach. BMC Genomics 9, 547.

Ross MG, Russ C, Costello M, Hollinger A, Lennon NJ, Hegarty R, Nusbaum C, Jaffe DB. (2013). Characterizing and measuring bias in sequence data. Genome Biol. 14, R51.

Rothschild LJ, Mancinelli RL. (1990). Model of carbon fixation in microbial mats from 3,500 Myr ago to the present. Nature. 345, 710-12.

Russell JA, Brady AL, Cardman Z, Slater GF, Lim DS, Biddle JF. (2014). Prokaryote populations of extant microbialites along a depth gradient in Pavilion Lake, British Columbia, Canada. Geobiology 12, 250-264.

Santos F, Peña A, Nogales B, Soria-Soria E, Del Cura MA, González-Martín JA, Antón J. (2010). Bacterial diversity in dry modern freshwater stromatolites from Ruidera Pools Natural Park, Spain. Syst Appl Microbiol. 33, 209-21.

Salek SS, Kleerebezem R, Jonkers HM, Witkamp GJ, van Loosdrecht MCM. Mineral CO_2 sequestration by environmental biotechnological processes. Trends Biotechnol. 2013, 31, 139-146.

Schneider D, Arp G, Reimer A, Reitner J, Daniel R. (2013). Phylogenetic analysis of a microbialite-forming microbial mat from a hypersaline lake of the Kiritimati atoll, Central Pacific. PLoS One. 8, e66662.

Schindler T, Graumann PL, Perl D, Ma S, Schmid FX, Marahiel MA. (1999). The family of cold shock proteins of *Bacillus subtilis.* Stability and dynamics in vitro and in vivo. J Biol Chem. 274, 3407-13.

Schmid AK, Howell HA, Battista JR, Peterson SN, Lidstrom ME. (2005). HspR is a global negative regulator of heat shock gene expression in *Deinococcus radiodurans*. Mol Microbiol. 55, 1579-90.

Schmieder R, Lim YW, Rohwer F, Edwards R. (2010). TagCleaner: identification and removal of tag sequences from genomic and metagenomic datasets. BMC Bioinformatics 11, 341.

Schmieder R, Edwards R (2011). Quality control and preprocessing of metagenomic datasets. Bioinformatics. 27, 863-4.

Schopf JW. (2006). Fossil evidence of Archean life. Philosophical Transactions of the Royal Society, B 361, 869-885.

Schulz A, Schumann W. (1996). HrcA, the first gene of the *Bacillus subtilis* dnaK operon encodes a negative regulator of class I heat shock genes. J. Bacteriol. 178, 1088-93

Scolnik PA, Walker MA, Marrs, BL (1980). Biosynthesis of carotenoids derived from neurosporene in *Rhodopseudomonas capsulata*. J Biol Chem 255, 2427–32

Shao C, Sun Y, Wang N, Yu H, Zhou Y, Chen C, Jia J. (2013). Changes of proteome components of *Helicobacter pylori* biofilms induced by serum starvation. Mol Med Rep. 2013 6, 1761-6.

Sheehan PM, Harris MT. Microbialite resurgence after the Late Ordovician extinction. (2004). Nature. 430, 75-8.

Sherley M, Gordon DM, Collignon PJ. (2004). Evolution of multi-resistance plasmids in Australian clinical isolates of *Escherichia coli*. Microbiology. 150, 1539-46

Simpson JT, Wong K, Jackman SD, Schein JE, Jones SJ, Birol I. (2009). ABySS: a parallel assembler for short read sequence data. Genome Res. 6, 1117-23.

Singh NK, Raichand R, Kaur I, Kaur C, Pareek S, Mayilraj S. (2013). *Exiguobacterium himgiriensis* sp. nov. a novel member of the genus *Exiguobacterium*, isolated from the Indian Himalayas. Antonie van Leeuwenhoek 103, 789-796.

Smith AM, Andrews JE, Uken R, Thackeray Z, Perissinotto R, Leuci R, Marca-Bel A. (2011). Rock pool tufa stromatolites on a modern South African wave-cut platform: partial analogues for Archaean stromatolites? Terra Nova 23, 375-381.

Spadafora A, Perri E, McKenzie JA, Vasconcelos C. (2010). Microbial biomineralization processes forming modern Ca:Mg carbonate stromatolites. Sedimentology 57, 27–40.

Sprachta S, Camoin G, Golubic S, Le-Campion T. (2001). Microbialites in a modern lagoonal environment: nature and distribution, Tikehau atoll (French Polynesia). Palaeogeo Palaeoclim, Palaeoecology. 175, 103-124.

Squyres SW, Andersen DW, Nedell SS, Wharton RA Jr. (1991). Lake Hoare, Antarctica: sedimentation through a thick perennial ice cover. Sedimentology. 38, 363-79.

Stal LJ. (2000). Cyanobacterial mats and stromatolites. Ecology of cyanobacteria: their diversity in time and space (Whiton BA & Potts M, eds), pp. 61-120. Kluwer academic publications, The Netherlands.

Stevenson JS. (1940). Mercury deposits of British Columbia. Bulletin No.5, British Columbia department of mines. Victoria, BC.

Summons RE, Jahnke LL, Hope JM, Logan GA. (1999). 2-Methylhopanoids as biomarkers for cyanobacterial oxygenic photosynthesis. Nature. 400, 554-7.

Suttle, AS. (2005). Viruses in the Sea. Nature 437, 356-36

Suzuki R, Shimodaira H. (2006). Pvclust: an R package for assessing the uncertainty in hierarchical clustering, Bioinformatics 22, 1540-1542.

Sverjensky DA, Lee N. (2010). The Great Oxidation Event and Mineral Diversification. Elements 6, 31-36

Takaichi S, Maoka T, Takasaki K, Hanada S. (2010). Carotenoids of *Gemmatimonas aurantiaca* (Gemmatimonadetes): identification of a novel carotenoid, deoxyoscillol 2-rhamnoside, and proposed biosynthetic pathway of oscillol 2,2'-dirhamnoside. Microbiology. 156, 757-63.

Tamura K, Peterson D, Peterson N, Stecher G, Nei M, and Kumar S. (2011). MEGA5: Molecular Evolutionary Genetics Analysis using Maximum Likelihood, Evolutionary Distance, and Maximum Parsimony Methods. Molecular Biology and Evolution 28, 2731-2739.

Tao L, Yao H, Cheng Q. (2007). Genes from a Dietzia sp. for synthesis of C40 and C50 β-cyclic carotenoids. Gene 386, 90-97.

Tarhan LG, Planavsky NJ, Laumer CE, Stolz JF, Reid RP. (2013). Microbial mat controls on infaunal abundance and diversity in modern marine microbialites. Geobiology. 11, 485-97.

Tats A, Remm M, Tenson T. (2006). Highly expressed proteins have an increased frequency of alanine in the second amino acid position. BMC Genomics. 7, 28.

Tesson B, Gaillard C, Martin-Jézéquel V. (2008). Brucite formation mediated by the diatom *Phaeodactylum tricornutum*. Mar. Chem. 109, 60-76.

Therkildsen MS, Isaksen MF, Lomstein BA. (1997). Urea production in the marine bacteria *Delaya venusta* and *Pseudomonas stutzeri* grown in a minimal medium. Aquatic Microb. Ecol. 13, 213-217.

Thompson JB, Ferris GF. (1990). Cyanobacterial precipitation of gypsum, calcite, and magnesite from natural alkaline lake water. Geology 18, 995-998.

Thompson JB, Schultze-Lam S, Beveridge TJ, Des Marais DJ. (1997). Whiting events: Biogenic origin due to the photosynthetic activity of *Cyanobacteria* picoplankton. Limnol. Oceanog. 42, 133-141.

Thompson RL, Zeng Q, Kelly L, Huang HK, Singer UA, Stubbea J, and Chisholm WS. (2011). Phage auxiliary metabolic genes and the redirection of cyanobacterial host carbon metabolism. PNAS 108, E757-64.

Toleman MA, Bennett PM, Bennett DM, Jones RN, Walsh TR. (2007). Global emergence of trimethoprim/sulfamethoxazole resistance in *Stenotrophomonas maltophilia* mediated by acquisition of sul genes. Emerg Infect Dis. 4, 559-65.

Tsuzuki M, Moskvin OV, Kuribayashi M, Sato K, Retamal S, Abo M, Zeilstra-Ryalls J, Gomelsky M. (2011). Salt stress-induced changes in the transcriptome, compatible solutes, and membrane lipids in the facultatively photosynthetic bacterium *Rhodobacter sphaeroides.* Appl Environ Microbiol. 77, 7551-9

Tu Q, He Z, Zhou J. (2014). Strain/species identification in metagenomes using genome-specific markers. Nucleic acids 42, e67

Untergasser A. DNA Miniprep using CTAB *Untergasser's Lab*. (2008). First accessed July 10, 2010 http://www.untergasser.de/lab/protocols/miniprep_dna_ctab_v1_0.htm

Van der Meer MTJ, Schouten S, de Leeuw JW, Ward DM. (2000). Autotrophy of green non-sulphur bacteria in hot spring microbial mats: biological explanations for isotopically heavy organic carbon in the geological record. Environ Microbiol. 2, 428-35.

Van Kranendonk MJ, Philippot P, Lepot K, Bodorkos S, Pirajno F. (2008). Geological setting of Earth's oldest fossils in the ca. 3.5 Ga Dresser Formation, Pilbara Craton, Western Australia. Precambrian Research 167, 93-124.

Varin T, Lovejoy C, Jungblut AD, Vincent WF, Corbeil J. (2012). Metagenomic analysis of stress genes in microbial mat communities from Antarctica and the High Arctic. Appl Environ Microbiol. 78, 549-59.

Vasconcelos C, Warthmann R, McKenzie JA, Visscher PT, Bittermann AG, van Lith Y. (2006). Lithifying microbial mats in Lagoa Vermelha, Brazil: Modern Precambrian relics?:Sedimentary Geology. 185, 175-183

Vijayalaxmi S, Anu Appaiah KA, Jayalakshmi SK, Mulimani VH, Sreeramulu K. (2013). Production of bioethanol from fermented sugars of sugarcane bagasse produced by lignocellulolytic enzymes of *Exiguobacterium sp.* VSG-1. Appl Biochem Biotechnol. 171, 246-60.

Vishnivetskaya TA, Kathariou S. (2005). Putative transposases conserved in Exiguobacterium isolates from ancient Siberian permafrost and from contemporary surface habitats. Appl Environ Microbiol. 71, 6954-6962.

Vishnivetskaya TA, Petrova MA, Urbance J, Ponder M, Moyer CL, Gilichinsky DA, Tiedje JM. (2006). Bacterial community in ancient Siberian permafrost as characterized by culture and culture-independent methods. Astrobiology 6, 400-414.

Vishnivetskaya TA, Kathariou S, Tiedje JM. (2009). The *Exiguobacterium* genus: biodiversity and biogeography. Extremophiles 13, 541-555.

Vishnivetskaya TA, Lucas S, Copeland A, Lapidus A, Glavina del Rio T, Dalin E, Tice H, Bruce DC, Goodwin LA, Pitluck S, Saunders E et al. (2011). Complete genome sequence of the Thermophilic Bacterium *Exiguobacterium* sp. AT1b. J. Bacteriol. 193, 2880-81.

Visscher PT, Reid RP, Bebout BM. (2000). Microscale observations of sulfate reduction: correlation of microbial activity with lithified micritic laminae in modern marine stromatolites. Geology 28, 919-922.

Wacey D, Kilburn RM, Saunders M, Cliff J, Brasier DM. (2011). Microfossils of sulphur-metabolizing cells in 3.4-billion-year-old rocks of Western Australia. Nature Geoscience 4, 698-702.

Wang J, Gao F, Liu Z, Qiao M, Niu X, Zhang KQ, Huang X. (2012). Pathway and molecular mechanisms for malachite green biodegradation in *Exiguobacterium* sp. MG2. PLoS One. 7(12):e51808.

Weihrauch D, Wilkie MP, Walsh PJ. (2009). Ammonia and urea transporters in gills of fish and aquatic crustaceans. J Exp Biol 212, 1716–1730.

White RA 3rd, Blainey PC, Fan HC, Quake SR. (2009). Digital PCR provides sensitive and absolute calibration for high throughput sequencing. BMC Genomics 10, 116.

White RA 3rd, Grassa CJ, Suttle CA. (2013). (a). First draft genome sequence from a member of the genus *Agrococcus*, isolated from modern microbialites. Genome Announc. 1, e00391-13.

White RA 3rd, Grassa CJ, Suttle CA. (2013). (b). Draft Genome Sequence of *Exiguobacterium pavilionensis* Strain RW-2, with Wide Thermal, Salinity, and pH Tolerance, Isolated from Modern Freshwater Microbialites. Genome Announc. 1, e00597-13.

White RA 3rd, Suttle CA. (2013). (c). The Draft Genome Sequence of *Sphingomonas paucimobilis* Strain HER1398 (Proteobacteria), Host to the Giant PAU Phage, Indicates That It Is a Member of the Genus Sphingobacterium (Bacteroidetes). Genome Announc. 1, e00598-13

Wickham H. (2009). ggplot2: elegant graphics for data analysis. Springer New York.

Wilson SA, Dipple GM, Power IM, Thom JM, Anderson RG, Raudsepp M, Gabites JE, Southam G. (2009). Carbon dioxide fixation within mine wastes of ultramafic-hosted ore deposits: examples from the Clinton Creek and Cassiar chrysotile deposits, Canada. Economic Geology 104, 95-112.

Wommack, E.K., Bhavsar, J., and Ravel, J. (2008). Metagenomics: read length matters. Appl Environ Microbiol. 74, 1453-63.

Wu YS, Yu GL, Li RH, Song LR, Jiang HX, Riding R, Liu LJ, Liu DY, Zhao R. (2014). Cyanobacterial fossils from 252 Ma old microbialites and their environmental significance. Sci Rep. 4, 3820.

Wu S, Zhu Y. (2012). ProPAS: standalone software to analyze protein properties. Bioinformation 8, 167-9.

Yamanaka K, and Inouye M. (1997). Growth-phase-dependent expression of cspD, encoding a member of the CspA family in *Escherichia coli.* J Bacteriol 179, 5126-30

Yang J, Wang C, Wu J, Liu L, Zhang G, Feng J. (2014). Characterization of a multiresistant Mosaic plasmid from a fish farm sediment *Exiguobacterium* sp. isolate reveals aggregation of functional clinic-associated antibiotic resistance genes. Appl Environ Microbiol. 4, 1482-8.

Yilmaz S, Allgaier M, Hugenholtz P. (2010). Multiple displacement amplification compromises quantitative analysis of metagenomes. Nat Methods. 7, 943-944.

Yoshimune K, Galkin A, Kulakova L, Yoshimura T, Esaki N. (2005). Cold-active DnaK of an Antarctic psychrotroph *Shewanella sp*. Ac10 supporting the growth of dnaK-null mutant of Escherichia coli at cold temperatures. Extremophiles. 2, 145-50.

Yumoto I, Hishinuma-Narisawa M, Hirota K, Shingyo T, Takebe F, Nodasaka Y, Matsuyama H, Hara I. (2004). *Exiguobacterium oxidotolerans* sp nov., a novel alkaliphile exhibiting high catalase activity. Int. J. Syst. Evol. Microbiol. 54, 2013-17.

Zamarreno DV, Inkpen R, May E. (2009). Carbonate crystals precipitated by freshwater bacteria and their use as a limestone consolidant, Appl Environ Microbiol. 75, 5981-90.

Zeigler Allen L, Allen EE, Badger JH, McCrow JP, Paulsen IT, Elbourne LD, Thiagarajan M, Rusch DB, Nealson KH, Williamson SJ, Venter JC, Allen AE. (2012). Influence of nutrients and currents on the genomic composition of microbes across an upwelling mosaic. ISME J. 6, 1403-14.

Zerbino DR, Birney E. (2008). Velvet: algorithms for de novo short read assembly using de Bruijn graphs. Genome Res. 18, 821-9.

Zhang JY, Liu XY, Liu SJ. (2010). *Agrococcus terreus* sp. nov. and *Micrococcus terreus* sp. nov., isolated from forest soil. Int J Syst Evol Microbiol. 60, 1897-903.

Zhang W, Hu X, Wang L, Wang X. (2014). Reconstruction of the carotenoid biosynthetic pathway of *Cronobacter sakazakii* BAA894 in Escherichia coli. PLoS One. 9, e86739.

Zhou J, He Q, Hemme CL, Mukhopadhyay A, Hillesland K, Zhou A, He Z, Van Nostrand JD, Hazen TC, Stahl DA, Wall JD, Arkin AP. (2011). How sulphate-reducing microorganisms cope with stress: lessons from systems biology. Nat Rev Microbiol. 9, 452-66.

Zlamala C, Schumann P, Kämpfer P, Rosselló-Mora R, Lubitz W, Busse HJ. (2002). *Agrococcus baldri* sp. nov., isolated from the air in the 'Virgilkapelle' in Vienna. Int J Syst Evol Microbiol. 52, 1211-6.